Nano-porous Materials from Diblock Copolymers and its Membrane Application

Szewczykowski, Piotr Przemyslaw

Publication date:
2009

Document Version
Publisher's PDF, also known as Version of record

Nano-porous Materials from Diblock Copolymers and its Membrane Application

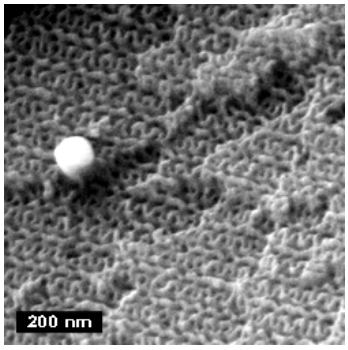

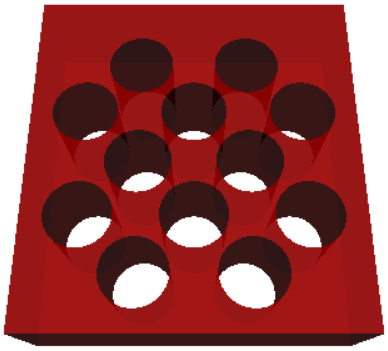

Piotr Szewczykowski
Ph.D. Thesis
2009

DTU Chemical Engineering
Department of Chemical and Biochemical Engineering

Nano-porous Materials from Diblock Copolymers and its Membrane Application

Piotr Szewczykowski

Ph.D. Thesis

February 2009

Danish Polymer Centre
Department of Chemical and Biochemical Engineering
Technical University of Denmark

2009 ISBN: 978-87-92481-06-1
Printed by J&R Frydenberg A/S
Copenhagen, Denmark

Preface

Work presented in this thesis was supported by grants given by the Danish Research Council for Technology and Production Sciences (FTP Grant no. 26-03-0271), DANSCATT centre sponsored by the Danish Natural Science Research Council.

Most of the experiments and analysis took place at Danish Polymer Centre, Department of Chemical and Biochemical Engineering and at Risø DTU National Laboratory for Sustainable Energy. Supervisors were Martin E. Vigild, Department of Chemical and Biochemical Engineering, Danish Polymer Centre, Technical University of Denmark and Sokol Ndoni, Department of Micro- and Nanotechnology, Technical University of Denmark.

First of all I would like to thank very much my supervisors: Martin Vigild and Sokol Ndoni for supporting me all the time, helping to solve many problems and teach me how the research should proceed. Working as a member of Martin's Vigild and Sokol's Ndoni group was a great pleasure and good school of group work. Here I would like to thank all the people with whom I had occasion to collaborate within our group and not only: Kenneth Andersen, Fenxiao Guo, Lars Schulte, Mathilde R. Jakobsen, Anne Grydgaard, Li Li, Astrid Jørgensen, Kaushal Sagar, Rolf H. Berg and Katja Jankova.

I would like to thank very much Kell Mortensen for great help with analysis of small angle neutron scattering data and for writing necessary programs. I also thank Gunnar Eigil Jonsson for help with solving problems connected to membranes.

For technical support I would like to thank: Thomas Geue from the Paul Scherrer Institute (Villingen, Switzerland) for providing beam time at the SANS2 instrument, Pia Wahlberg from the Danish Technological Institute, (Høje Taastrup, Denmark) for help with scanning electron microscopy, Jens Wenzel Andreasen from Risø DTU National Laboratory for Sustainable Energy for introduction to small angle x-ray scattering, Flemming Bjerg Grumsen from Department of Mechanical Engineering, DTU for help with transmission electron microscopy, Bente Lundgård from Department of Chemical and Biochemical Engineering, DTU for help with size exclusion chromatography, Christian Rein Hansen from Copenhagen University for help with atomic force microscopy, Marina Kustova from Department of Chemistry, DTU for help with nitrogen adsorption, Brian R. Pauw for help with graphics preparation in POV-ray program and Kim Chi Szabo from Polymer Centre, DTU for general help in the lab.

Finally special thanks to my family for great support, especially to my beloved wife and daughter.

Kgs. Lyngby, Denmark
08 February 2009

Synopsis

This thesis is a study on characterization and membrane application of nano-porous materials from diblock copolymers. The study of nano-porous materials obtained from self-organizing block copolymers is a research field of increasing focus both on scientific and the technological aspects. This project aimed to understanding and creating nano-porous material from block copolymers, based on the selective removal of the minority block from self-organized block copolymers. The ambition was to generate the necessary know-how in order to obtain promising results for at least one final application. Quite many potential applications of nano-porous materials can be found in the literature. Such material can be used for highly selective membrane preparation and it is further investigated in this thesis.

Nano-porous material presented here was prepared from diblock copolymers synthesized (not by me) by living anionic polymerization. The majority block consisted of polyisoprene or 1,2-polybutadiene, whereas the minority block consisted of polydimethylsiloxane (PDMS) in all cases. Depending on the block copolymer composition two different morphologies were obtained and investigated: hexagonally packed cylinders morphology (HEX) and gyroid morphology (GYR). Samples with HEX morphology were aligned by mechanical shearing. Since glass transition temperature of the major block T_g is below room temperature, samples were cross-linked to avoid pores collapsing. Final nano-porous material was obtained after selective etching the minority block of PDMS. The prepared nano-porous material was characterized by electron microscopy, scattering techniques and nitrogen adsorption.

The influence of crosslinking degree on pores stability was investigated on samples with HEX morphology prepared from polyisoprene-*b*-polydimethylsiloxane. Not sufficiently crosslinked samples had collapsed pores in the dry state. Such sample was placed in deuterated toluene and analyzed by using small angle neutron scattering (SANS). Process of drying the sample was analyzed by SANS also. Conclusion from this part was that pores can be reopened after placing the sample in a proper solvent and closed again after sample drying.

Nano-porous samples obtained from 1,2-polybutadiene-*b*-polydimethylsiloxane with gyroid morphology were used for membrane application. Gyroid morphology was chosen for this purpose, since nano-pores do not have to be aligned in order to assure percolation between two sides of the membrane. Alignment of channels would be necessary in case of HEX morphology. Samples in a form of discs were investigated. Formation of a skin layer on the disc side which had a contact with air during solvent casting was observed. Polishing of the sample with a sand paper was performed in order to remove this skin layer and these two kinds of samples were compared for gas and liquids fluxes and separation properties. The setup for this purpose was designed. Separation properties of nano-porous samples were investigated by filtration of polyethylene glycols molecules of different molecular weight dissolved in a mixture of methanol and water. Collected

permeates were analyzed by size exclusion chromatography (SEC) and retention curves were compared.

In conclusion samples with a skin layer showed better separation properties comparing to polished samples. From the other side, polished samples showed much higher fluxes. The ideal material for membrane application should be much thinner, with high flux and separation properties.

This interesting and promising research area could be definitely continued by following researchers, since this is a first project investigating membrane application of nano-porous material within Sokol Ndoni and Martin E. Vigild group.

Dansk Resumé

Denne afhandling omhandler undersøgelser vedrørende karakterisering og membran anvendelse af nano-porøse materialer fremstillet ud fra selvorganiserende diblock copolymerer. Forskning i nano-porøse materialer er et ekspanderende forsknings-område med fokus på både videnskabelige og teknologiske aspekter. Dette projekt havde til formål at forstå og fremstille nano-porøse materialer ud fra block copolymerer baseret på selektiv fjernelse af minoritets blokken i selvsorganiserede diblock copolymerer. Ambitionen var at generere den nødvendige know-how med henblik på at få lovende resultater i mindst en endelig applikation. I litteraturen findes mange potentielle anvendelser af nano-porøse materialer. Sådanne materialer kan bruges til fremstilling af meget selektive membraner, hvilket er undersøgt yderligere i denne afhandling.

De nano-porøse materialer, der omtales i det følgende, var fremstillet af diblock copolymerer syntetiseret (ikke personligt) ved levende anionisk polymerisering. Majoritetsblokken af den benyttede block copolymer bestod af enten polyisopren eller 1,2-polybutadien, mens minoritetsblokken bestod af polydimethylsiloxane (PDMS). Afhængigt af sammensætningen blev to forskellige morfologier undersøgt: hexagonalt pakket cylinder morfologi (HEX) og gyroid morfologi (GYR). Prøver med HEX morfologi blev ensrettet ved hjælp af mekanisk klipning. Da glasovergangstemperaturen T_g af den største blok er under stuetemperatur, blev prøverne krydsbundet for at undgå at porerne ville kollapse. Nano-porøsiteten blev opnået ved selektiv ætsning af minoritetsblokken af PDMS. Materialet blev karakteriseret ved elektronmikroskopi, sprednings teknikker og kvælstof adsorption.

Krydsbindingsgradens indflydelse på stabiliteten af porerne blev undersøgt på prøver fremstillet af polyisopren-*b*-polydimetylsiloxan med HEX morfologi. Prøver uden tilstrækkelig krydsbinding havde kollapsede porer i tør tilstand. En prøve blev placeret i deutereret toluen og analyseret ved hjælp af småvinkel neutron spredning (SANS). Endvidere blev tørringsprocessen af prøven analyseret med SANS. Konklusionen på denne del var, at porerne kan genåbnes ved at anbringe prøven i en velegnet solvent og genlukkes ved tørring.

Nano-porøse prøver fremstillet af 1,2-polybutadien-*b*-polydimetylsiloxan med GYR morfologi blev anvendt som membran. GYR morfologi blev udvalgt til dette formål, da nano-porerne i denne struktur ikke behøver at blive ensrettet for at sikre perkolation gennem membranen. Ensretning af kanalerne vil være nødvendigt i tilfælde af HEX morfologi. Disc-formede prøver blev undersøgt, og dannelse af et overfladelag på den side, som havde kontakt med luft under solvent strengstøbning støbning, blev observeret. En prøve blev poleret med sand papir med henblik på at fjerne overfladelaget, og prøver med og uden overfladelag blev sammenlignet for gas og væske flux og separations egenskaber. Opsætningen til dette formål blev udformet. Separations egenskaberne for de nano-porøse prøver blev undersøgt ved filtrering af polyethylen glycol molekyler med forskellige molmasser opløst i en blanding af methanol og vand. Indsamlet permeat blev analyseret ved hjælp af størrelseskromatografi størrelse SEC og retentions kurverne blev

sammenlignet.
Det konkluderes, at prøver med overfladelag viste bedre separations egenskaber sammenlignet med polerede prøver. Derimod viste polerede prøver langt højere flux. Det ideelle materiale til membranen applikationen bør være meget tyndere, med stor flux, og separations egenskaber.

Dette interessante og lovende forskningsområde har potentiale for yderligere efterforskning, da det er det første projekt, der omhandler anvendelse af membran fremstillet af nano-porøst materiale i Sokol Ndoni og Martin E. Vigild gruppen.

Contents:

List of abbreviations:

Table 1 Symbols

Symbol	Description
b	Average bond length
b_i	Scattering length of the monomer or the solvent molecule
C_n	Characteristic ratio calculated as a function of chain length
d	Specific mass (mass density) of monomer or solvent
d_{10}	Distance between scattering plane 10
D_k	Knudsen diffusion coefficient
f_A	Volume fraction of block A
I	Scattering intensity
J	Volume flux
k	Boltzmann constant
l	Membrane thickness
m	Mass of monomer or solvent molecule
M_w	Weight average molecular weight
M_N	Number average molecular weight
n	number of covalent chain bonds
N	Degree of polymerization
P	Pressure
T_g	Glass transition temperature
T_{OOT}	Order-order temperature
T_{ODT}	Order-disorder temperature
q	Scattering vector
r	Pore radius
R	Gas constant
R_h	Hydrodynamic radius
R_g	Radius of gyration
R_o^2	Mean square end-to-end distance
w_A	Mass fraction of block A
ε	Surface porosity
λ	Wavelength; mean free path
χ	Flory interaction parameter
ρ	Scattering length density
σ	Collision cross-section
θ	Scattering angle
τ	Tortuosity factor

Table 2 Abbreviations

Symbol	Description
ABS	Acrylonitrile-butadiene-styrene terpolymer
AFM	Atomic force microscope
BCC	Body centred cubic morphology
BD	Poli(butadiene-*b*-polydimethylsiloxane)
BET	Brunauer-Emmett-Teller method
BJH	Barrett-Joyner-Halenda method
d-MeOH	Deuterated methanol
d-Tol	Deuterated toluene
DCP	Dicumyl peroxide
DLS	Dynamic light scattering
GYR	Gyroid morphology
HEX	Hexagonally packed cylinders morphology
HF	Hydrogen fluoride
ID	Poli(isoprene-*b*-polydimethylsiloxane)
LAM	Lamellar morphology
MeOH	Methanol
NMR	Nuclear magnetic resonance
NPM	Nano-porous material
PB	Polybutadiene
PCEMA	poly(2-cinnamoylethyl methacrylate)
PDI	Polydispersity index
PDMS	Polydimethylsiloxane
PEG	Polyethylene glycol
PI	Polyisoprene
PMMA	poly(methyl methacrylate)
PO	poly(propylene oxide)
PPS	Poly(4-vinylphenyl-dimethyl-2-propoxysilane)
PPQ	Poly(phenylquinoxaline)
PS	polystyrene
P*t*BA	Poly(*tert*-butyl acrylate)
PVC	Polyvinylchloride
SAN	Styrene-acrylonitrile alternating copolymer
SANS	Small angle neutron scattering
SAXS	Small angle x-ray scattering
SEC	Size exclusion chromatography
SEM	Scanning electron microscopy
TBAF	Tetrabutylammonium fluoride
TEM	Transmission electron microscopy
THF	Tetrahydrofurane

List of Tables:

List of Figures

Introduction

Polymers built from one type of monomer are defined as homopolymers. Polymer built up from different monomers could be called as heteropolymer.[1] In particular case, when polymer consists only two different mers we talk about copolymer. Depending on the sequence that two different monomers are bonded together we can distinguish copolymer types like: random, alternating, graft and block copolymers. Block copolymers can be distinguished to: di-, tri- or ter- block copolymers,[2] depending on the amount of blocks in one polymer molecule, which is schematically presented in Figure 1. Polymer which consists of three different mers is called terpolymer.

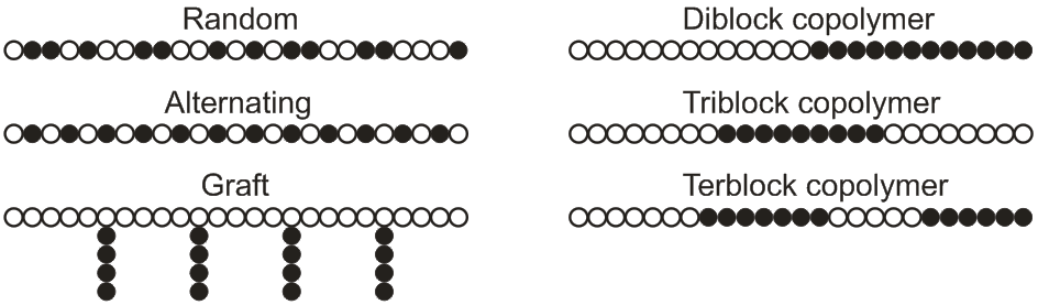

Figure 1 Schematic presentation of different copolymers and block copolymers types.

Copolymer will have different properties than homopolymers of same mers. Its properties depend on the ratio of mers. Copolymers are well known materials which find many applications in our every day life. SAN – is alternating copolymer of styrene-acrylonitrile, which is used as a cover for car batteries. Known example of terpolymer (build from three different monomers) is ABS – acrylonitrile-butadiene-styrene, which is used as a different kind of covers or pipes thanks to its mechanical resistance.

Block copolymers are much more difficult to obtain comparing to altenating or random copolymers, but they give something instead.

Self-organization of diblock copolymers

Block copolymers have a wonderful property of organizing itself into different morphologies in the nanoscale.[3] This comes from the fact that two chemically incompatible polymer chains want to separate into different phases. This phenomenon is only partly allowed, since two blocks are combined together by a covalent bond. The chemical bond joining two different blocks will be at the interface between phases of one and the other block. Microdomains of separated phase will be similar to polymer chains in size. Two main parameters which influence the morphology of self-organized diblock copolymer are: temperature and volume fraction of block A (f_A) to block B.[4] Schematic phase diagram for diblock copolymer is presented on Figure 2. In fact phase diagrams are rather presented in the form, where instead of temperature χN parameter is used. N is degree of polymerization and χ is Flory interaction parameter, which is inversely proportional to the temperature, so the disorder state would be at the bottom of a diagram.[5]

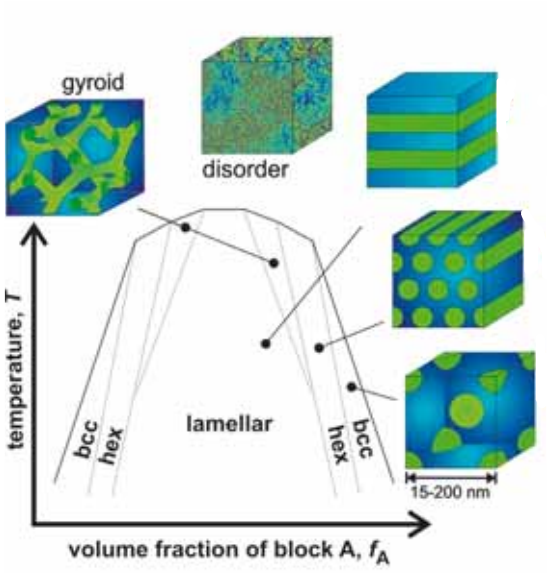

Figure 2 Schematic presentation of different morphologies depending on volume fraction of one block and temperature.

Block A is marked by blue and block B by green color. Considering bottom part of the diagram it is seen, that for equal volume fraction of each block ($f_A = f_B = 0.5$) block copolymer is organized into lamellar morphology (LAM). By increasing volume fraction of block A, following morphologies can be obtained: gyroid (GYR) morphology; hexagonally packed cylinders morphology (HEX) and body centered cubic (BCC) morphology. The same morphologies but with reversed phases can be obtained by decreasing volume fraction of block A below $f_A = 0.5$. On the diagram it can be seen, that at given volume fraction of block A, the morphology can be change by increasing the

temperature. The temperature at which copolymer morphology changes from one to the other is referred as order-order temperature (T_{OOT}). There is a maximum temperature for a given volume fraction of block A, at which ordered state is observed. Above this maximum temperature copolymer molecule can mix freely, which is called as disorder state. This temperature at which block copolymer changes from organized morphology into disordered mixture is called order-disorder temperature (T_{ODT}).

Similar schematic phase diagram for triblock copolymers is much more complicated [6] and is not taken in consideration here, since only diblock copolymers will be discussed in the thesis.

Obtaining soft matter like this with highly ordered structures in the nanoscale creates interest in finding an application for such material. Removing the minority block from one of the morphologies could give very regular porous material, with well defined pores of diameters in nanometers. Such porous material is called nano-porous material (NPM).

Nano-porous materials preparation.

Synthesis of block copolymer is an initial, difficult and crucial step in order to prepare nano-porous material. Depending on the polydispersity index (PDI), which is a ratio between weight average M_w and number average M_N molecular weight, we get more or less uniform material with predictable microstructure in a polymer melt. Length of the block will influence the diameter of the finally obtained pores. In conventional polymerization techniques (free radical polymerization) high PDI is obtained since chain transfer and termination processes are happening. These undesirable processes can be almost eliminated in living polymerization techniques.[7] In living polymerization firstly monomer A is synthesized and polymer chain is left active or “living”. Monomer B is synthesized after that. Block copolymers of low PDI are obtained in lesser degree from atom transfer radical polymerization also.[8]

An alignment of the microdomains can be (but not necessarily for all morphologies) the following preparation step, after the synthesis. This refers especially to hexagonally packed cylinders morphology. HEX morphology can be very interesting from the commercial, application point of view. In the polymer melt HEX microdomains will be randomly oriented. It means that in finally prepared nano-porous material there should be nano-channels without access to the sample surface. Efficiency of such material, independently on its application, will be probably not sufficient. The crucial operation here is proper alignment of all cylinders in one given direction. Mechanical shear forces are mainly presented in publications,[9] but also electric field,[10][11] magnetic field, [12] solvent evaporation[13] or thermal annealing.[14]

Finally, in order to get nano-porous material the minority block needs to be selectively removed. After such operation new voids and new surfaces will be created. Here we have

two cases. In the first case the majority block is below its glass transition temperature T_g, so created pores can survive. In the second case the majority block is above its T_g and the pores formed during the removal of the minority block collapse under the action of internal Laplace pressure.[15] In order to keep nano-pores the majority block needs to be additionally supported. It can be done by cross-linking. After that operation the minority block can be removed by etching.

Such a nano-porous material needs to be characterized by different techniques and many promising applications can be found for NPM. Fabrication development of NPM is schematically presented on Figure 3.

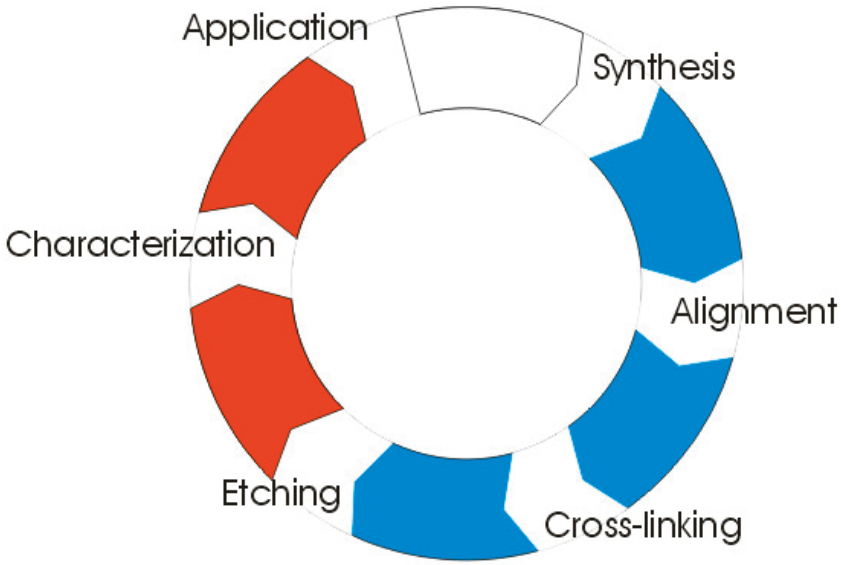

Figure 3 Fabrication development of NPM.

Applications of nano-porous materials

Nano-porous materials derived from block copolymers hold potential for many different nano-technological applications[16][17][18], and are also candidate materials for smart applications. An obvious application of nano-porous block copolymer based materials is in membrane technology. A smart membrane could for example be used in controlled or selective diffusion which depends on the nature of the feed liquid for the membrane. Such a membrane would offer exceptional characteristics in separation processes with the option of including a valve effect which could allow the membrane to be open or closed for filtration of a liquid.

NPM based on block copolymers can be also used as support for catalysts, since its high internal surface area. Most widely NPM were tried to be used as templates in nanolithography.

Historical development of nano-porous materials

Historical development of nano-porous materials (NPM) based on block copolymers was summarized by M. A. Hillmyer in 2005.[19] According to his literature research the mile stones for further applications of NPM were put between 1988 and 1997. First publication presenting preparation of nano-porous, which could be used as membrane, was reported in 1988 by J. S. Lee et al.[20] Fabrication of NPM in this very first paper reflects the scheme presented in Figure 3, except that no effort was put to align the channels. ABA triblock copolymer of poly(4-vinylphenyl-dimethyl-2-propoxysilane)-*b*-polyisoprene-*b*-poly(4-vinylphenyl-dimethyl-2-propoxysilane) [PPS-PI-PPS] was synthesized by anionic polymerization and thin film of block copolymer with lamellar morphology was solvent casted. PPS block was crosslinked by hydrolysis of alkylsiloxane part of molecule and PI block was etched by ozonolysis. Like in this thesis NPM was investigated by SEM and nitrogen adsorption. No scattering techniques were used by J. S. Lee. The same group published similar paper in 1989, where the same NPM fabrication strategy is used and three morphologies are investigated: lamellar, cylindrical and spherical.[21]

D.R. Smith and D.J.Meier presented in 1992 a new method for staining NPM samples with ruthenium tetroxide for better distinguish of morphologies by TEM investigation. [22] In this paper they used polystyre-*b*-polydiene copolymers (polyisoprene and polybutadiene) and showed the efficiency of etching polybutadiene block with ozone, without influencing polystyrene matrix.

The interesting way of preparation NPM was presented in 1993 by J. Hendrick et al.[23] Authors describe final material as ‘nanofoam’. In this publication authors prepared triblock copolymer with thermally stable poly(phenylquinoxaline) [PPQ] as a majority block and unstable poly(propylene oxide) [PO] or poly(methyl methacrylate) [PMMA] as a minority block. Voids were obtained during heating the material above decomposition temperature for PO or PMMA block.
Work presenting potential use of nano-porous film as a template for nanolithography was published in 1996 by P. Mansky et al.[24] They prepared a polystyrene-polybutadiene block copolymer with HEX morphology, and cylinders were oriented by solvent evaporation. Polybutadiene block was etched by ozonolysis like in previous cases. Results presented in this publication inspired further work in the nanolithography field with NPM as a template.

Lie et al. presented in 1997 preparation of a skin layer with potential use as membrane. [25]. In this publication a film from poly(*tert*-butyl acrylate)-*b*-poly(2-cinnamoylethyl methacrylate) [P*t*BA-*b*-PCEMA] with hexagonally packed cylinders was prepared.

PCEMA was photo cross-linked and *tert*-butyl groups in P*t*BA were cleaved by hydrolysis.

A method to prepare NPM with gyroid morphology was presented in 1997 by T. Hashimoto.[26] Here in this article authors use PS-PI block copolymer where PI block is etched by ozonolysis. Authors cover the surface of prepared channels by nickel and suggest its potential use as membrane reactors.

According to Hillmyers manuscript[19] above mentioned articles are a kind of research base from which many other ideas and applications developed.

In above articles polydiene blocks were used as minority blocks to be etched by ozonolysis. In 2003 S. Ndoni et al presented preparation of NPM based on PS-PDMS block copolymer, were hydrogen fluoride HF was used to etch PDMS block.[27] Spherical and gyroid morphology was investigated in this paper. In the next step the same group proposed an alternative technique for etching PDMS by using tetrabutylammoniumfluoride (TBAF).[28] This technique is used in the following sections presented in this thesis and is presented in details in Paragraph 1.5.

Aim of PhD project and research contents

The aim of the project was to find at least one application and characterize nano-porous material prepared from diblock copolymers.

In this work two morphologies of NPM presented in Figure 2 were taken into consideration: hexagonally packed cylinders and gyroid morphology. Diblock copolymer used to prepare nano-porous material consists of polydiene (polyisoprene[28] PI or polybutadiene PB) majority block and polydimethylsiloxane (PDMS) minority block. First attempt was to prepare NPM according to general scheme presented in Figure 3. Preparation presented in this work starts from the point where block copolymer melt was already synthesized by other person: Lars Schulte. Characterization and comparison of different samples was very important. Prepared samples were characterized by scanning electron microscopy (SEM) and transmission electron microscopy (TEM). These two techniques allowed for direct confirmation of assumed morphologies and measuring of pore diameters and distances between different planes. Pore size distribution for analyzed samples was done by nitrogen adsorption. Small angle x-ray scattering (SAXS) technique played very important role during studies, since without any complicated sample treatment and preparation allowed for identification of bulk samples morphology, confirmation of alignment in case of hexagonally packed cylinders and analysis of distances between scattering planes, which could be compared with electron microscopy results.

Not sufficiently crosslinked samples with collapsed pores after etching were put in consideration also. These non nano-porous samples were prepared at different cross-linking degrees for samples based on polyisoprene. In this work samples cross-linked to

14, 20 and 38 mol % of crosslinker in relation to mol of double bonds in polyisoprene were presented. Samples characterized firstly in the dry state were placed in different solvents and analyzed by small angle neutron scattering (SANS).

Finally butadiene based samples with gyroid morphology were investigated for membrane application. After designing the necessary set up samples were investigated for three different gases permeability (hydrogen, nitrogen and carbon dioxide) and than for separation of polyethylene glycol (PEG) molecules dissolved in mixture of methanol (MeOH) and water. Polyethylene glycols were analyzed by dynamic light scattering (DLS) in order to know hydrodynamic radius of molecules used for separation experiments. Permeates were analyzed by size exclusion chromatography (SEC).

Thesis outline

Since in this work many different samples were used, which were based on polyisoprene or polybutadiene and consists of hexagonally packed cylinders morphology or gyroid morphology, the thesis organization including information about which samples are presented in which chapter is schematically shown on Figure 4.

Chapter 1 presents the way of preparation of all samples used in the thesis. Chapter 2 presents the experimental techniques and specimen preparation. Chapter 3 presents the results of characterization nano-porous samples with different techniques. Chapter 4 presents the results of investigating non-nanoporous samples with SANS. Chapter 5 finally presents the results of using gyroid samples as membranes.

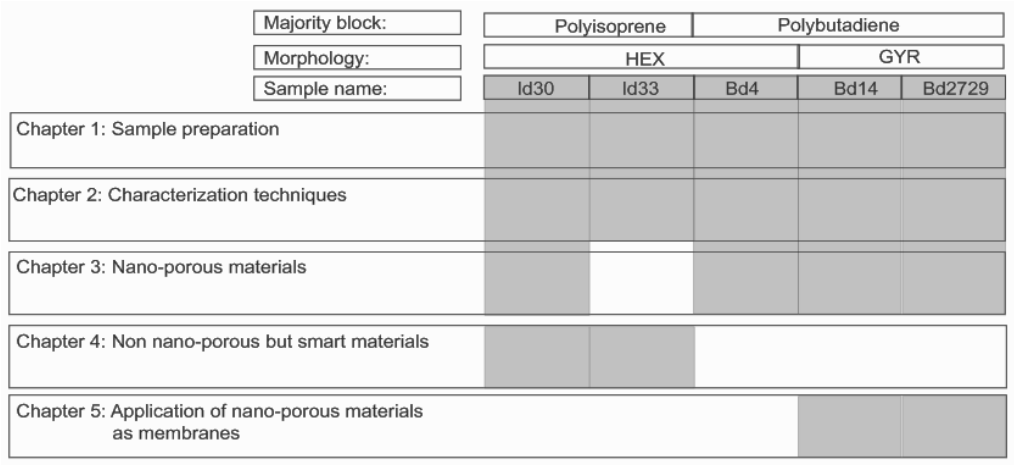

Figure 4 Organization of the thesis.

1. Sample preparation

To make nanoporous material the synthesized mother polymer was taken via several intermediate steps marked by blue in Figure 3.

1.1. Nomenclature

In order to keep track of the process described above, the following nomenclature was used for the samples. Block copolymer precursors' names reflects the monomer composition of the block copolymers: *D* stands for D_3 (the cyclic trimer of dimethylsiloxane), *B* stands for butadiene and *I* for isoprene. A sample number is added after the two letters which uniquely identifies the synthesis batch, like: ID30; ID33; BD4 or BD14. Batches BD27 and BD29 were aimed to reach GYR morphology. This morphology was obtained after mixing 2 parts of BD27 with one part of BD29. Samples obtained in this way are coded as BD2729.

Crosslinked polydiene block copolymers are named by adding an 'x' to the block copolymer name; if necessary, a number reflecting the relative crosslinking degree is attached to the *x*.

Etched samples are named by adding a suffix '*e*' to the name of the crosslinked sample, e.g. ID30-x14e. All the nanoporous samples presented in this thesis were prepared by the reaction of PDMS with tetrabutylamonium fluoride (TBAF).

1.2. Synthesis

PI-PDMS and 1,2-PB-PDMS block copolymers was prepared by sequential 'living' anionic polymerization under Argon[29] by Lars Schulte. *Sec*-buthyllithium was used as initiator for all the polymerizations. 1,2-PB-PDMS was polymerized in tetrahydrofurane (THF); hexane at 40 ± 2°C was the solvent of polymerization for the PI block in PI-PDMS. An equivolume mixture of hexane and THF at 0 ± 1°C was used as solvent of polymerization for the PDMS block in PI-PDMS. The reaction times were 10 h and 60-70 h for the formation of the PI and the PDMS blocks, respectively. The temperature of

polymerization of 1,3-butadiene in THF was either -40 ± 5°C or -20 ± 3°C, with polymerization times of 13 h and 3 h respectively. The building unit of PDMS, hexamethyl-cyclotrisiloxane (D_3), was added as a THF solution into the reactor containing the living polybutadienyl Lithium (pale green-yellow) at the respective temperatures mentioned above. The temperature was then gradually increased to 0°C and D_3 was left to polymerize for up to 3 days at 0 ± 1°C. The complete crossover from the hydrocarbon to the siloxyl Lithium was associated with color disappearance within few minutes from the addition of D_3. At that stage of each synthesis a 3-5 ml sample was taken out of the polymerization reactor. These samples were used for the characterization of the molar mass and molar mass distribution of the hydrocarbon blocks in the block copolymers. After the formation of the PDMS block, all the samples were terminated with a three times molar excess of trimethylchlorosilane. The finished polymers were isolated from the polymerization solutions by first precipitating and washing in excess methanol and than by drying under vacuum over night.

1.2.1. Characterization of the block copolymer precursors

Table 3 summarizes properties of 6 block copolymer precursors samples used in this thesis. The molar masses of the hydrocarbon blocks showed in the second column of Table 3 were determined by size exclusion chromatography (SEC). The SEC results combined with the compositional information from ^{1}H-NMR allowed calculating the total average mass values of the block copolymers listed in the third column. The polydispersity index of the block copolymer sample (fourth column in Table 3) was determined by SEC. The mass and volume fraction of PDMS block is summarized in fifth and sixth column in Table 3 respectively. The morphology at room temperature was determined by small angle x-ray scattering (SAXS) measurements.

precursor sample	$<M_n>$[a] [g/mol]	$<M_n>_{total}$[b] [g/mol]	PDI_{total}[c]	w_{PDMS}[d]	f_{PDMS}[e]	*Morphology* [SAXS]	T_{ODT} [C°]
ID30	10 764	15600	1.04	0.31	0.30	HEX	280
ID33	10 530	14200	1.1	0.26	0.26	HEX	225
BD4	10 400	15000	1.22	0.308	0.294	HEX	260
BD14	6 300	10700	1.04	0.408	0.392	GYR	207
BD27	10400	16030	1.06	0.404	0.420	n.m.	n.m.
BD29	5800	8600	1.05	0.413	0.430	n.m.	n.m.

Table 3 Characteristics of the precursor diblock copolymers. [a]Number average molecular weight of the polydiene block as obtained by ^{1}H-NMR. [b]Number average molecular weight of the diblock molecule obtained by SEC and ^{1}H-NMR. [c]Polydispersity index obtained by SEC. [d]Mass fraction of PDMS determined by ^{1}H-NMR. [e]Volume fraction of PDMS at 20 °C calculated from density values: ρ_{PI} = 0.900 g/cm^3, $\rho_{1,2\text{-}PB}$ = 0.902 g/cm^3 and ρ_{PDMS} = 0.966 g/cm^3. [30][31] The morphology was determined by Small Angle X-ray Scattering and the order-disorder temperature (T_{ODT}) was determined by rheology measurements.

The information about apparatuses used for characterization of the block copolymer precursors is included below.

Chromatography

The molar mass and molar mass distribution Size Exclusion Chromatography (SEC) in stabilized THF was used to determine the molar mass and molar mass distribution of the copolymer blocks. SEC equipment consisted of two mixed-D columns (Polymer Laboratories) and a triple detector setup (Viscotec) (right angle light scattering, viscometer and differential refractometer).

Spectroscopy

The average composition of the diblock copolymers were determined by proton magnetic resonance spectroscopy, ^{1}H-NMR in a 250 MHz Avance DPX 250 Bruker instrument.

Rheology

Rheological measurements were used to determine the order-disorder transition temperature (T_{ODT}) of the synthesized polymers. The viscoelastic properties of the diblock copolymers were investigated by isothermal and temperature-gradient dynamic mechanical measurements on a Rheometrics RS 800 rheometer using parallel plate geometry. The temperature was changed continuously with a rate of 2.5 ^{o}C/min.

1.3. Solvent casting and alignment

Samples were prepared in two different ways. Structurally isotropic material was obtained by solvent casting. 0.2 – 0.8 g block copolymer samples were dissolved in 10 ml of THF and such solution was poured into Petri Dish of 30 mm diameter. Solvent was than evaporated at room temperature under the flow of Argon and polymer films of 0.3 – 1 mm thickness were obtained.

Structurally aligned samples were obtained by extrusion of polymer melt with extrusion device with a rectangular die. Films of 1.0 mm thickness and 10 mm width were obtained by pressing polymer melt through the die. The extrusion device is presented on Figure 5.

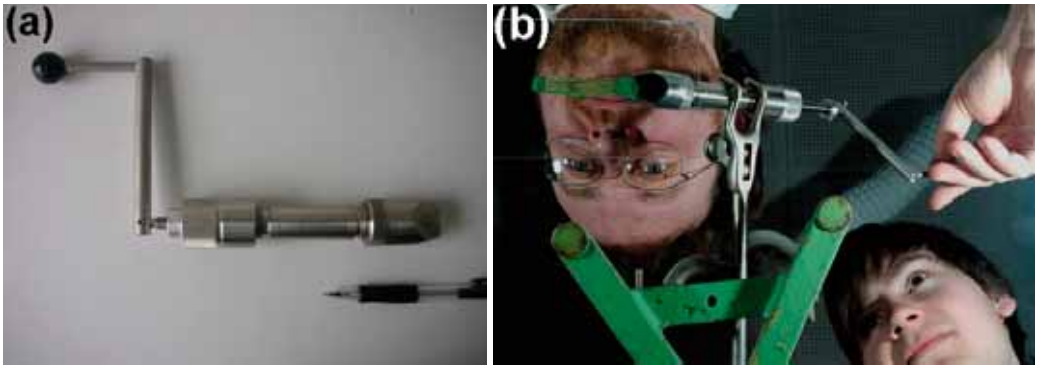

Figure 5 a: Extrusion device used for alignment of the hexagonal morphology with the rectangular die on the right. b: The polymer is squeezed out of the tube through the rectangular die by turning the handle clockwise. Picture taken by Bo Jarner.

The following Cartesian coordinate system was used to describe extrusion experiment: extrusion direction corresponds to x – axis, the die thickness and width correspond to y and z axis respectively.

All samples based on polyisoprene (ID30 and ID33) were shear aligned, whereas all polybutadiene samples with gyroid morphology (BD14, BD27 and BD29) were solvent casted. Samples of polybutadiene with hexagonal morphology (BD4) were prepared in both ways.

In order to avoid air bubbles during extrusion process, sample ID30 was heated to 140 ^{o}C for 2 hours in nitrogen atmosphere before loading the extruder. This was done to decrease the polymer viscosity in order to release the majority of air trapped in polymer. In case of sample ID33 and BD4 approximately 6g of polymer was dissolved in 60 ml THF and cast in a glass covered by aluminum foil at the bottom. After solvent evaporation the aluminum foil was rolled, placed in the extruder and squeezed. The polymer was extruded onto microscopy cover glasses prior to the cross-linking procedure.

1.4. Cross-linking

Dicumyl peroxide (*bis((α,α-dimethylbenzyl) peroxide*) (DCP) (Merck) was used as the crosslinker for all samples. For dosage of DCP a reference to the total number (mole) of double bonds in the sample in question was taken. All presented samples were crosslinked under an Argon atmosphere for 2 hours at 140^{o}C in homemade stainless steel cup screw container equipped with two valves. An o-ring ensured gas-tight closing of the container, two valves allowed to control the atmosphere inside the container. The stainless container is presented on Figure 6.

Figure 6 Steel chamber used for the sample cross-linking under inert atmosphere. The polymer sample is in the Petri dish. The lid contains a fluorinated rubber o-ring (not visible) for a tight closure. The two valves visible on the lid are used to replace air with inert atmosphere.

Samples based on polyisoprene and based on polybutadiene were prepared in slightly different ways.

Sample ID30 was crosslinked in a step-by-step procedure. For the first cross-linking step an amount of DCP was scaled off which equal 6 molar % relative to the moles of double bonds in the sample volume (i.e. mole DCP/mole double bonds = 0.06). The 6 molar % DCP was placed next to the polymer in a homemade stainless steel cap screw cylinder equipped with two valves (Figure 6). Nitrogen gas was run through the cylinder for few minutes and then the cylinder was tightened and placed in a preheated oven at 140 ^{o}C for two hours with a nitrogen atmosphere as an additional precaution.[32] After baking, the cylinder was rapidly cooled down and the sample was placed in a vacuumed round bottom flask at 130 ^{o}C for one hour to get rid of any accumulation of by-products. This procedure was repeated 6 times. Finally, a total of 37.7 molar % of DCP had been added to the sample. This sample was code named ID30-x38.

All ID33 samples were prepared for the purpose of small angle neutron scattering (SANS) measurements, which will be presented in details in Chapter 4. There was the whole series of differently cross-linked samples prepared, but here only two, the most interesting ID33 samples are in discussion. These samples cross-linked to 14% and 20% mol of DCP were prepared in the following way. Firstly a microscopy glass with extruded polymer was placed at the bottom of the metal cylinder. 2% DCP was placed on top of extruded polymer. After 2h of crosslinking at 140^{o}C the cylinder was cooled down and 6% DCP was placed this time on aluminum foil next to the microscopy glass. In this case DCP enters gas phase and crosslink the polymer. Again after 2h of crosslinking at 140^{o}C the cylinder was cooled down and another 6% DCP was placed on aluminum foil. In this way sample crosslinked to 14% was obtained. After repeating the last step 20% crosslinked sample was produced. These samples were called ID33-x14 and ID33-x20 respectively.

In case of samples based on polybutadiene (BD4; BD14; BD27 and BD29) around 1 mol% of DCP relative to the double bonds in the polybutadiene block was enough to ensure pore stability after the etching process. For all samples the polymer was dissolved together with DCP in tetrahydrofurane (THF) and solvent casted in a Petri dish under gentle argon flow. All samples were crosslinked at 140°C for 2h. Two presented samples with HEX morphology were crosslinked to 0.8% (aligned) and 2% (solvent casted) and named BD4-x0.8 and BD4-x2 respectively. All BD samples with GYR morphology were 1% crosslinked.

The overall expected reaction for the free radical cross-linking of PI could be schematized as shown in Figure 7.

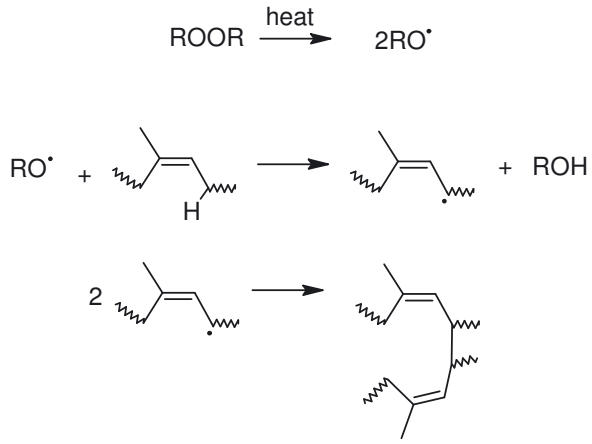

Figure 7 Scheme for cross-linking of PI by thermal treatment with peroxide.

The thermally generated free radicals from the peroxide cleave allylic hydrogens from the PI chain, forming free radicals and the combination of two such radicals from different chains produces a crosslink. The double bonds remain intact in the above scheme. For the case of PI, one peroxide molecule generates in average one (or less) cross-link. Other reactions that convert the double bonds into single bonds and/or crosslinks become important at high temperature and/or high degree of crosslinking.[33]

The situation is quite different in the case of cross-linking of 1,2-PB by peroxides. At the same crosslinking conditions as for PI, just one single addition of less than 2 molar % of DCP relative to the double bonds was sufficient to generate glassy material. The crosslinking reaction in this case is a chain reaction, where one peroxide molecule can generate more than one crosslink. This can only happen by direct involvement of double bonds as shown in Figure 8.

The alcoxy radical produced from the thermal scission of the peroxide (Figure 8a) initiates the reaction by generating a free radical onto the polymer either by subtraction of

allylic hydrogen or by direct attack on the double bond (Figure 8 b). Both the tertiary and the secondary carbon free radicals thus produced can start a chain reaction on the double bonds of PB (propagation), as shown in Figure 8 c and d. In each propagation step of the reaction chain a cross-link and a new free radical on the polymer chain are formed. A crosslinking cluster thus forming is ended either by transfer of free radical to other molecules (e.g. by subtraction of an allylic H) or by recombination of two free radicals (not shown). This last is a true termination reaction and may produce merge of two crosslinking clusters. Increased reaction time augments the fraction of peroxide transformed into free radicals and therefore the number of kinetic chains. The half-life of DCP at 140°C (from measurements in dodecane solution) is estimated to 1.5 h;[34] therefore more than 90% of DCP is expected to be decomposed after 6 h at 140°C.

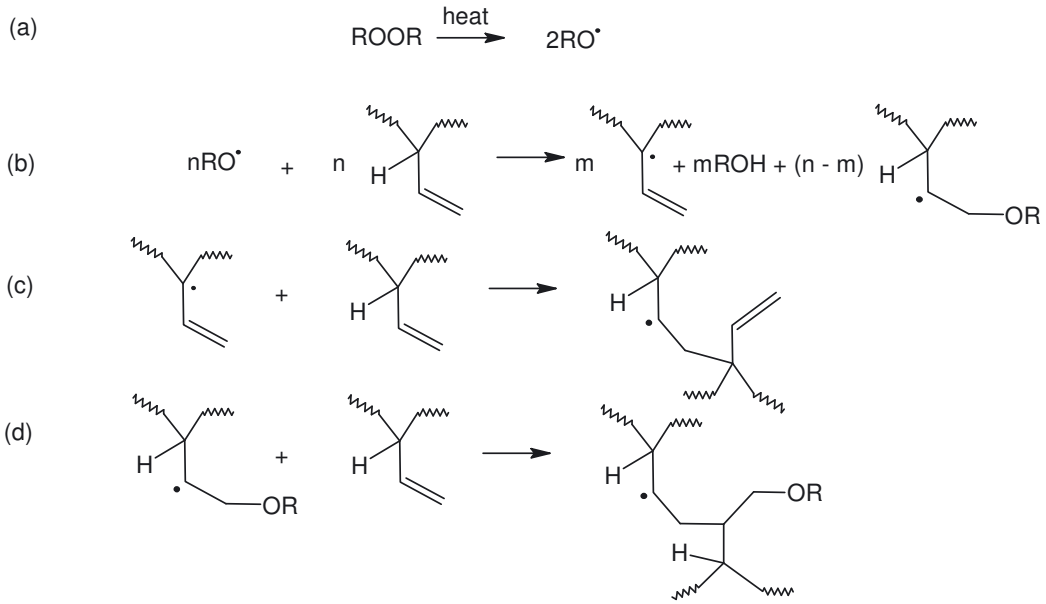

Figure 8 Suggested cross-linking scheme of 1,2-PB by heating in inert atmosphere in the presence of peroxide.

1.5. Etching

A solution of 1 M tetrabutylammonium fluoride (TBAF) in THF from Aldrich was used as cleaving reactant for removing the PDMS blocks from all the samples presented in this thesis. TBAF etching procedure was previously used by others.[35] Five times molar excess of TBAF relative to the PDMS repeating unit was used to etch the cross-linked samples. Etched samples were placed in pure THF and than in mixtures of THF and methanol in order to avoid cracks. Finally samples were kept in pure methanol before gradual solvent evaporation under Argon stream.

Sample ID30-x38 was soaked in THF overnight before etching for better access of TBAF. The samples were stirred in the TBAF solution for 4 hours followed by washing in THF three times of 20 min each. Solvent was evaporated under vacuum at 130 ^{o}C and the weight loss was measured in the dry state. This procedure was repeated four times until the total loss of mass was equal to the mass of the PDMS content of the sample.

Samples ID33-x and BD-x were not soaked in THF prior to etching, but kept in TBAF for 36 hours. All etched samples were code named by adding the suffix 'e' for etching to the sample name, hence this sample becomes ID30-x38e etc.

Cleavage with TBAF probably proceeds via the so-called S_N2-Si pathway (Figure 9) known from the rapid cleavage of silyl ethers to alcohols by treatment with 2-3 eq. TBAF in THF at 25^{o}C[36][37]

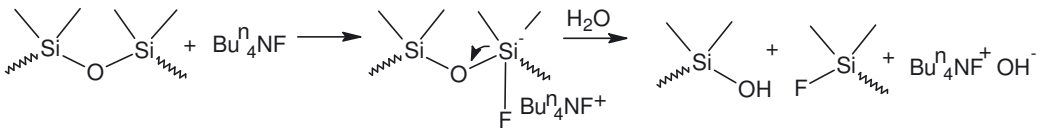

Figure 9 Proposed PDMS cleaving reaction mechanism by TBAF through the S_N2-Si pathway, which involves a pentacoordinate silicone anion. The wavy lines depict the polymer chain.

1.6. Overview of treated, etched materials

Code names of all samples presented in the thesis are summarized in the first column of Table 4. Following columns contain information about morphology, alignment and chapter number in which sample is put into discussion. '*shr*' means that sample was aligned by using shearing forces during extrusion process, and '*sc*' means that sample was solvent casted.

Sample name	*Morphology*	*shr/sc*	*Chapter nr*
ID30-x38e	HEX	shr	3; 4
ID33-x14e	HEX	shr	4
ID33-x20e	HEX	shr	4
BD4-x2e	HEX	sc	3
BD4-x0.8e	HEX	shr	3
BD14-x1e	GYR	sc	3; 5
BD2729-x1e	GYR	sc	3; 5

Table 4 Summarization of samples code names (first column) together with its morphology (second column). Third column contains information if sample was extruded, shear aligned (*shr*) or prepared by solvent casting (*sc*). Last column says in which chapters samples are in focus.

Chapter 3 puts in consideration characterization of nanoporous samples, so it includes all samples from Table 4 except for ID33 samples. Samples ID33-x14e and ID33-x20e were not nanoporous after etching process and are discussed together with nanoporous sample ID30-x38e in Chapter 4. Chapter 5 considers only samples with GYR morphology, which were investigated for its potential membrane application.

2. Characterization techniques

Techniques used to characterize crosslinked and etched samples from Chapter 1 are presented here. Each technique is firstly described shortly, to explain its principles. The technical information about apparatus is given next and specimen preparation is presented after that. By 'specimen' we here understand already crosslinked or crosslinked and etched sample, ready to be characterized.

2.1. Electron microscopy

Scanning electron microscopy (SEM) and transmission electron microscopy (TEM) were used as very important methods of sample characterization. These two methods, specially SEM gives us direct and quite straight forward way to interpret results confirming nanoporosity and morphology of investigated samples. The main difference between these two methods is that in case of SEM we scan the sample surface and collect scattered electrons, wherever in case of TEM electrons penetrate the sample, which is very schematically presented on Figure 10:

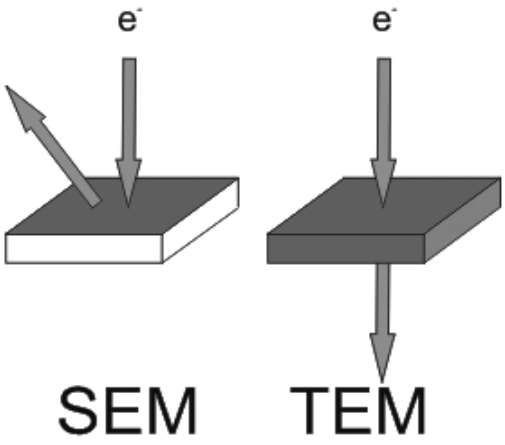

Figure 10 Schematic presentation of difference between the scanning (SEM) and transmission (TEM) electron microscopy.

2.1.1. Scanning electron microscopy

Principle

Scanning Electron Microscopy is used to investigate the sample surface and reveal high resolution images of a sample. Electron beam is scanned on the surface and penetrates it. When an electron beam hits the sample surface it reveals various secondary emissions from the specimen like secondary electrons, backscattered electrons or x-rays.

The electron source is mainly tungsten filament or field emission gun. Electron beam energy is usually between 1 and 30 kV. Since in case of investigation of polymers charging effect is very often observed it is operated at low voltage (1-3 kV).[38] The scheme of SEM is presented on Figure 11:

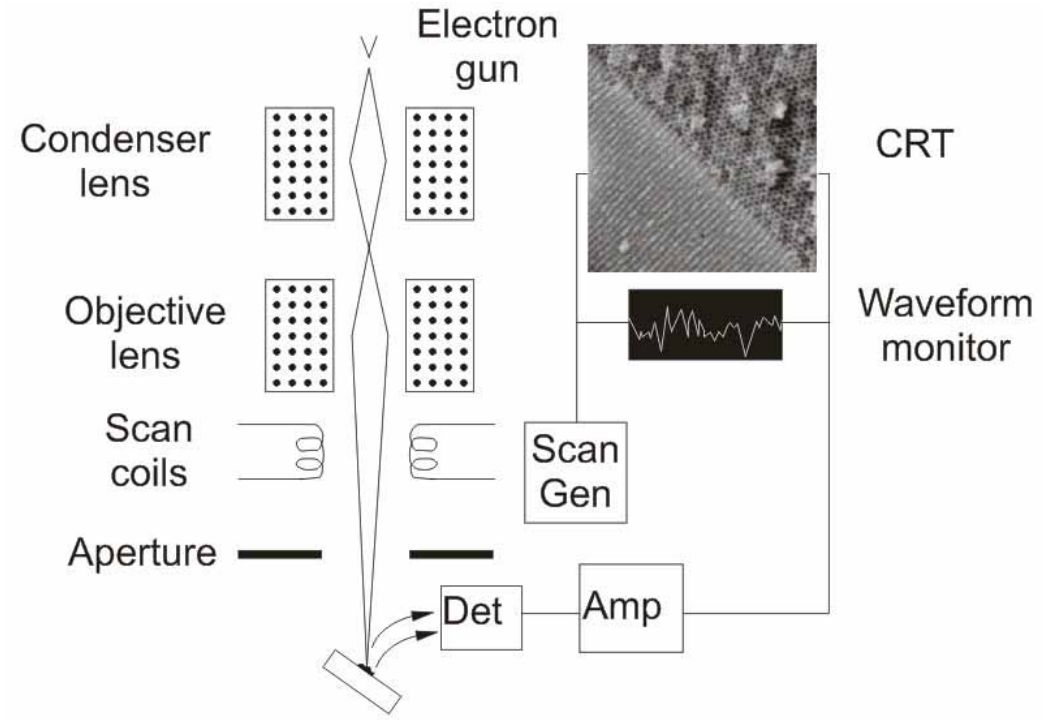

Figure 11 Schematic of scanning electron microscopy (SEM). [39]

The electron beam is demagnified by condenser lenses to 2-10 nm diameter size. In older type of microscopes the scan coils are used to scan the specimen surface by electron beam. The emitted electrons from specimen surface hit the detector which counts the number of these electrons or other radiation.

Apparatus

All samples presented were investigated in a Zeiss 1540 EsB Gemini SEM instrument at 1-3 kV electron beam acceleration.

Specimen preparation

Sample for SEM was prepared by freeze fracturing a piece of nanoporous polymer film in liquid nitrogen; the piece was than mounted onto an aluminum specimen mount using Ted Pella double coated carbon conductive tabs and CCC Carbon Adhesive (Electron Microscopy Science). Sample was sputter-coated with 2-3 nm gold layer in a Polaron SC7640 and kept under vacuum in the microscopy chamber for 14-16 hours before scanning.

2.1.2. Transmission Electron Microscopy

Principle

In case of TEM the electron beam hits a very thin sample and penetrates it, where some electrons go through the sample and the other are adsorbed. The scheme of TEM is presented on Figure 12:

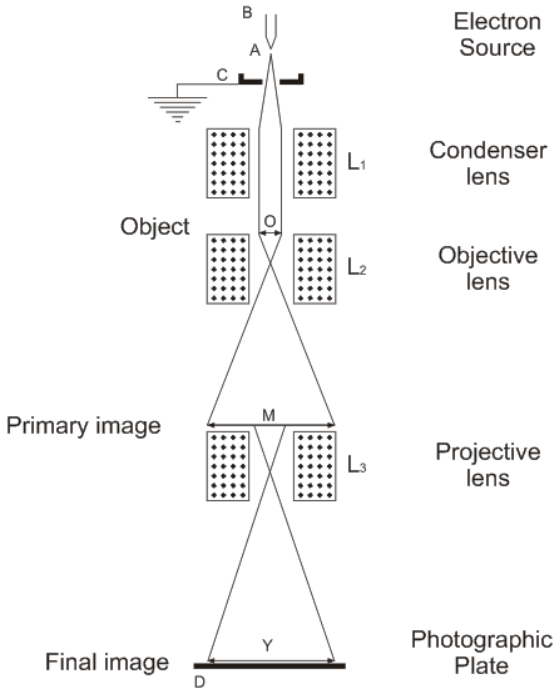

Figure 12 Schematic of transmission electron microscopy (TEM).[40]

Apparatus

Samples were investigated in a Jeol 3000F transmission electron microscope (TEM)

Specimen preparation

Sample preparation for TEM was performed by placing a piece of the sample in an Agat mortar filled with liquid nitrogen and crushed into a fine powder. Then the mortar was filled with approximately 2 ml of toluene (Fluka, 99.8% pure) and the suspension was transported to a small glass. The glass with suspension was placed in an ultrasonic water bath (Branson, Model B1510-MT) for 30 min to separate particles. A drop of the suspension was deposited on a Holey Carbon film on a 300 mesh copper grid. Finally, the toluene was evaporated and the sample analyzed by TEM.

2.2. Scattering techniques

To be able to interpret the results some basic knowledge about scattering is necessary. The details explaining the interpretation of scattering results from HEX sample is included in Appendix A.

For the purpose of farther reading it is probably worth to mention, that the main scattering peak position is marked by '*', so q^* is value of scattering vector from the main scattering planes. Distance between main scattering planes is marked in the same way: d^*. For HEX morphology $d^*=d_{10}$; for GYR morphology $d^*=d_{211}$.

2.2.1. Small angle x-ray scattering (SAXS)

SAXS technique is very important characterization technique, since it gives very first indication of the morphology of nanoporous sample. This technique characterizes bulk properties of the sample in indirect method.[41]

Principle

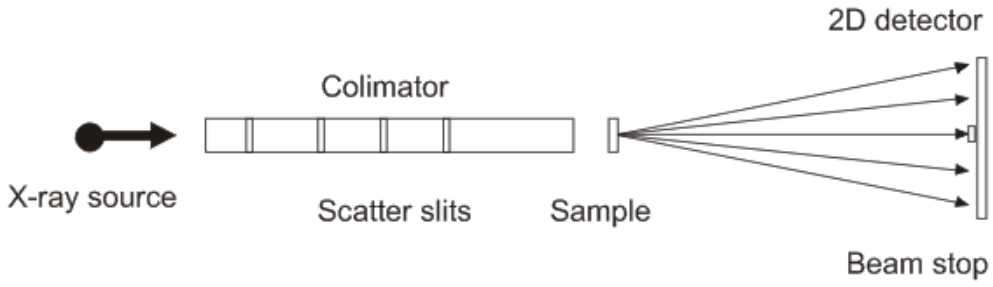

Figure 13 Schematic presentation of SAXS installation.

Apparatus

Small angle x-ray scattering (SAXS) was performed using the rotating anode lab-source at Risø-DTU. The wavelength of the x-rays was $\lambda = 1.54$ Å. A two dimensional position sensitive wire detector in a distance of 1435 mm from the sample was used to collect scattered radiation. The ID30 mother block copolymer was measured at the SAXS instrument at the Department of Chemistry, Aarhus University, Denmark. Experimental conditions were identical, apart from sample-detector distance of 1085 mm.

Specimen preparation

No special treatment of the sample was necessary for SAXS measurements. Samples were temporary fixed to the metal plate with holes on goniometer.

2.2.2. Small angle neutron scattering (SANS)

Principle

Neutrons can be obtained from reactor sources, electron accelerator sources or spallation neutron sources which is the one used for experiments presented here. The problem with neutron sources is that they have quite low efficiency in general and can causes breaks in the evaluable beam. The source at the Paul Scherrer Institute (PSI) is the only one of its kind the continuous spallation neutron source which produces $1.1 \cdot 10^{14}$ $n \cdot cm^{-2} \cdot s^{-1}$.

The name: spallation neutron source comes from the fact, that contrary to the reactor and electron accelerator sources this one does not disintegrate the nuclei in target atom The accelerated proton hits the target (lead atom) and causes the increase in the internal energy, which is released by evaporating neutrons. One proton causes about 10 neutrons to escape from atom.

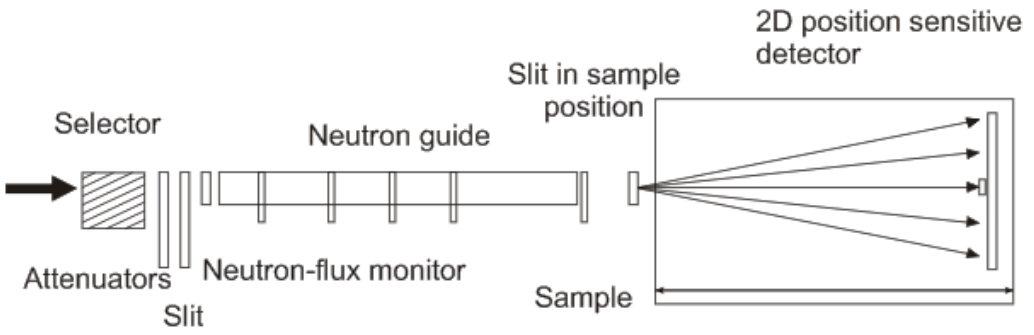

Figure 14 Neutron scattering apparatus. [42]

Neutrons coming out from the spallation neutron source have a high energy. To slow down the neutrons the **moderator** is used. This is generally a material with light nuclei. Neutrons collide with this material and lose their energy. Liquid deuterium is used as a

moderator at PSI. There are no perfect moderators and always some of neutrons will manage to get through the moderator without colliding.

In scattering experiments the q value (look in Appendix A) is a very important parameter. In order to obtain correctly analyzed results we have to define q values very precisely. That is why the neutrons wavelength λ and the scattering angle θ has to be very well defined. In order to get the stream of neutrons of one wavelength we use the so called **monochromators** of two possible kinds: crystal monochromators and mechanical velocity selection monochromators. The later is used at PSI.

In order to precisely measure the θ angle the neutron beam has to be well defined. Such process is called **collimation**. This is in principle a long tube with many diaphragms.

Apparatus

Samples were investigated using the small angle neutron scattering instrument SANS-II at SINQ, Paul Scherrer Institute (PSI) in Villigen, Switzerland.[42] The incoming neutrons were monochromized by a mechanical velocity selector and collimated in the six meter long collimation section. The scattered neutrons were detected by a two dimensional ^{3}He Detector. Neutrons wavelength was 6.37 Å.

Specimen preparation
Samples were placed in glass cuvettes. In case of the swelling experiments the cuvettes were filled with approximately 2 ml of solvent just before placing in the sample chamber and starting scattering measurement. During the swelling process time resolved scattering data was collected over 60 or 300 s intervals. Some samples were measured for longer time when necessary (1200 or 3600 s).

2.3. Nitrogen adsorption

Principle

Nitrogen adsorption technique can reveal such information like: specific surface area, pore size distribution or pore volume for a given porous material. In general nitrogen gas molecules are adsorbed on the surface of porous material. Nitrogen is adsorbed by physisorption.[43]

The results are presented in form of isotherm. Such plots present the amount of adsorbed nitrogen versus equilibrium pressure at constant temperature.

Apparatus

The instrument Micromerities ASAP 2020 Surface Area and Porosity Analyzer was used for investigation.

Specimen preparation

No particular sample preparation was needed for performing nitrogen adsorption.[44] Samples of about 0.1g were used for analysis.

3. Nano-porous materials

In this part samples which were porous after cross-lining and etching will be discussed. Firstly samples with hexagonal morphology are described and then sample with gyroid morphology.

3.1. Hexagonal morphology

Looking at the cross-section of the ideal hexagonally packed cylinders domain we will see a regular hexagon, presented on Figure 15. The pore radius *r* and distance between the main scattering planes d_{10} can be directly investigated by SEM or TEM technique.

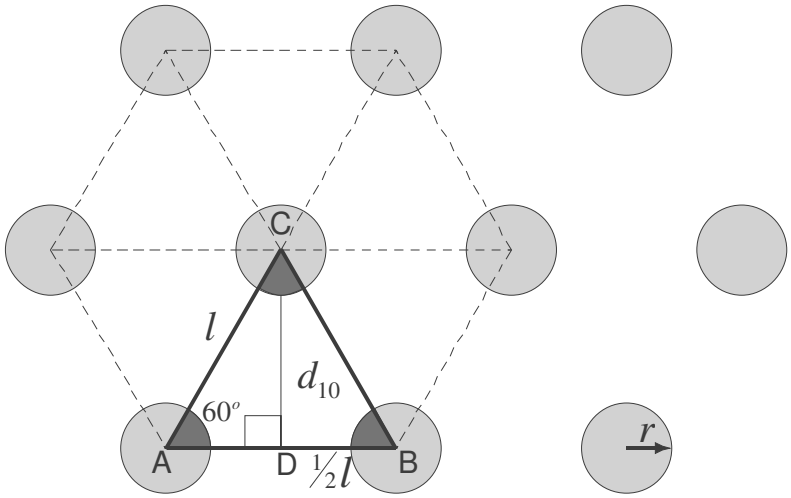

Figure 15 Cross-section of hexagonally packed cylinders domain.

By SAXS d_{10} can be obtained. If d_{10} is known (from SAXS measurements) than we can calculate l, since:

$$l^2 = d_{10}^2 + \left(\frac{1}{2}l\right)^2 \Rightarrow l = \frac{2\sqrt{3}}{3}d_{10} \qquad \text{Equation (1)}$$

The area of triangle ABC is area occupied by polydiene and PDMS $\Delta ABC = polydiene + PDMS$ and it can be expressed as:

$$P_{\Delta ABC} = \frac{1}{2} l \cdot d_{10}$$ Equation (2)

The area occupied by PDMS in this triangle is:

$$P_{PDMS} = \frac{\pi r^2}{2}$$

where r is pore diameter. P_{PDMS} can be calculated as a value of PDMS volume fraction f_{PDMS} in area of triangle ABC:

$$P_{PDMS} = f_{PDMS} \cdot P_{\Delta ABC}$$ Equation (3)

Finally we get:

$$r = \sqrt{f_{PDMS} \cdot \frac{2\sqrt{3}}{3\pi} \cdot d_{10}^2}$$ Equation (4)

This pore radius is based on the assumption, that the density of the crosslinked polydiene matrix remain unchanged before and after ething PDMS.

3.1.1. Polyisoprene based sample

Following the preparation of cross-linking and etching described in Paragraph 1.4 and 1.5 respectively the sample ID30-x38e was characterized by both microscopy and SAXS experiments.

SAXS

Figure 16a shows azimuthally reduced SAXS data (1-D) representing the three steps of preparing samples from the precursor polymer; the mother (original) sample (ID30), the cross-linked sample (ID30-x38) and the cross-linked and etched sample (ID30-x38e). Figure 16b shows two dimensional (2-D) raw data profile for ID30-x38e sample. In case of the strongly cross-linked sample ID30-x38 we observe scattering which gives evidence to a hexagonal structure by the presence of the higher order peaks at ratios of $\sqrt{3}$ and $\sqrt{7}$ with respect to the primary scattering peak q^*. The multi-peak profile of the etched sample (ID30-x38e) also shows much stronger scattering intensity compared to the cross-linked sample (ID30-x38), which is a natural consequence of the increase of contrast between the cavity voids and the PI matrix compared to the PI/PDMS contrast. Such evolution of the scattering profile, following the preparatory steps to fabricate nano-

porous material, is expected and observed in other samples. [27] For the sake of better display of the data the scattering intensity values of ID30 melt have been multiplied by the factor indicated in the illustration.

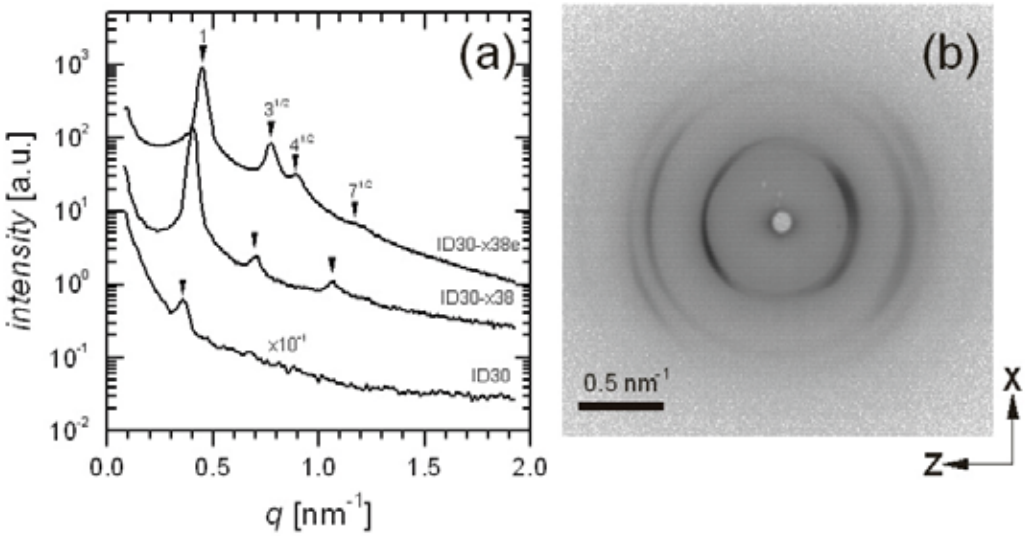

Figure 16 SAXS of ID30 sample a: Upper plot presents one dimensional (1-D) SAXS profiles of cross-linked and etched ID30-x38e sample with characteristic q ratios marked by reversed triangles. Middle plot presents 1-D profile of crosslinked only sample ID30-x38 and bottom profiles presents polymer melt. b: two dimensional (2-D) scattering profile of shear aligned sample ID30-x38e.

Here we observe that the primary scattering peak moved towards higher values upon cross-linking and subsequent etching. The peak position of the primary Bragg peak for polymer melt, cross-linked only and etched samples is $q^* = 0.35$ nm^{-1}; $q^* = 0.40$ nm^{-1} and $q^* = 0.45$ nm^{-1} This indicates a small shrinkage of the domain structure resulting from both of the processes, and is evident from the values for the d_{10} Bragg spacing derived from the positions of the primary scattering peaks listed in Table 5 (and also inTable 6) Each preparatory step (cross-linking and etching) results in an approximate decrease of the Bragg lattice spacing of about 14% in the first step and 12% in the second step. Based on SAXS data the pore radius was calculated accordingly to Equation (4). The 2-D scattering profile Figure 16b shows evidence of sample alignment, as the intensity of the scattering along the Debye-Scherrer rings is not uniform. Such alignment is to be expected as the sample was extruded through the dye prior to cross-linking and etching. The extrusion causes directional alignment of the cylindrical PDMS domain along the shear direction X.

Electron microscopy

In a left panel of Figure 17 the result of conducting TEM on sample ID30-x38e is presented. The hexagonal arrangement of circular cavities is visible. The micrograph captures a sample section, which shows the normal projection of the structure along the cylinder axis with slight misalignment. The pore radius of 3.8 ± 0.5 nm was estimated by

fitting circular cross-sections to various areas of the micrograph. From the projection of the structure illustrated on left panel of Figure 17 it is possible to estimate the distance between the primary (10) Bragg scattering planes to be d^*_{TEM} = 14.8 ± 1.2 nm. The measured values of pore radius and distance from each other corresponds to a volume fraction of pores equal to 30% - in excellent agreement with the pristine block copolymer composition. Structural data for ID30 sample is presented inTable 5. SEM picture presented on the right panel of Figure 17 reveals hexagonal pattern of cylinders, but picture quality is not good. Pore size can be estimated in the same way as in case of TEM picture and it is 5.4 ± 1.7 nm. SEM picture quality does not allow to estimate the distance between the primary (10) Bragg scattering planes.

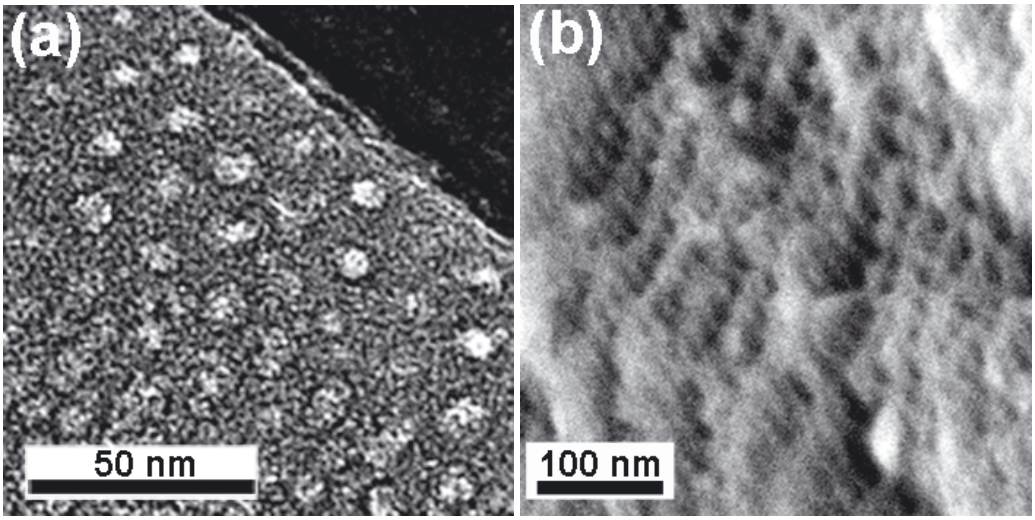

Figure 17 a: Transmission electron micrograph and b: scanning electron micrograph of the nano-porous sample ID30-x38e.

3.1.2. Polybutadiene based samples

SAXS

The result of small angle x-ray scattering from solvent casted sample is presented on Figure 18. The left plot is one dimensional plot with values of q/q^* marked. The right plot presents the two-dimensional results. In case of solvent casted sample we observe the equal ring, when in case of shear aligned sample we observed two spots of higher intensity which indicated orientation of cylinders.

Here only the SAXS profile of solvent casted sample was presented.

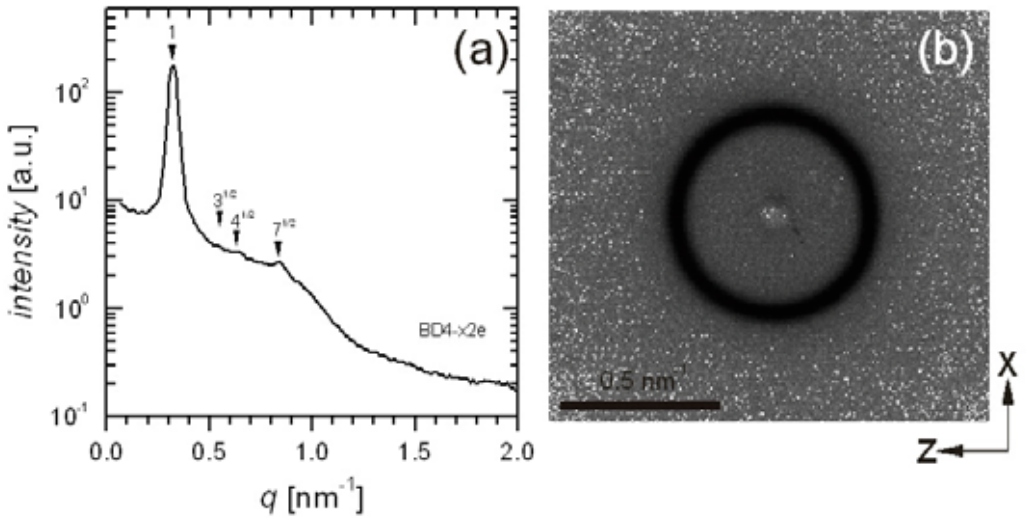

Figure 18 a: One dimensional (1-D) SAXS profiles of solvent casted, cross-linked and etched BD4-x2e sample with characteristic *q* ratios marked by reversed triangles. b: two dimensional (2-D) scattering profile of sample BD4-x2e.

Electron microscopy

Scanning electron microscopy pictures of solvent casted sample BD4-x2e are presented on Figure 19 and on Figure 20.

On Figure 19 a we can clearly see the bending of cylinders. White stripes seen on the picture are the empty cylinders. Figure 19 b shows the distance between the cylinders centers, which is estimated 20 ± 2 nm.

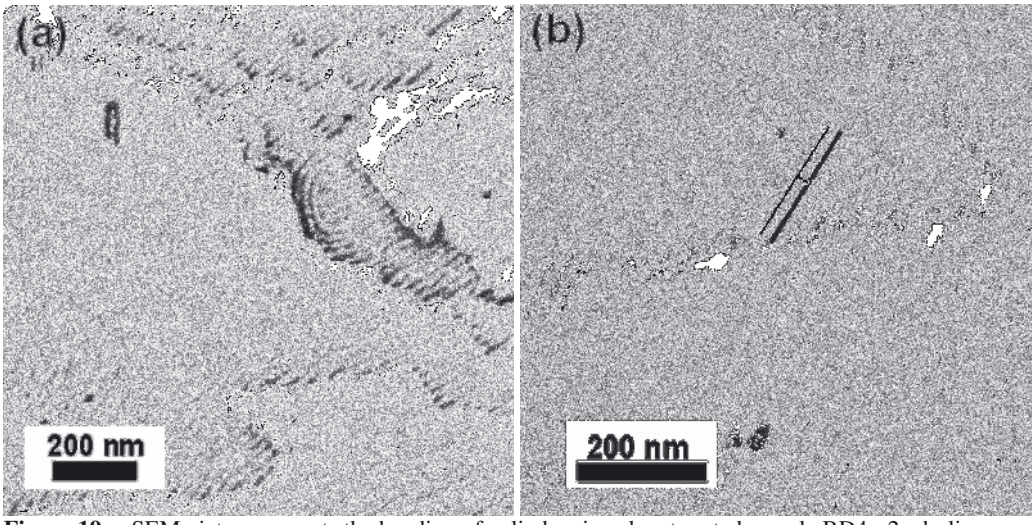

Figure 19 a: SEM picture presents the bending of cylinders in solvent casted sample BD4-x2e; b: lines indicate the distance between cylinders center.

Figure 20 b shows different projections of the hexagonally packed cylinders within one SEM picture. The inlet, which is magnified on Figure 20 a presents the hexagons of the cylinders. Measured pore diameter *2r* from this picture is 8 ± 2 nm. In the upper right corner of the right panel we can see the cross-sections of the cylinders. From Figure 20 we can also measure the distance between the main scattering planes d_{10}, which is 18 ± 3 nm.

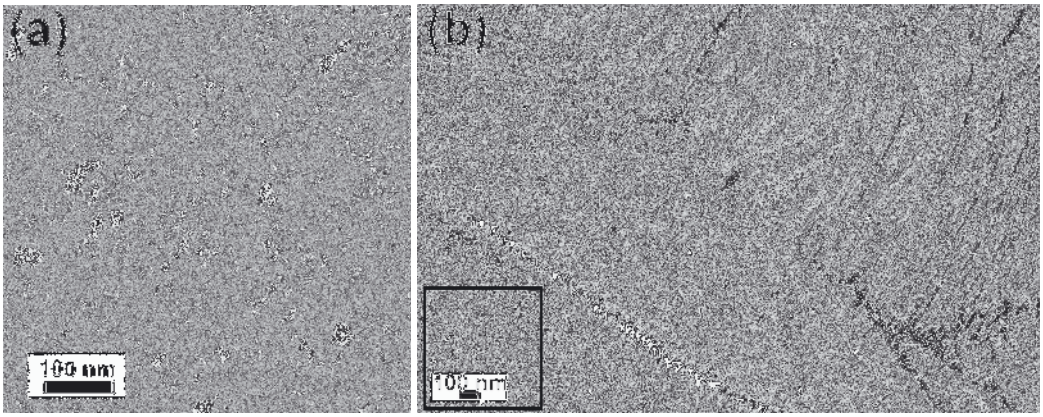

Figure 20 SEM picture of solvent casted sample A. Left panel is the magnification of the right panel inlet, presenting hexagonal pattern of cylinders.

SEM picture of shear aligned sample BD4-x0.8e is presented on Figure 21. This picture clearly shows the hexagonal pattern and cross-section of the cylinders within one domain. The measured pore diameter was 8 ± 1 nm. The distance between pore centers was found to be 23 ± 2 nm and the distance between the main scattering planes d_{10}, was 14 ± 3 nm.

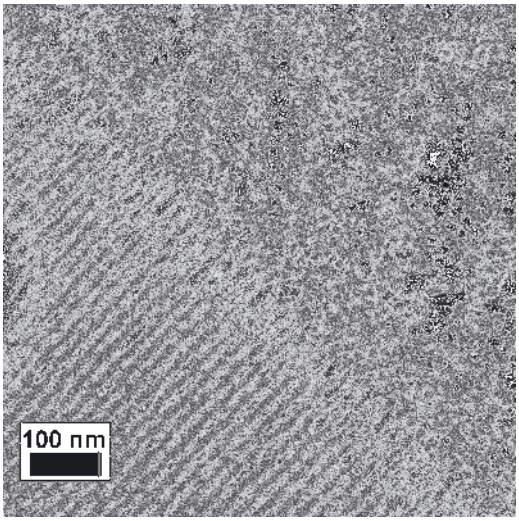

Figure 21 SEM picture of shear aligned sample BD4-x0.8e.

TEM result of solvent casted sample BD4-x2e is presented on Figure 22. This picture very clearly shows the regular pattern of hexagonally packed cylinders. The measured pore diameter was 8 ± 1 nm.

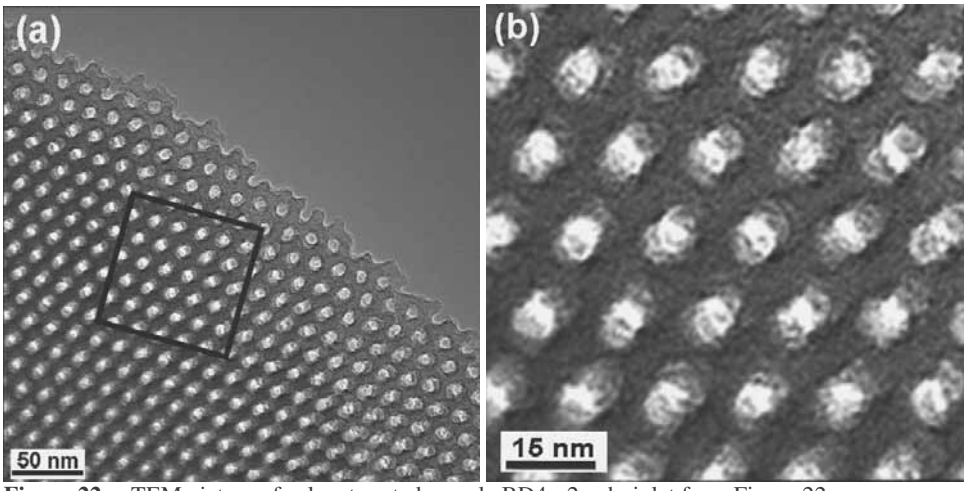

Figure 22 a: TEM picture of solvent casted sample BD4-x2e. b: inlet from Figure 22 a.

3.2. Gyroid morphology

The gyroid morphology of diblock copolymers has been characterized by many authors. [45][46] It is a bicontinuous cubic structure which shows a $Ia\bar{3}d$ symmetry. Single unit cell of this morphology consist of 16 tripods, where each tripod is connected to the other one which is twisted by 70.53°. Depending if tripods are twisted clockwise or counter clockwise we get two interpenetrating, chiral networks. Figure 23 presents graphic presentation of a diblock copolymer unit cell with GYR morphology. Both networks marked by green and red colour presents the minority block (PDMS in case of samples presented in this thesis). They were marked in this way to visualize, that these are two networks.

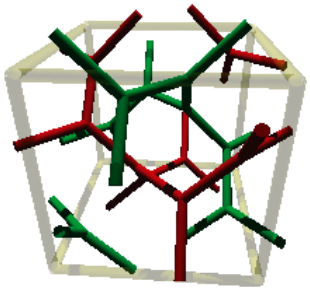

Figure 23 Graphic presenting a gyroid unit cell.

The complexity of gyroid morphology is presented on Figure 24, which was created by combination of unit cells presented above. Two interpenetrating networks are distinguished in the same way by red and green color. Graphic was prepared in POV-ray program by Piotr Szewczykowski with help of Brian R. Pauw.

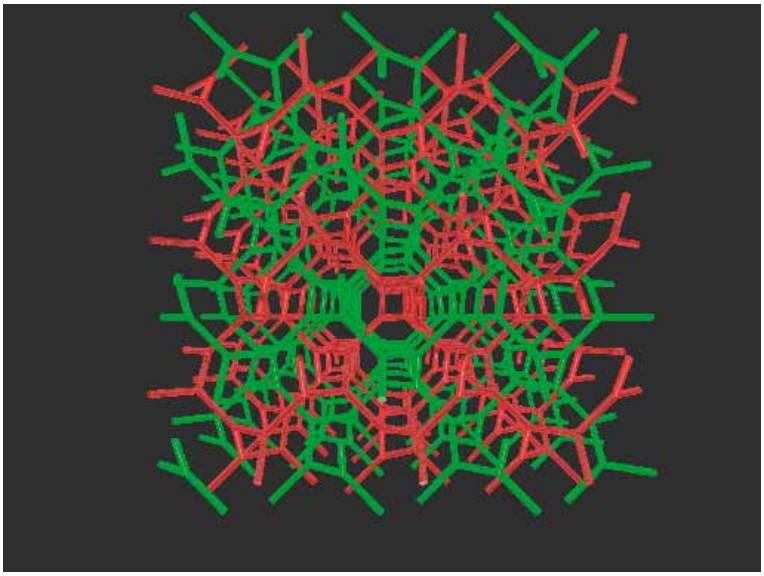

Figure 24 Gyroid interpenetrating network

Two interpenetrating networks (distinguished by red and green color) of the minority block in diblock copolymer with gyroid morphology. Graphic was prepared in POV-ray program by Piotr Szewczykowski with help of Brian R. Pauw.

SAXS

SAXS profile from the gyroid sample is much more difficult for interpretation comparing to hexagonally packed cylinders morphology. The upper plot in Figure 25 a shows one dimensional (1-D) scattering profile from cross-linked and etched, nano-porous sample BD14-x1e. The characteristic ratio of scattering vector q has the following values: $6^{½}$, $8^{½}$, $14^{½}$, $16^{½}$, $20^{½}$, $22^{½}$, $24^{½}$, $26^{½}$, $30^{½}$, $32^{½}$, $38^{½}$, $40^{½}$, $42^{½}$ and $50^{½}$. The interpretation of the peaks can be found in literature. [46]

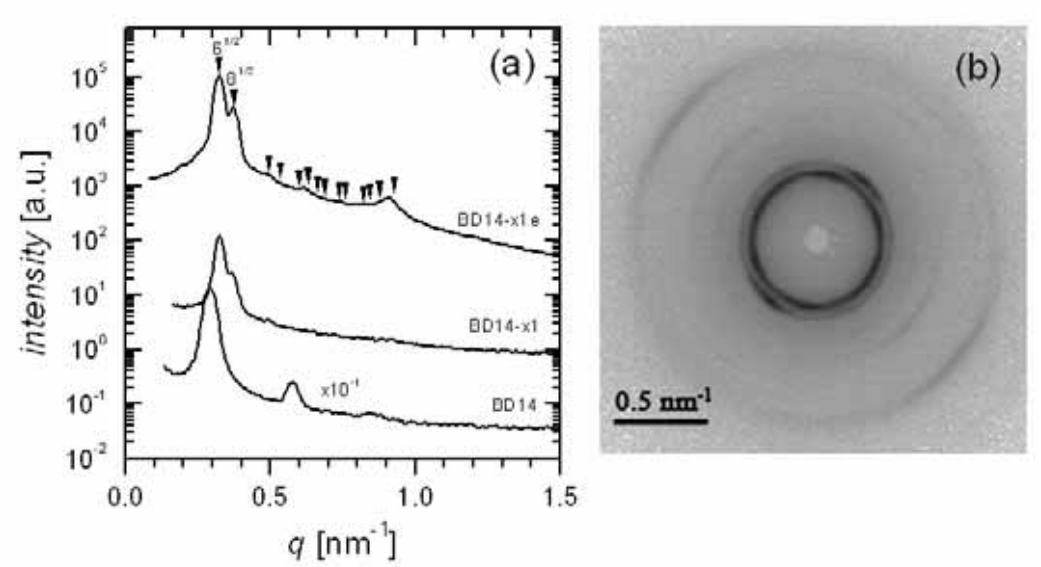

Figure 25 a: Upper plot presents one dimensional (1-D) SAXS profiles of cross-linked and etched BD14-x1e sample with characteristic q ratios marked by reversed triangles. Middle plot presents 1-D profile of crosslinked only sample and bottom profiles presents polymer melt. b: two dimensional (2-D) scattering profile of etched sample BD14-x1e.

Figure 25 a shows the 1-D scattering profiles of polymer melt (BD14), cross-linked only sample (BD14-x1) and finally cross-linked and etched sample (BD14-x1e). The characteristic q ratios for gyroid morphology are marked on 1-D profile of etched sample by reversed, black triangles. The bottom profile of polymer melt shows three peaks which are in equal distance to each other. This is characteristic to the lamellar (LAM) structure. During the cross-linking, polymer is heated up and it reaches the following order to order transition temperatures T_{OOT} measured by rheology. At 68°C it changes to hexagonally perforated lamellae (HPL) and at 106°C it reaches gyroid morphology, this is just below the boiling point of cross-linking agent (130°C), and this morphology is 'captured' in cross-linked sample. The scattering intensity of cross-linked only sample almost does not change comparing to polymer melt. Scattering intensity of BD14 melt was divided by 10 for better illustration. It can be seen that polymer changed morphology to GYR after cross-linking, since characteristic peaks appeared ($6^{½}$ and $8^{½}$). Scattering intensity for etched sample clearly increased, since volume filled by PDMS is now

vacuum, so contrast increased. Figure 25 b presents two-dimensional scattering profile of cross-linked and etched BD14-x1e sample.

SEM

Investigation of the gyroid morphology with electron microscopy is quite complex, since we observe different surface morphologies depending on the fracture of the sample. Projections along different directions occur as characteristic patterns like: “knitting”, “wishbone” or “wagon wheel”.[47][48] Figure 26a shows a “knitting” pattern which results from cut along the (211) symmetry plane of unit cell. This result from SEM corresponds very well to the computer graphics in Figure 26b.[49][50] Bright phase corresponds to the 1,2-polybutadiene whereas dark phase corresponds to the pores. A graphical representation of the gyroid network is shown on Figure 26c.

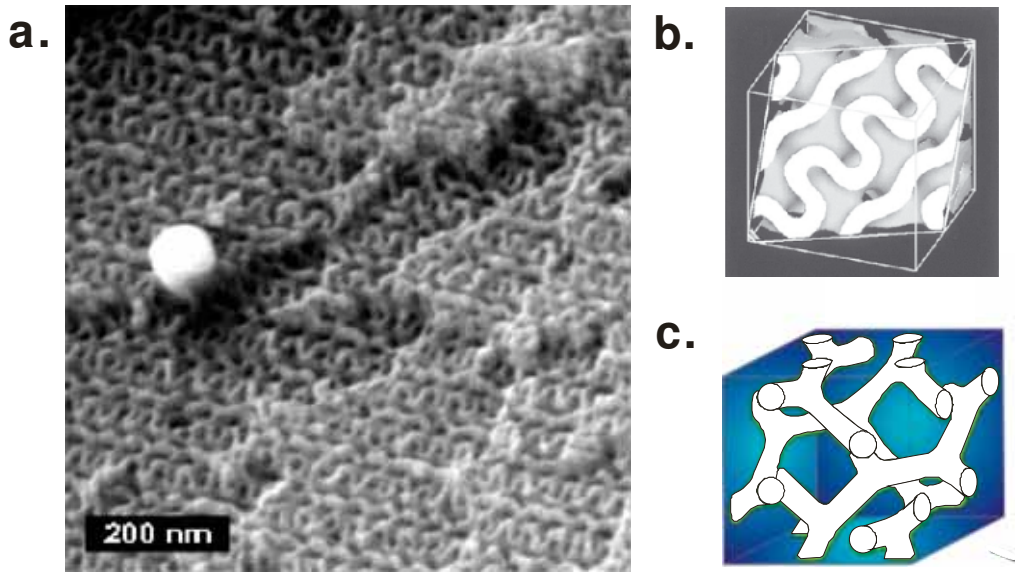

Figure 26 a. SEM picture of “knitting” pattern of nanoporous sample. B. Computer graphic presenting a two dimensional cut along the (211) plane [49] c. Graphic presentation of the gyroid network. The pore diameter is expected to vary in the gyroid morphology, with a maximum expected at the 3-branch zones and a minimum at half distance between two branches.

Nitrogen adsorption

The observed nitrogen gas physisorption isotherm fitted to the Type IV isotherm which is characteristic for mesoporous (2-50 nm pore diameter) adsorbents. The hysteresis loop was of type H1 which indicated quite uniform pores.[43] The specific surface area calculated from BET method for nanoporous sample was 260 ± 30 m^2/g. The pore size distribution obtained from BJH method showed the pore diameter in the range of 15±4 nm.

3.3. Summarization

Table 5 compares the structural data of polyisoprene and polybutadiene based samples.

STRUCTURAL DATA									
	ID30			BD4					BD14
		aligned			solvent casted		aligned		solvent casted
preparation step	precursor	cross-linked	etched	precursor	cross-linked	etched	cross-linked	etched	etched
Sample codes	ID30	ID30-x38	ID30-x38e	BD4	BD4-x2	BD4-x2e	BD4-x0.8	BD4-x0.8e	BD14-x1e
SAXS									
q^* [nm^{-1}]	0.35	0.40	0.45	0.30	n.m.	0.32	n.m.	0.33	0.32
$d^*=2\pi/q^*$ [nm]	17.8	15.6	14.0	21.1	n.m.	19.5	n.m.	19.3	19.4
r [nm]	5.9	5.2	4.6	6.9	n.m.	6.4	n.m.	6.3	-
TEM									
d^* [nm]			14.8 ± 1.2			15 ± 2			-
r [nm]			3.8 ± 0.5			4 ± 0.5		4 ± 0.5	-
SEM									
d^* [nm]			n.a.			18 ± 3		14 ± 3	19.3 ± 2.5
r [nm]			5.4 ± 1.7			4 ± 1		4 ± 0.5	6 ± 1
Nitrogen adsorption									
r [nm]						6 ± 1.5		6.5 ± 1.5	7.5 ± 2
Internal surface area [m^2/g]			n.m.			85		70	260 ± 30

Table 5 Summarization of characterization results for nano-porous samples with hexagonally packed cylinders morphology. 'n. a.' and 'n. m.' mean 'not available' and 'not measured' respectively.

4. Non nano-porous but 'smart' material

Smart polymeric materials attract major attention amongst researchers within applied as well as basic science.[51][52][53][54][55] Such materials are characterized by having predetermined responses to external stimuli, which for example can be electrical, mechanical or chemical. Often the response takes the form of a change in shape or size, possibly induced by a phase transition. Polymeric actuators are prominent examples of such materials, where electrical energy results in mechanical motion.[56] A very simple stimulus is temperature change which is exploited in thermo responsive systems by controlling a volume phase transition of the material.[57] Other chemical stimuli which trigger a shift of physio-chemical properties could be change in pH, selective solubility of a solvent or a change in salt concentrations. Especially di-block copolymers show structural changes when exposed to solvents which interact differently with the polymer blocks. This is the case for block copolymer-based micelles induced by using a specific solvent at a given temperature[58] or selective swelling of block copolymer melts which causes phase transitions and morphology changes.[59] However, these phenomena do not traditionally qualify block copolymers as smart materials, although there are examples of solvent triggered stimuli responsive materials which are used to create smart surfaces based on forms of block copolymers.[60]

In Chapter 3 it was shown how polydiene-based diblock copolymers containing polydimethylsiloxane (PDMS) establish a fine and versatile platform for creating nano-porous materials with plentiful opportunities for combining synthesis to obtain nano-structured materials of different morphologies and chemical composition. Various procedures can be used to modify or functionalise the matrix material.[27][28][61][62] As it was already mentioned in *Introduction* the nano-porous structures are crucially dependent on the nature and the mechanical strength of the matrix material. In case of matrices which are not crystalline or glassy at room temperature (as is the case with polydienes) it is necessary to reinforce the matrix by cross-linking the polymer in order to have a structure which remains stable after the selective etching of the expendable block during the process of fabricating the nano-porous material. In an earlier report by F. Guo et al,[61] with whom I had a pleasure to work, a series of samples with relatively low degrees of cross-linking in the matrix domain was characterized and it was observed that the nanostructure and porosity apparently is not detectable by small angle scattering measurements after finishing the fabrication procedure. It is reasonable to describe these materials as *collapsed*, but it is unresolved what the characteristics, morphology and physio-chemical properties are for these materials, which all have been treated in such a

way that the expendable component of the precursor diblock copolymer matrix was quantitatively removed.

The aim of the work presented in this Chapter 4 is to conduct a comparative structural study of nano-porous samples of high and low degrees of matrix cross-linking. The samples are produced from the same (or similar) precursor block copolymer molecules. On one hand the samples which are highly cross-linked and subsequently etched give well defined nano-porous materials, and constitute the benchmark for the study. On the other hand the samples of low cross-linking degree are collapsed and do not produce a well defined nano-porous material. This study is primarily based on Small Angle Neutron Scattering (SANS) measurements of the effect of exposing the collapsed samples to specific liquids, namely a solvent and a non-solvent to the matrix material. Transmission Electron Microscopy (TEM) and Small-Angle X-ray Scattering (SAXS) were used to characterise the dry samples without the presence of any solvent. From this study information about the structure and nature of the low degree cross-linked samples is obtained. Collapsed materials are tested for possible smart behaviour.

4.1. Material preparation, characterization and SANS data reduction

Block copolymer synthesis

According to Figure 4 samples described in this chapter derive from two batches of polymerization: ID30 and ID33. The volume fraction of PI was targeted $w_{PI} = 0.7$ for both polymerizations (ID30 and ID33) to give comparative block copolymer systems with hexagonally distributed cylinders of PDMS in a matrix of PI. Data for the parent samples ID30 and ID33 are summarized in Table 3.

Alignment

In order to get optimal insight into the structural properties, as determined by the SANS experiment, the morphology of all the ID30 and ID33 samples were aligned into a simple texture by extruding the polymer melt. The procedure of alignment was already described in Paragraph 1.3.

Crosslinking

The samples were cross-linked to different degrees by using dicumyl peroxide (bis(α,α-dimethylbenzyl) peroxide) (DCP) from Merck. Details for cross-linking procedure were presented already in Paragraph 1.4. Three samples are discussed in this chapter. One sample ID30 was crosslinked to 38%, where two ID33 samples were cross-linked to 14 and 22%. The code names of crosslinked samples are ID30-x38; ID33-x14 and ID33-x20 respectively.

Etching

A solution of 1 M tetrabutylammonium fluoride (TBAF) in THF from Aldrich was used as cleaving reactant for removing the PDMS blocks. Etching procedure for sample ID30 and ID33 was already presented in Paragraph 1.5.

Swelling and solvents uptake

The weight of the dry piece of a sample was measured before the sample was placed in approximately 1 ml of solvent. The weight of the sample was measured again after soaking in solvent for 24 hours.

Characterization

Accordingly to Paragraph 1.2.1bloc copolymer precursors were characterized by Size Exclusion Chromatography (SEC); ^{1}H-NMR and rheology.

Sample ID30-x38e was investigated transmission electron microscope (TEM). Specimen preparation and information about apparatus were presented in Paragraph 2.1.2.

Polymer precursors, cross-linked only samples and etched samples were investigated with small angle x-ray scattering (SAXS) technique. Etched samples were investigated in dry state and in two different solvent with small angle neutron scattering (SANS): in deuterated methanol and deuterated toluene. Specimen preparation and information about apparatus were presented in Paragraph 2.2.

SANS data reduction

The procedure of data reduction and plot preparation is described in Appendix B. It is important to mention, that q values, distances between scattering planes and pore diameters are expressed in Å in this chapter, since the received raw data from SANS were presented in Å unit (neutron wavelength and calculated q value).

4.2. Results and discussion

Firstly, the data on the precursor diblock copolymers are presented and the two samples derived from these, which result from following the prescribed procedure to generate nano-porous polymers. The two samples differ only in the expected degree of cross-linking of the matrix component. Interestingly, these two samples display very different structural properties, as witnessed below in the section describing results of SAXS measurements. Secondly, we show the results of a more detailed study using SANS. The SANS measurements gauge the structural response of the samples to various solvents and shed light on morphological differences of the two samples generated from the similar diblock copolymer parent melts.

4.2.1. Characteristics of precursors and cross-linked, etched material

Block copolymer parent samples

Two PI-PDMS block copolymers ID30 and ID33 were synthesized by anionic "living" polymerization as described in Paragraph 1.2. Table 3 in Paragraph 1.2.1 lists the characteristics of these precursor diblock copolymers. SEC and/or ^{1}H-NMR were applied in order to obtain the molecular weights of the PI block, the total weight of the two block copolymers, the polydispersity index, and the weight and volume fraction of PDMS. SAXS measurements showed that the morphology of both samples is hexagonally ordered cylinders (HEX) of PDMS in a matrix of PI. Rheological studies determined the order-disorder temperature (T_{ODT}).

Preparation of samples by cross-linking and etching

Experience of previous students in the NPM research group is that effective cross-linking of PI requires several treatments with peroxide. Previously, it was reported that five to six additions of fresh peroxide was necessary to obtain sufficient mechanical stability of the PI network after etching with HF.[28] The expected mechanism of cross-linking the PI chains was discussed in Paragraph 1.4. Expected mechanism of etching PDMS with TBAF was presented in Paragraph 1.5.

Structural results

TEM results for ID30-x38e were presented and discussed in Paragraph 3.1.1 (see Figure 17). The structure data for ID30 sample were summarized in Table 5. These data are now repeated in Table 6 for easier comparison between ID30 and ID33 samples discussed in this chapter. Similarly SAXS profiles of ID30 polymer melt, cross-linked and etched samples were presented in Figure 16. They are now repeated in Figure 28 which shows azimuthally reduced SAXS data representing the three steps of preparing samples from the precursor polymer; the mother (original) sample (ID), the cross-linked sample (ID-x) and the cross-linked and etched sample (ID-xe).

Figure 28 also shows corresponding SAXS profiles of reduced data for one of the samples (ID33-x20e) from the ID33 polymer, which was cross-linked to lower degrees prior to etching. For the purpose of illustration the scattering data values for ID33 were divided by 10^4 and the values for ID33-x20e were multiplied by 10. Following the etching procedure small angle scattering from the nano-structure is almost absent and only a very weak indication of a scattering peak remains. Assuming that the volume of PI does not change following cross-linking and etching, and that the pores in etched sample are reduced to points, we can estimate a relationship between the Bragg distance of (10) planes in the etched nano-porous sample (d_{10}^E) and the cross-linked sample (d_{10}^X). Figure

27 presents cross-section of hexagonally packed cylinders, with marked distance between the main scattering planes d_{10} .

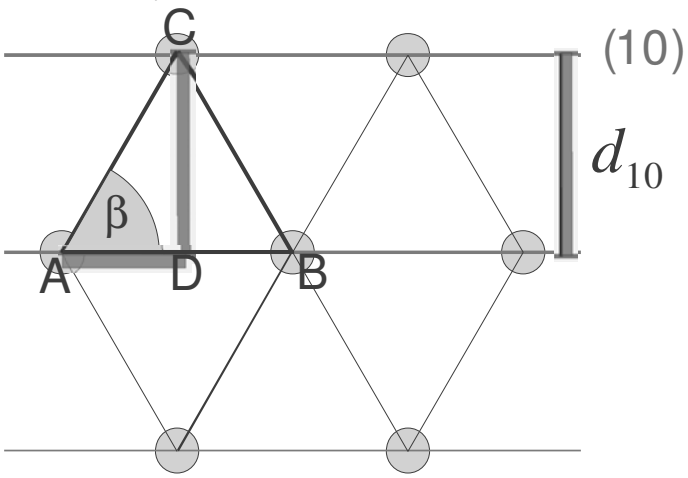

Figure 27 Geometrical construction for calculating main scattering peak position for collapsed pores.

Since we talk about hexagonally packed cylinders, we say that the area of ΔABC is equal to the volume of PI and PDMS:

$$\Delta ABC = PI + PDMS = (d_{10})_X \cdot AD \qquad \text{Equation (5)}$$

Knowing the experimental value of *q** for ID33-x20 (see Table 6) we calculate AD value, which is:

$$\tan\beta = \tan 60^o = \frac{d_{10}}{AD} \Rightarrow AD = \frac{d_{10}}{\tan 60^o} = \frac{d_{10}}{\sqrt{3}} = \frac{\sqrt{3}\cdot d_{10}}{3}, \qquad \text{Equation (6)}$$

so

$$\Delta ABC = PI + PDMS = (d_{10})_X \cdot \frac{\sqrt{3}\cdot (d_{10})_X}{3} \qquad \text{Equation (7)}$$

Since the volume fraction of PI in the melt is 0.74 (Table 3) and we assume it doesn't change after crosslinking and etching , the PI fraction is:

$$PI = \Delta ABC \cdot 0.74 = \frac{\sqrt{3}}{3}\cdot (d_{10})_X \cdot (d_{10})_X \cdot 0.74 \qquad \text{Equation (8)}$$

The volume of the PI does not change (assumption) and the distance between the 10 planes change after etching, so:

$$\frac{\sqrt{3}}{3}\cdot (d_{10})_X \cdot (d_{10})_X \cdot 0.74 = \frac{\sqrt{3}}{3}\cdot (d_{10})_E \cdot (d_{10})_E \qquad \text{Equation (9)}$$

$$d_{10}^E = \sqrt{0.74}\cdot d_{10}^X \qquad \text{Equation (10)}$$

Now we can estimate a peak position for the etched sample based on the conditions above. We get d_{10}^{E} = 121 Å which corresponds to q^* = 0.0521 Å^{-1} for ID33-x20e which is marked by an open triangle in the insert in Figure 28. Close inspection of the scattering profile leads to the identification of a scattering peak at q^* = 0.0513 Å^{-1} which is marked by solid triangle and listed in Table 6 for ID33-x20e. This value is less than 2% smaller than the expected value, which means that the pores probably do not shrink to the point-like conditions as assumed in Equation 10.Anyhow, based on the weakness of the peak in this scattering profile it is not possible to claim any sort of structure of the sample in the nano-porous regime, which is probed by the SAXS measurement.

Attempts of obtaining electron micrographs of the nano-structure in these samples (ID33-x14e and ID33-x20e) were conducted in vain. From this evidence it is concluded that there is no nano-porous structure in the as-prepared dry samples from the batch of ID33. In comparison with the ID30 batch the only difference in the sample preparation is the degree of cross-linking. Judging from the preparation procedure it is fair to conclude that the ID30 batch was cross-linked to relatively higher degrees than the ID33 batch. This leads to speculations that the cross-linking of the ID33 samples was not sufficient to withhold the internal forces, which arise from creating the internal surface of the nano-porus structure and we will describe these samples as being *collapsed*. This is in agreement with our findings from a similar polydiene block copolymer based system. [61] It is noteworthy that the scattering from samples ID33-x14 and ID33-x14e showed similar behavior as illustrated in Figure 28 and the values of q^* listed in Table 6 are almost identical.

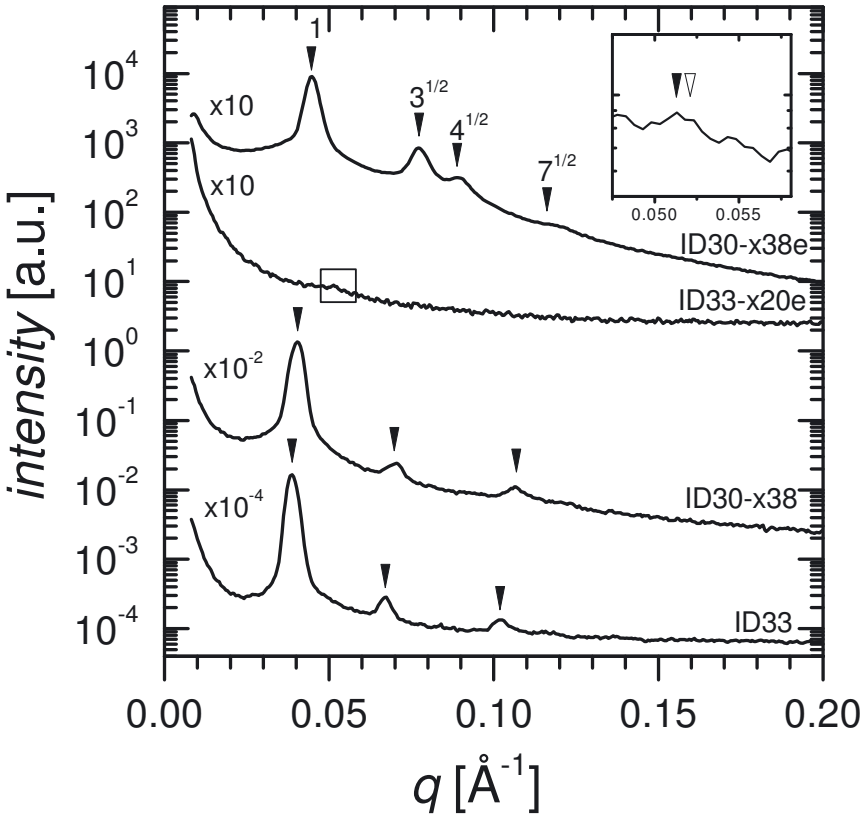

Figure 28 Azimuthally averaged SAXS data of the original, the cross-linked and the etched samples. In order to separate plots for better presentation, the intensity values for the ID33 and ID30-x38 profile were divided by 10^4 and by 10^2 respectively, while intensity values for ID33-x20e and ID30-x38e were multiplied by 10. For sample names please see text. The primary peak position (q^*) is marked by numeral '1' and higher order reflections are marked accordingly showing the indications of a hexagonal structure. The insert in the top right corner magnifies the scattering curve for sample ID33-x20e in the vicinity of the 0.05 $Å^{-1}$ scattering vector. The open triangle for indicates the expected peak position for a nano-porous structure (see text) and the closed triangle marks the estimated peak position of this very weak scattering peak.

Typical for both batches of ID30 and ID33 was that the primary scattering peak moved towards higher values upon cross-linking and subsequent etching as it was already mentioned in Paragraph 3.1.1

By comparing the values of q_{10} of the ID33-sample series with the corresponding ID30-series we see that the q_{10}-values of the ID33-samples are 9-10% higher than those of ID30. This is expected as the number average molecular weight of the ID30 mother sample is approximately 10% larger than the weight of the ID33 mother sample, as can be seen in Table 3.

STRUCTURAL DATA, DRY								
	ID30			ID33				
preparation step	precursor	cross-linked	etched	precursor	cross-linked		etched	
Sample codes	ID30	ID30-x38	ID30-x38e	ID33	ID33-x14	ID33-x20	ID33-x14e	ID33-x20e
TEM								
d_{10} [Å]			148 ± 12				no visible structure	no visible structure
SAXS								
q_{10} [Å^{-1}]	0.0354	0.0402	0.0448[a]	0.0387	0.0452	0.0448	0.0489[b]	0.0513[b]
$2\pi/q_{10}=d_{10}$ [Å]	178	156	140	162	139	140	128	122
SANS								
q_{10} [Å^{-1}]		0.0406	0.0425[a]		0.0426	0.0426	no Bragg peak	no Bragg peak
$2\pi/q_{10}=d_{10}$ [Å]		155	143		147	147	n.a.	n.a.
Nanoporosity			present				absent	absent

Table 6 Structural data for dry samples (without exposure to solvents). The results of Bragg spacing (d_{10}) measurements are listed for TEM, SAXS and SANS experiments. The apparent condition of the porous structure for the etched samples is summarized in the bottom line by either 'present' or 'absent'. [a]Very strong peak. [b]Very weak peak. Data accuracy for SAXS and SANS is about 1% and 5% respectively.

4.2.2. SANS investigation of morphology responses to selected solvents.

As mentioned in the previous section, we have two kinds of samples of different degrees of cross-linking which render very different structures: nano-porous and collapsed. The sample derived from ID30 is a straight forward nano-porous structure. The samples derived from ID33 apparently show no nano-structure and the sample morphology is ill-defined by SAXS and TEM measurements. In this section we will attempt to resolve the peculiar morphology difference between samples from batches ID30 and ID33 which both have been cross-linked and etched.

Before investigating sample response to various solvents we present the SANS profiles of the dry samples ID30-x38e in Figure 29(a) (open symbols) and ID33-x20e in Figure 29(b) (open symbols). This data is in agreement with the SAXS data displayed in Figure 28. SANS peak positions are listed in Table 6. The SANS data shows a well defined peak for ID30-x38e, and the absence of any constructive Bragg scattering for ID33-x20e. This confirms our preliminary findings from the SAXS measurements that the structure of the

lesser cross-linked material (ID33-x20e) is collapsed and cannot be resolved or characterized by small angel scattering data.

In the following sections we will investigate how these samples behave when exposed to respectively a non-solvent and a solvent for the cross-linked PI matrix. We do this in the hope that such investigation can shed light on the nature of the unresolved structure of the collapsed material (samples ID33-x20e and ID33-x14e). The expectations for a non-solvent are that it will percolate into nano-cavities without changing the dimensions of the PI matrix. When using a deuterated liquid the contrast factor between cavity and matrix will be greatly enhanced and in this way amplify otherwise weak Bragg scattering. On the other hand, the expectation for a solvent is that the sample will undergo swelling, and that the matrix will change dimensions.

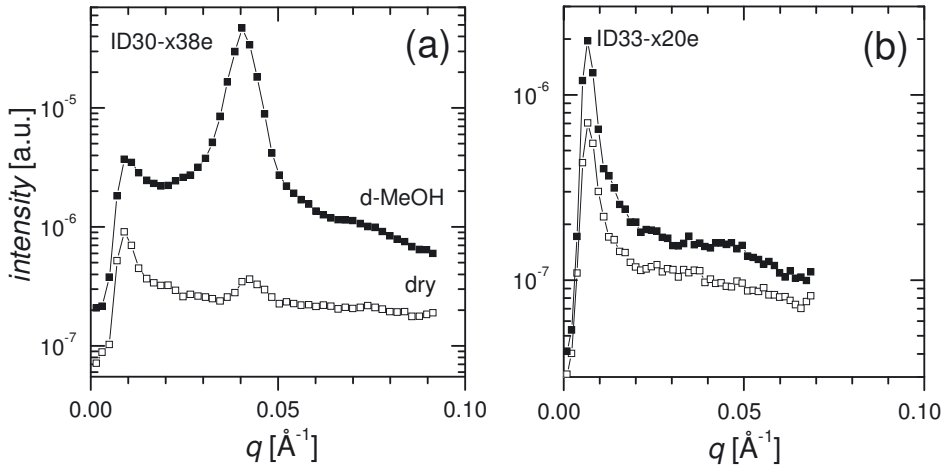

Figure 29 (a) Azimuthaly averaged SANS profiles of the raw scattered intensity of sample ID30-x38e. (b) Ditto for sample ID33-x20e. Scattering from samples in the dry state is depicted by open symbols, and scattering from samples placed in d-methanol is depicted by closed symbols.

Exposure to a non-solvent

The first solvent exposure experiment is one which should attempt to fill out the nano-porous cavities without changing the dimensions of the PI matrix. Methanol is a non-solvent for the cross-linked PI-matrix, so we expect that after placing the sample in the d-methanol it does not swell the sample, but some solvent may percolate into the porous bulk structure. The resulting scattering for the nano-porous sample (ID30-x38e) is illustrated in Figure 29(a) (closed symbols). We observe a highly enhanced peak intensity of the neutron scattering. This is in good agreement with expectations that the liquid percolates into the nano-pores. The data is recorded after the sample was submerged for 131 minutes in d-methanol. Values for peak position are listed in Table 8, together with the gravimetrical mass uptake. We notice a small shift of the peak position of some 4% to lower values, which indicates that the structure is undergoing some swelling. This is

supported by the observation that the samples seem to take up 0.83% more solvent than the cavity volume accounts for.

We can compare the intensity ratio of the dry and wet scattering data with theoretical expectations. The scattering intensity is directly proportional to the contrast factor:[63]

$$I(q) \propto (\rho_A - \rho_B)^2 \qquad \text{Equation 11}$$

ρ_A and ρ_B are scattering length densities of the two components or domains A and B (f.x. the two blocks in the pristine block copolymer or in this case the matrix polymer and vacuum or solvent in the etched system). The scattering length densities can be expressed as: $\rho = b_i \cdot d_i / m_i$, where the index i is either A or B; and b_i is the scattering length of the monomer or the solvent molecule, respectively; d_i is the specific mass (mass density) of monomer or solvent; and m_i is the mass of monomer or solvent molecule as known from the chemical formula. Calculated values for different neutron-contrast factors for PI relative to deuterated methanol (methanol-d4), deutereted toluene (toluene-d8) and air (i.e. vacuum) are presented in Table 7.

	PI	**methanol-d4**	**toluene-d8**	**vacuum (air)**
d [kg·m^{-3}]	856	889	910	
m_i [Da]	68.12	36.07	100.21	
ρ [m^{-2}]	$2.52 \cdot 10^{13}$	$5.81 \cdot 10^{14}$	$5.47 \cdot 10^{14}$	
$(\rho_{PI}-\rho_{solvent})^2$ [m^{-4}]		$3.09 \cdot 10^{29}$	$2.72 \cdot 10^{29}$	$6.35 \cdot 10^{26}$

Table 7 Contrast factors for PI versus methanol-d4, toluene-d8 and vacuum (air). Contrast factors are presented in the bottom row of the table. d [kg·m^{-3}]; m_i [Da] and ρ [m^{-2}] are mass density of monomer or solvent, the mass of monomer or solvent molecule and scattering length density respectively.

The ratio of the wet and dry scattering intensities should equal the ratio of the contrast factors between PI/methanol-d4 and PI/vacuum. From Table 7 we can see that assuming similar structure, the expected scattering ratio between the intensity of the Bragg scattering from the methanol filled system and the dry system should be approximately 490. From the scattering data we extract the ratio of the wet and dry scattering intensities by measuring the area of the scattering peaks. This gives a factor of approximately 380 which is a little lower, but in the range of the expected intensity increase. A reason for the lower value is probably that the deuterated methanol penetrates the cross-linked PI matrix and to some extend causes some swelling of the matrix due to the solvent uptake as discussed above. Hence the wet system will have a reduced contrast factor.

The exposure of the ID33-x20e sample to deuterated methanol did not yield any change of the scattering as judging from the SANS profile in Figure 29 (b) (closed symbols). The scattering remains indecisive and does not characterize the morphology of the sample beyond the level of being collapsed in agreement the dry SANS and SAXS data. The data indicates that there is no trace of the original structure left in the sample, which could facilitate a guided percolation of the non-solvent. As we may conclude from the methanol

uptake measurements reported in Table 8 the ID33-based samples soak up less than 10% non-solvent without any detectable structural indications from the scattering. Scattering data for samples placed in deuterated solvents are summarized in Table 8.

STRUCTURAL DATA, WET (SANS)						
	ID30		ID33			
preparation step	cross-linked	etched	cross-linked		Etched	
sample codes	ID30-x38	ID30-x38e	ID33-x14	ID33-x20	ID33-x14e	ID33-x20e
in d-methanol						
q_{10} [Å^{-1}]	0.0393	0.0407[a]			n.a.	0.0427[b]
$2\pi/q_{10}=d_{10}$ [Å]	160	154			n.a.	147
mass uptake [wt%]		41			4	5
in d-toluene						
q_{10} [Å^{-1}]	0.0353	0.0390[a]	0.0386	0.0347	0.0374[a]	0.0400[a]
$2\pi/q_{10}=d_{10}$ [Å]	178	161	163	181	168	157

Table 8 Structural data from SANS measurements of wet samples exposed to the deuterated solvents: d-methanol and d-toluene. Also included is the degree of percolation as measured by the relative gravimetrical mass uptake of the non-solvent. [a]Very strong peak. [b]Very weak peak.

Exposure to a solvent

The second solvent exposure experiment is an attempt to swell the complete sample matrix and study the effect of this to the sample structure. Toluene is a solvent for the PI-matrix. Placing the sample in toluene will cause swelling of the cross-linked matrix.

As illustrated in Figure 30 this led to a dramatic change of the scattering fingerprint of the collapsed samples ID33-x20e. The two dimensional detector response shows the scattering collected over 300 seconds. Figure 30(a) shows the scattering from the dry data as already discussed above and presented azimuthally averaged in Figure 29 (b). After being submerged in deuterated toluene for 2.5 hours a very strong scattering signal is observed. The two dimensional scattering is anisotropic, which is in perfect agreement with the extrusion processing during sample preparation. Hence, the sample holds a memory of both the originally templated diblock morphology and the preparation alignment procedure, which persists matrix cross-linking and nano-porous etching. At the end of the preparation procedure the dry sample renders no structure, but when the cross-linked matrix is swollen by a solvent the nano-structered morphology balloons up. In the terminology of polymer gels the swollen material exhibits dual porosity, one set of pores being related to the cross-linked matrix and the other to the precursor block copolymer morphology. This data allows a precise identification of the Bragg peak position. The scattering peak positions of the swollen ID33-x14e and ID33-x20e samples are very close to the similar peak position of the swollen nano-porous ID30-x38e, as seen in Table 8.

This is in good agreement with the stochiometric data presented in Table 3, which show that the mother polymers ID30 and ID33 are almost of same molecular weights.

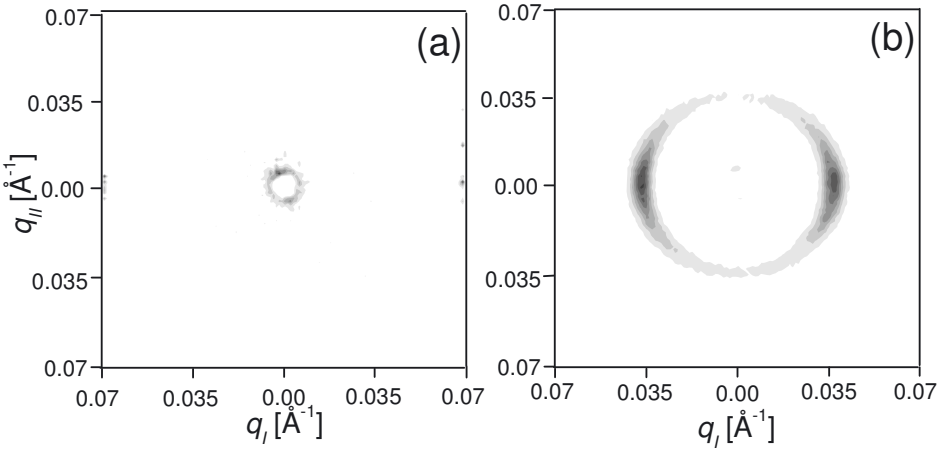

Figure 30 (a) 2D scattering pattern on the detector recorded for the sample in the dry state without any solvent exposure (a) and for ID33-x20e and ID33-x14e (b). 2D scattering pattern in the wet state is presented on (b) and (d) for ID33_x20e after 2.5 h and ID33-x14e after 5.5 h respectively. SANS was collected for 300 s in both cases. 3D plots showing the intensity scale for ID33-x14e are presented on right panels.

The effect of exposure to deuterated toluene is compared for both nano-porous and collapsed samples in Figure 31. As expected, when exposed to toluene the nano-porous sample (ID30-x38e) in Figure 31 (a) show a peak position which indicates a structure of wider separated Bragg planes than both the dry sample and the sample exposed to methanol. Values for the peak position and the Bragg plane separation are given in Table 8.

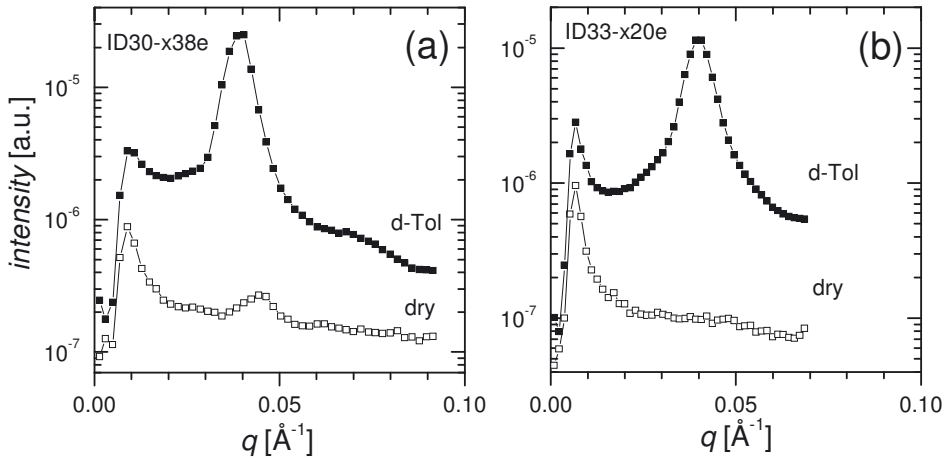

Figure 31 Azimuthally averaged SANS profile of (a) sample ID30-x38e and (b) ID33-x20e in the dry state (open symbols) and after submerging in d-toluene (closed symbols).

Swelling, kinetics of collapsed structure

In order to test how well a collapsed sample will reproduce the original template morphology, the sample ID33-x14e was subjected to repetitive cycles of swelling in d-toluene followed by drying in air. This was done on-line the SANS instrument and enabled investigation of the kinetics of the swelling as well as the reproducibility of cycles of swelling and drying.

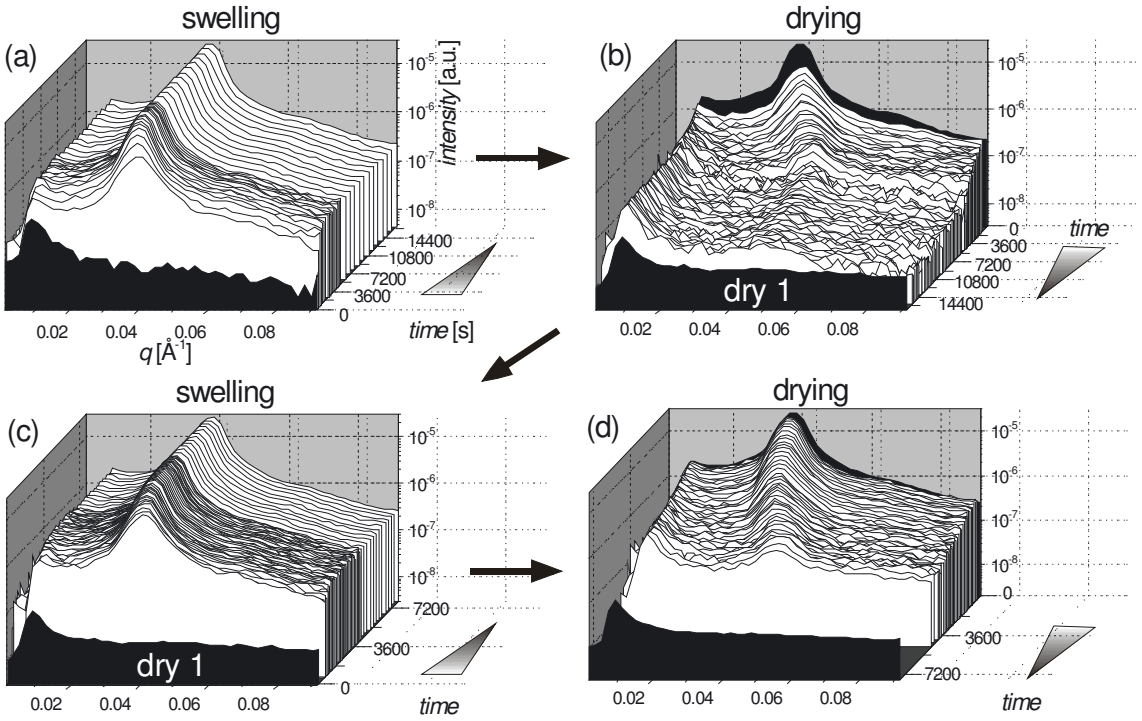

Figure 32 Time evolution of repeated swelling and drying as observed in the azimuthally averaged SANS profiles. The initial and resulting dry states are shown at the front of each sequence of data which shows the scattering intensity versus scattering vector q. The sample ID33-x14e was exposed to (a) swelling, (b) drying, (c) repeated swelling and (d) drying. Notice the direction of the time axis is alternatively reversed for clarity of the evolution of the scattering profiles.

Figure 32 shows the time evolution of two swelling-drying cycles. The azimuthally averaged SANS profiles of scattering intensity versus scattering vector q show evidence of the structural changes in the sample. The scattering from the dry state of the sample is indicated in black at the front of Figure 32(a). There is no scattering peak from nanostructure in the dry sample. After submerging the sample into d-toluene the first 60 s frame of scattering was recorded with a time delay of 4.5 min. This is due to the handling procedure of introducing the solvent and the safety routine for the neutron exposure. A scattering peak is clearly evident at this time and the scattering vector q^* at peak intensity maximum decreases following time in agreement with an increase of the real space dimensions of the material structure.

Figure 32(b) presents the scattering recorded during sample drying. The lastly recorded wet scattering profile from the swelling is put at the back of this series of profiles for comparison and marked in black. As anticipated the peak position at maximum intensity increases and the intensity drops over time. After four hours the scattering peak is almost gone. Following subsequent drying of the sample in air for 6 hours and another two hours

in a vacuum chamber the resulting scattering marked “dry 1” is displayed in the black scattering curve at the front of the figure. This scattering gives proof that the swelling-induced nanostructure (in the form of a peak of intensity) has completely gone. Back at the starting point the sample was exposed to a second swelling experiment and the resulting evolution on the scattering is documented in Figure 32 (c). The effect of the d-toluene solvent is identical to the first cycle. Finally, the sample was dried for the second time. The evolution in the scattering does not completely reproduce the evolution of the first drying sequel. Drying conditions were not subjected to particular control and the two drying experiments are not comparable in a detail that justifies a close relative inspection of the two cycles. However, the scattering data of the swelling behaviour is a more precise intrinsic measurement of the interaction between solvent and sample, and the two swelling sequences will be compared in the following section. A fully dried sample was obtained after 3 hours, which shows no nano-structured scattering. Hence, we can conclude that the two swelling-drying cycles resulted in repeated appearance and disappearance of the nano-structure. We interpret this as being in fact an opening and closing of nano-porous voids, which are templated into the collapsed sample by the original morphology of the diblock precursor polymer ID33. Also the sample reproduced the originally introduced alignment by the shear extrusion preparation process as evidenced by the 2D scattering profile, which shows strong equatorial peaks similar to those of Figure 30. In conclusion, this set of data shows that the collapsed material exhibits memory of the sample history on two accounts, namely precursor morphology and preparatory alignment.

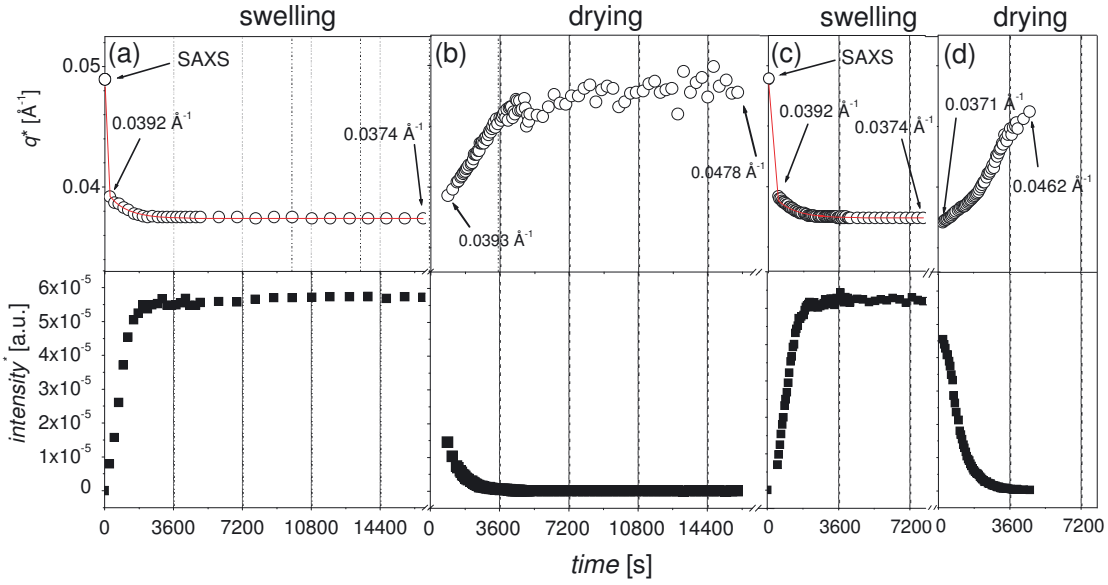

Figure 33 Time evolution as observed by changes of the peak position q^* (upper panel, open symbols) and the peak intensity I_{max} (lower panel, closed symbols). The data is the same as illustrated in Figure 32, where sample ID33-x14e was exposed to (a) swelling, (b) drying, (c) repeated swelling and (d) repeated drying. For the two swelling sequences a double decaying exponential function is used to fit the change of of peak position q^*.

A quantitative representation of the swelling-drying cycles is presented in Figure 33 which shows the details of the changes of peak scatting position (q*) in the upper panel and changes of peak intensity (Imax) in the lower panel. In Figure 33(a) the first observable value of q* is 0.0392 Å^{-1} (after the time delay of 4.5 min mentioned above). This value can be compared to the value obtained by SAXS for this sample in the collapsed dry state, which is listed in Table 6 and indicated at time 0 in the figure. We assume that this value is an upper limit to the value of q*. Following time, q* decreases to a lower value within half an hour, which after 4 hours 40 min remains at 0.0374 Å^{-1}. The time development of q* is nicely reflected in the evolution of the increasing peak intensity Imax, which is shown in a linear plot and also levels off after approximately half an hour and remains constant for the duration of the experiment.

At this point the sample was removed from the solvent and placed on the beam line in an empty cuvette cell to dry. Figure 33 (b) shows the effect of this drying procedure. The first 60 s frame of scattering is recorded 15 min after removing the sample from d-toluene. This time was enough for the value of q* to increase to 0.0393 Å^{-1}. It takes approximately 1.5 hours to reach the upper level for the value of q* which after 4 hours 26 min is fluctuating around 0.0478 Å^{-1}. This value is very close to the q* SAXS value indicated in Figure 33(a). The determination of the value of q* is rather uncertain at this

time of the data sampling, because the scattering peak is very much reduced as can be seen in Figure 32(b). The trend for the change in I_{max} nicely follows the change of q^*. In Figure 33(c) and Figure 33(d) we see a repeating behaviour for q^* and I_{max}, and that the parameters cycle between the same limits as observed in the first cycle of swelling and drying.

The estimation of the characteristic swelling times in toluene is made by fitting the decay of q^* as a function of time in toluene with exponential functions. The appearance of the scattering peak is due to scattering length density contrast generated as a result of pore opening in the swelling process and the absolute value of the scattering vector q^* is inversely related to the length scale of the material. In the presence of toluene the collapsed PI material behave as a visco-elastic gel, and the swelling of such materials cannot be described as a simple solvent diffusion process.[64] The existence of a shear modulus puts constrains to the shapes a polymer gel can take during swelling. A detailed description of the swelling of the material in a good solvent is not possible at the present, mainly due to missing information at times below 200 s. However, by estimation of the y-value of the data point at $t = 0$ to be equal to the value obtained from the SAXS measurement (see Table 6) the result of fitting of a double exponential decaying function to the experimental data of q^* for the both swelling sequences is presented by the red line in Figure 33 (a) and (c). The fitting function is:

$$q^*(t) = q_\infty \cdot [1 - a \times \exp(-bt) - c \times \exp(-dt)]^{-1} \qquad \text{Equation 12}$$

with a = 0.0610; b = 0.0010; c = 0.1742 and d = 0.2709. q_∞ is the asymptotic value of q^*(t) at very long times. This indicates that the swelling process consists of at least two processes – one fast and one slow – both driven by the same mechanism. The fast process is probably related to the swelling in the close skin layer at the polymer surface and is too fast to be measured by the procedure adopted in this study. The time constant for the slow process is 1000 s. The same characteristic time was found for the scattering intensity shown in the lower panels of Figure 33 (a) and (c).

4.3. Conclusions

Structure and behaviour was examined of a collapsed material which was identically prepared from diblock copolymer precursors as that of a benchmark nano-porous material except for the degree of cross-linking of the elastomeric PI matrix. At first sight the sample displayed no structural evidence as investigated by TEM, SAXS and SANS measurements of dry specimens, while the nano-porous benchmark material displayed hexagonally ordered cavities in agreement with the precursor morphology. However, this cross-linked material exhibited interesting properties as a gel when exposed to solvent which swells the PI matrix. A nano-structure is dormant and recovers inside the gel in such a fashion that the anticipated porosity is re-established, which matches the nanostructure of the benchmark nano-porous material under similar solvent conditions. The appearance of structure seems to be driven by a process, which swells the matrix and inflates the cavities, which are vacated by the original expendable block copolymer

component. These results resemble observations by Durkee et al. in a study on the microstructure in cross-linked diblock copolymer gels, which reported on solvent-filled open channels inside a network of swollen PI.[65] Furthermore, the structure also exhibits perfect agreement with the process of extrusion that was part of the preparation procedure. This was evidenced by anisotropic scattering caused by the presence of elongated (solvent filled) cavity structures aligned in the extrusion direction. Hence the collapsed elastomeric material has memory of the original precursor morphology and the preparatory extrusion alignment. Upon cycles of swelling and drying the nano-structure shows up and disappears – reversibly, which suggests that the presence and absence of solvent can open and close the cavities. Very interestingly, the cavities are not prune to be opened by non-solvents to the matrix, which suggests that the nature of the liquid (solvent or non-solvent) could control the state of the material in e.g. a membrane application. This means that the material could have some "smart" application in advanced separation systems and maybe used as a form of valve, where the liquid polarity would be the controlling external stimuli.

5. Application of nano-porous materials as membranes

Pore size and size distribution determine the separation properties of porous membranes. Separation and selectivity depend also on enthalpic interactions with the pore surfaces, therefore on the surface area and surface chemistry.[66][67][68] Size discrimination of membranes relevant for molecular filtration is expected to be significantly more effective with membranes having pores in the range of nanometer instead of micrometers.

Potential application as separation media is mentioned in almost any article on nanoporous materials (NPs) obtained from diblock copolymers.[18][27][69] Most of the existing literature reports focus on NPs with hexagonally packed cylindrical morphology (HEX) and cylindrical cavities oriented perpendicularly to the main surface of the membrane. Orientation of the cylinders in the flow direction (perpendicularly to the main surface) is necessary in order to use the material as a membrane.[70] Yang *et. al.* showed that thin nanoporous films of HEX morphology can be used indeed as an ultrafiltration media, for example to separate viruses.[71] In the case of membranes prepared from diblock copolymers, the gyroid (GYR) morphology is an interesting alternative to the hexagonal morphology. GYR is an isotropic cubic structure of $Ia\bar{3}d$ symmetry, as it was already mentioned in paragraph 3.2, and therefore porosity percolation is warranted with no need for structure pre-alignment procedures. One disadvantage relates to the difficulty of preparation of the gyroid morphology, since it occurs in a narrow range of the diblock copolymer micro phase diagram, i.e. in a narrow range of composition, chain length and temperature.[72] However once the boundaries of the GYR morphology are experimentally determined in the micro-phase diagram, samples of this morphology can be routinely synthesized by the advanced polymerization techniques.

5.1. Membrane material

According to Figure 4 and Table 4, only samples based on polybutadiene, with GYR morphology will be considered in Chapter 5. Four samples numbered as 1, 2, 3 and 4 are summarized in Table 9. Sample nr 1 was prepared from solvent casted BD14 polymer, whereas samples nr 2-4 were prepared from solvent casted BD2729. Characteristics of precursor polymer were already presented in Paragraph 1.2.1, Table 3. The solvent

casting operation was described at the beginning of Paragraph 1.3. The amount of polymer was calculated to obtain sample of 0.5 mm thickness.

All samples were cross-linked by dicumyl peroxide (DCP) at 140^{o}C for 2h. DCP was dissolved together with polymer in tetrahydrofurane (THF) before solvent casting. Details for cross-linking were already presented in Paragraph 1.4.
After the cross-linking 14 mm diameter discs were cut out of the cross-linked film, by using round knife, as presented on Figure 34.

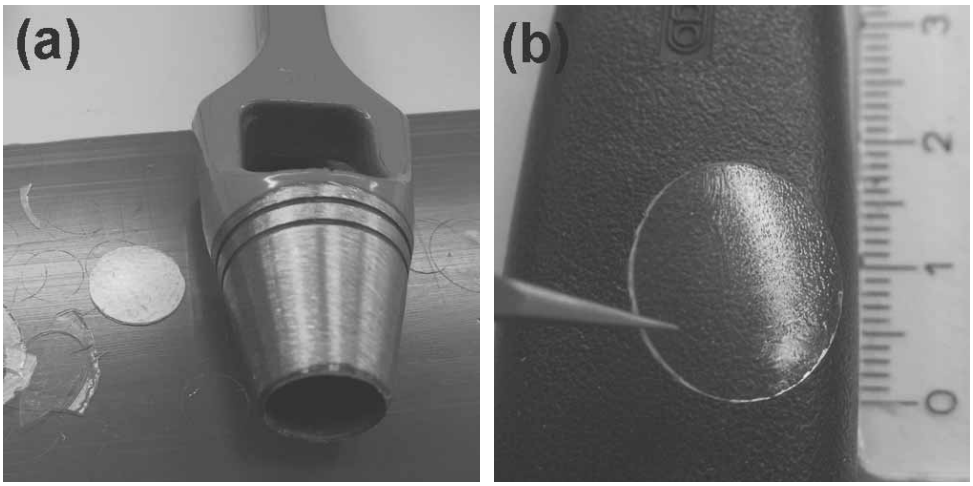

Figure 34 a. Round knife used for cutting a 14 mm diameter disc from cross-linked sample b. Sample disc.

For the purpose of further discussion two sides of the sample disc are distinguished. The side of the disc, which stacked to the bottom of a Petri dish, is called: 'glass' side. The side of the disc which had a contact with air, during solvent casting is called: 'air' side.

All samples discussed here were etched by using 1M solution of tetrabutylammonium fluoride (TBAF) in tetrahyfrofurane (THF). According to established procedure 5 times molar excess of TBAF relative to the PDMS repeating unit and a reaction time of 36h assure quantitative removal the PDMS block. After etching, the samples were rinsed in THF, mixtures of THF with methanol and at the end with pure methanol, before sample drying. This procedure, together with etching reaction was already presented in Paragraph 1.5.

Polishing operation of sample surface is introduced, since the assumption of the skin layer formed on the air side of the sample disc. This phenomenon will be explained further. Sample nr 1 was not polished. Sample nr 2 was polished only on the air side and samples nr 3-4 were polished on both sides. This information is placed in the third column of Table 9, where 'a' and 'g' stands for 'air' side and 'glass' side respectively. Samples were polished firstly on the air side with Waterproof Silicon Carbide Paper FEPA P#1000 by Struers. Sand-paper was wet with water and sample disc was moved on paper surface by a finger. In order to avoid any leaking of gas or liquid during filtration experiments, a 10,00-2,00 NBR 70 o-ring by M-Seals was glued by epoxy resin to the

glass side of sample discs 2-4. Glass side was polished only within the inert diameter of the o-ring.

Samples were checked for gas permeability and filtration experiments. Samples nr 1 and 4 were checked for both medium, whereas sample nr 3 was checked only for gas permeability and sample nr 2 was checked for filtration only. This is presented in a forth column of the Table 9, where G and S refers to 'gases and 'solutions'. Feeds used for filtration experiments for samples 1, 2 and 4 are summarized in the last column of Table 9. Details for feeds are presented in Paragraph 5.2.4.

One commercial ultrafiltration membrane from Alfa Laval (GR61PP) was investigated as a reference for nano-porous material. This is a polysulphone membrane on a polypropylene support. The active membrane area was 36.3 cm^2, as calculated from the internal diameter of the o-ring (6.8 cm).

Sample name:	Sample precursor:	Polishing a/g:	Gas/Solution G/S	Feed:
1	BD14-x1e	-	G/S	A, B, C
2	BD2729-x1e	a	S	B
3	BD2729-x1e	a/g	G	-
4	BD2729-x1e	a/g	G/S	F
GR61PP	-	-	S	D, E

Table 9 Summarization of polybutadiene based samples with GYR morphology used for membrane application.

5.2. Membrane performance

5.2.1. Setup

The set up, which is the final solution of many previous versions, is presented on Figure 35b. On part a. we can see the overview of set up. Nitrogen gas (1) was used to create a pressure on the feeding side of the membrane. Next elements are: pressure gauge (2), manometer (3), security valve (4), membrane device (5) and a glass (6) to collect a permeate at the end of outlet tube.
The membrane was mounted in the homemade stainless steel device, which is schematically presented on Figure 35b.

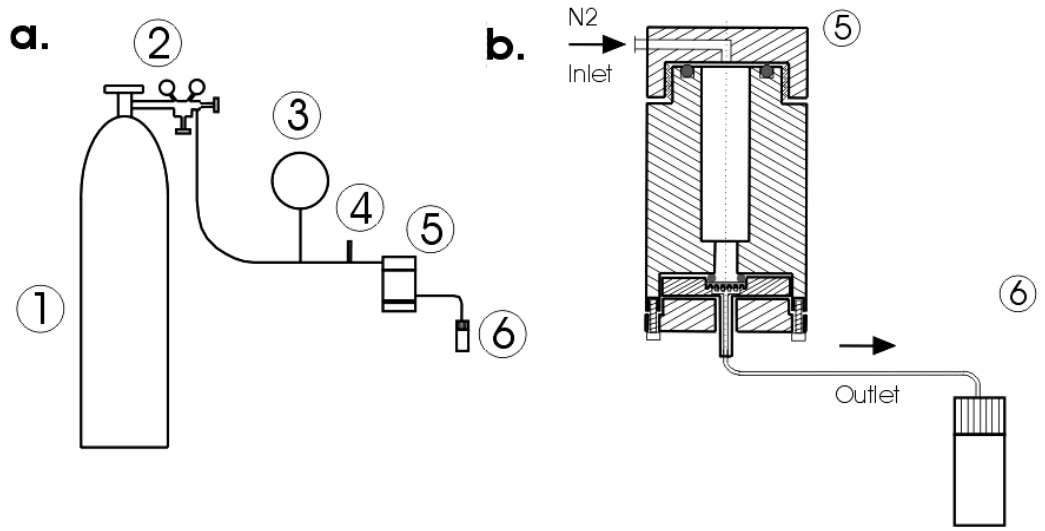

Figure 35 Schematic presentation of set up elements. Scheme a. shows the overview, which consists of: 1. nitrogen gas bottle; 2. gas reducer with valves; 3. manometer; 4. security valve; 5. membrane device; 6. permeate collecting glass. Scheme b. presents details of final version of membrane device with o-rings marked by red color.

The membrane device can withstand 50 bar pressure and can be filled in by 10 ml of liquid. Magnetic stirrer can be placed inside the device. Membrane sample is placed in the support with drainage system made of PVC. Permeate is collected through the drainage channels and the outlet tube to a 1 ml glass. Glass has marked 0.2 ml scale. Drainage part and whole membrane device is showed on Figure 36.

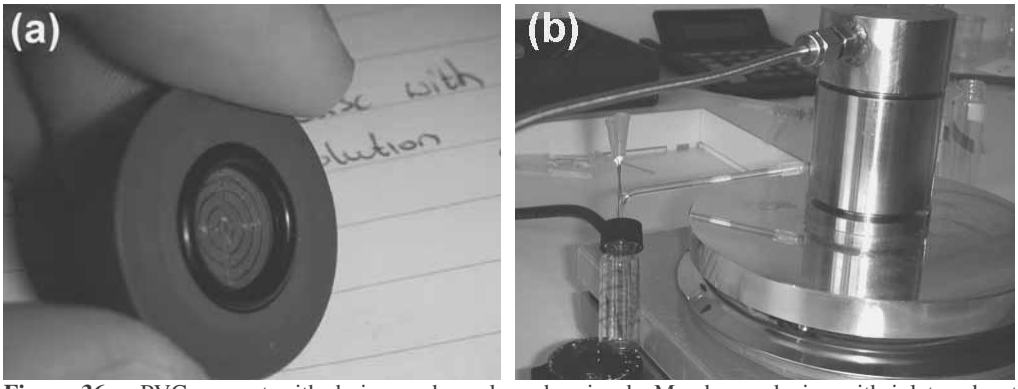

Figure 36 a. PVC support with drainage channels and o-ring b. Membrane device with inlet and outlet together with collecting glass.

Gas fluxes were measured on the same set up, except that a bubble flow meter was used instead of the collecting glass (element nr 6 on Figure 35).

The setup used for the investigation of the commercial membrane is similar to the scheme of Figure 35b, however the membrane device is bigger and made from glass and PVC. The device was filled with 400 ml of liquid in this case.

5.2.2. Gas fluxes

Fluxes of three different gases: nitrogen, hydrogen and carbon dioxide (all by AGA) were calculated from the speed of bubble displacement in the bubble flow meter.

5.2.3. Pure Solvents

Fluxes of pure solvents: methanol/water 80/20 volume ratios were calculated from the measurement of time needed to collect a given volume of permeate. Sample nr 1 was additionally measured for methanol/water 20/80 flux.

5.2.4. PEG solutions

Solutions of polyethylene glycol samples of different molecular weight: 1 kg/mol from Merck, 3 kg/mol, 8 kg/mol, 10 kg/mol, 12 kg/mol from Fluka, 56 kg/mol from Polymer Laboratories and 100 kg/mol from Serva was filtered through the NP disc.

Polyethylene glycols were dissolved in a mixture of methanol (MeOH) and water (80:20 volume ratio) in case of Feed A, B, D and F. 20% of water was added in order to ensure better dissolution of high molecular weight PEG. Pure methanol and 80:20 MeOH:H_2O penetrate exclusively the pore volume.[61]. Feed C and E was prepared by dissolving polyethylene glycols in a mixture of methanol/water (20:80 volume ratio).

Firstly the solution of PEG 1 kg/mol, PEG 10 kg/mol and PEG 100 kg/mol in MeOH/water (80:20) was prepared. The concentration of each of the components was 0.5mg/ml. This solution is called Feed A and was prepared for unpolished sample nr 1. Such a wide range of molecular weights was chosen for the preliminary experiment aiming at a first estimation of the cut off value. A more accurate determination of such a value was achieved at a second step by using five PEG samples covering the more restricted M.W. range 1 – 35 kg/mol. The solution of PEG 1 kg/mol, PEG 3 kg/mol, PEG 8 kg/mol, PEG 12 kg/mol and PEG 35 kg/mol with concentration of 0.5 mg/ml for each of the components in MeOH/water (80:20) is called Feed B in the following. This feed was used for filtration experiment for sample nr 1 and polished sample nr 2. The third feed solution with same concentration of polymer in MeOH/water (20:80) is referred to as Feed C and was prepared for sample nr 1.

In the case of the commercial membrane GR61PP solutions of five PEG (1k-35k) samples with individual concentration of 2 mg/ml were prepared either in methanol/water 80/20 (Feed D) or in methanol/water 20/80 (Feed E).
Solution of PEG 1 kg/mol, PEG 3 kg/mol, PEG 8 kg/mol, PEG 12 kg/mol and PEG 56 kg/mol with concentration of 0.5 mg/ml for each of the components in MeOH/water (80:20) is called Feed F and was examined on sample nr 4

All the feeds used for filtration are summarized in Table 10.

Feed	PEG (kg/mol)	Concentration (g/liter)	Solvent (methanol/water v/v)
A	1+10+"230"	0.5	80/20
B	1+3+8+12+35	0.5	80/20
C	1+3+8+12+35	0.5	20/80
D	1+3+8+12+35	2	80/20
E	1+3+8+12+35	2	20/80
F	1+3+8+12+56	0.5	80/20

Table 10 Feeds used for separation experiments. Polyethylene glycols of different molecular weights (second column) and given concentration of each PEG (third column) were dissolved in two mixtures of methanol and water (described by the volume fractions in the last column)

At least 0.6 ml of permeate was collected for each sample. Flux was measure for each 0.2 ml of collected volume.

The commercial membrane was treated similarly to the nanoporous membrane. The membrane was mounted in the separation device filled with 400 ml 80 methanol :20 water and left overnight without any stirring or pressure. Next day the mixture of methanol (80%) and water (20%) was percolated and the Feed D was filtered and the permeates at 1 bar, 2 bar and 3 bar of pressure were collected and analyzed by size exclusion chromatography. The mixture of methanol (80%) and water (20%) was percolated again. The mixture of methanol (20%) and water (80%) was run through the membrane. Feed E was filtered and the permeate at 1 bar, 2 bar and 3 bar pressure was collected and analyzed by size exclusion chromatography.

5.3. Characterization techniques

5.3.1. SEM and nitrogen adsorption

Specimen preparation and information about apparatus for SEM and nitrogen adsorption was already presented in Paragraph 2.1.1 and Paragraph 2.3 respectively.

5.3.2. Atomic Force Microscope AFM

Atomic Force Microscope is used to investigate surface morphology. It is based on measurements of interaction forces between investigated surface and a probe, which moves on the surface without damaging it. [73]

Atomic Force Microscope by Asylum Research, model MFP-3D^{TM} was used to investigate the samples surfaces.

Samples were placed on a silicon wafer and fixed by epoxy resin. Glass side and air side of unpolished sample and air side of polished sample was checked.

5.3.3. Size Exclusion Chromatography SEC

The size separation performance of the membranes was quantified by Size Exclusion Chromatography (SEC) of the feed and the collected permeate solutions. Water was the eluent at a flow rate of 0.6 ml/min. The sample injection volume was 40µl and the column used was Waters Ultrahydrogel™ 250 6µm 7.8 x 300 mm GPC column. The SEC setup consists of a 717plus Autosampler, a 600 Controller and a 410 Refractive Index Detector, all from Waters™.

5.3.4. DLS

Dynamic Light Scattering experiments were done at Risø National Laboratory by using Brookhaven-BI-2000 SM system with 35 mW HeNe Laser, 633 nm (Red). Measurements were operated at 100% attenuator and pinhole of different diameter (100, 200, 400 or 1000µm).

The same polyethylene glycols as used to prepare the feed solutions plus additional PEG standard (97.4 kg/mol) were dissolved in 3 ml of methanol/water (80/20) as presented in Table 11:

PEG [kg/mol]	Producer:	Concentration [mg/ml]
1	Merck 807488	20
3	Fluka 81230	20
8	Fluka 81268	10
10	Fluka 81280	10
12	Fluka 81285	10
35	Fluka 81310	5
55.6	Polymer Laboratories 20833-10	3
97.35	Polymer Laboratories 20835-9	2
230	Serva 33125	2

Table 11 Molecular weights of PEG (first column), used for solution in methanol/water 80/20. PEG producer and solution concentration are in second and third column respectively.

Around 2.5 ml of each sample was filtered by using 5 ml syringe with 0.2 µm Supor® Membrane on Acrodisc® Syringe Filter by Pall-life Science prior to measurements.

5.4. Results and discussion

5.4.1. Structure

SEM, Nitrogen adsorption

SEM and nitrogen adsorption results for cross-linked and etched nano-porous sample with GYR morphology was already presented in Paragraph 3.2.

Atomic Force Microscopy (AFM)

Unpolished sample

Two sides of solvent casted, cross-linked and etched samples were investigated under AFM. The air side and glass side of unpolished BD14 sample are presented on Figure 37 a and b respectively.

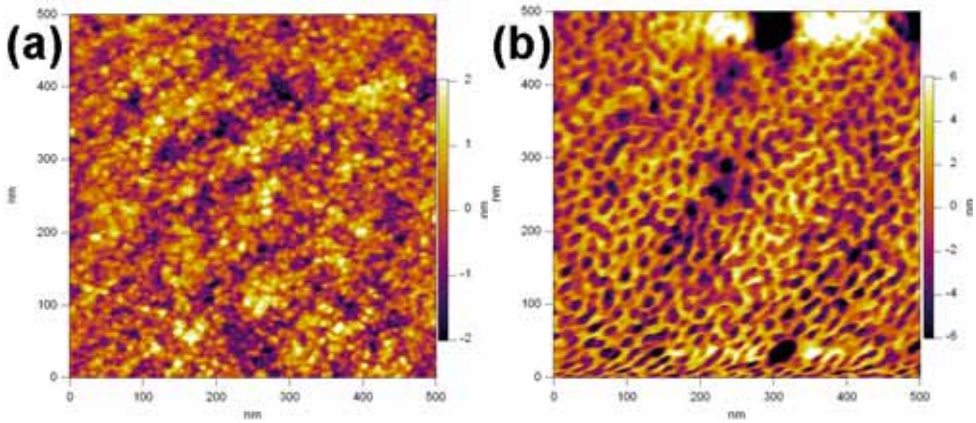

Figure 37 a. air side and b. glass side of unpolished sample BD14-x1e

Definitely the difference between the air and glass side can be seen. Air surface is almost flat, without clear holes or channels. Glass surface is very interesting, since it does not look perfectly gyroid, but we can see some channels. The pore size can be estimated to be: 11±1 nm.

The surface on the air side presented on Figure 37a is probably related to the presence of a skin layer. The skin layer exists on at least one side of the investigated samples. The presence of such a skin layer is plausible due to contribution of interfacial energy in the free energy balance at the sample boundaries. For example, given the low surface tension of the PDMS block in the precursor polymer it will be energetically favorable for the polymer interface to air to be enriched with PDMS. Therefore it is qualitatively expected that the lamella morphology, thermodynamically stable up to 100°C in the bulk, be stable even at higher temperature at the polymer-air interface.[74] If this phase transition

'retardation' is more than 10°C, then the probability that a thin (few tens of nanometer) layer at the interface gets crosslinked at a less opened morphology than the gyroid bulk is increased.

Zooming out the picture of glass side we can observe very big holes which are randomly distributed on bigger area, as shown in Figure 38.

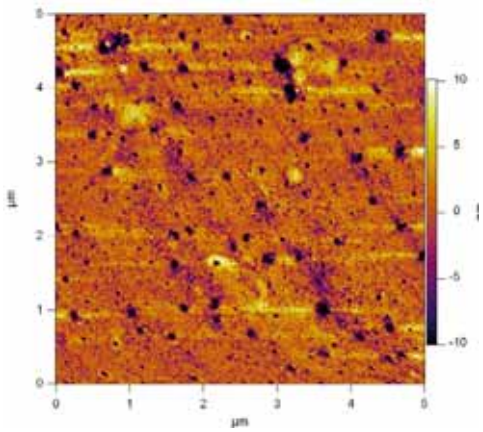

Figure 38 glass side of unpolished sample BD14-x1e at lower magnification. Clearly we can see large holes distributed on the whole surface.

Looking at the 3D picture of the glass side (not shown) the deepness of the holes was analyzed to be 70 – 80 nm deep. Since investigated film are 0.5 mm thick, there is no risk that these large diameter holes penetrate whole sample. These deep channels could be caused by adhesion between crosslinked polymer and Petri dish glass. Small pieces of polymer could retain on glass surface during removing the sample. It could also be caused by dust left on glass.

Polished samples

Sample polished by sand paper revealed porous gyroid morphology as presented on Figure 39. The result obtained by AFM fits very well to SEM results of gyroid morphology presented in Figure 26.

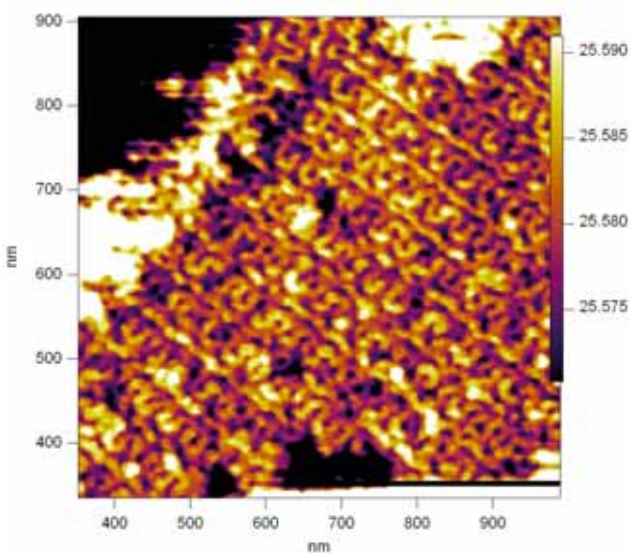

Figure 39 Projections of gyroid morphology on sample surface after polishing with sand paper.

5.4.2. Membrane performance

Gas fluxes

Knudsen flow is observed when a mean free path λ of gas molecules is larger or comparable to the pore size that we observe. Viscous flow occurs mainly for large pore size ($r \rangle 10 \mu m$), when the mean free path of gas molecules is much smaller than pore size. This is schematically presented on Figure 40[75]:

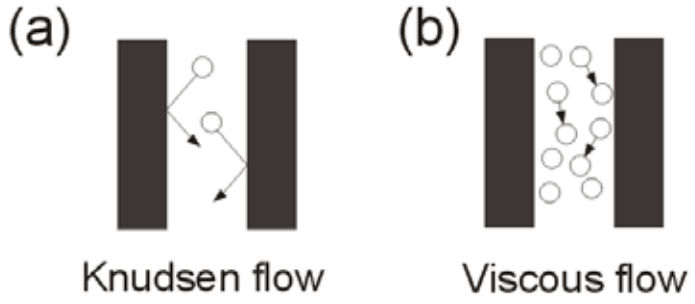

Figure 40 Schematic presentation of a: Knudsen flow and b: viscous flow

The mean free path is calculated as:[76]

$$\lambda = \frac{kT}{\sqrt{2}\sigma P} \qquad \text{Equation 13}$$

Where:

k	- Boltzmann constant $\left[J \cdot K^{-1}\right]$
T	- temperature $\left[K\right]$
σ	- collision cross-section $\left[m^2\right]$
P	- pressure $\left[Pa\right]$

The mean free path of Hydrogen gas is higher (98.7 nm) compared to the mean free path of nitrogen (62.0 nm) and carbon dioxide (51.3 nm) at standard conditions (0°C, 1bar) whereas the mean free paths of the last two gases is similar.

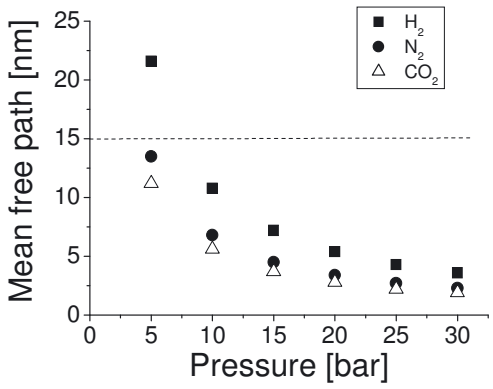

Figure 41 Mean free path of hydrogen, nitrogen and carbon dioxide at different pressures

Since the pore diameter of the nanoporous material is in average 15 nm, that is smaller or similar to the mean free path in all the pressure range tested (Figure 41), the Knudsen diffusion was expected to be the principal regime of gas diffusion in the present experiments [75]:

$$J = \frac{\varepsilon \cdot D_k \cdot \Delta P}{R \cdot T \cdot \tau \cdot l} \qquad \text{Equation 14}$$

Where:

J	- volume flux $\left[m^3 \cdot m^{-2} \cdot s^{-1}\right]$
ε	- surface porosity
D_k	- Knudsen diffusion coefficient $\left[m^2 \cdot s^{-1}\right]$
ΔP	- pressure difference $\left[Pa\right]$
R	- gas constant $\left[J \cdot K^{-1} \cdot m^{-3}\right]$
T	- temperature $= \left[K\right]$
τ	- pore tortuosity
l	- membrane thickness $\left[m\right]$

Since Knudsen diffusion coefficient D_k (Equation 15) is reciprocally proportional to the square root of gas molecular weight, we expect the highest flux for hydrogen and the lowest flux for carbon dioxide.

$$D_k = 0.66 \cdot r \sqrt{\frac{8 \cdot R \cdot T}{\pi \cdot M_w}} \qquad \text{Equation 15}$$

Where:

r - pore radius $[m]$

R - gas constant $\left[J \cdot K^{-1} \cdot mol^{-1}\right]$

T - temperature $[K]$

M_w - molecular weight $\left[kg \cdot mol^{-1}\right]$

Surface porosity ε is defined as ratio of pores area to the area of the whole membrane. In case of perpendicularly aligned HEX morphology the porosity ε is equal to the volume fraction f_{vol} of the pores. For the isotropic gyroid morphology the porosity is assumed to scale with the power of dimentionality, therefore the surface porosity ε is related to the volume porosity f_{vol} by $\varepsilon = (f_{vol})^{2/3}$. With $f_{vol} = 0.40$, $\varepsilon = 0.54$.

The tortuosity factor is a ratio between the length of the way gas molecule needs to travel to go through the membrane to the membrane thickness. In case of cylindrical pores aligned perpendicularly to the membrane surface the tortuosity factor would be equal to 1. The tortuosity factor for the gyroid morphology could not be found in the literature and is used as fitting parameter.

Results on fluxes of three different gases through nanoporous sample nr 1 are presented in Figure 42. Fluxes were normalized to 0.1 mm sample thickness. Hydrogen flux is much higher than nitrogen and carbon dioxide. The flux of CO2 is slightly lower than N2 for pressures up to 30 bar and slightly higher for 35 and 40 bar.

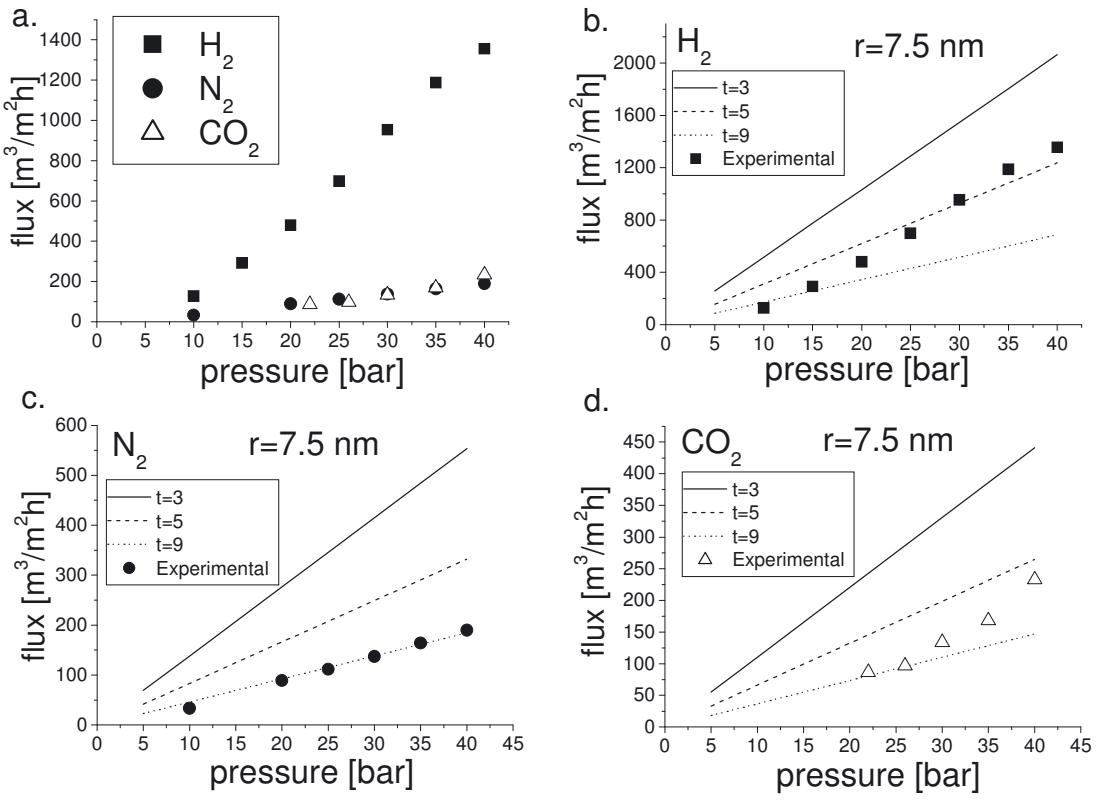

Figure 42 Sample nr 1 a: Experimental fluxes of H_2 (squares), N_2 (circles) and CO_2 (triangles); b, c and d: experimental (symbols) and theoretical values of flow according to Knudsen equation for pore diameter: 7.5 nm and at four different tortuosity factors: t=3 (solid line); t=5 (dash line); and t=9 (dot line). Fluxes are normalized to 0.1 mm sample thickness.

The pore radius was taken 7.5 nm and the experimental data for all the three gases fall between the tortuosity τ values 5 and 9 (Figure 42). Linear extrapolations of the data trends in Figure 42 b, c to zero flux yield 'residual' pressure values between 3.3 and 13 bars. This deviation from the prediction of eq. 14, is probably related to the presence of a skin layer. The case of CO_2 in Figure 42 d is more uncertain due to difficulties in measuring the flux of this gas with the bubble meter. The possible reason for such difficulties is related to the instability of bubbles in the presence of CO_2. Reliable data on the flux of CO_2 for pressures below 22 bars could not be obtained as shown in Figure 42 d.

Results for samples nr 3 and 4, which were polished on both sides of a disc, are presented in Figure 43 and Figure 44 respectively.

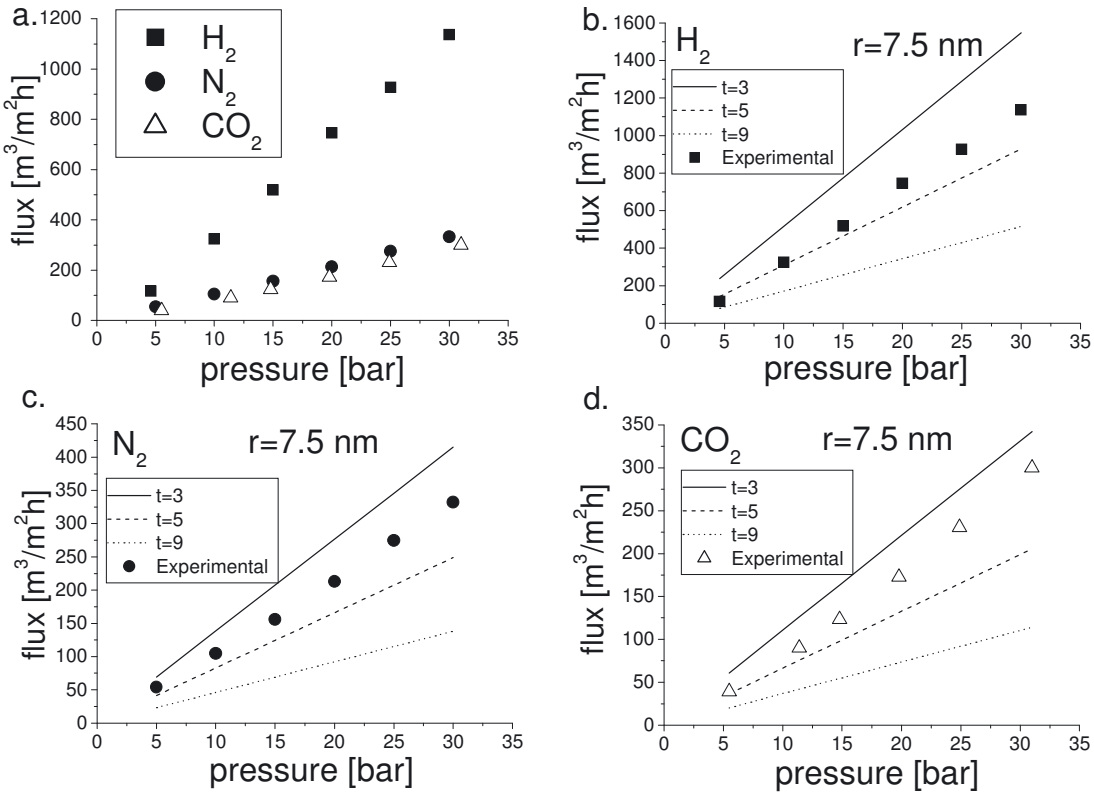

Figure 43 Sample nr 3 a: Experimental fluxes of H_2 (squares), N_2 (circles) and CO_2 (triangles); b, c and d: experimental (symbols) and theoretical values of flow according to Knudsen equation for pore diameter: 7.5 nm and at four different tortuosity factors: t=3 (solid line); t=5 (dash line); and t=9 (dot line). Fluxes are normalized to 0.1 mm sample thickness.

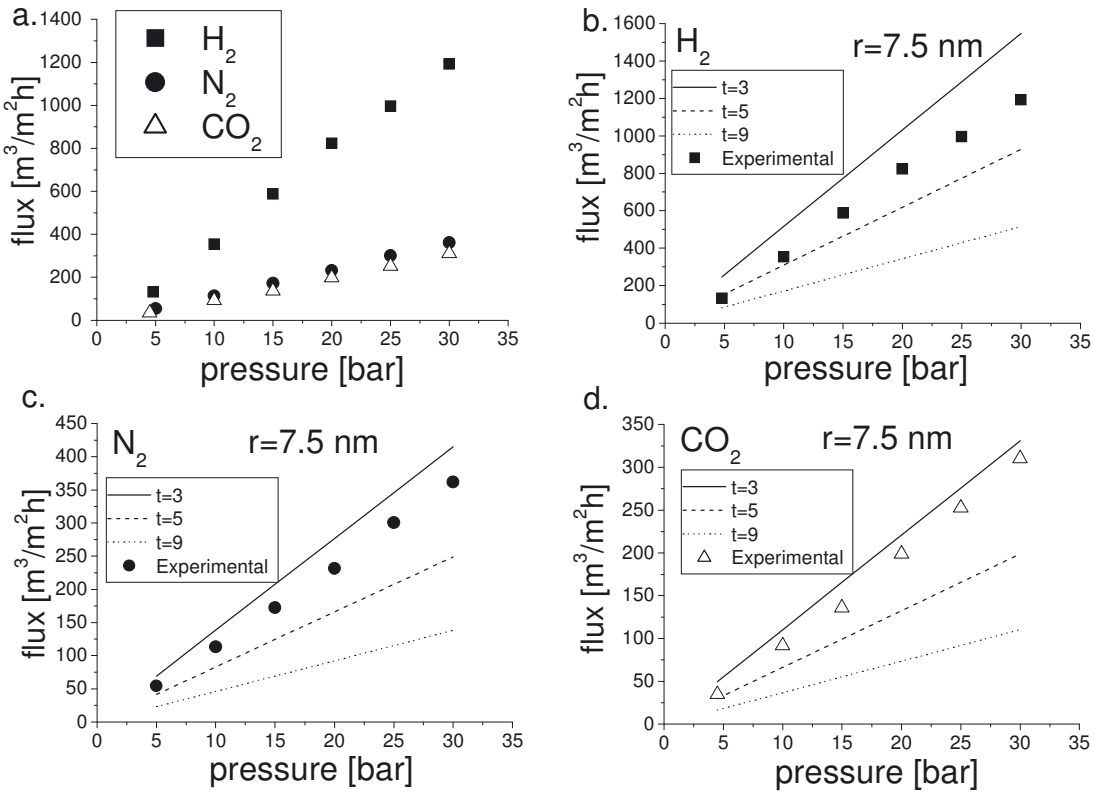

Figure 44 Sample nr 4 a: Experimental fluxes of H_2 (squares), N_2 (circles) and CO_2 (triangles); b, c and d: experimental (symbols) and theoretical values of flow according to Knudsen equation for pore diameter: 7.5 nm and at four different tortuosity factors: t=3 (solid line); t=5 (dash line); and t=9 (dot line). Fluxes are normalized to 0.1 mm sample thickness.

Permeability coefficient in Barrer, permeability coefficient ratios, value of fitted tortuosity factor and pressure values for flux extrapolated to zero are summarized in Table 12.

Sample nr:	polishing:	Permeability coefficient[Barrer]		
		H_2	N_2	CO_2
1	-	$9.72 \cdot 10^5$	$1.62 \cdot 10^5$	$1.68 \cdot 10^5$
3	a/g	$1.26 \cdot 10^6$	$3.98 \cdot 10^5$	$3.15 \cdot 10^5$
4	a/g	$1.38 \cdot 10^6$	$4.28 \cdot 10^5$	$3.48 \cdot 10^5$

sample:	polishing:	Permeability coefficient ratio		
		H_2/ N_2	H_2/ CO_2	N_2/ CO_2
1	-	6.00	5.79	0.98
3	a/g	3.17	4.00	1.26
4	a/g	3.22	3.97	1.23

sample:	polishing:	Tortuosity factor		
		H_2	N_2	CO_2
1	-	9.01	5.22	6.56
3	a/g	4.20	3.82	3.62
4	a/g	3.90	3.50	3.31

sample:	polishing:	Pressure [bar] at zero flux		
		H_2	N_2	CO_2
1	-	7.88	3.33	13.00
3	a/g	1.86	0.59	2.42
4	a/g	1.41	0.82	1.65

Table 12 Results for measuring flux of three different gases: H_2, N_2 and CO_2 for two polished samples nr 3 and nr 4 and one unpolished sample nr 1. First part (from top) summarizes gas permeability coefficient expressed in Barrer (1 Barrer = 10^{-10} cm^3 (STP) $\cdot cm \cdot cm^{-2} \cdot s^{-1} \cdot cmHg^{-1}$). Second part presents ratios of permeability coefficients and third part gives tortuosity factors fitted to Knudsen flow equation. The last (bottom) part of the table shows pressure values (bar) after extrapolating experimental data to zero flux value.

All values in Table 12 for samples nr 3 and nr 4 are close to each other, but very different from data for sample nr 1. Permeability coefficient for all three gases increased after polishing (c.a. 36% for hydrogen, 155% for nitrogen and 97% carbon dioxide). Fitted tortuosity factor shows lower value. For polished sample it falls between 3.3 and 4.2. Finally pressure value for flux extrapolated to zero moves to lower values.

Pure solvent flux

Fluxes of pure solvents for all samples, normalized to 0.1 mm thickness are summarized in Table 14 and its more detailed version: Table 15. Flux for sample nr 1 checked for MeOH/water 80/20 for the first time is 0.16. It is much higher for sample nr 2 (1.44 $dm^3 \cdot m^{-2} \cdot h^{-1} \cdot bar^{-1}$), which was polished only on the air side, and even higher for sample nr 4 (2.71 $dm^3 \cdot m^{-2} \cdot h^{-1} \cdot bar^{-1}$) which was polished on both sides. This indicates, similarly like

in case of gas measurements, that indeed skin layer is removed during the polishing process.

In case of unpolished sample nr 1 very high pressure needed to be applied (38 ± 1 bar) to observe 1 - 2 $dm^3 \cdot m^{-2} \cdot h^{-1}$ flux at 0.5 mm sample thickness. After polishing this thickness falls to 0.3 mm, 4 times lower pressure is applied (10 bar) and the flux is 4.6 $dm^3 \cdot m^{-2} \cdot h^{-1}$ for sample nr 2 and 9 $dm^3 \cdot m^{-2} \cdot h^{-1}$ for sample nr 4.

Already mentioned skin layer is one of the explanations for very low flux in case of unpolished sample nr 1. Additionally the highly networked gyroid porous morphology could disturb the laminar flow and increase the resistance to flow, constituting a second possible reason.

Size separation of polymers in solution

Results of polymer characterization by DLS

Results of dynamic light scattering obtained with 400 μm pinhole are presented in Table 13. The selection of the pinhole opening in front of the detector was a balance between acceptable photon count rate and quality of correlation function.

Experimental			Literature			Theoretical		
PEG [kg/mol]:	Average $R_h \times 2$ [nm]:	Conc. [mg/ml]:	PEG [kg/mol]:	Average $R_h \times 2$ [nm]:	Conc. [mg/ml]:	PEG [kg/mol]:	$R_g \times 2$ [nm]	$R_h \times 2$ [nm]
1	1.55	20	1.45	2.26	30.98	1	2.94	1.99
3	3.74	20	3.35	3.58	18.23	3	5.81	3.94
8	5.23	10	8.5	5.84	6.50	8	10.47	7.09
10	7.72	10				10	11.97	8.11
12	11.33	10	11.84	6.98	6.00	12	13.36	9.04
35	16.43	5	35	13.18	3.80	35	25.39	17.19
55.6	21.08	3				55.6	33.52	22.69
97.35	36.21	2	100	23.9	1.82	97.35	46.91	31.76
230	46.83	2				230	78.57	52.38

Table 13 Hydrodynamic diameter average value from dynamic light scattering. Literature experimental data and calculated values (see the discussion related to fig. 5 in the main text) are presented for comparison

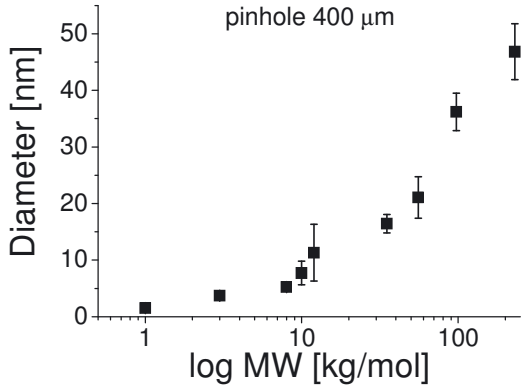

Figure 45 Diagram showing experimental results for hydrodynamic diameter for PEG molecules.

The experimental results for hydrodynamic diameters of PEG samples were compared to theoretical values calculated in the following way. First the radius of gyration R_g for PEG molecules was calculated as:

$$R_g = \frac{1}{6} \cdot R_o^2 \qquad \text{Equation 16}$$

where:

R_o^2 - mean square end-to-end distance

R_o^2 in a good solvent, as is the case of PEG in the (methanol : water) mixed solvent, is expressed as:

$$\overline{R}_o^2 = C_n \cdot n^{1.2} \cdot b^2 \qquad \text{Equation 17}$$

where:

C_n - the characteristic ratio calculated as a function of chain length[77]

n - number of covalent chain bonds

b - average bond length

C_n value tells us about the flexibility-rigidity of the polymer chain. If the polymer makes one step from starting point, than there is a question: where will be the next step? If it is totally random in case is flexible chain, than we say that C_n value is 1. It has to take some additional steps in order to cover with the initial step if the chain has some rigidity. C_n value depends on bonds number in the chain and in case of high molecular weight PEG $C_n \approx 4$. Based on reference mentioned above, we take $C_n = 3.81$ for PEG 1 kg/mol and $C_n = 4$ for all higher mol weights.

Number of covalent chain bonds can be calculate easily, since we now the mass of PEG repeating unit: 44.05 g/mol and molecular weight of PEG. Obtained number of repeating

units per chain has to be multiplied by 3, since there are 3 covalent bonds in the backbone of PEG repeating unit chain:

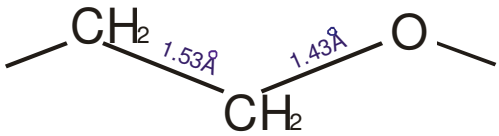

Figure 46 Repeating unit of poly(ethylene glycol) molecule.

Finally the average bond length b in above equation is calculated as the sum of bond length in the backbone of repeating unit cell ($1 \cdot 1.53\text{Å} + 2 \cdot 1.43\text{Å}$) divided by its number (we have 3 bonds), which gives $b = 1.46\text{Å}$.

The value of mean square end-to-end distance depends on the solvent we use and this changes the power to which we rise n value. $\overline{R}_o^2 = C_n \cdot n \cdot b^2$ if we use the Θ-solvent. In Θ-solvent polymer chain has not preferential to solvent or polymer. In case of good solvent (better than Θ-solvent) polymer chain will prefer to meet solvent molecules than other polymer chains, so it will swell and the end-to-end distance will increase. In good solvent we have $n^{1.2}$.

The calculated values for the diameter of gyration ($2R_g$)as a function of molecular weight are presented by the solid line in the double logarithmic plot of Figure 47:

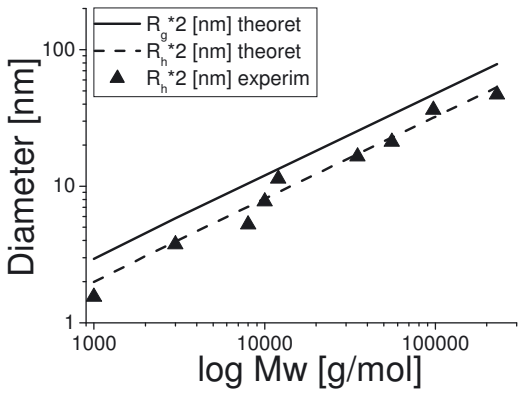

Figure 47 Diameter of gyration (solid line) $2R_g\ [nm]$ calculated from Equation 4; hydrodynamic diameter (dash line) $2R_h\ [nm]$ calculated from the theoretical $R_g\ [nm]$ as described in the main text; experimental data of hydrodynamic diameter $2R_h\ [nm]$ obtained from dynamic light scattering results (triangles).

The 2xR_g values are collected in the eighth column of Table 13. In order to compare the calculated results with the experimental values a proportionality factor between R_g and

R_h was needed; such a factor was found in the literature[78] : $R_h \approx \frac{2}{3} R_g$. The ratio between theoretical gyroid diameter and experimental hydrodynamic diameter was calculated for PEG 35; 55.6 and 97.35 kg/mol than. The average value is 1.48, which fits perfect to literature value: $\frac{R_g}{R_h} \approx \frac{3}{2}$. Based on this ratio values of the theoretical hydrodynamic diameter, $2R_h\left[nm\right]$ were calculated and presented by the segmented line in Figure 47. Values of hydrodynamic diameter are collected in the last column of Table 13. Experimental results of $2R_h\left[nm\right]$ from dynamic light scattering are shown by triangles in Figure 47.

Experimental results from dynamic light scattering are also compared with experimental literature data[79] from quasi-elastic light scattering for polyoxyethylene (POE) prepared in phosphate-buffered saline at 25°C. These data are listed in the middle section of Table 13. The overall comparison of our experimental data with the combined literature experimental data and the calculated values is considered satisfactory.

Size separation (ultrafiltration) through the gyroid membrane

Unpolished sample nr 1

10 ml of Feed A (Table 10) which is a solution of PEG 1 + 10 + 100 kg/mol in methanol/water 80/20, and Sample 1 (nanoporous disc) were placed in the filtration device. Permeates were analysed by SEC. The 1st Permeate means the first 0.8 ml of permeate collected in the 1ml glass and analysed by SEC. 2nd Permeate and 3rd Permeate were the following 0.8 ml and 0.6 ml of collected volume respectively. Results are presented in Figure 48 a, as the detector response in milivolts vs. retention time in minutes. The fluxes of all the PEG solutions were similar to the fluxes of the solvents. Fluxes listed in Figure 48 a are fluxes in $dm^3 \cdot m^{-2} \cdot h^{-1}$ for not normalized sample thickness (0.53 mm) at 38 bar pressure.

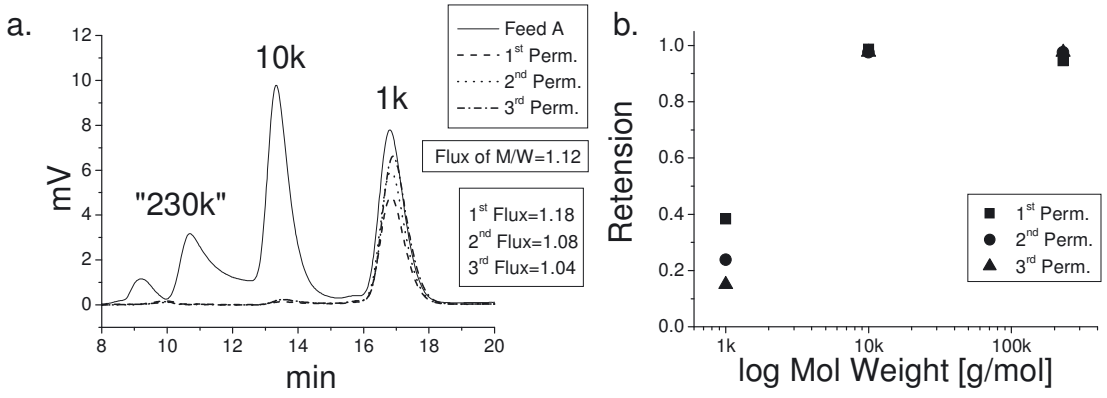

Figure 48 a) Size exclusion chromatography results of filtration Feed A on Sample nr 1. . b) Retention curve based on the analysis of feed and permeates' peaks height

The "PEG 100 000 [g/mol]" showed a bimodal distribution in SEC with MW values of each peak of 230 kg/mol and 60 kg/mol, respectively.

The retention (R) value (Figure 48b) is calculated as: $R = 1 - \frac{C_P}{C_F}$, where C_p and C_F are the concentration [mg/ml] of the permeate and the feed respectively. Knowing the concentration of each of PEG in the Feed A (0.5 mg/ml) the permeate concentration was found from the ratio of permeate and feed peak height.

From the Figure 48 it is seen that the membrane is permeable for PEG 1 kg/mol and the retention for this polymer decreases in the successive collected permeates. The peak for PEG 230 kg/mol in all permeates is virtually gone and the retention for these molecules is close to 1.

The same disc of sample nr 1 was used to filter Feed B (Table 10), which is a solution of PEG 1+3+8+12+35 kg/mol in methanol/water 80/20. Permeates were analysed by SEC. The 1st, 2nd and 3rd Permeate mean the first, second and third 0.8 ml of permeate collected. Results are presented in Figure 49.

The retention values of the 2nd and 3rd permeates were almost identical as shown in Figure 49 b. The retention profile is almost consistent with the profile of Figure 48 b.
Experimental results were compared with a model from literature.[80] In this model the maximum retention of each PEG was calculated for the following values of nanopore diameter: 8 nm, 10 nm, 12 nm and 15 nm. The results are presented in Figure 49 c. The experimental results follow the prediction for a pore diameter of 12 nm, which is within the measured by nitrogen adsorption: 15 ± 4 nm.

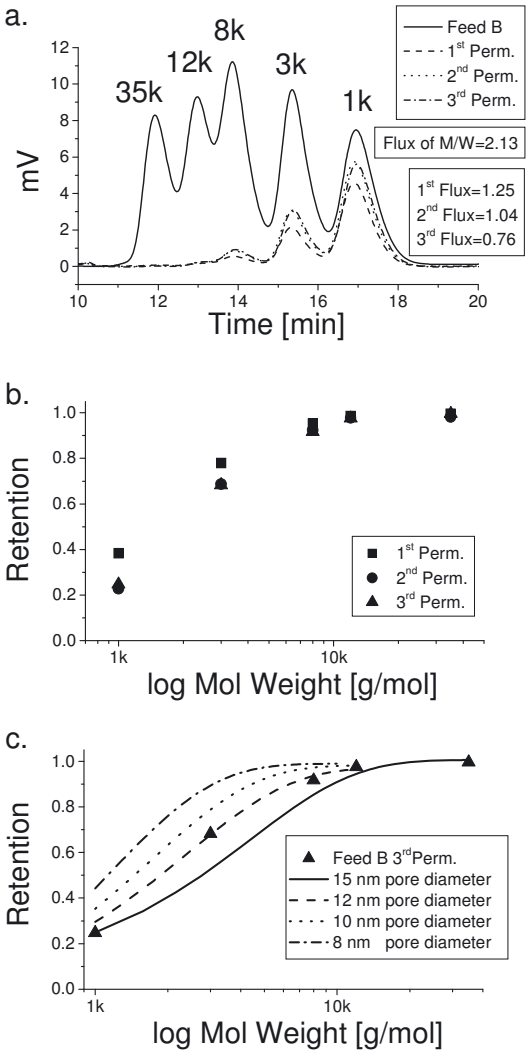

Figure 49 a) Size exclusion chromatography results of filtration Feed B (PEG 1+3+8+12+35 kg/mol in methanol/water 80/20) on Sample nr 1 b) Retention curve based on the analysis of feed and permeates peaks height. c) Comparison between the retention curve for 3rd Perm from experimental data and calculated maximum retentions for four different pore sizes.

Sample nr 1 was stored in methanol for 99 days. After a preconditioning in methanol/water 20/80 the disc was used to filtrate Feed C (Table 10), which is a solution of PEG 1+3+8+12+35 kg/mol in methanol/water 20/80. Four successive permeates (three times 0.8 ml and last one 0.6 ml) were collected and analysed by SEC. The results are presented in Figure 50. Again a good reproducibility of retention profile was observed after the first permeate, as shown in Figure 50 b.

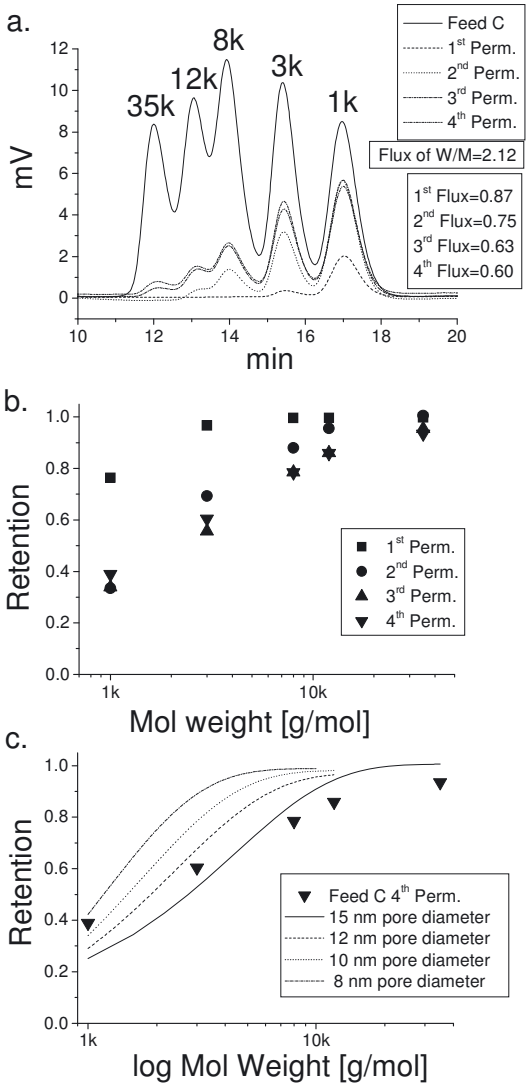

Figure 50 a) SEC results after filtration of Feed C (PEGs in methanol/water 80/20) by using sample nr 1 at 40 bar b) retention profiles of four profiles c) Comparison between the retention curve for 3rd Perm from experimental data and calculated maximum retentions for four different pore sizes.

The large difference between 1st and following permeates can come from the fact, that sample was soaked in methanol before PEG filtration. 1st permeate is diluted by solvent left in the sample. 3rd and 4th permeate show the steady state is reached. Same tendency is observed for Feed A (Figure 48) and Feed B (Figure 49).

The separation properties of a commercial polysulphone membrane, GR61PP by Alfa Laval were investigated and compared to the properties of the nanoporous sample. The results of Feed D (Table 10), which is a solution of PEG 1+3+8+12+35 kg/mol in

methanol/water 80/20, filtration after overnight membrane conditioning in methanol/water 80/20 are presented in Figure 51

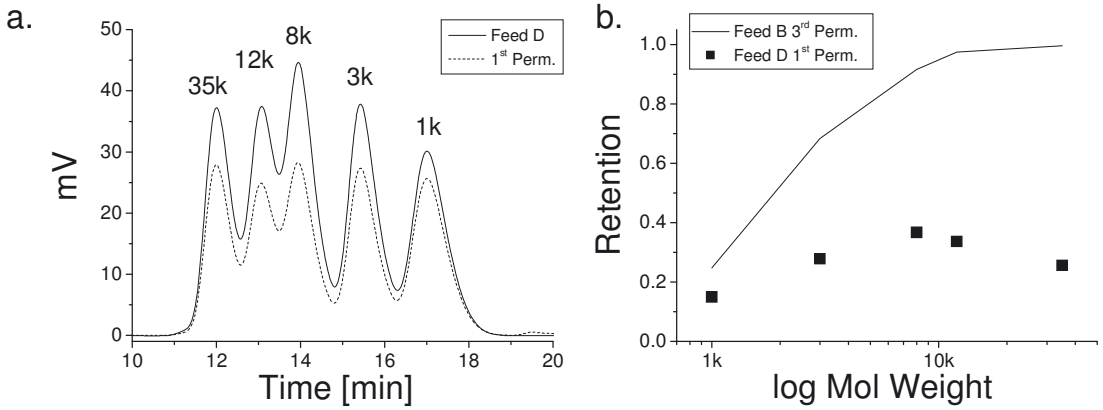

Figure 51 Separation curves for GR61PP. Figure 51 a shows curves for Feed D and the following permeate. Figure 51 b compares the retention curves for Feed B through the nanoporous disc (see Figure 49) and the filtration of Feed D through the commercial membrane.

The separation performance of the nanoporous disc was little sensitive to the change of solvent tested in this work, while the sulphone membrane did not show satisfactory separation in the methanol-rich solvent (see Figure 51). The performance of the commercial membrane was also very sensitive to pressure variations. The retention profiles of the nanoporous disc in the two kinds of solvents are superposed as lines in Figure 51 and Figure 52 b and they show at least as good selectivity as the polysulphone membrane when this last performs best.

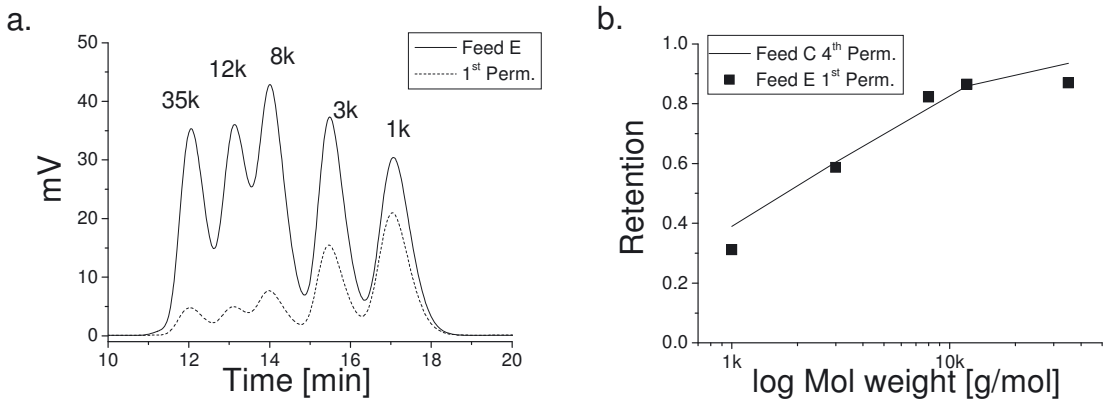

Figure 52 Separation curves for GR61PP. Figure 52 a shows curves for Feed E and the following permeate. Figure 52 b presents the retention curves for commercial membrane and nanoporous sample.

The measured fluxes, of the order of 1 $l\ m^{-2}\ h^{-1}$ at 40 bars, are extremely low. The huge disk thickness in the ultrafiltration membrane context and the presence of the skin layer are the two main reasons responsible for the low flux. The flux at thickness 1 μm and 1 bar can be extrapolated to 13 $l\ m^{-2}\ h^{-1}$ assuming inverse and direct proportionality of flux on thickness and pressure, respectively. For comparison, the flux through the well-performing polysulphone membrane at 1 bar was 26 $l\ m^{-2}\ h^{-1}$.

Polished samples nr 2 and 4

Firstly 10 ml of Feed B (Table 10) which is a solution of PEG 1 + 3 + 8 + 12 + 35 kg/mol in methanol/water 80/20, and Sample nr 2 (nanoporous disc) were placed in the filtration device. Permeates were collected and analysed by SEC in the same way as for sample nr 1, except that this time 5 following permeates were analysed. Results are presented in Figure 53. Flux listed in Figure 53 a are fluxes in $dm^3 \cdot m^{-2} \cdot h^{-1}$ for not normalized sample thickness after polishing an air side (0.34 mm) at 11 bar pressure.

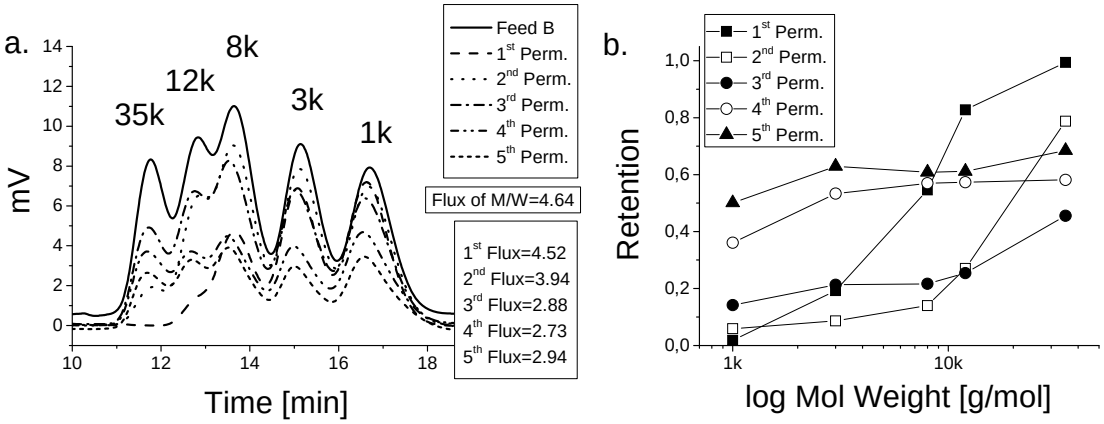

Figure 53 a) Size exclusion chromatography results of filtration Feed B on Sample nr 2. b) Retention curve based on the analysis of feed and permeates' peaks height

The result for the 1st collected permeate was very promising. 35 k PEG molecules were separated and quite sharp cut-off curve was obtained at high flux. Unfortunately in 2nd permeate 35 k molecules peak appeared, increased at 3rd permeate and than stabilized for 4th and 5th permeate. In the same time peak for low molecular weight PEG decreased. The effect is, that the retention curve presented in Figure 53 b get more and more flatten with each following permeate. Such observations could indicate high concentration polarization. Closed look at the setup design revealed, that there was probably not sufficient stirring in the membrane device. Magnetic stirrer does not operate close to the membrane surface, which means that there is some "dead" volume in which there is no stirring. This volume is marked by blue color on Figure 54 .

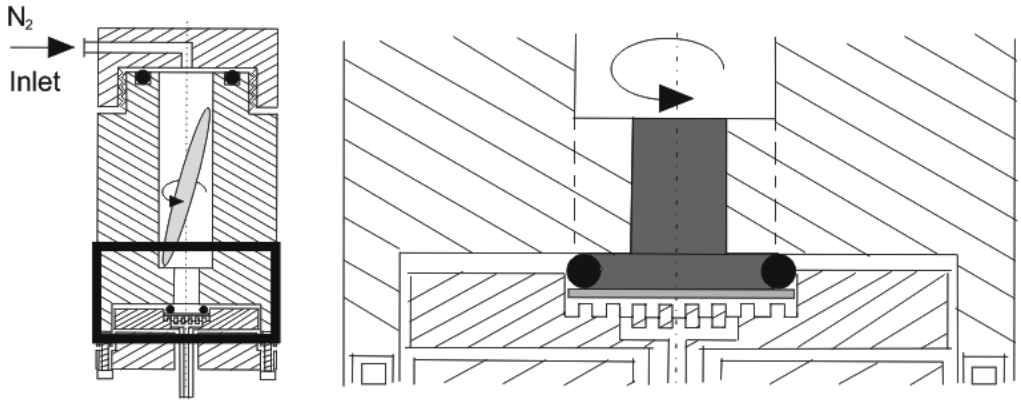

Figure 54 Scheme of membrane device. The inset points out the 'dead' volume marked by blue color. Sample disc is marked by yellow color.

Lack of stirring causes very high concentration polarization. If we assume, that there is sufficient stirring, than concentration of PEG molecules at the membrane surface should be very close to the concentration in the bulk of feed solution (C_b). Concentration in the permeate (C_{p1}) will be lower. This is what we observed for the first collected permeate (red curve on Figure 53).

In case of not sufficient stirring concentration of high molecular weight molecules increases close to the membrane surface, comparing to feed concentration in the bulk. In such situation, even though the membrane could separate molecules, its concentration in the permeate is very high (C_{p2}) and it will be closer and closer to the feed concentration with the following permeates collected. This is schematically presented on Figure 55.

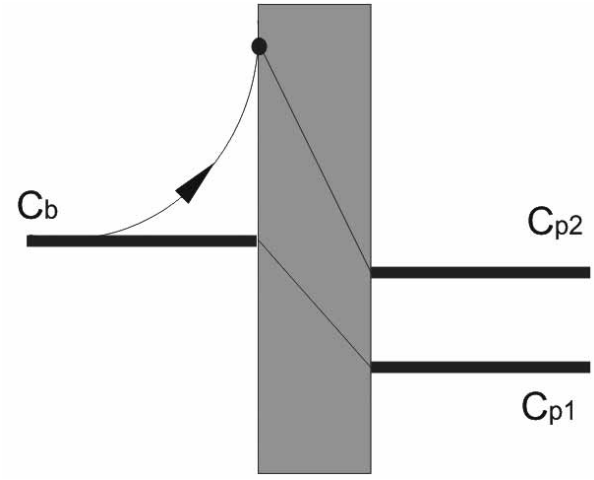

Figure 55 Shematic presentation of concentration polarization. C_b stands for concentration in the bulk and C_p stands for concentration in the permeate.

Polished on both sides sample nr 4 was analyzed for filtration of Feed F (Table 10). In order to minimize the concentration polarization sample was cleaned after each permeate collected. After collecting first permeate device was filled with 10 ml of MeOH/water 80/20 without removing the sample. 0.6 ml of pure solvent was collected and analyzed by SEC. Than sample was removed and cleaned by rinsing both sides with methanol. Sample was placed back in the membrane device and again 0.6 ml of MeOH/water was collected. After 2nd permeate sample was removed and rinsed with methanol. Finally the 3rd permeate was collected.

SEC results together with retention curve are presented on Figure 56 a and b respectively. Fluxes listed in Figure 56 a are fluxes in $dm^3 \cdot m^{-2} \cdot h^{-1}$ for not normalized sample thickness after polishing both sides (0.30 mm) at 10 bar pressure. The average fluxes in $dm^3 \cdot m^{-2} \cdot h^{-1} \cdot bar^{-1}$] after normalization to 0.1 mm thickness are summarized in Table 14 and detailed information showing fluxes for each collected 0.2 ml volume is presented in Table 15.

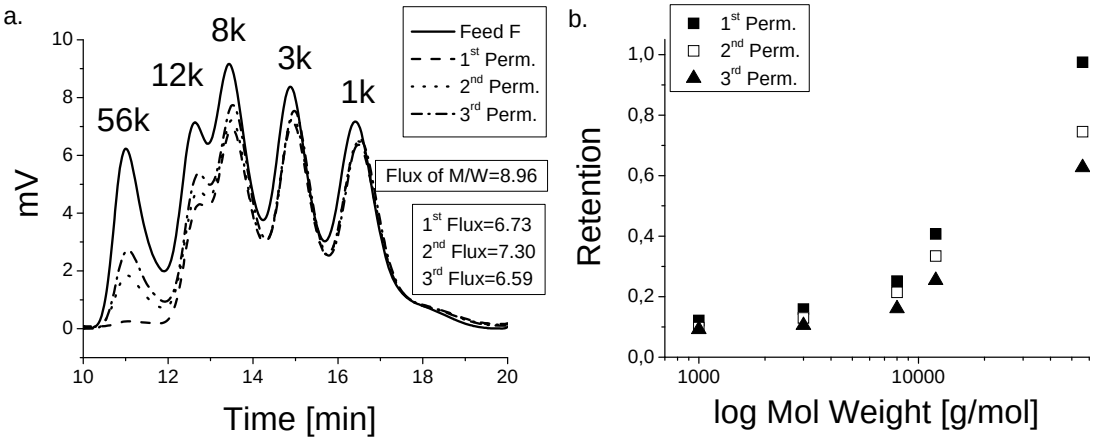

Figure 56 a) Size exclusion chromatography results of filtration Feed F on Sample nr 4. b) Retention curve based on the analysis of feed and permeates' peaks height

Again the first collected permeate shows retention for 56k very close to 1, but with the fallowing 2nd and 3rd permeate even this higher molecular weight peak appeared.

Fluxes normalized to 0.1 mm thickness for each 0.2 ml (Table 15) are much higher comparing unpolished sample nr 1 and to polished on the air side sample nr 2 also. Within the first permeate collection, the flux falls down from 2.77 $dm^3 \cdot m^{-2} \cdot h^{-1}$ for the first 0.2 ml, to 1.61 for third 0.2 ml. The flux of pure solvent increases to 2.81 $dm^3 \cdot m^{-2} \cdot h^{-1}$ value after cleaning the sample with methanol. Similarly decreasing of flux was observed during collecting 2nd and 3rd permeate. Flux increased during cleaning the sample with MeOH/water in between 2nd and 3rd permeates. SEC results from collected pure solvent in presented in Figure 57. As expected the peak height is reversed comparing to the

results from permeates. 56 k peak disappears after second cleaning following the 1st permeates collection. Cleaning after 2nd permeate shows 56 k peak,

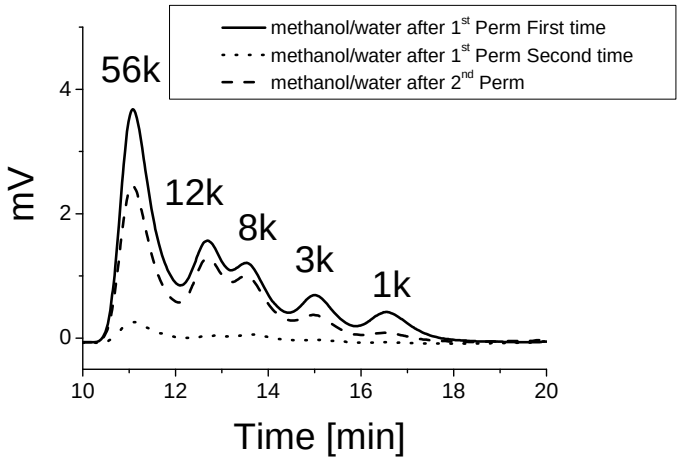

Figure 57 Size exclusion chromatography results of cleaning Sample nr 4 after filtration PEG solution Feed F.

To confirm correct sealing of the membrane additional experiment was done. 2 ml of permeates from Feed F PEG solution was collected overnight at 10 bar pressure. 56 k peak appeared after SEC analysis, so previous results should not be caused by any leakage caused by unsealing the membrane device during cleaning operation.

		Flux [$dm^3 \cdot m^{-2} \cdot h^{-1} \cdot bar^{-1}$] Normalized to 0.1 mm thickness				
	Sample nr:	1			2	4
Solution:	Feed:	A	B	C	B	F
MeOH/Water 80/20	Average:	0.16	0.31	0.29	1.44	2.71
1st Permeate	Average	0.18	0.18	0.15	1.40	2.04
MeOH/Water 80/20	Average					2.18
MeOH/Water 80/20	Average					2.81
2nd Permeate	Average	0.15	0.14	0.11	1.22	2.21
MeOH/Water 80/20	Average					2.54
3rd Permeate	Average	0.13	0.10	0.08	0.89	1.99
4th Permeate	Average			0.08	0.93	
5th Permeate	Average				1.00	

Table 1 Flux [$dm^3 \cdot m^{-2} \cdot h^{-1} \cdot bar^{-1}$] average values normalized to 0.1 mm thickness for samples nr 1, 2 and 4.

		Flux [$dm^3 \cdot m^{-2} \cdot h^{-1} \cdot bar^{-1}$] Normalized to 0.1 mm thickness				
	Sample:	1			2	4
Solution:	Feed:	A	B	C	B	F
MeOH/Water 80/20	1st 0.2 ml	0.16	n. n.	0.35	1.47	2.74
	2nd 0.2 ml	0.16	n. n.	0.29	1.34	2.68
	3rd 0.2 ml	0.15	0.32	0.29	1.49	2.71
	4th 0.2 ml	-	0.30	0.26	-	-
	5th 0.2 ml	-	-	0.24	-	-
	Average	**0.16**	**0.31**	**0.29**	**1.44**	**2.71**
1st Permeate	1st 0.2 ml	0.23	0.24	0.20	1.46	2.77
	2nd 0.2 ml	0.15	0.17	0.14	1.27	1.73
	3rd 0.2 ml	0.16	0.16	0.16	1.46	1.61
	4th 0.2 ml	0.15	0.15	0.12	-	-
	Average	**0.18**	**0.18**	**0.15**	**1.40**	**2.04**
MeOH/Water 80/20	1st 0.2 ml					1.86
	2nd 0.2 ml					2.15
	3rd 0.2 ml					2.53
	Average					**2.18**
MeOH/Water 80/20	1st 0.2 ml					2.78
	2nd 0.2 ml					2.89
	3rd 0.2 ml					2.76
	Average					**2.81**
2nd Permeate	1st 0.2 ml	0.12	n. n.	0.10	1.23	2.30
	2nd 0.2 ml	0.14		0.14	1.29	2.29
	3rd 0.2 ml	0.16	0.17	0.10	1.14	2.04
	4th 0.2 ml	0.14	0.10	0.10	-	-
	Average	**0.15**	**0.14**	**0.11**	**1.22**	**2.21**
MeOH/Water 80/20	1st 0.2 ml					2.67
	2nd 0.2 ml					2.72
	3rd 0.2 ml					2.24
	Average					**2.54**
3rd Permeate	1st 0.2 ml	0.13	0.10	0.08	0.93	2.48
	2nd 0.2 ml	0.13	0.11	0.08	0.85	1.92
	3rd 0.2 ml					1.58
	4th 0.2 ml	-	0.10		-	-
	Average	**0.13**	**0.10**	**0.08**	**0.89**	**1.99**
4th Permeate	1st 0.2 ml			0.09	0.79	
	2nd 0.2 ml			0.08	1.07	
	3rd 0.2 ml			0.07		
	4th 0.2 ml			-	-	
	Average			**0.08**	**0.93**	
5th Permeate	1st 0.2 ml				1.12	
	2nd 0.2 ml				1.03	
	3rd 0.2 ml				0.84	
	4th 0.2 ml				-	
	Average				**1.00**	

Table 2 Table is more detailed version of Table 1.Flux [$dm^3 \cdot m^{-2} \cdot h^{-1} \cdot bar^{-1}$] for each collected 0.2 ml of permeate is presented. All values are normalized to 0.1 mm sample thickness. Few fluxes were not noticed even though the permeate volume was collected.

5.5. Conclusions

Cross-linked 1,2-polybutadiene nanoporous films of gyroid (GYR) morphology, having 40% porosity and pore cross-sectional diameter of 15 ± 4 nm were tested as ultrafiltration membranes. Formation of a skin layer during sample preparation process was observed. In order to remove this skin layer samples needed to be polished. Polishing sample surface with a sand paper is a quite tough method and other, gentler method should be used for this purpose (plasma treatment). It was difficult to control equal thickness at each point of a sample prepared in a way described above.

The fluxes of different gases (hydrogen, nitrogen and carbon dioxide) through thick nanoporous films were firstly measured. Removing the skin layer increases the fluxes of all three gases and minimizes the fitting parameter – tortuosity factor. Experimental data for polished samples fits better to Knudsen flow equation. Additionally extrapolation of experimental data to zero flux for unpolished sample crosses the pressure axis at 3.3-13 bar, whereas in case of polished samples it goes down to 0.6 – 2.4 bar which indicates that polishing indeed removes the skin layer.

Fluxes of pure solvents for both types of samples were measured and compared. The molecular size cut-off of the films was afterwards determined by the filtration of polyethylene glycol (PEG) molecules of different molecular weight dissolved in methanol/water 80/20 or 20/80 mixtures. Permeates and feeds were analyzed by size exclusion chromatography (SEC). Fluxes of pure solvents, PEG solutions and separation properties revealed huge differences between polished and unpolished samples.

Fluxes on unpolished samples are extremely low, but unpolished samples showed nice separation properties. A cut-off value in the range between 8 and 12 [kg/mol] was found for unpolished sample, corresponding to molecular hydrodynamic diameters of 7-9 nm, as determined by Dynamic Light Scattering. In case of unpolished sample it was rather properties of a skin layer that a bulk material showing separation properties. Unpolished sample is more like an asymmetric membrane.

The membrane characteristics of the unpolished GYR nanoporous polymer were compared with one commercial polysulphone ultrafiltration membrane. The GYR membranes were robust to changes in the methanol/water mixtures, while the commercial membrane lost its ultrafiltration characteristics at high methanol content.

Fluxes and separation properties of nano-porous sample after removing a skin layer change dramatically. Fluxes of pure solvents increased for polished samples. In case of sample polished on both sides at 10 bar pressure flux of 9 $dm^3 \cdot m^{-2} \cdot h^{-1}$ was obtained, whereas for unpolished sample 38 bar pressure was needed to get flux of 1 $dm^3 \cdot m^{-2} \cdot h^{-1}$. Similar tendency was observed during filtration experiments. Unfortunately increasing the flux after polishing did not went together with increasing separation properties. Only the first collected permeates showed nice cut-off curves, where 35 and 56 [kg/mol] PEGs were separated. First suspicious was, that polishing the sample with rough sand paper

caused deep scratches of micrometer size on sample surface. This could cause not enough sealing by the o-ring. Even though o-ring was glued by epoxy resin to unpolished surface and sample was polished inside the o-ring, problem remained. This indicated, that probably setup design has some drawback and closer look up showed not enough stirring, which caused concentration polarization. This can explain why only the first permeates showed good cut-off curves. To solve this problem the part of membrane device presented in Figure 54 should be changed. Metal marked by green dashed lines should be removed, so the stirrer could operate directly on membrane surface.

In general samples prepared in form of thick discs are not the best way to use nano-porous material for membrane application. Even though the main experiments were performed on nano-porous discs, afford was put to prepare thin film. Few techniques were tried, but were not successful. Lately quite promising results of thin film preparation were obtained by placing viscous solution of polymer on teflon support and rolling polymer to a thin film. This work can be continued in order to produce thin gyroid films.

6. References

(1) M. Rubinstein and R. H. Colby; Polymer Physics, Oxford University Press, USA 2006

(2) N. Hadjichristidis; S. Pispas and G. A. Floudas; Block Copolymers – Synthetic Strategies, Physical Properties and Applications, Wiley – InterScience, 2003

(3) T. P. Lodge; Block Copolymers: Past Successes and Future Challenges *Macromol. Chem. Phys.* **2003**, *204*, 265-273

(4) F. S. Bates; G. H. Fredrickson; Block Copolymer Thermodynamics: Theory and Experiment *Annu. Rev. Phys. Chem.* **1990**, *41*, 525-557

(5) E. L. Thomas and R. L. Lescanec; Phase Morphologies in Block Copolymer Systems *Philosophical Transactions: Physical Sciences and Engineering*, **1994**, *348*, 149-166

(6) P. Tang; F. Qiu; H. Zhang and Y. Yang; Morphology and Phase Diagram of Complex Block Copolymers: ABC Star Triblock Copolymers *J. Phys. Chem. B* **2004**, *108*, 8434-8438

(7) O. W. Webster; Living Polymerization Methods *Science* **1991**, *251*, 887-893

(8) F. Guo, K. Jankova, L. Schulte, M.E. Vigild and S. Ndoni; One-Step Routes from Di- and Triblock Copolymer Precursors to Hydrophilic Nanoporous Poly(acrylic acid)-*b*-polystyrene, *Macromolecules* **2008**, *41*, 1486-1493

(9) T. Tepe; M. F. Schultz; J. Zhao; M. Tirrell; F. S. Bytes; K. Mortensen; K. Almdal; Variable Shear-Induced Orientation of a Diblock Copolymer Hexagonal Phase *Macromolecules* **1995**, *28*, 3008-3011

(10) B. Ashok; M. Muthukumar and T. P. Russell; Confined thin film diblock copolymer in the presence of an electric field *J. Chem. Phys.* **2001**, *115*, 1559-1564

(11) T. Thurn-Albrecht; J. DeRouchey; T. P. Russell and H. M. Jaeger; Overcoming Interfacial Interactions with Electric Fields *Macromolecules* **2000**, *33*, 3250-325

(12) C. Osuji; P. J. Ferreira; G. Mao; C. K. Ober; J. B. Vander Sande and E. L. Thomas; Alignment of Self-Assemble Hierarchical Microstructure in Liquid Crystalline Diblock Copolymers Using High Magnetic Fields *Macromolecules* **2004**, *37*, 9903-9908

(13) I. Tokarev; R. Krenek; Y. Burkov; D. Schmeisser; A. Sidorenko; S. Minko and M. Stamm; Microphase Separation in Thin Films of Poly(styrene-*b*-4-vinylpyridine) Copolymer-2-(4'-Hydroxybenzeneazo)benzoic Acid Assembly *Macromolecules* **2005**,*38*, 507-516

(14) R. J. Albalak; E. L. Thomas and M. S. Capel; Thermal Annealing of roll-cast triblock copolymer films *Polymer* **1997**, *38*, 3819-3825

(15) V. Muralidharan; C. Y. Hui; Stability of Nanoporous Materials *Macromol. Rapid. Commun.* **2004**, *25*, 1487-1490

(16) D. A. Olson; L. Chen and M. A. Hillmyer; Templating Nanoporous Polymers with Ordered Block Copolymers *Chem. Mater.* **2008**, *20*, 869–890

(17) J. -M. Ha; J. H. Wolf; M. A. Hillmyer and M. D. Ward; Polymorph selectivity under nanoscopic confinement *J. Am. Chem. Soc.***2004**, *126*, 3382-3383

(18) C. Park; J. Yoon and E. L. Thomas; Enabling nanotechnology with self assembled block copolymer patterns *Polymer*, **2003**, *44*, 6725-6760

(19) M. A. Hillmyer; Nanoporous Materials from Block Copolymer Precursors *Adv.Polym. Sci.***2005**, *190*, 137-181

(20) J.-S. Lee; A. Hirao; S. Nakahama; Polymerization of Monomers Containing Functional Silyl Groups. 5. Synthesis of New Porous Membranes with Functional Groups *Macromolecules* **1988**, *21*, 274-276

(21) J.-S. Lee; A. Hirao; S. Nakahama; Polymerization of Monomers Containing Functional Silyl Groups. 7. Porous Membranes with Controlled Microstructures *Macromolecules* **1989**, *22*, 2602-2606

(22) D. R. Smith and D. J. Meier; New techniques for determining domain morphologies in block copolymers *Polymer* **1992**, *33*, 3777-3782

(23) J. Hedrick; J. Labadie; T. Russell; D. Hofer and V. Wakharker; High temperature polymer foams *Polymer*, **1993**, *34*, 4717-4726

(24) P. Mansky; C. K. Harrison; P. M. Chaikin; R. A. Register and N. Yao; Nanolithographic templates from diblock copolymer thin films *Appl. Phys. Lett.* **1996**, *68*, 2586-2588

(25) G. Liu; J. Ding; A. Guo; M. Herfort and D. Bazett-Jones; Potential Skin Layer for Membranes with Tunable Nanochannels *Macromoelcules* **1997**, *30*, 1851-1853

(26) T. Hashimoto, K. Tsutsumi and Y. Funaki, Nanoprocessing Based on Bicontinuous Microdomains of Block Copolymers: Nanochannels Coated with Metals *Langmuir* **1997**, *13*, 6869-6872

(27) S. Ndoni; M. E. Vigild and R.H. Berg; Nanoporous Materials with Spherical and Gyroid Cavities by Quantitative Etching of Polydimethylsiloxane in Polystyrene-Polydimethylsiloxane Block Copolymers *J. Am. Chem. Soc.* **2003**, *125*, 13366-13367

(28) M.S. Hansen, M.E. Vigild, R.H. Berg and S. Ndoni; Nanoporous Crosslinked Polyisoprene – Polydimethylsiloxane Block Copolymer *Polymer Bulletin* **2004**, *51*, 403-409.

(29) S. Ndoni, C.M. Papadakis, K. Almdal and F.S. Bates; Laboratory-scale setup for anionic-polymerization under inert atmosphere *Rev. Sci. Instrum.* **1995,** *66*, 1090-1095

(30) J.E. Mark editor Polymer Data Handbook, Oxford University Press, 1999

(31) J. Brandrup and E.H. Immergut, Polymer Handbook, 3rd ed., New York, John Wiley & Sons, 1989

(32) K. Andersen; Diplom Thesis **2005**, Technical University of Denmark, Department of Chemical Engineering, Lyngby, Denmark

(33) D. W. van Krevelen, editor, Properties of Polymers, 1990, Elsevier, Amsterdam, Oxford, New York, Tokyo

(34) *Encyclopedia of Polymer Science and Engineering*, 1985-1989, 2nd ed., Vol.14, John Wiley & Sons, New York

(35) K.A. Cavicchi; A.S. Zalusky; M.A. Hillmyer and T.P. Lodge; An Ordered Nanoporous Monolith from an Elastomeric Crosslinked Block Copolymer Precursor *Macromol. Rapid. Commun*., **2004**, *25*, 704-709

(36) E. J. Corey and A. Venkateswarlu; Protection of hydroxyl groups as tert-butyldimethylsilyl derivatives *J. Am. Chem. Soc.***1972**, *94*, 6190-6191

(37) E. J. Corey and B. B. Snider; Total Synthesis of (+/-) Fumagillin *J. Am. Chem. Soc.***1972**, *94*, 2549-2550

(38) L. C. Sawyer and D. T. Grubb Polymer Microscopy, Springer, 1996

(39) P.J. Goodhew, J. Humphreys and R. Beanland Electron Microscopy and Analysis, Taylor & Francis, London & New York, 2001

(40) M. W. Ladd The Electron Microscope Handbook: Specimen Preparation and Related Laboratory Procedures; Ladd Research Industries, Inc 1973

(41) B. Chu and B. S. Hsiao; Small Angle X-ray Scattering of Polymers *Chem. Rev.***2001**,*101*, 1727-1761

(42) P. Strunz, K. Mortensen and S. Janssen, SANS-II at SINQ: installation of the former Risø-SANS facility *Physica B*, 350 **2004**,*350*, e783 – e786

(43) G.E. Knözinger and J. Weitkamp editors, Handbook of Heterogenous Catalysis, Vol.2, Wiley-VCH, Weinheim, 1997

(44) M.R. Jakobsen and A. Grydgaard, Bechelor "Nano Cavities in Polymeric Materials", B.Sc. Thesis, Technical University of Denmark, 2006

(45) R. Eskimergen; K. Mortensen and M. Vigild; Shear Instability of a Gyroid Diblock Copolymer *Macromolecules* **2005**, *38*, 1286-1291

(46) M.E. Vigild; K. Almdal; K. Mortensen; I. W. Hamley; J.P.A. Fairclough and A.J. Ryan, Transformations To and From the Gyroid Phase in a Diblock Copolymer *Macromolecules*,**1998,** *31*, 5702-5716

(47) D.A. Hajduk, P.E. Harper, S.M. Gruner, C.C. Honeker, G. Kim, E.L. Thomas and L.J. Fetters, The Gyroid: A New Equilibrium Morphology in Weakly Segregated Diblock Copolymers, Macromolecules, 27 (1994) 4063-4075

(48) S. L. Aggarwal; Structure and properties of block polymers and multiphase polymer systems: an overview of present status and future potential *Polymer*, **1976**, *17*, 938-956

(49) T. Hashimoto, K. Tsutsumi and Y. Funaki, Nanoprocessing Based on Bicontinuous Microdomains of Block Copolymers: Nanochannels Coated with Metals, *Langmuir*, **1997,** *13*, 6869-6872

(50) T. Hashimoto, Y. Nishikawa and K. Tsutsumi, Identification of the "Voided Double-Gyroid-Channels": A New Morphology in Block Copolymers, *Macromolecules*, **2007**, *40*, 1066-1072

(51) Z. G. Wei; R. Sandstrom and S. Miyazaki; Shape-memory materials and hybrid composites for smart systems *Journal of Material Science* **1998**, 33, 3743-3762

(52) Q. B. Pei and O. Inganas; Conjugated polymers and the bending cantilever method: Electrical muscles and smart devices *Advanced Materials* **1992**, 4, 277-278

(53) W. A. Gazotti; G. Casalbore-Miceli; A. Geri; A. Berlin and M. A. De Paoli; An All-Plastic and Flexible Electrochromic Device Based on Elastomeric Blends *Advanced Materials* **1998**, *10*, 1522

(54) J. T. Koberstein; D. E. Duch; W. Hu; T. J. Lenk; R. Bhatia; H. R. Brown; J. P. Lingelser and Y. Gallot; Creating smart polymer surfaces with selective adhesion properties *Journal of Adhesion* **1998**, *66*, 229-249

(55) E. S. Gil and S. A. Hudson; Stimuli-reponsive polymers and their bioconjugates *Progress in Polymer Science* **2004**, 29, 1173-1222

(56) R. H. Baughman; Conducting polymer artificial muscles *Synthetic Metals* **1996**, *78*, 339-353

(57) M. E. Harmon; M. Tang and C. W. Frank; A microfluidic actuator based on thermoresponsive hydrogels *Polymer* **2003**, 44, 4547-4556

(58) K. Mortensen and J. S. Pedersen; Structural study on the micelle formation of poly(ethylene oxide)-poly(propylene oxide)-poly(ethylene oxide) triblock copolymer in aqueous solution *Macromolecules* **1993**, *26*, 805-812

(59) K. Mortensen; K. Almdal; R. Kleppinger; N. Mischenko; H. Reynaers; Networks of gel-forming triblock copolymer solutions: In situ SANS and rheological measurements *Physica B* **1997**, *241*, 1025-1028

(60) R. Yerushalmi; A. Scherz; M. E. van der Boom and H. B. Kraatz; Stimuli responsive materials: new avenues toward smart organic devices *Journal of Materials Chemistry* **2005**, *15*, 4480-4487

(61) F. Guo; J. W. Andreasen; M. E. Vigild and S. Ndoni; Influence of 1,2-PB Matrix Cross-Linking on Structure and Properties of Selectively Etched 1,2-PB-*b*-PDMS Block Copolymers *Macromolecules* **2007**, *40*, 3669-3675

(62) F. Guo; K. Jankova; M. E. Vigild and S. Ndoni; Hydrophilic Nanoporous 1,2-Polybutadiene Via Surface-Initiated Atom Transfer Radical Polymerization *Polymer Preprints* **2008**, *49*, 540

(63) J.S. Higgins and H.C Benoît, Polymers and Neutrons Scattering, Oxford University Press, 1997

(64) Y. Li and T. Tanaka; Kinetics of swelling and shrinking of gels *J. Chem. Phys*. **1990**, *92*, 1365-1371

(65) D. A. Durkee; E. D. Gomez; M. W. Ellsworth; A. T. Bell and N. P. Balsara; Microstructure and solvent distribution in cross-linked diblock copolymer gels *Macromolecules*, **2007**, *40*, 5103-5110

(66) G. Liu, J. Ding, A. Guo, M. Herfort and D. Bazett-Jones, Potential Skin Layers for Membranes with Tunable Nanochannels, *Macromolecules*, **1997,** *30*, 1851-1853

(67) G.Liu, J. Ding and S. Stewart, Preparation and Properties of Nanoporous Triblock Copolymer Membranes, *Angew. Chem. Int. Ed.*,**1999**, *38*, 835-838

(68) G. Jonsson, Molecular Weight Cut-Off Curves for Ultrafiltration Membranes of Varying Pore Sizes, *Desalination*, **1985**, *53*, 3-10

(69) K.A. Cavicchi, A.S. Zalusky, M.A. Hillmyer and T.P. Lodge, An Ordered Nanoporous Monolith from an Elastomeric Crosslinked Block Copolymer Precursor, *Macromol. Rapid Commun*., **2004**, *25*, 704-709

(70) S.H. Kim, M.J. Misner, T. Xu, M. Kimura and T.P. Russell, Highly Oriented and Ordered Arrays from Block Copolymers via Solvent Evaporation, *Advanced Materials*, **2004**, *16*, 226-231

(71) S.Y. Yang, I. Ryu, H.Y. Kim, J.K. Kim, J.K., S.K. Jang and T.P. Russell, Nanoporous Membranes with Ultrahigh Selectivity and Flux for the Filtration of Viruses, *Advanced Materials*, **2006**, *18*, 709-712

(72) A. K. Khandpur, S. Förster, F.S. Bates, I.W. Hamley, A.J. Ryan, W. Bras, K. Almdal, and K. Mortensen, Polyisoprene-polystyrene Diblock Copolymer Phase Diagram near the Order-Disorder Transition, *Macromolecules*, **1995**, *28*, 8796-8806

(73) G. Binnig; C. F. Quate and Ch. Gerber; Atomic Force Microscope, *Physical review letters,* **1986**, *56*, 930-933

(74) N. Wu, A. Zheng, Y. Huang and H. Liu, Morphology of Poly(styrene-*block*-dimethylsiloxane) Copolymer Films, Journal of Applied Polymer Science, **2007**, *104*, 1010-1018

(75) M. Mulder, Basic principles of membrane technology, Kluver, Dordrecht, 2003

(76) P.W. Atkins, Physical chemistry 6th ed., Oxford University Press, 1998

(77) P.J. Flory, Statistical mechanics of chain molecules, Interscience publishers, New York, 1969

(78) G.R. Strobl, The Physics of Polymers, Springer, Berlin, 1996

(79) J.K. Armstrong, R,B. Wenby, H.J. Meiselman and T.C. Fisher, The Hydrodynamic Radii of Macromolecules and Their Effect on Red Blood Cell Agregation, *Biophysical Journal*, **2004**, *87*, 4259-4270

(80) G. Jonsson and C.E. Boesen, Water and Solute Transport Through Cellulose Acetate Reverse Osmosis Membranes, *Desalination*, **1975,** *17*, 146-165

7. Appendices

Appendices named by the following alphabet letters as: A, B, C, D, E, F are attached below. Page numeration for each appendix starts from 1 again.

Appendix A – describes interpretation of small angle scattering results from nano-porous sample with hexagonally packed cylinders morphology

Appendix B – describes the procedure of data reduction from small angle neutron scattering experiments

Appendix C – Article: “Elastomers with reversible nano-porosity” Published in Macromolecules.

Appendix D – Article: “Gyroid membranes made from nanoporous block copolymers” Article is going to be resubmitted to Journal of Membrane Science

Appendix E – Article: “Nanoporous Materials from Stable and Metastable Structures of 1,2 – Polybutadiene-Polydimethylsiloxane Block Copolymers” Article is going to be resubmitted to Journal of Polymer Science Part A: Polymer Chemistry

Appendix F – Article: “Controlled Photo-Oxidation of Nanoporous Polymers” Article published in Macromolecules

A

Small angle scattering on hexagonally packed cylinders morphology

Basic principles
q vector and Bragg's Law

Scattering vector $\overline{q}$ is described as the difference between the scattered wavevector $\overline{K}_s$ and incident wavevector $\overline{K}_i$ (Equation 1)

$$\overline{q} = \overline{K}_s - \overline{K}_i \qquad \textbf{Equation 1}$$

The geometrical construction of scattering vector $\overline{q}$ is presented on Figure 1, where θ is the angle between the incident and scattered wavevector. We assume here that the interaction between the sample and x-ray occurs as elastic scattering, which means there is no energy loss and the length of incident and scattered wavevector stays the same: $\overline{K}_i = \overline{K}_s$.

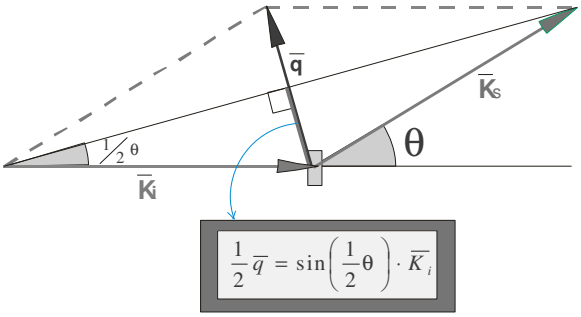

Figure 1 Geometrical construction of scattering vector $\overline{q}$ **.**

From Figure 1 we see that we can write scattering vector $\overline{q}$ as:

$$\overline{q} = 2 \cdot \sin\left(\frac{1}{2}\theta\right)\overline{K} \qquad \textbf{Equation 2}$$

where $\overline{K} = \frac{2\pi}{\lambda}$ and λ is a wavelength of incident x-ray.

Now we can show that the scattering vector $\overline{q}$ is inversely proportional to the distance between the scattering planes d , by applying Bragg's Law, which geometrical interpretation is shown on Figure 2.

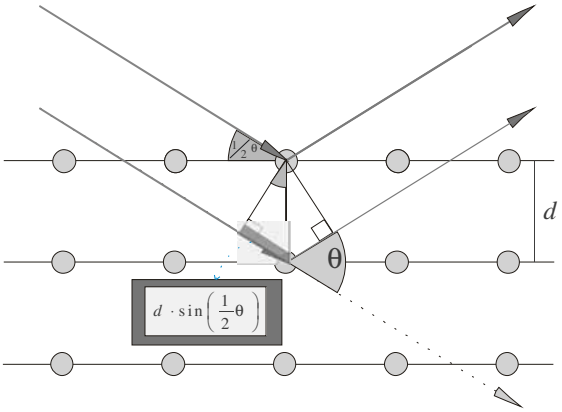

Figure 2 Bragg's Law of diffraction

Two incident x-rays scattered on the given plane, are staying in phase only if additional distance traveled by the second x-ray is equal or multiplication of x-ray wavelength λ. In such case we get enhance of scattering intensity, which happens only at given angle θ. Than Bragg's Law (Equation 3) has to be fulfilled:

$$n \cdot \lambda = 2 \cdot d \cdot \sin\left(\frac{1}{2}\theta\right) \qquad \textbf{Equation 3}$$

Taking d from Equation 3, and putting $\lambda = \frac{2\pi}{\overline{K}}$ and than $\overline{K}$ from Equation 2 we get:

$$d = \frac{n \cdot \lambda}{2 \cdot \sin\left(\frac{1}{2}\theta\right)} = \frac{n \cdot 2\pi}{2 \cdot \sin\left(\frac{1}{2}\theta\right) \cdot \overline{K}} = \frac{n \cdot 2\pi \cdot 2 \cdot \sin\left(\frac{1}{2}\theta\right)}{2 \cdot \sin\left(\frac{1}{2}\theta\right) \cdot \overline{q}} = \frac{n \cdot 2\pi}{\overline{q}} \qquad \textbf{Equation 4}$$

This shows indeed that scattering vector $\overline{q}$ is inversely proportional to the distance between the scattering planes d.

Scattering from nanoporous sample of HEX morphology

The following consideration is done under the assumption that we know we have nanoporous sample with pores showing hexagonally packed cylinders. Now we want to predict what results we will get from scattering experiment.

In hexagonally packed cylinders domain, where all cylinders are oriented in one direction, we choose the origin point of our coordinate system and we mark to vectors: x and y (Figure 3). In this case with two coordinates we can mark scattering planes, where the main scattering planes (10) have the highest distance to each other d. It means that the scattered signal from these planes will occur at lowest $\overline{q}$ value. The distance d between scattering the following scattering planes: (11), (21) and (31) decreases, which means that scattering peaks from these planes will come out at higher $\overline{q}$ values.

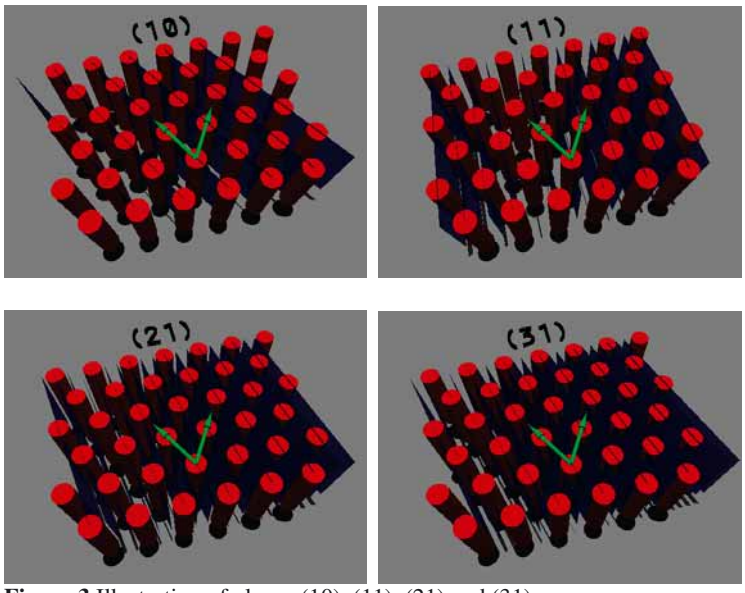

Figure 3 Illustration of planes (10), (11), (21) and (31).

Now depending on the synthesized block copolymer and chain length the distance d between the scattering planes can differ from one HEX sample to the other. In order to indentify HEX morphology independently of sample preparation we want to find the ratio of the distance between the main scattering planes d_{10}^{*} and the following scattering planes: d_{11}, d_{21} and so on.

The starting point is the assumption that the distances between the (10) planes are equal to 1. Since cylinders arrangement is hexagonal, than the β angle on Figure 4 should be 30^{o}. Than we can write:

$$\tan\beta = \frac{d_{11}}{d_{10}^{*}} \Rightarrow \tan 30^{o} = \frac{d_{11}}{d_{10}^{*}} \Rightarrow \frac{1}{\sqrt{3}} = \frac{d_{11}}{d_{10}^{*}} \Rightarrow \frac{d_{10}^{*}}{d_{11}} = \sqrt{3}$$

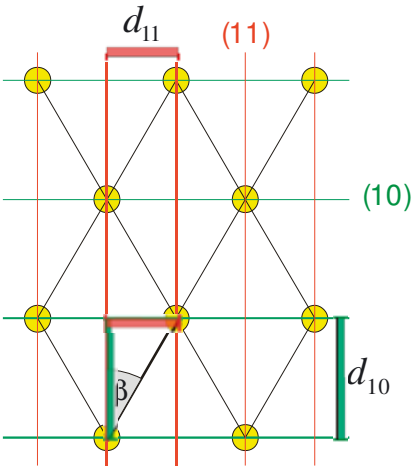

Figure 4 Distance between the (10) and (11) scattering planes in hexagonally packed cylinders.

Finding the ratio of $\frac{d^*_{10}}{d_{21}}$ is more complicated. Here we have to focus on ABC triangle presented on Figure 5.

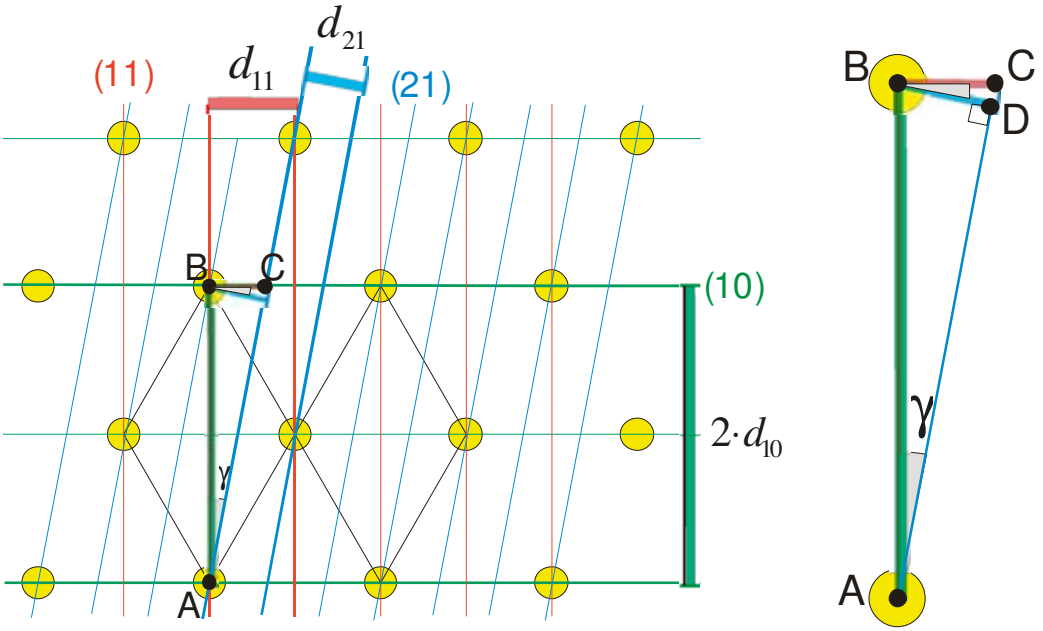

Figure 5 Distance between the (10), (11) and (21) scattering planes in hexagonally packed cylinders.

From the Figure 5 we can see that $BC = \frac{1}{3} \cdot 2d_{11}$ so $\tan\gamma = \frac{BC}{AB} = \frac{\frac{2}{3} \cdot d_{11}}{2 \cdot d_{10}^*}$. We can find γ from $\gamma = \tan^{-1} \frac{\frac{2}{3}}{2} \cdot \frac{1}{\sqrt{3}} = \tan^{-1} \frac{1}{3\sqrt{3}} = \tan^{-1} \frac{\sqrt{3}}{9} \Rightarrow \gamma = 0.19 rad = 10.89^o$

From Figure 5 we can see, that γ angle is equal to angle CBD. Now we can calculate $\cos\gamma = \frac{d_{21}}{\frac{2}{3} d_{11}} = \frac{3 \cdot d_{21}}{2 \cdot d_{11}} \Rightarrow \frac{d_{21}}{d_{11}} = \frac{2}{3}\cos\gamma$. Since $\tan\gamma = \frac{\frac{2}{3} d_{11}}{2d_{10}^*} = \frac{d_{11}}{3d_{10}^*}$ and $\frac{d_{11}}{d_{10}^*} = \frac{1}{\sqrt{3}}$ than $\tan\gamma = \frac{1}{3\sqrt{3}}$. The relation between $\cos\gamma$ and $\tan^2\gamma$ can be found as:

$$\tan^2\gamma = \frac{\sin^2\gamma}{\cos^2\gamma} = \frac{1-\cos^2\gamma}{\cos^2\gamma} = \frac{1}{\cos^2\gamma} - 1 \Rightarrow \cos\gamma = \frac{1}{\sqrt{\tan^2\gamma + 1}}$$

Now we can find $\frac{d_{21}}{d_{10}^*}$:

$$d_{21} = d_{11}\frac{2}{3}\cos\gamma = d_{11}\frac{2}{3}\frac{1}{\sqrt{\tan^2\gamma+1}} = \frac{d_{10}^*}{\sqrt{3}}\frac{2}{3}\frac{1}{\sqrt{\tan^2\gamma+1}}$$

$$\frac{d_{21}}{d_{10}^*} = \frac{2}{3\sqrt{3}} \cdot \frac{1}{\sqrt{\left(\frac{1}{3\sqrt{3}}\right)^2 + 1}} = \frac{2}{3\sqrt{3}} \cdot \frac{1}{\sqrt{\left(\frac{1}{27}\right) + 1}} = \frac{2}{3\sqrt{3}\sqrt{\frac{28}{27}}} = \frac{2}{3\sqrt{\frac{3 \cdot 4 \cdot 7}{3 \cdot 9}}} = \frac{1}{\sqrt{7}}$$

The ratio of the distance between the main scattering plane d_{10}^* and following scattering planes together with the ration of q values to q_{10}^* are summarized in Table 1.

(10)	(11)	"2(10)"	(21)
$\frac{d_{10}^*}{d_{10}^*} = 1$	$\frac{d_{10}^*}{d_{11}} = \sqrt{3}$	$\frac{2 \cdot d_{10}^*}{d_{10}^*} = \sqrt{4}$	$\frac{d_{10}^*}{d_{21}} = \sqrt{7}$
$\frac{q_{10}^*}{q_{10}^*} = 1$	$\frac{q_{11}}{q_{10}^*} = \sqrt{3}$	$\frac{2 \cdot q_{10}^*}{q_{10}^*} = \sqrt{4}$	$\frac{q_{21}}{q_{10}^*} = \sqrt{7}$

Table 1 The ratio of the distance between the main scattering planes d_{10}^* and following scattering planes (second raw) and ration of q values for following scattering planes and q_{10}^* (third raw).

To explain the value of $\sqrt{4}$ we have to look at Figure 6. For the scattering from (10) planes we assume, that the additional way of x-ray beam is equal to the wavelength,

so $n = \lambda$. If the scattering is really coming from the planes of distance $2 \cdot d_{10}^{*}$, than the additional way of x-ray beam (half of it is marked by blue) will be twice longer $n = 2$. If the scattering peak is indeed coming from $2 \cdot d_{10}^{*}$, than according to Equation 4 the peak should appear at lower q values. But the peak we characterize with $\sqrt{4}$ value is coming at the higher q. Twice long additional way of the x-ray beam ($n = 2 \cdot \lambda$) we can also get by tilting the same plane in such a way, that again we fulfill the Brag equation (second order scattering plane). From Equation 4 we know that for $n = 1$ (1^{st} order scattering) $q_{10}^{*} = \frac{2\pi}{d_{10}^{*}}$ and for $n = 2$ (2^{nd} order scattering) $q_{10}^{*} = \frac{4\pi}{d_{10}^{*}}$. That gives us:

$$\frac{2^{nd}\ order}{1^{st}\ order} = \frac{4\pi}{d_{10}^{*}} \cdot \frac{d_{10}^{*}}{2\pi} = \frac{2 \cdot d_{10}^{*}}{d_{10}^{*}} = 2 = \sqrt{4}$$

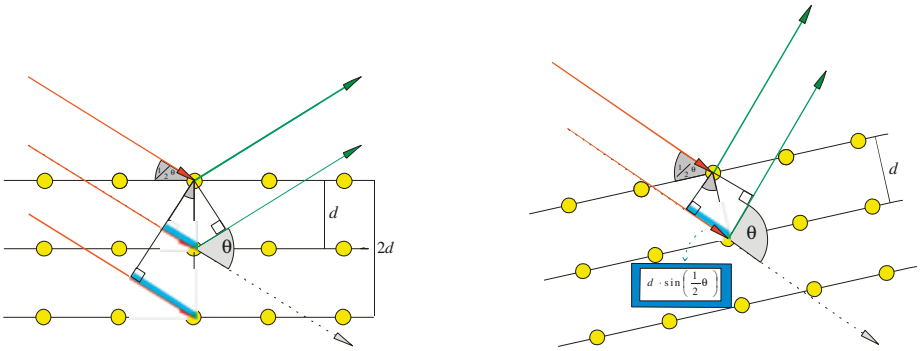

Figure 6 Scattering of the x-ray beam before (left) and after sample tilting (right).

The fallowing scattering peaks from HEX morphology occur at $\frac{q}{q^{*}}$ ratio equal to: $\sqrt{9}$, $\sqrt{12}$, $\sqrt{13}$ [i]

The schematic presentation of the scattering from the main planes (10) and (11) planes can be seen on Figure 7. In case of all cylinders oriented in one direction we will see two spots on two-dimensional detector. Two spots closest to the beam center, at lowest scattering vector value q^{*} correspond to scattering from (10) planes. Next two spots correspond to scattering from (11) planes.

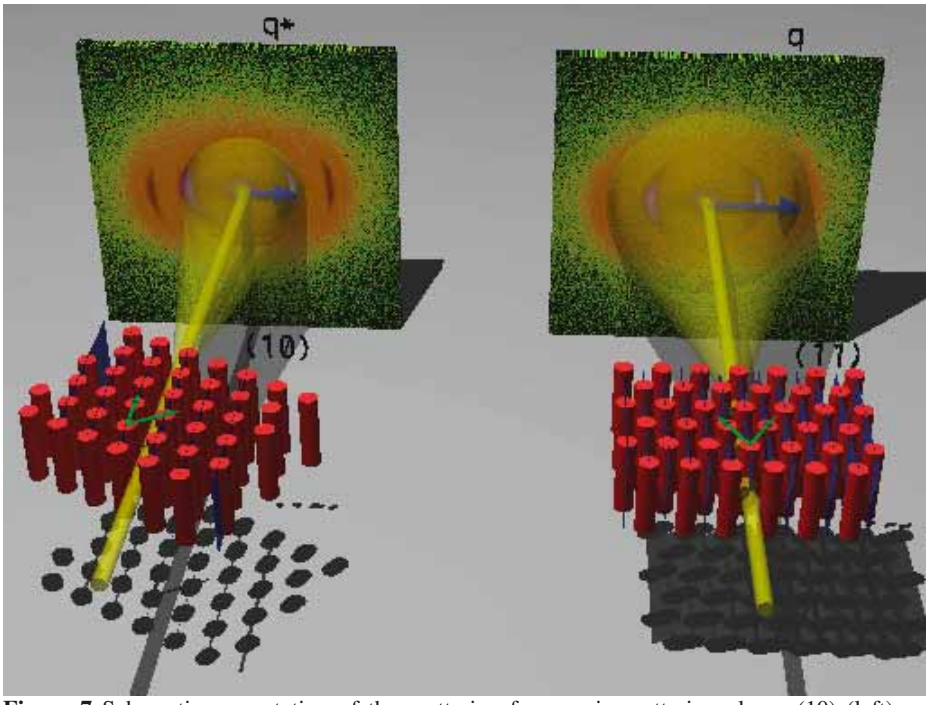

Figure 7 Schematic presentation of the scattering from main scattering planes (10) (left) and scattering from (11) planes (right). The two-dimensional scattering results come from original recorded data (file 2289 Ntb2 p 56).

After integration by using software, we get the plot of scattering intensity vs scattering vector q. From the plot we can read the q values for each peak and calculate the corresponding distance between the scattering planes d, based on Equation 4. Now to confirm that given peaks come from scattering from planes (10), (11), 2(10) and (21) we need to calculate ratios of $\frac{q}{q^*}$ or $\frac{d^*}{d}$ and to see if indeed they are close to values of $1, \sqrt{3}, \sqrt{4}$ and $\sqrt{7}$.

[i] B.Chu and B.S.Hsiao, Small-Angle X-ray Scattering of Polymers, Chem. Rev., 101 (2001) 1727-1761

B

Contents

1. Programs

The following programs (Table 1) were used to reduce the data and prepare the plots:

Program:	Author:
dscan.exe	Kell Mortensen
newlam.exe	Kell Mortensen
go-scan.bat	Kell Mortensen
db.exe	Kell Mortensen
radial.exe	Kell Mortensen
erad.exe	Kell Mortensen
lorentz.par	Kell Mortensen
res.par	Kell Mortensen
fit.par	Kell Mortensen
vaxfit.exe	Kell Mortensen
xyz.exe	Kell Mortensen
wgnuplot.exe	free software
Origin 6.1	commercial software
Excell	commercial software

Table 1

2. Procedure scheme

The procedure of data reducing and plot preparation is schematically presented on Figure 1:

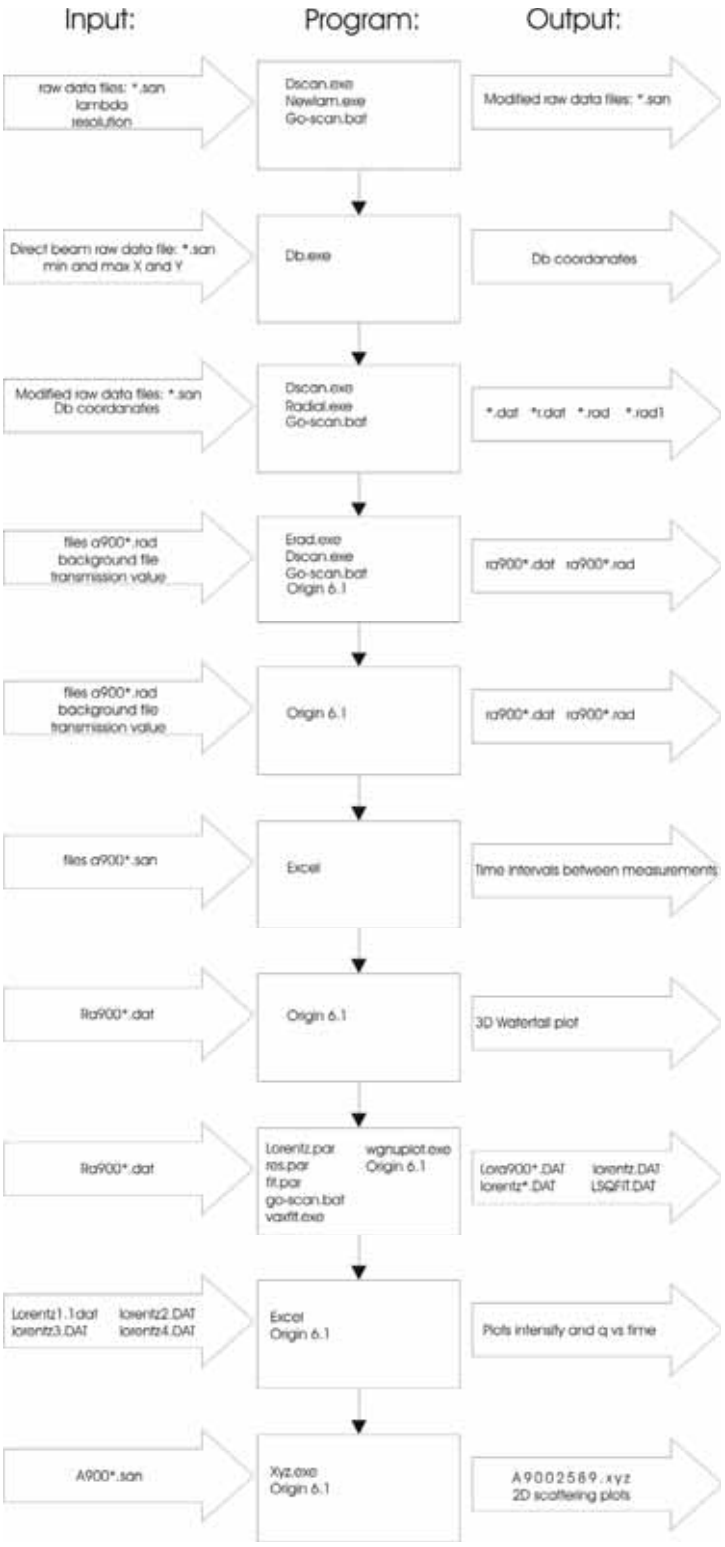
Input:
Program:
Output:
raw data files: *.san
lambda
resolution
Dscan.exe
Newlam.exe
Go-scan.bat
Modified raw data files: *.san
Direct beam raw data file: *.san
min and max X and Y
Db.exe
Db coordanates
Modified raw data files: *.san
Db coordanates
Dscan.exe
Radial.exe
Go-scan.bat
*.dat *r.dat *.rad *.rad1
files a900*.rad
background file
transmission value
Erad.exe
Dscan.exe
Go-scan.bat
Origin 6.1
ra900*.dat ra900*.rad
files a900*.rad
background file
transmission value
Origin 6.1
ra900*.dat ra900*.rad
files a900*.san
Excel
Time intervals between measurements
lra900*.dat
Origin 6.1
3D Watertall plot
lra900*.dat
Lorentz.par
res.par
fit.par
go-scan.bat
vaxfit.exe
wgnuplot.exe
Origin 6.1
Lora900*.DAT lorentz.DAT
lorentz*.DAT LSQFIT.DAT
Lorentz1.1.dat lorentz2.DAT
lorentz3.DAT lorentz4.DAT
Excel
Origin 6.1
Plots intensity and q vs time
A900*.san
Xyz.exe
Origin 6.1
A9002589.xyz
2D scattering plots

Figure 1

3. NewLam procedure

Raw data files were collected every 60s or 300s in most of the experiments. The machine did not record the lambda value λ (neutron wave length) during these short periods of time and it could not calculate the q value since:

$$\overline{q} = 2 \cdot \sin\left(\frac{1}{2}\theta\right)\overline{K}$$

where $\overline{K} = \frac{2\pi}{\lambda}$

That is why we have to input the lambda value to get the q values column. To do it we use two programs:

dscan.exe
newlam.exe

dscan.exe is a program which scans the input files and uses given procedure, like newlam in this case.

In the Command Prompt window we input data as presented on Figure 2. Here we will scan raw data files from a9002585.san to a9002637.san. The λ is 6.37Å and the resolution is 0.105.

```
 ** Input LIST-FILE with data file names, or
 ** Input Pre-letter of data-file,(def=s0):        a900
 ** Input File-extension, (def=san):               san
 ** Input First File:                              2585
 ** Input Last File:                               2637
 ** Input Routine:                                       newlam

 ** NewLam input **

** Input New Lambda and resolution (Lambda   Resolution):    6.37 0.105
** TYPE:   go-scan  **
```

Figure 2

Before typing “go-scan” comment, we can check the list of the files we are going to scan, procedure and input values by opening go-scan.bat file.
In case we would like to scan only every second or third file etc. we can delete unnecessary file from the list and save changes in go-scan.bat file.

Modified output file has the same name as the input file like: a9002585.san

4. Direct beam procedure

In order to integrate data from modified *.san file and get the file with q values column and scattering intensity values column we need to have a beam center coordinates.
Direct beam transmission file has to be found. Direct beam file: a9002456.san is closest to files a9002585.san-a9002637.san.

db.exe program is used to find direct beam coordinates. In Command Prompt window (Figure 3) the "db" command is used and as input value we write the direct beam file name and max and min values of X and Y.

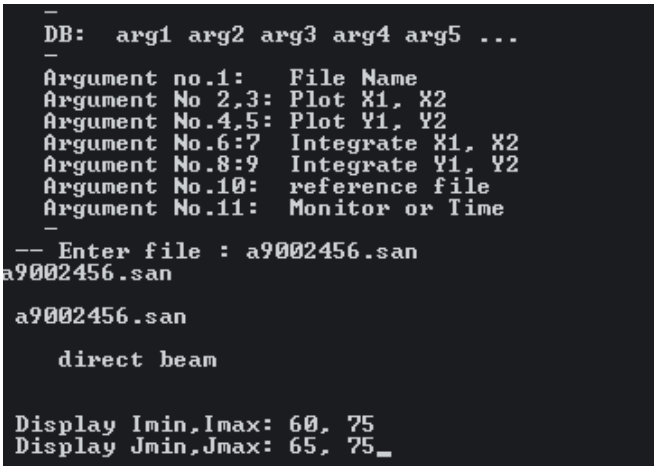

Figure 3

Finally we get matrix presented on Figure 4.

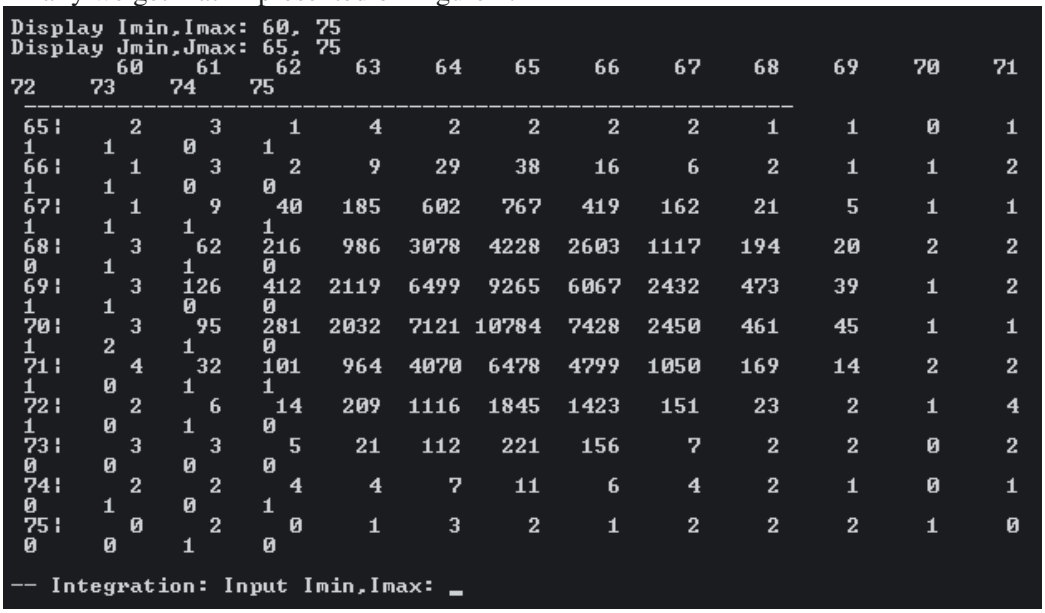

Figure 4

From this matrix we can see, that the highest value is: 10784 and that is for coordinates: X: 65 and Y: 70, so it is within the min and max values we declared.

Continuing procedure in the Command Prompt window (Figure 5) we get the precise direct beam coordinates, which in this case are: <X0,Y0>; 65.023 and 69.682.

```
-- Integration: Input Imin,Imax: 60,75
-- Integration: Input Jmin,Jmax: 65,75
-- Input reference sample for transmission:

** Center coordinates (X0,Y0):   65.023  69.682
** FWHM;          X-coordinate:     2.78,  Y-coordinate:     2.77
** Integrated intensity:       0.9610E+05  in total number of pixels:    176
  ** db.dat **
```

Figure 5

5. Rad procedure

Now as we have the centre coordinates we can start rad procedure. We will integrate raw data and we will get a file with q column and Intensity column.

We use two programs:

dscan.exe
radial.exe

Like in the newlam procedure we open Command Prompt window and we input data as presented on Figure 6.

```
 ** Input LIST-FILE with data file names, or
 ** Input Pre-letter of data-file,(def=s0):        a900
 ** Input File-extension, (def=san):              .san
 ** Input First File:                             2585
 ** Input Last File:                              2637
 ** Input Routine:                                      rad
 ** RADIAL input **

 ** Scaling relative to Monitor(def) or Time:
 ** Input Center (X,Y) (def=saved):                    65.023, 69.682
  ** Circular Standard, Saved in Param (P), , No(N) or Individual name:
          Input MASK (def=C):
 **  Circular(def) or Angular:
** TYPE:   go-scan  **
```

Figure 6

We want to scan modified *.san files and use “rad” procedure. Direct beam coordinates are already known so we type the values. Before typing “go-scan” we can check the list

of the files we are going to scan and remove unnecessary files by opening go-scan.bat file.

After scanning we get new output files:
a9002585.dat
a9002585r.dat
a9002585.rad
a9002585.rad1

In *.rad file we can find information about wavelength, sample to detector distance, center values or about time for data collection for a given sample.

If we plot a900*.dat file in Origin, than we can get scattering intensity vs. scattering vector plot, but these data do not subtract the background. In order to do it we need "erad" procedure.

6. Erad procedure

In order to subtract the background from the data file we use the following programs:
dscan.exe
erad.exe
Origin 6.1

As the background sample I was using scattering file from pure water sample. Very important is to check if sample to detector distance is the same for sample file and a background. For files a9002585.san to a9002637.san the background file is a9001965.san.

In Command Prompt window dscan.exe is used, as on Figure 7.

```
 ** Input LIST-FILE with data file names, or
 ** Input Pre-letter of data-file,(def=s0):        a900
 ** Input File-extension, (def=san):              rad
 ** Input First File:                             2585
 ** Input Last File:                              2637
 ** Input Routine:                                      erad

 ** ERAD input **

** Input SAMPLE transmission (def=1):
** Input SAMPLE Background file:              a9001965.rad
** Input Backgr. transm. (def=1):
** Input Boron. file:
** Input Normalization file:
**  Input cst. to be subtr. (def=0):
**  Input const. prefactor (def=1):
** TYPE:   go-scan  **
```

Figure 7

Here we have to specify the files to be scanned and background file we want to use. Again we can check the list of the files we are going to scan and remove unnecessary files by opening go-scan.bat file. After scanning the files the new output files are created:

ra900*.dat
ra900*.rad

If we open the file: a9002585.dat (before background subtraction) in the Notepad, than we find out that the intensity values in the second column are positive numbers. Wherever in case of ra9002585.dat (after background subtraction) we find out that the intensity values in the second column are negative numbers. It means that the intensity of water sample (a9001965.dat) was higher than our sample a9002585.dat.

To check the difference files I open the Origin 6.1 program and "Import Multiple ASCII" a9001965.dat and a9002585.dat are ploted in Origin 6.1 program as presented on Figure 8.

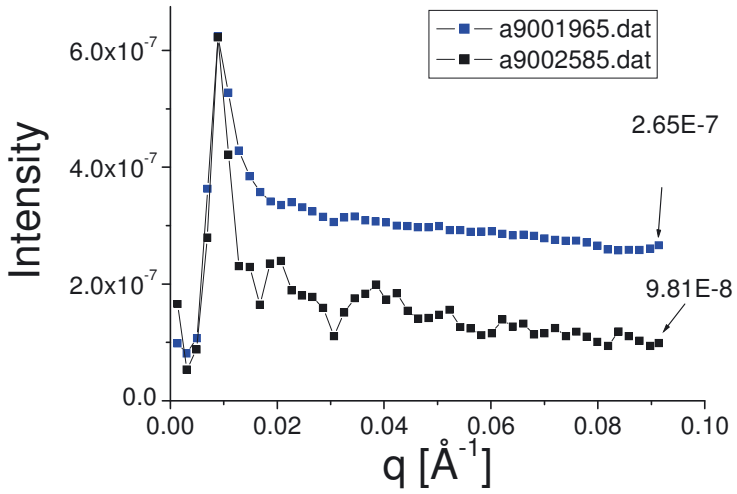

Figure 8

The ratio between the sample and water intensity is:

$$\frac{sample}{water} = \frac{a9002585.dat}{a9001965.dat} = \frac{1E-7}{2.6E-7} = 0.39$$

The Intensity level of sample is 61% lower than water. To increase the sample intensity values to the water background we run the erad procedure once again except we change the Input SAMPLE transmission to: 0.61. If the intensity values are still negative than we repeat the procedure until obtaining positive values.

7. Time intervals between files

Single plots of scattering intensity vs. scattering vector q can be plotted in Origin 6.1. We just need to import file: ra900****.dat or a900****.dat and make a plot.
In order to prepare the 3D Waterfall plot of scattering intensity vs. scattering vector q vs time in Origin 6.1 program we have to calculate the time intervals between each sample firstly. We include some "empty" files in between to show time intervals between measurements. Each empty file placed in between is equivalent of 60 s.
In the sample chamber we had the rotating sample holder in which we could place 3 or 4 samples together. Here I present calculations when 4 different samples were placed in position nr 6, nr 5, nr 4 and nr 3. Computer saves the data file for sample in pos nr 6, 5, 4, 3 and than it goes back to position 6. We have to calculate the time which pass between measurements for each sample.

In case of measurement of swelling sample in d-Toluene or percolation of d-MeOH, as "Time 0" we take the moment when we start to fill the sample quvete with liquid. On Waterfall plot at time zero we present the file in the dry state.
In the presented case the time between filling quvete with d-Toluene and starting SANS measurement is 10s.
Apparatus was programmed to start measurements from POS 6 and it measures sample for 60s. It takes 15s to move to POS 5 than. Finally when it finishes measure our sample in POS 3 it is 295s (10+3*15+4*60s) since placing in the d-Toluene (Figure 9). It moves back to POS 6 than and continuous the program.

Column A in Figure 10 is the file name. File a9002589.san represent sample measured in the dry state for 300s. This file will be placed at zero time. Column B and C in Figure 10 is what time the measurement starts and finishes. To find this data we have to open a9002589.san file in Word.doc.

File a9002593.san is finished at 19:32. Next file a9002597.san starts at 19:37 (5 min difference) and measurement is for 60s so file a9002597.san is finished after 655s (column E in Figure 10) since placing the sample in d-Toluene. 655s is 295 s plus 6 minutes (column D in Figure 10).

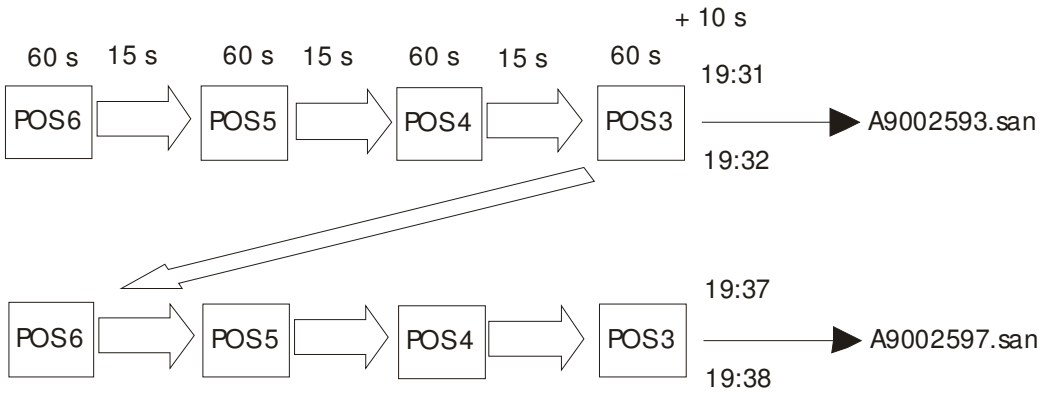

Figure 9

	A	B	C	D	E	F
1		measurement time			SET nr 35 d-Toluene	
2	nr of file	start	end	Time difference	Time [s]	
3	2589	19:05	19:10		0	
4					55	
5					115	
6					175	
7					235	
8	2593	19:31	19:32		**295**	
9					355	
10					415	
11					475	
12					535	
13					595	
14	2597	19:37	19:38	00:06	**655**	
15					715	
16					775	
17					835	
18					895	
19					955	
20	2601	19:43	19:44	00:12	**1015**	

Figure 10

8. 3D Waterfall plot preparation

Now we can open the Origin program.

From upper menu choose: Import multiple ASCII and import files: ra9002***.dat we want to present on 3D Waterfall plot. In presented case I include files: ra9002585(+4n).dat - ra9002637.dat

Mark the data worksheet with data of the first file you want to present. In case of SET 35 I mark RA9002589 worksheet. Go to upper menu and choose: Plot – 3D XYY – 3D waterfall-OK.
Since in RA9002589 worksheet column A(X) stays for q values and column B(Y) stays for Intensity values, we have to choose these columns to be plotted in Waterfall window (Figure 11):

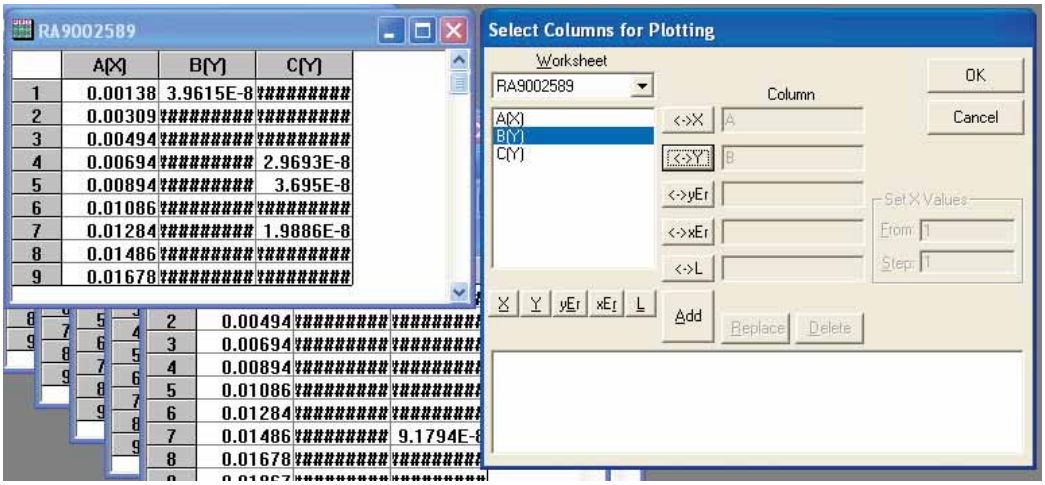

Figure 11

We get a Graph1 with x axis of q values and y axis of Intensity values. Now if we want to add more files we click in the upper left corner of Graph1 window and add files described as: ra9002***_b, where b stands for column B in worksheet (Figure 12):

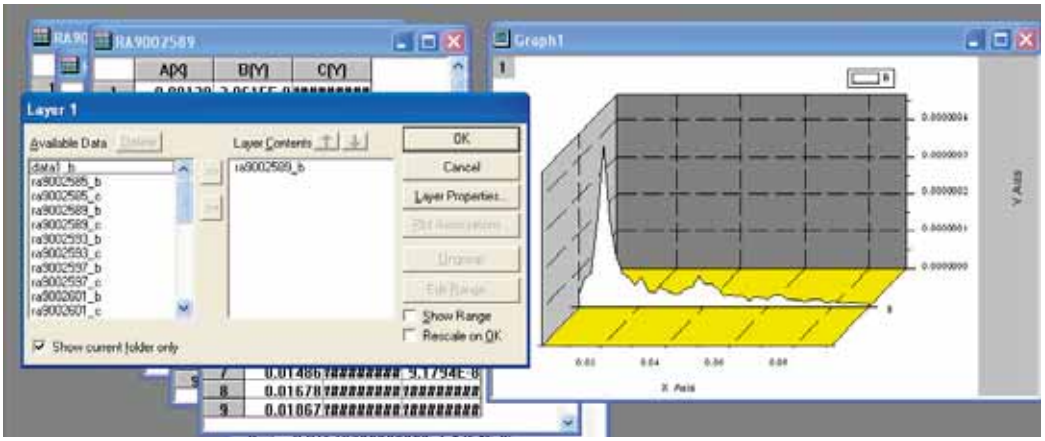

Figure 12

We get a waterfall plot with each file marked as B on z axis. Since the plot which is closest to us is the last file, we want to reverse it.
Double click on z axis and from new window choose scale and exchange “from”: and “to”:

We get the waterfall plot with files standing next to each other.
Now we want to change z scale to Time [s] scale and to separate files which are on Waterfall plot by the distance depending on how much time was left from one file to the other. We open again the excel file (Figure 10).
Now, file nr 2589 is our starting point. This is the file with dry sample measurement. According to previous considerations presented on Figure 9 and Figure 10 we place 4

empty data worksheet between file 2589 and 2593. This is not 100% accurate (we miss 5 seconds), but this is to present change in plot in nice graphical way. 1D plots are 100% accurate.

We go back to Waterfall Origin plot and we create new empty data worksheets. We click on Graph1 in upper left corner ("1") and move empty data worksheets to correct position.

9. Fit Lorentz function

Now we will try to fit Lorentzian function to our dry file nr 2589. In case of just one file we can do it by hand. In Origin 6.1 program I find data worksheet: RA9002589.dat and prepare a plot of Intensity vs q. We can choose Data Selector from the upper menu, position the Selectors and choose: Analysis – Fit Lorentzian than.

In case of many files we use programs:

lorentz.par
res.par
fit.par

I open the Command Prompt window and after writing notepad lorentz.par command we open notepad window in which we can find starting parameters we can change. 0 in the second column means that all parameters will be fitted. 1 means that a given value is fixed.
In the same time we can plot file RA9002589.dat in Origin 6.1 and by choosing Screen Reader option and we check peak intensity value. It is around: 7.5E-8 and q position is around 0.038. Correlation length I give as 1.E+02. As background I start with: 1E-8 (Figure 13).

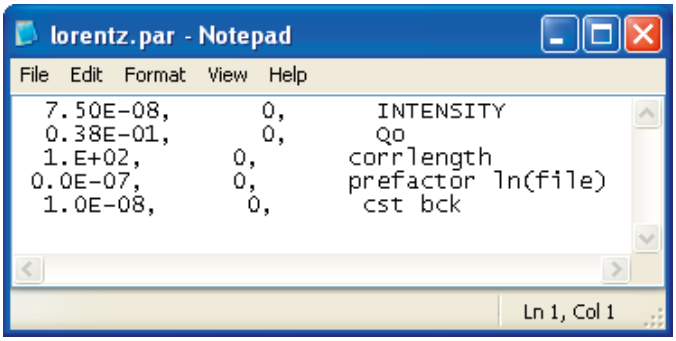

Figure 13

We save changes in Lorentz.par file.

Now we want to scan this single file. As I look at the plot in the Origin 6.1 I can see that the peak is somewhere between q: 0.03Å and 0.05Å. I will dscan for 0.03-0.05Å q value.

In the Command Prompt window I use dscan command and I specify the min and max q values (Figure 14):

```
 ** Input LIST-FILE with data file names, or
 ** Input Pre-letter of data-file,(def=s0):          ra900
 ** Input File-extension, (def=san):                rad
 ** Input First File:                               2589
 ** Input Last File:                                2589
 ** Input Routine:                                        vaxfit

 ** Vaxfit input **

** Input Fitting Routine (gauss,lotentz,...):          lorentz
** Qmin:              0.03
** Qmax:              0.05
** TYPE:   go-scan  **
```

Figure 14

Again to check the files which are going to be scanned I write the command notepad go-scan.bat and notepad window is opened. In this case there is only one file to be scanned, given in the second column: ra9002589.rad. First column gives the name of the procedure: vaxfit. Third column gives the name of function to be fitted and the last two columns show the minimum and maximum q values:

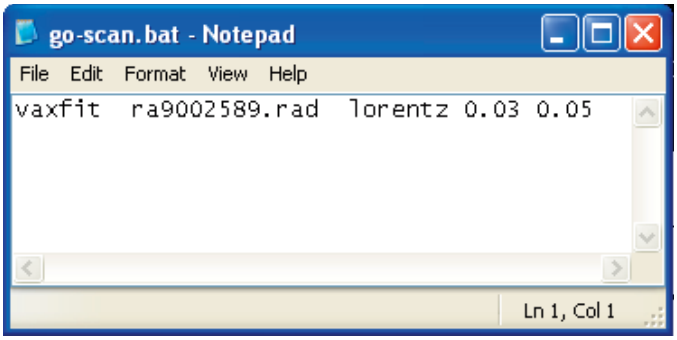

Figure 15

After scanning we created files:

lora9002589.DAT
lorentz.DAT
lorentz1.DAT
lorentz2.DAT
lorentz3.DAT
lorentz4.DAT
LSQFIT.DAT

Now I want to check how my lorentzian fit to Intensity vs q scale plot. I have two ways. I can open Origin 6.1 program and import: lora9002589.DAT file and plot it together with RA9002589.dat file. In the Origin we can see that it totally doesn't fit:

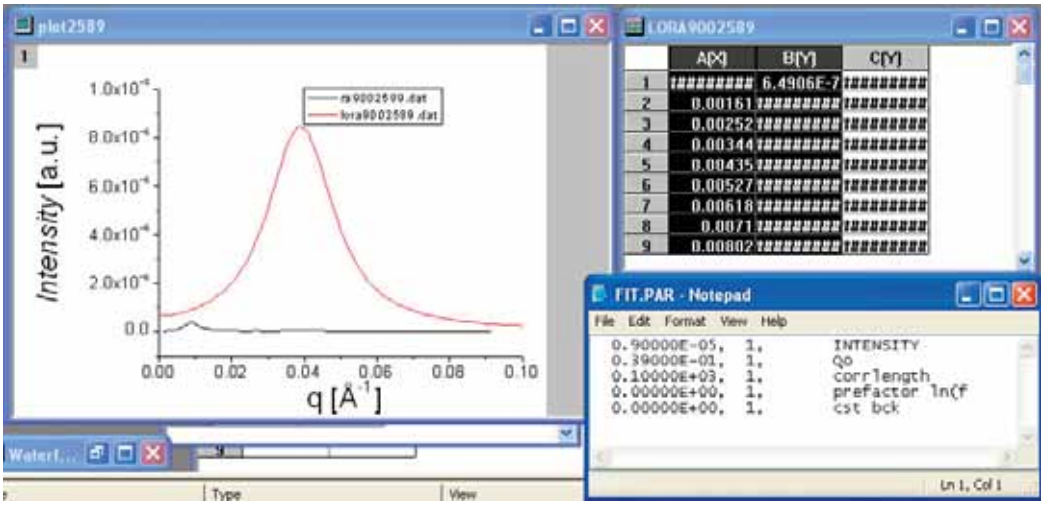

Figure 16

Fitting parameter we can find in fit.par program.

I can also look at these files by using wgnuplot.exe program. We get the same result as in Origin (Figure 17):

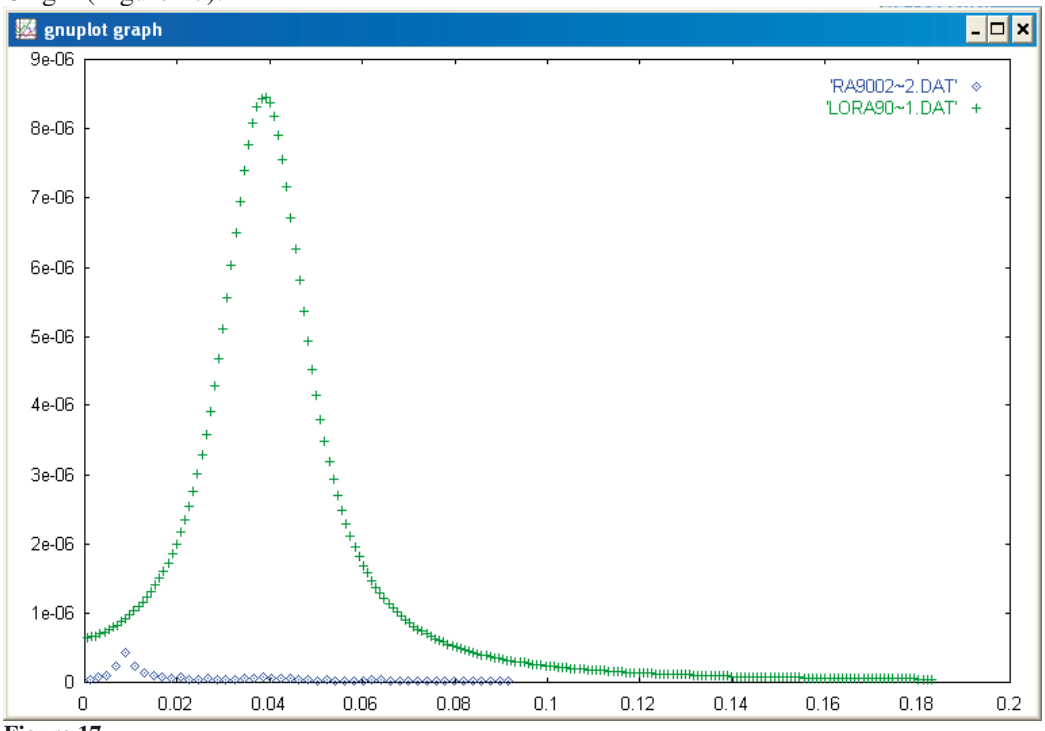

Figure 17

Now we want to fit lorenzian in better way. I choose new lorentz.par parameters:

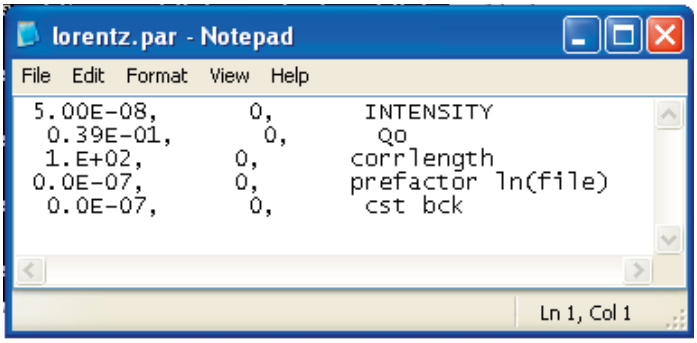

Figure 18

And again I will use dscan (like on Figure 14) but for q from:0.03 to 0.47

Now I check how it fits in Origin again. Now it fits much better:

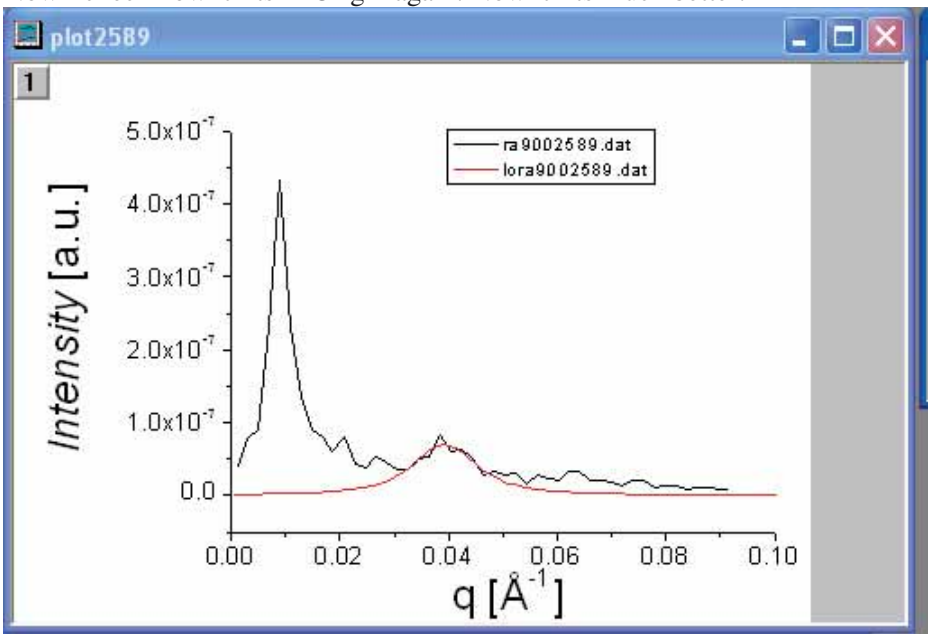

Figure 19

We can now check the fitting parameters by writing in Command Prompt notepad fit.par command again (Figure 20):

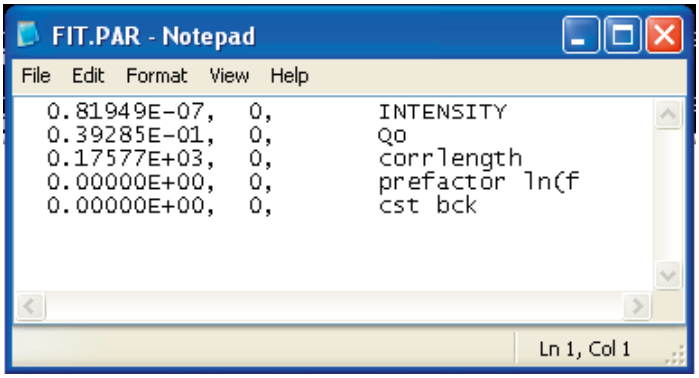

Figure 20

In case we would like to fit lorenzian function to next dscan file than after writing in Command Prompt notepad go-scan.bat we write copy fit.par lorentz.par (Figure 21) in between each file we want to scan. It means that fitted parameters after scanning one file will be used as starting parameters to dscan next file.

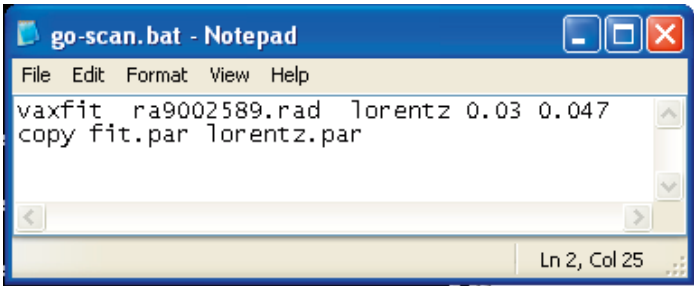

Figure 21

10. Plots of Intensity, Q, Corr funct and Baskground vs Time

Now to check the Intensity, Q, Corr function and Bacground, I have to open with Notepad files:

lorentz1.DAT

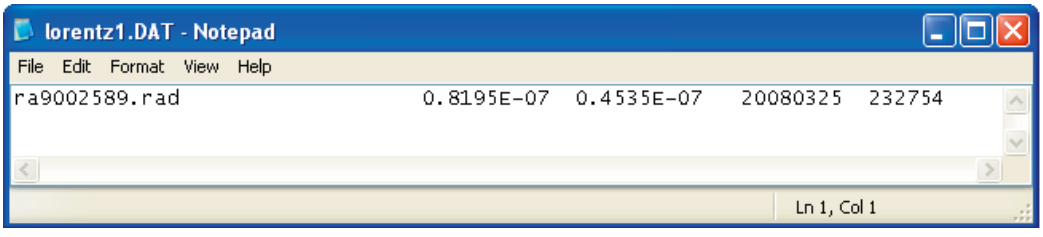

Figure 22

lorentz2.DAT
lorentz3.DAT
lorentz4.DAT
respectively.
I copy these data to new excel worksheet called:

Plots-bck fitted-2.xls

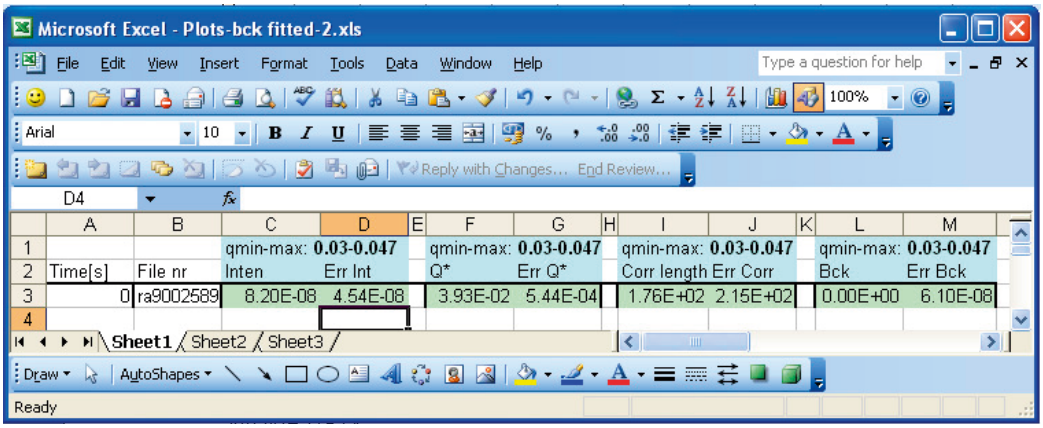

Figure 23

These data I use to prepare plots of Intensity, Q, Corr function and Bacground vs Time in Origin 6.1 respectively.

Before next dscan I have to delete:
lorentz1.DAT
lorentz2.DAT
lorentz3.DAT
lorentz4.DAT
lorentz.DAT
LSQFIT.DAT

11. 2D plots

The last step is to create 2D plots.
I use program: xyz.exe

Now in Command Prompt I write xyz:

```
arg1:

arg2,3:
arg4,5:
  -
  transform SANS-data to Qx,Qy,I:
  -
  Argument no.1:   File Name
  Argument No.2,3: Min and Max Pixel (X)
  Argument No.4,5: Min and Max Pixel (X)
  -
 ** Input file name:          a9002589.san
 -- file:                     a9002589.san

 ** Input Horizontal Pixel: Min, Max:
 Applied X-range:                    1         128
 Applied Y-range:                    1         128
arg1:

        id33_shr_Ic_dry
```

Figure 24

File a9002589.xyz was created. Now we open Origin program and we import ASCII file: a9002589.xyz to new data worksheet. From upper menu we choose:
Edit-convert to matrix-direct
We created Matrix1
Again we choose upper menu: Plot 3D – Contour Color Fill. After adjusting picture size and color scale Picture is ready (Figure 25).

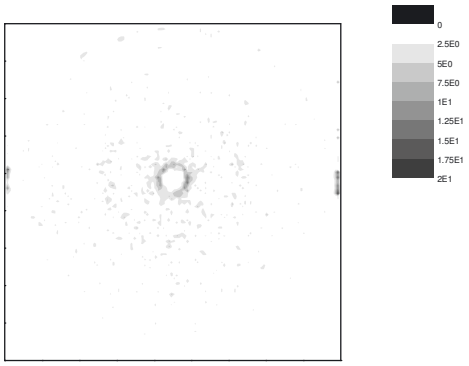

Figure 25

C

5636 *Macromolecules* **2009**, *42*, 5636–5641
DOI: 10.1021/ma900198k

Macromolecules
ARTICLE

Elastomers with Reversible Nanoporosity

Piotr P. Szewczykowski,[†] Kenneth Andersen,[†,‡] Lars Schulte,[†,‡] Kell Mortensen,[§] Martin E. Vigild,*[,†,⊥] and Sokol Ndoni*[,‡]

[†]*Danish Polymer Centre, Department of Chemical and Biochemical Engineering, Technical University of Denmark, DK-2800 Kgs. Lyngby, Denmark,* [‡]*Department of Micro and Nanotechnology, Technical University of Denmark, DK-4000 Roskilde, Denmark, and* [§]*Biophysics Group, Department of Basic Sciences and Environment, University of Copenhagen, DK-1871 Frederiksberg C, Denmark.* [⊥]*Presently: Dean of Undergraduate Studies and Student Affairs, Technical University of Denmark.*

Received January 29, 2009; Revised Manuscript Received June 6, 2009

ABSTRACT: An elastomer was created via cross-linking a diene block of a polyisoprene−polydimethylsiloxane (PI−PDMS) block copolymer in the ordered state of hexagonal morphology, followed by the quantitative removal of the PDMS component. The elastomer material collapsed following etching of the PDMS and apparently showed no resulting nanoporosity or structure resembling the precursor morphology in contrast to similar polydiene-based nanoporous material. However, the collapsed elastomer displayed surprising properties when exposed to a solvent. In the gel state the material recovers the original nanostructure and displays liquid-filled cavities. Upon several cycles of swelling and drying the cavities open and close in a reversible fashion. When exposed to a nonsolvent, the material remains collapsed. This discriminating behavior of liquid-material interaction holds potential for the use of these materials in advanced separation or load-release systems.

Introduction

Smart polymeric materials attract major attention among researchers within applied as well as basic science.[1−5] Such materials are characterized by having predetermined responses to external stimuli, which for example can be electrical, mechanical, or chemical. Often the response takes the form of a change in shape or size, possibly induced by a phase transition. Polymeric actuators are prominent examples of such materials, where electrical energy results in mechanical motion.[6] A very simple stimulus is temperature change which is exploited in thermoresponsive systems by controlling a volume phase transition of the material.[7] Chemical stimuli which trigger a shift of physicochemical properties could be a change in pH, selective solubility of a solvent, or a change in salt concentrations. Especially diblock copolymers show structural changes when exposed to solvents that interact differently with the polymer blocks. This is the case for block copolymer-based micelles induced by using a specific solvent at a given temperature[8] or selective swelling of block copolymer melts which causes phase transitions and morphology changes.[9] However, these phenomena do not traditionally qualify block copolymers as smart materials, although there are examples of solvent-triggered stimuli responsive materials which are used to create smart surfaces based on forms of block copolymers.[10]

Nanoporous materials derived from block copolymers hold potential for many different nanotechnological applications[11,12] and are also candidate materials for smart applications. An obvious application of nanoporous block copolymer-based materials is in membrane technology. A smart membrane could for example be used in controlled or selective diffusion which depends on the nature of the feed liquid for the membrane. Such a membrane would offer exceptional characteristics in separation processes with the option of including a valve effect which could allow the membrane to be open or closed for filtration of a liquid.

In our previous work we have shown how polydiene-based diblock copolymers containing polydimethylsiloxane (PDMS) establish a fine and versatile platform for creating nanoporous materials. Opportunities are plentiful for combining synthesis to obtain nanostructured materials of different morphologies and chemical composition with various procedures to modify or functionalize the matrix material.[13−16] The nanoporous structures are crucially dependent on the nature and the mechanical strength of the matrix material. In the case of matrices that are not crystalline or glassy at room temperature (as is the case with polydienes), it is necessary to reinforce the matrix (for example, by cross-linking the polymer) in order to have a structure which remains stable after selective etching of the expendable block during the process of fabricating the nanoporous material. In an earlier report we have characterized a series of samples with relatively low degrees of cross-linking of the matrix domain and observed that the nanostructure and porosity apparently are not detectable by small-angle scattering measurements after finishing the fabrication procedure.[13] It is reasonable to describe these materials as *collapsed*, but it is unresolved what the characteristics, morphology, and physicochemical properties are for these materials, which all have been treated in such a way that the expendable component of the precursor diblock copolymer matrix was quantitatively removed.

The aim of the work presented here is to conduct a structural study of collapsed samples (of low degrees of matrix cross-linking), which in the dry state do not produce well-defined nanoporous material. This study is primarily based on small-angle neutron scattering (SANS) measurements. Of special interest is the effect of exposing the collapsed samples to specific liquids, namely a solvent and a nonsolvent to the matrix material. Transmission electron microscopy (TEM) and small-angle X-ray scattering (SAXS) were used to characterize the dry samples.

*Corresponding authors. E-mail: mev@kt.dtu.dk (M.E.V.); sokol.ndoni@nanotech.dtu.dk (S.N.).

 Published on Web 07/15/2009

Table 1. Characteristics of the Precursor Diblock Copolymer

precursor sample	$\langle M_n \rangle_{PI}$[a] [g/mol]	$\langle M_n \rangle_{total}$[b] [g/mol]	PDI_{total}[c]	w_{PDMS}[d]	f_{PDMS}[e]	morphology [SAXS]	T_{ODT} [°C]
ID33	10 530	14 200	1.1	0.26	0.26	HEX	225

[a] Number-average molecular weight of the polyisoprene block as obtained by ^{1}H NMR. [b] Number-average molecular weight of the diblock molecule obtained by SEC and ^{1}H NMR. [c] Polydispersity index obtained by SEC. [d] Mass fraction of PDMS determined by ^{1}H NMR. [e] Volume fraction of PDMS at 20 °C calculated from density values: $\rho_{PI} = 0.900$ g/cm^3 and $\rho_{PDMS} = 0.966$ g/cm^3.[20,21] The morphology was determined by small-angle X-ray scattering (SAXS), and the order−disorder temperature (T_{ODT}) was determined by rheology measurements.

From this study we will gain information on the structure and nature of the low degree cross-linked samples and test these collapsed materials for possible smart behavior.

Experimental Section

Material Preparation. *Block Copolymer Synthesis*. The PI−PDMS block copolymer was prepared by sequential "living" anionic polymerization under an inert argon atmosphere as described elsewhere.[17] Samples described in this article derive from the ID33 batch of polymerization. The capital letters represent the chemical structure of the block copolymer, where PI is indicated by letter "I" and the PDMS is indicated by letter "D". The number following the letters "ID" is the batch number. The volume fraction of PI was targeted at $w_{PI} = 0.74$ to give a block copolymer system with hexagonally distributed cylinders of PDMS in a matrix of PI. Data for the parent sample ID33 are summarized in Table 1.

Alignment of Hexagonal Structure. In order to get optimal insight into the structural properties, as determined by the SANS experiment, the morphologies of the samples were aligned into a simple texture by extruding the polymer melt. For this purpose an extrusion device with a rectangular die of cross section 1×10 mm and 20 mm in length was constructed. Approximately 6 g of polymer was dissolved in 60 mL of tetrahydrofuran (THF) and cast in a glass covered by aluminum foil at the bottom. After solvent evaporation the aluminum foil was rolled, placed in the extruder, and squeezed. This helped to avoid bubbles in the extruded polymer. The polymer was extruded onto microscopy cover glasses prior to the cross-linking procedure.

Cross-Linking. The samples were cross-linked by using dicumyl peroxide (bis(α,α-dimethylbenzyl) peroxide) (DCP) from Merck in a step-by-step procedure. For dosage of DCP we make reference to the total number (mole) of double bonds in the sample in question. For the first cross-linking step an amount of DCP was scaled off which equal 2 mol % relative to the moles of double bonds in the sample volume (i.e., mol DCP/mol double bonds = 0.02). The 2 mol % of DCP was placed directly on the sample surface inside a homemade stainless steel cap screw cylinder equipped with two valves. Nitrogen gas was run through the cylinder for few minutes, and then the cylinder was tightened and placed in a preheated oven at 140 °C for 2 h with a nitrogen atmosphere as an additional precaution.[18] After baking, the cylinder was rapidly cooled down, and the sample was placed in a vacuumed round-bottom flask at 130 °C for 1 h to get rid of any accumulation of byproduct. For subsequent cross-linking steps an amount equivalent of 6 mol % of DCP was used. This procedure was repeated 2−3 times to give samples ID33-x14 and ID33-x20, where "x" symbolizes the cross-linking and the numeral refers to the total amount of added DCP (in mol %).

Etching of PDMS. A solution of 1 M tetrabutylammonium fluoride (TBAF) in THF from Aldrich was used as cleaving reactant for removing the PDMS blocks. Five times molar excess of TBAF relative to the PDMS repeating unit was used to etch the cross-linked PI−PDMS samples. The reaction time was 24 h at room temperature. The samples were rinsed with THF and methanol prior to drying. Samples were code named by adding the suffix "e" for etching to the sample name; hence, the sample names become ID33-x14e and ID33-x20e.

Characterization Techniques. *Chromatography*. Size exclusion chromatography (SEC) in stabilized THF was used to determine the molar mass and molar mass distribution of the copolymer blocks. SEC equipment consisted of two mixed-D columns (Polymer Laboratories) and a triple detector setup (Viscotec) (right angle light scattering, viscometer, and differential refractometer).

Spectroscopy. The diblock copolymer average composition was determined by proton magnetic resonance spectroscopy (^{1}H NMR) in a 250 MHz Avance DPX 250 Bruker instrument. Raman (Renishaw system 3000) and Fourier transform infrared FT-IR (Perkin-Elmer Spectrum) spectroscopies were used to monitor the number of double bonds before and after cross-linking and etching of the PI−PDMS.

Rheology. Rheological measurements were used to determine the order−disorder transition temperature (T_{ODT}) of the synthesized polymers. The viscoelastic properties of the diblock copolymers were investigated by isothermal and temperature-gradient dynamic mechanical measurements on a Rheometrics RS 800 rheometer using parallel plate geometry. The temperature was changed continuously with a rate of 2.5 °C/min.

Electron Microscopy. Samples were investigated in a Jeol 3000F transmission electron microscope (TEM). Preparation for microscopy was performed by placing a piece of the sample in an Agat mortar filled with liquid nitrogen and crushed into a fine powder. Then the mortar was filled with ∼2 mL of toluene (Fluka, 99.8% pure), and the suspension was transported to a small glass. The glass with suspension was placed in an ultrasonic water bath (Branson, Model B1510-MT) for 30 min to separate particles. A drop of the suspension was deposited on a holey carbon film on a 300 mesh copper grid. Finally, the toluene was evaporated and the sample analyzed by TEM.

SAXS. Small-angle X-ray scattering (SAXS) was performed using the rotating anode lab source at Risø DTU. The wavelength of the X-rays was $\lambda = 1.54$ Å. A two-dimensional position-sensitive wire detector in a distance of 1435 mm from the sample was used to collect scattered radiation.

SANS. Samples were investigated using the small-angle neutron scattering instrument SANS-II at SINQ, Paul Scherrer Institute (PSI) in Villigen, Switzerland,[19] using 6 m collimation with entrance and exit pinholes equal to 16 and 6 mm, respectively. The sample-to-detector distance was 6 m, and the neutron wavelength was 6.37 Å.

Samples were placed in glass cuvettes. In case of the swelling experiments the cuvettes were filled with ∼2 mL of solvent just before placing in the sample chamber and starting scattering measurement. During the swelling process time-resolved scattering data were collected over 60 or 300 s intervals. Some samples were measured for longer time when necessary (1200 or 3600 s).

Results and Discussion

First, we present data on the precursor diblock copolymer and the samples derived from this, which result from following the prescribed procedure. Second, we show the results of a more detailed study using SANS. The SANS measurements gauge the structural response of the samples to various solvents and shed light on the morphological identity of the collapsed samples.

Characteristics of Precursors and Cross-Linked, Etched Material. *Block Copolymer Parent Sample*. A PI−PDMS

block copolymer (ID33) was synthesized by anionic "living" polymerization as described above. Table 1 lists the characteristics of the precursor diblock copolymer. SEC and/or ^{1}H NMR were applied in order to obtain the molecular weights of the PI block, the total weight of the block copolymer, the polydispersity index, and the weight and volume fraction of PDMS. SAXS measurements showed that the morphology of the parent sample is hexagonally (HEX) ordered cylinders of PDMS in a matrix of PI. Rheological studies determined the order−disorder temperature (T_{ODT}).

Preparation of Samples by Cross-Linking and Etching. Generally, our experience is that effective cross-linking of PI requires several treatments with peroxide. Previously, we have reported that five to six additions of fresh peroxide was necessary to obtain sufficient mechanical stability of the PI network after etching with HF.[14] Figure 1 presents the expected mechanism of cross-linking the PI chains.[22] High temperature causes the dicumyl peroxide molecule to split into two radicals. These radicals attack the allylic hydrogen in PI, and new radicals are created within the chain. When two radicals on different chains react with each other, a cross-link is created, without changing the double bond which is untouched by this reaction. One peroxide molecule generates on average one (or less) cross-link. At high temperature and high cross-linking degrees the double bonds can take part in additional cross-linking.

TBAF etching procedure was previously used by others.[23] The mass loss due to etching is a first good indication of rendering a nanoporous material if it approaches the sample mass of PDMS. Fractions of mass losses following the etching procedure were respectively 0.26 and 0.23 for ID33-x14e and ID33-x20e. The data show good agreement between the fraction of mass loss and the original weight fraction of PDMS (w_{PDMS}) listed in Table 1. This supports the conclusion that the PDMS block was quantitatively removed. Sample ID33-x20e shows a slight deficit in this comparison, which may mean that the removal of PDMS is not perfect in this particular sample.

Structural Results. Following the preparation of cross-linking and etching described above, the samples were characterized by both SAXS experiments and microscopy. Structural data for the dry samples (which are not exposed to any form of solvent) are presented in Table 2.

Figure 2 shows azimuthally reduced SAXS data representing the three steps of preparing a sample from the precursor polymer: the mother (original) sample (ID33), the cross-linked sample (ID33-x20), and the cross-linked and etched sample (ID33-x20e). In case of the precursor polymer the scattering gives evidence to a hexagonal structure by the presence of the higher order peaks at ratios of $\sqrt{3}$ and $\sqrt{7}$ with respect to the primary scattering peak q^*. After cross-linking the higher order scattering peaks have vanished, but an intense primary peak remains, which very likely is Bragg scattering from the ordered structure which is still present in the sample. The peak position is shifted to little higher q values, which is indicative of a slight shrinkage. Although a natural consequence of the selective etching is an increase of contrast between the cavity voids and the PI matrix compared to the contrast between PDMS and PI, the ID33-x20e sample gives no nanoporous scattering profile following the preparatory steps as observed in other samples.[24] The absence of any indication of a nanoporous structure for the collapsed sample is similar to previous observations.[13]

In the inset in Figure 2 a position on the q scale is marked, which is calculated assuming that the volume of the cross-linked PI matrix (a soft elastomer) does not change or is influenced in any way during selective etching of the PDMS minority component. As etching progresses, the cylindirical

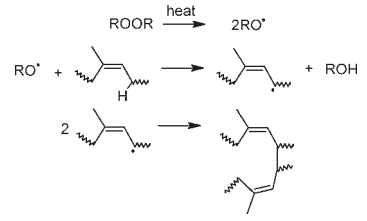

Figure 1. Scheme for cross-linking of PI by thermal treatment with a peroxide.

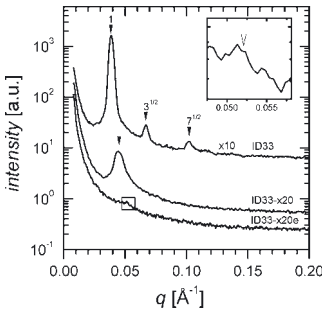

Figure 2. Azimuthally averaged SAXS data of the original precursor (ID33), the cross-linked (ID22-x20), and the etched (ID33-x20e) samples. In order to separate plots for better presentation, the top scattering profile is multiplied by a factor of 10. The primary peak position (q^*) is marked by numeral "1" and higher order reflections are marked accordingly showing the indications of a hexagonal structure. The inset in the top right corner magnifies the scattering curve for sample ID33-x20e in the vicinity of the 0.05 Å^{-1} scattering vector. The open triangle indicates the maximum expected peak position for a vanishing nanoporous structure (see text). The weak peak at 0.051 Å^{-1} hints the presence of a slight contrast (change of PI density) at the centers of the collapsed cylindrical cavities.

Table 2. Structural Data for Dry Samples (without Exposure to Solvents) and Wet Samples[a]

	dry					wet (in d-toluene)	
	precursor	cross-linked		etched		etched	
sample codes	ID33	ID33-x14	ID33-x20	ID33-x14e	ID33-x20e	ID33-x14e	ID33-x20e
SAXS q_{10} [Å^{-1}]	0.0387	0.0452	0.0448	0.0489[b]	0.0513[b]		
$2\pi/q_{10} = d_{10}$ [Å]	162	139	140	128	122		
SANS q_{10} [Å^{-1}]		0.0426	0.0426	no peak	no peak	0.0374	0.0400
$2\pi/q_{10} = d_{10}$ [Å]		147	147			168	157

[a] The results of Bragg spacing (d_{10}) measurements are listed for SAXS and SANS experiments. Data accuracy for SAXS and SANS is about 1% and 5%, respectively. [b] This is an observation of a very weak "bump" in the q-position, which indicates the maximum q-value possible given conditions discussed in the text.

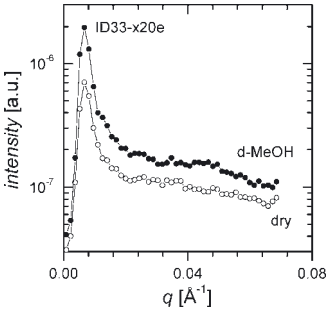

Figure 3. Azimuthally averaged SANS profiles of the raw scattered intensity of sample ID33-x20e. Scattering from the sample in the dry state is depicted by open symbols, and scattering from the sample placed in d-methanol is depicted by closed symbols. The high intensity at very low q is parasitic scattering due collimation of the neutron beam and background intensity.

PDMS domains reduce in size and cause a shrinking of the hexagonal structure. As the etching is complete the cylindrical domains have totally collapsed, all PDMS is removed, and there is no longer any scattering contrast in the polymer. A position on the q scale can be calculated based on the peak position of the cross-linked polymer prior to etching, which is equivalent to the highest possible q value of scattering from the etched collapsed system. The very small peak at 0.051 $Å^{-1}$ can be interpreted as due to small PI density modulation at the centers of the collapsed cylindrical domains.

Attempts of obtaining electron micrographs of the nanostructure in samples ID33-x14e and ID33-x20e were conducted in vain. From this evidence we conclude that there are no nanopores in the as-prepared dry samples from the batch of ID33.

SANS Investigation of Morphology Responses to Selected Solvents. Before investigating sample response to various solvents, we present the SANS profiles of the dry sample ID33-x20e in Figure 3 (open symbols). The SANS data show an absence of any constructive Bragg scattering for ID33-x20e, which is in agreement with the collapsed state, as discussed in the previous section.

In the following sections we will investigate how the sample behaves when exposed to respectively a nonsolvent and a solvent for the cross-linked PI matrix. We do this in the hope that such investigation can shed light on the nature of the unresolved structure of the collapsed material. The question is whether a nonsolvent will percolate into the PI matrix by reopening the original nanocavities. When using a deuterated liquid, the contrast factor between filled cavity and matrix will be greatly enhanced and in this way amplify otherwise weak Bragg scattering. On the other hand, the expectation for a solvent is that the sample will undergo swelling and that the matrix will change dimensions.

Exposure to a Nonsolvent (Methanol). Methanol is a nonsolvent for the cross-linked PI matrix. The exposure of the ID33-x20e sample to deuterated methanol did not yield any change of the scattering as judging from the SANS profile in Figure 3 (closed symbols). The scattering remains indecisive and does not characterize the morphology of the sample beyond the level of being collapsed in agreement with the dry SANS and SAXS data. The data indicates that there is no trace of the original structure left in the sample, which could facilitate a guided percolation of the nonsolvent.

Exposure to a Solvent (Toluene). Toluene is a solvent for the cross-linked PI matrix. The second liquid exposure

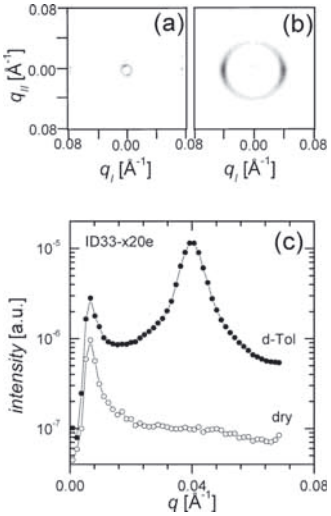

Figure 4. Two-dimentional scattering patterns recorded for the sample ID33-x20e in (a) the dry state without any solvent exposure and (b) in the wet state where the same sample was placed in d-toluene for 150 min. SANS data were collected for 300 s in both cases. The azimuthally averaged data are compared in (c).

experiment is an attempt to swell the complete sample matrix and study the effect of this on the sample structure. Placing the sample in toluene will cause swelling of the cross-linked matrix.

As illustrated in Figure 4, this led to a dramatic change of the scattering fingerprint of the collapsed sample ID33-x20e. The two-dimensional detector response shows the scattering collected over 300 s. Figure 4a shows the scattering from the dry sample. After being submerged in deuterated toluene for 2.5 h a very strong scattering signal is observed as illustrated in Figure 4b. Obviously, the solvent swells the sample and apparently fills out the empty pore cavities. The two-dimensional scattering is anisotropic, which is in perfect agreement with the extrusion processing during sample preparation. Hence, the sample holds a memory of both the originally templated diblock morphology and the preparation alignment procedure, which persists matrix cross-linking and nanoporous etching. At the end of the preparation procedure the dry sample renders no structure, but when the cross-linked matrix is swollen by a solvent, the nanostructured morphology makes its presence. The azimuthally integrated scattering pattern in Figure 4c allows a precise identification of the Bragg peak position. The scattering peak positions of the swollen ID33-x14e and ID33-x20e samples are relatively close to each other (as seen in Table 2) and in good agreement with the preparatory procedure which suggest that the higher cross-linked sample exhibits the smaller Bragg spacing of the swollen polymer and vice versa.

Swelling Kinetics of Collapsed Structure. Finally, we want to test how well a collapsed sample will reproduce the behavior of exhibiting nanoporous structure during swelling. In order to do this, the sample ID33-x14e was subjected to repetitive cycles of swelling in d-toluene followed by drying in air. This was done online in the SANS instrument and enabled investigation of the kinetics of the swelling as well as the reproducibility of cycles of swelling and drying.

Figure 5 shows the time evolution of two swelling−drying cycles. The azimuthally averaged SANS profiles of scattering

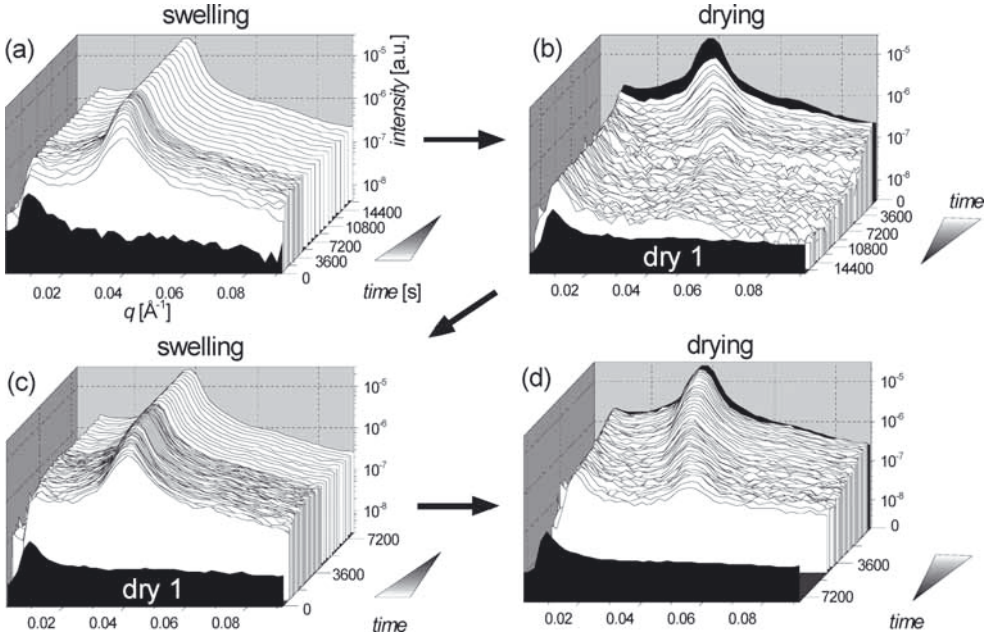

Figure 5. Time evolution of repeated swelling and drying as observed in the azimuthally averaged SANS profiles. The initial and resulting dry states are shown at the front of each sequence of data which shows the scattering intensity versus scattering vector q. The sample ID33-x14e was exposed to (a) swelling, (b) drying, (c) repeated swelling, and (d) repeated drying. Notice the direction of the time axis is alternatively reversed for clarity of the evolution of the scattering profiles.

intensity versus scattering vector q show evidence of the structural changes in the sample. The scattering from the dry state of the sample is indicated in black at the front of Figure 5a. There is no scattering peak from nanostructure in the dry sample. After submerging the sample into d-toluene the first 60 s frame of scattering was recorded with a time delay of 4.5 min. This is due to the handling procedure of introducing the solvent and the safety routine for the neutron exposure. A scattering peak is clearly evident at this time, and the scattering vector q^* at peak intensity maximum decreases following time, in agreement with an increase of the real space dimensions of the material structure.

Figure 5b presents the scattering recorded during sample drying. The last recorded wet scattering profile from the swelling is put at the back of this series of profiles for comparison and marked in black. As anticipated, the peak position at maximum intensity increases and the intensity drops over time. After 4 h the scattering peak is almost gone. Following subsequent drying of the sample in air for 6 h and another 2 h in a vacuum chamber the resulting scattering marked "dry 1" is displayed as the black plot at the front. This scattering gives proof that the swelling-induced nanostructure (in the form of a peak of intensity) has completely gone. Back at the starting point the sample was exposed to a second swelling experiment, and the resulting evolution on the scattering is documented in Figure 5c. The effect of the d-toluene solvent is identical to the first cycle. Finally, the sample was dried for the second time as illustrated in Figure 5d. The evolution in the scattering does not completely reproduce the evolution of the first drying sequel. Drying conditions were not subjected to particular control, and the two drying experiments are not comparable in a detail that justifies a close relative inspection of the two cycles. However, the scattering data of the swelling behavior are a more precise intrinsic measurement of the interaction between solvent and sample, and the repeated swelling sequences will be the subject of work to follow and future publications.

A fully dried sample was obtained after 3 h, which shows no nanostructured scattering. Hence, we can conclude that the two swelling−drying cycles resulted in repeated appearance and disappearance of the nanostructure. We interpret this as being in fact an opening and closing of nanoporous voids, which are templated into the collapsed sample by the original morphology of the diblock precursor polymer ID33. Also, the sample reproduced the originally introduced alignment by the shear extrusion preparation process as evidenced by the 2D scattering profile, which shows strong equatorial peaks similar to those of Figure 4b. In conclusion, this set of data shows that the collapsed material exhibits memory of the sample history on two accounts, namely precursor morphology and preparatory alignment.

Conclusions

We have examined the structure and behavior of a collapsed elastomeric PI-matrix material which was prepared from diblock copolymer precursors by cross-linking and selective etching of the minority block. At first sight the sample displayed no structural evidence as investigated by TEM, SAXS, and SANS measurements of dry specimens. However, this cross-linked material exhibited interesting properties as a gel when exposed to solvent which swells the PI matrix. A nanostructure is dormant and recovers inside the gel in such a fashion that the anticipated porosity is re-established, which matches the nanostructure of the precursor block copolymer material. The appearance of structure seems to be driven by a process, which swells the matrix and

inflates the cavities, which are vacated by the original expendable block copolymer component. These results resemble observations by Durkee et al. in a study on the microstructure in cross-linked diblock copolymer gels, which reported on solvent-filled open channels inside a network of swollen PI.[27] Furthermore, the structure also exhibits perfect agreement with the process of extrusion that was part of the preparation procedure. This was evidenced by anisotropic scattering caused by the presence of elongated (solvent filled) cavity structures aligned in the extrusion direction. Hence, the collapsed elastomeric material has memory of the original precursor morphology and the preparatory extrusion alignment. Upon cycles of swelling and drying the nanostructure shows up and disappears—reversibly, which suggests that the presence and absence of solvent can open and close the cavities. Very interestingly, the cavities are not prone to be opened by nonsolvents to the matrix, which suggests that the nature of the liquid (solvent or nonsolvent) could control the state of the material in e.g. a membrane application. This means that the material could have some "smart" application in advanced separation systems and maybe used as a form of valve, where the liquid polarity would be the controlling external stimuli.

Acknowledgment. This work was supported by a grants given by the Danish Research Council for Technology and Production Sciences (FTP Grant 26-03-0271), DANSCATT centre sponsored by the Danish Natural Science Research Council. The authors thank Thomas Geue at the Paul Scherrer Institute (Villingen, Switzerland) for providing beam time at the SANS 2 instrument, Pia Wahlberg at the Danish Technological Institute (Høje Taastrup, Denmark), for help with SEM and Fengxiao Guo at the Department of Chemical Engineering, DTU (Kgs. Lyngby, Denmark), for sample preparation. M.E.V. is grateful for support given by Kaj Hansen's Foundation (Danalim Prisen).

References and Notes

(1) Wei, Z. G.; Sandstrom, R.; Miyazaki, S. *J. Mater. Sci.* **1998**, *33*, 3743–3762.
(2) Pei, Q. B.; Inganas, O. *Adv. Mater.* **1992**, *4*, 277–278.
(3) Gazotti, W. A.; Casalbore-Miceli, G.; Geri, A.; Berlin, A.; De Paoli, M. A. *Adv. Mater.* **1998**, *10*, 1522.
(4) Koberstein, J. T.; Duch, D. E.; Hu, W.; Lenk, T. J.; Bhatia, R.; Brown, H. R.; Lingelser, J. P.; Gallot, Y. *J. Adhes.* **1998**, *66*, 229–249.
(5) Gil, E. S.; Hudson, S. A. *Prog. Polym. Sci.* **2004**, *29*, 1173–1222.
(6) Baughman, R. H. *Synth. Met.* **1996**, *78*, 339–353.
(7) Harmon, M. E.; Tang, M.; Frank, C. W. *Polymer* **2003**, *44*, 4547–4556.
(8) Mortensen, K.; Pedersen, J. S. *Macromolecules* **1993**, *26*, 805–812.
(9) Mortensen, K.; Almdal, K.; Kleppinger, R.; Mischenko, N.; Reynaers, H. *Physica B* **1997**, *241*, 1025–1028.
(10) Yerushalmi, R.; Scherz, A.; van der Boom, M. E.; Kraatz, H. B. *J. Mater. Chem.* **2005**, *15*, 4480–4487.
(11) Olson, D. A.; Chen, L.; Hillmyer, M. A. *Chem. Mater.* **2008**, *20*, 869–890.
(12) Hillmyer, M. A. *Adv. Polym. Sci.* **2005**, *190*, 137–181.
(13) Guo, F.; Andreasen, J. W.; Vigild, M. E.; Ndoni, S. *Macromolecules* **2007**, *40*, 3669–3675.
(14) Hansen, M. S.; Vigild, M. E.; Berg, R. H.; Ndoni, S. *Polym. Bull.* **2004**, *51*, 403–409.
(15) Ndoni, S.; Vigild, M. E.; Berg, R. H. *J. Am. Chem. Soc.* **2003**, *125*, 13366–13367.
(16) Guo, F.; Jankova, K.; Vigild, M. E.; Ndoni, S. *Polym. Prepr.* **2008**, *49*, 540.
(17) Ndoni, S.; Papadakis, C. M.; Almdal, K.; Bates, F. S. *Rev. Sci. Instrum.* **1995**, *66*, 1090–1095.
(18) Andersen, K.; Diplom, K. Thesis, Dept. of Chemical Engineering, Technical University of Denmark, Lyngby, Denmark, **2005**.
(19) Strunz, P.; Mortensen, K.; Janssen, S. *Physica B* **2004**, *350*, e783–e786.
(20) Mark, J. E., Ed. *Polymer Data Handbook*; Oxford University Press: New York, 1999.
(21) Brandrup, J.; Immergut, E. H. *Polymer Handbook*, 3rd ed.; John Wiley & Sons: New York, 1989.
(22) Krevelen, V. D. W., Ed. *Properties of Polymers*; Elsevier: Amsterdam, 1990.
(23) Cavicchi, K. A.; Zalusky, A. S.; Hillmyer, M. A.; Lodge, T. P. *Macromol. Rapid Commun.* **2004**, *25*, 704–709.
(24) Ndoni, S.; Vigild, M. E.; Berg, R. H. *J. Am. Chem. Soc.* **2003**, *125*, 13366–13367.
(25) Higgins, J. S.; Benoît, H. C. *Polymers and Neutrons Scattering*; Oxford University Press: New York, 1997.
(26) Li, Y.; Tanaka, T. *J. Chem. Phys.* **1990**, *92*, 1365–1371.
(27) Durkee, D. A.; Gomez, E. D.; Ellsworth, M. W.; Bell, A. T.; Balsara, N. P. *Macromolecules* **2007**, *40*, 5103–5110.

D

Gyroid membranes made from nanoporous block copolymers.

Piotr Szewczykowski[1], Gunnar Jonsson[1], Rolf H. Berg[2], Martin E. Vigild[1], Sokol Ndoni[2*]*

[1]Department of Chemical and Biochemical Engineering,

Technical University of Denmark, DK-2800 Kgs. Lyngby, Denmark.

[2]Department of Micro- and Nanotechnology, Technical University of Denmark,

Frederiksborgvej 399, DK-4000 Roskilde, Denmark

Telephone: +45 4677 4784

Fax: +45 4677 4791

pps@kt.dtu.dk; gj@kt.dtu.dk; rolf.berg@risoe.dk; mev@kt.dtu.dk; sokol.ndoni@risoe.dk;

ABSTRACT Nanoporous films of well-defined porosity and pore size can be prepared from self-organizing model block copolymer precursors. In the present study we test a cross-linked nanoporous 1,2-polybutadiene of double gyroid (GYR) morphology, with porosity 40% and pore cross-section diameter of 15 ± 4 nm as a potential candidate material for ultrafiltration membranes. Self-supporting nanoporous discs of 0.5 mm

thickness, prepared by solvent casting were firstly tested relative to fluxes of different fluids: nitrogen, carbon dioxide, hydrogen and mixtures of methanol and water. The molecular size cut-off of the same membranes was afterwards determined by the filtration of polyethylene glycol (PEG) molecules of different molecular weight dissolved in methanol/water 80/20 or 20/80 mixtures. Permeates and feeds were analyzed by size exclusion chromatography. A cut-off value lying between 8000 and 12000[g/mol] was found, corresponding to molecular hydrodynamic diameters of 7-9 nm, as determined by Dynamic Light Scattering. The membrane characteristics of the GYR nanoporous polymer were compared with one commercial polysulphone ultrafiltration membranes. The GYR membranes were robust to changes in the methanol/water mixtures, while the commercial membrane lost its ultrafiltration capability at high methanol content.

KEYWORDS ultrafiltration membranes, nanoporous, block copolymers, gyroid morphology.

MANUSCRIPT TEXT

Introduction Pore size and size distribution determine the separation properties of porous membranes. Separation and selectivity depend also on enthalpic interactions with the pore surfaces, therefore on the surface area and surface chemistry [1] [2][3]. Size discrimination of membranes relevant for molecular filtration is expected to be significantly more effective with membranes having pores in the range of nanometer instead of micrometers.

Potential application as separation media is mentioned in almost any article on nanoporous materials (NPs) obtained from diblock copolymers [4][5][6]. Most of the

existing literature reports focus on NPs with hexagonally packed cylindrical morphology (HEX) and cylindrical cavities oriented perpendicularly to the main surface of the membrane. Orientation of the cylinders in the flow direction (perpendicularly to the main surface) is necessary in order to use the material as a membrane [7]. Yang *et. al.* showed that thin nanoporous films of HEX morphology can be used indeed as an ultrafiltration media, for example to separate viruses [8]. In the case of membranes prepared from diblock copolymers, the gyroid (GYR) morphology is an interesting alternative to the hexagonal morphology. GYR is an isotropic cubic structure of $Ia\bar{3}d$ symmetry and therefore porosity percolation is warranted with no need for structure pre-alignment procedures. One disadvantage relates to the difficulty of preparation of the gyroid morphology, since it occurs in a narrow range of the diblock copolymer micro phase diagram, i.e. in a narrow range of composition, chain length and temperature [9]. A strict control of the polymerization process is necessary in order to reduce the composition and chain length dispersities. This is possible by application of special polymerization techniques such as living anionic polymerization [10] and in lesser degree atom transfer radical polymerization [11]. However once the boundaries of the GYR morphology are experimentally determined in the micro-phase diagram, samples of this morphology can be routinely synthesized by these advanced techniques. A 1,2-polybutadiene-*b*-polydimethylsiloxane (1,2-PB-PDMS) diblock copolymer with GYR morphology was prepared by sequential living anionic polymerization. Since both blocks of the copolymer have glass transition temperatures below the room temperature it is necessary to crosslinkg the majority block before selectively removing the minority block. Otherwise

the pores formed during the removal of the minority block would collapse under the action of internal Laplace pressure [12].

The gyroid morphology of diblock copolymers has been characterized by many authors [13]. To the best of our knowledge this is the first report investigating the possibility to use a GYR NP as an ultrafiltration membrane.

The rest of the paper is organized as follows. The characterization of structure and especially the porosity of the nanoporous material will be firstly reported. The membrane specific characterization such as gas and solvent permeability follows. The central part of this paper is the study of size separation of polymer solutions by means of the gyroid nanoporous membranes. The obtained results are finally compared with ultrafiltration of same polymer solutions by commercial membranes.

Experimental

This section comprises three main themes: 1. Membrane material, 2. Membrane performance and 3. Characterization techniques.

Membrane material

The precursor block copolymer 1,2-polybutadiene-*b*-polydimethylsiloxane was synthesized by living anionic polymerization [14].

Dicumyl peroxide (*bis(α,α-dimethylbenzyl) peroxide*) (DCP) (Merck) was used as crosslinker. 1 mol% of DCP relative to the double bonds in the polybutadiene block was sufficient to ensure pore stability after the etching process. The polymer was dissolved together with DCP in tetrahydrofurane (THF) in a Petri dish. The mass of the dissolved polymer before crosslinking was calculated to ensure 0.5 mm polymer film thickness after solvent evaporation. After the crosslinking 14mm diameter discs were cut out of the

crosslinked film. The details of the crosslinking reaction and the procedure can be found elsewhere [14].

1M solution of tetrabutylammonium fluoride (TBAF) in tetrahydrofurane (THF) (Aldrich) was used to etch the minority block PDMS from the crosslinked copolymer. According to established procedure 5 times molar excess of TBAF relative to the PDMS repeating unit and a reaction time of 36 h guarantee quantitative removal of the PDMS block. More information about the etching mechanism and the procedure can be found elsewhere [14]. After etching, the samples were rinsed in THF, mixtures of THF with methanol and at the end with pure methanol, before sample drying.

One commercial ultrafiltration membrane from Alfa Laval was investigated as a reference for our material. This is a polysulphone membrane on a polypropylene support. The active membrane area was 36.3 cm^2, as calculated from the internal diameter of the o-ring (6.8 cm).

Membrane performance

A simple set up (Figure 1) was used for the filtration experiments. Nitrogen was the gas used to create pressure on the feeding side of the membrane. The main parts of the setup are schematically shown in Figure 1; they comprise a pressure gauge, a security valve, stainless steel pipes and a membrane fixture. The membrane was mounted in a home-made stainless steel fixture (Figure 1a). The drainage system of the device is made of PVC. Permeate is collected through the drainage channels and the outlet tube to a 1 ml glass with marked 0.2ml scale, as shown in Figure 1 b.

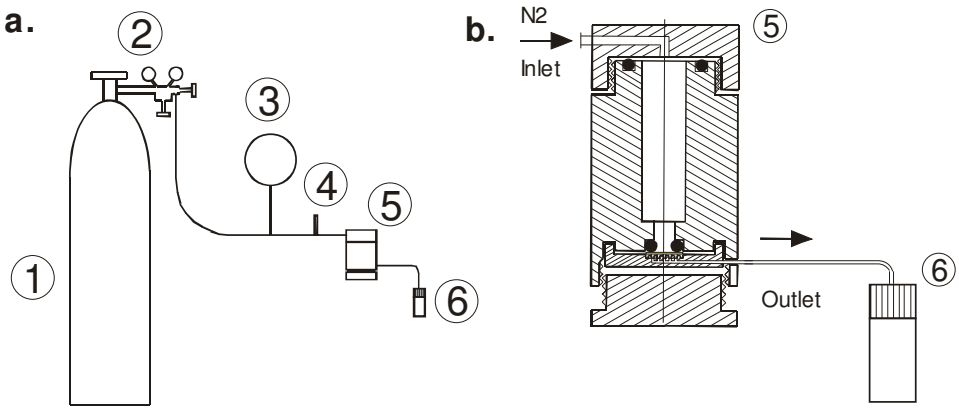

Figure 1 Schematics of filtration setup. a. Set up overview consists of: 1. nitrogen bottle, 2. gas reducer with valves, 3. manometer, 4.security valve, 5. membrane device, 6. permeate collecting glass b. Details of membrane device.

Gas fluxes were measured on the same set up, except that a bubble flow meter was used instead of the collecting glass (element nr 6 in Figure 1).

The setup used for the investigation of the commercial membrane is similar to the scheme of Figure 1a, however the membrane device is bigger and made from glass and PVC. The device was filled with 400 ml of liquid in this case.

Fluxes of three different gases: nitrogen, hydrogen and carbon dioxide (all by AGA) were calculated from the speed of bubble displacement in the bubble flow meter.

Fluxes of pure solvents: methanol/water 80/20 and 20/80 volume ratios were calculated from the measurement of time needed to collect a given volume of permeate.

Solutions of polyethylene glycol samples of different molecular weight: 1 kg/mol from Merck, 3 kg/mol, 8 kg/mol, 10 kg/mol, 12 kg/mol, 35 kg/mol from Fluka, and 100 kg/mol from Serva were filtered through the NP disc.

Polyethylene glycols were dissolved in a mixture of methanol (MeOH) and water (80:20 volume ratio) 20% of water was added in order to ensure better dissolution of high molecular weight PEG. Pure methanol and 80:20 MeOH:H_2O penetrate exclusively the pore volume [14].

Firstly the solution of PEG 1 kg/mol, PEG 10 kg/mol and PEG 100 kg/mol in MeOH/water (80:20) was prepared. The concentration of each of the components was 0.5mg/ml. This solution is called Feed A. Such a wide range of molecular weights was chosen for the preliminary experiment aiming at a first estimation of the cut off value. A more accurate determination of such a value was achieved at a second step by using five PEG samples covering the more restricted M.W. range 1 – 35 kg/mol. The solution of PEG 1 kg/mol, PEG 3 kg/mol, PEG 8 kg/mol, PEG 12 kg/mol and PEG 35 kg/mol with concentration of 0.5 mg/ml for each of the components in MeOH/water (80:20) is called Feed B in the following. The third feed solution with same concentration of polymer in MeOH/water (20:80) is referred to as Feed C.

In the case of the commercial membrane GR61PP solutions of the same five PEG samples with individual concentration of 2 mg/ml were prepared either in methanol/water 80/20 (Feed D) or in methanol/water 20/80 (Feed E).

All the feeds used for filtration are summarized in Table 1.

Feed	PEG (kg/mol)	Concentration (g/liter)	Solvent (methanol/water v/v)
A	1+10+100	0.5	80/20
B	1+3+8+12+35	0.5	80/20
C	1+3+8+12+35	0.5	20/80
D	1+3+8+12+35	2	80/20
E	1+3+8+12+35	2	20/80

Table 1 Feeds used for separation experiments. Polyethylene glycols of different molecular weights (second column) and given concentration of each PEG (third column) were dissolved in two mixtures of methanol and water (described by the volume fractions in the last column)

The commercial membrane was treated similarly to the nanoporous membrane. The membrane was mounted in the separation device filled with 400 ml 80 methanol :20 water and left overnight without any stirring or pressure. Next day the mixture of methanol (80%) and water (20%) was percolated and the Feed D was filtered and the permeates at 1 bar, 2 bar and 3 bar of pressure were collected and analyzed by size exclusion chromatography. The mixture of methanol (80%) and water (20%) was percolated again. The mixture of methanol (20%) and water (80%) was run through the membrane. Feed E was filtered and the permeate at 1 bar, 2 bar and 3 bar pressure was collected and analyzed by size exclusion chromatography.

Characterization techniques

Each sample for Scanning Electron Microscopy (SEM) was prepared by crushing a piece of the NP film in an agat mortar filled with liquid nitrogen. Fragments were then

fixed on the aluminum specimen mount covered by the Ted Pella double-coated carbon tabsand additionally stabilized by CCC Carbon Adhesive (Electron Microscopy Science). Samples were first sputter-coated with a 2-3 nm layer of gold in a Polaron SC7640 instrument. Then after 12-14h in the microscopy chamber the samples were investigated by Scanning Electron Microscopy (SEM) on a Zeiss 1540 EsB Gemini SEM at 2kV electron beam accelerating voltage.

The instrument Micromerities ASAP 2020 Surface Area and Porosity Analyzer was used for investigation. Samples of about 0.1g were used for analysis. No particular sample preparation was needed for performing nitrogen adsorption [15].

In all cases the mass of disc was measured in the dry state and in the wet state after equilibration in methanol.

The size separation performance of the membranes was quantified by Size Exclusion Chromatography (SEC) of the feed and the collected permeate solutions. Water was the eluent at a flow rate of 0.6 ml/min. The sample injection volume was 40µl and the column used was Waters Ultrahydrogel^{TM} 250 6µm 7.8 x 300 mm GPC column. The SEC setup consists of a 717plus Autosampler, a 600 Controller and a 410 Refractive Index Detector, all from Waters^{TM}.

Dynamic light scattering experiments were done at the Risø National Laboratory by using Brookhaven-BI-2000 SM system with 35 mW HeNe Laser, 633 nm (Red). The polyethylene glycols used to prepare the feed solutions (see table 1) and two additional PEG standards (97.4 and 55.6kg/mol) by Polymer Laboratories were dissolved each in 3 ml of methanol/water (80/20). The solutions were filtered through 0.2 µm Supor®

Membrane on Acrodisc® Syringe Filter by Pall-Life Science prior to measurements. Solutions were investigated at different pinhole diameters: 100; 200; 400 and 1000 µm.

Results and discussion

Structure

Investigation of the gyroid morphology with electron microscopy is quite complex, since we observe different surface morphologies depending on the fracture of the sample. Projections along different directions occur as characteristic patterns like: “knitting”, “wishbone” or “wagon wheel”[16]. Figure 2a shows a “knitting” pattern which results from cut along the (211) symmetry plane of unit cell. This result from SEM corresponds very well to the computer graphics in Figure 2b [17] [18]. Bright phase corresponds to the 1,2-polybutadiene whereas dark phase corresponds to the pores. A graphical representation of the gyroid network is shown on Figure 2c.

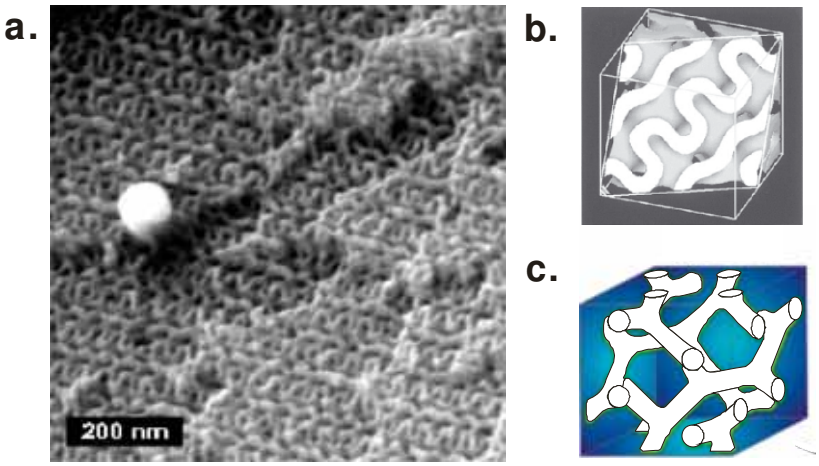

Figure 2 a. SEM picture of “knitting” pattern of nanoporous sample. b. Computer graphic presenting a two dimensional cut along the (211) plane c. Graphical presentation of the gyroid network. The pore diameter is expected to vary in the gyroid morphology,

with a maximum expected at the 3-branch zones and a minimum at half distance between two branches.

The observed nitrogen gas physisorption isotherm fitted to the Type IV isotherm which is characteristic for mesoporous (2-50 nm pore diameter) adsorbents. The hysteresis loop was of type H1 which indicated quite uniform pores [19]. The specific surface area calculated from BET method for nanoporous sample was 278 m^2/g. The pore size distribution obtained from BJH method showed the pore diameter in the range of 15±4 nm.

Measurement of porosity by methanol uptake

A direct and simple measurement of a nanoporous sample's porosity requires two gravimetric data: the mass of the dry sample and the mass of the wet sample after equilibration in methanol. In a previous publication [14] evidence was presented on the exclusive access of methanol into the pore volume. The measured porosity by this method is 0.39 ± 0.01, which is within experimental uncertainty equal to the calculated porosity from the block copolymer composition data.

Membrane performance

Gas and solvent membrane permeability

Gas fluxes

Results on fluxes of three different gases through nanoporous discs are presented in Figure 3. Hydrogen flux is much higher than nitrogen and carbon dioxide. The flux of CO_2 is slightly lower than N_2 for pressures up to 30 bar and slightly higher for 35 and 40 bar.

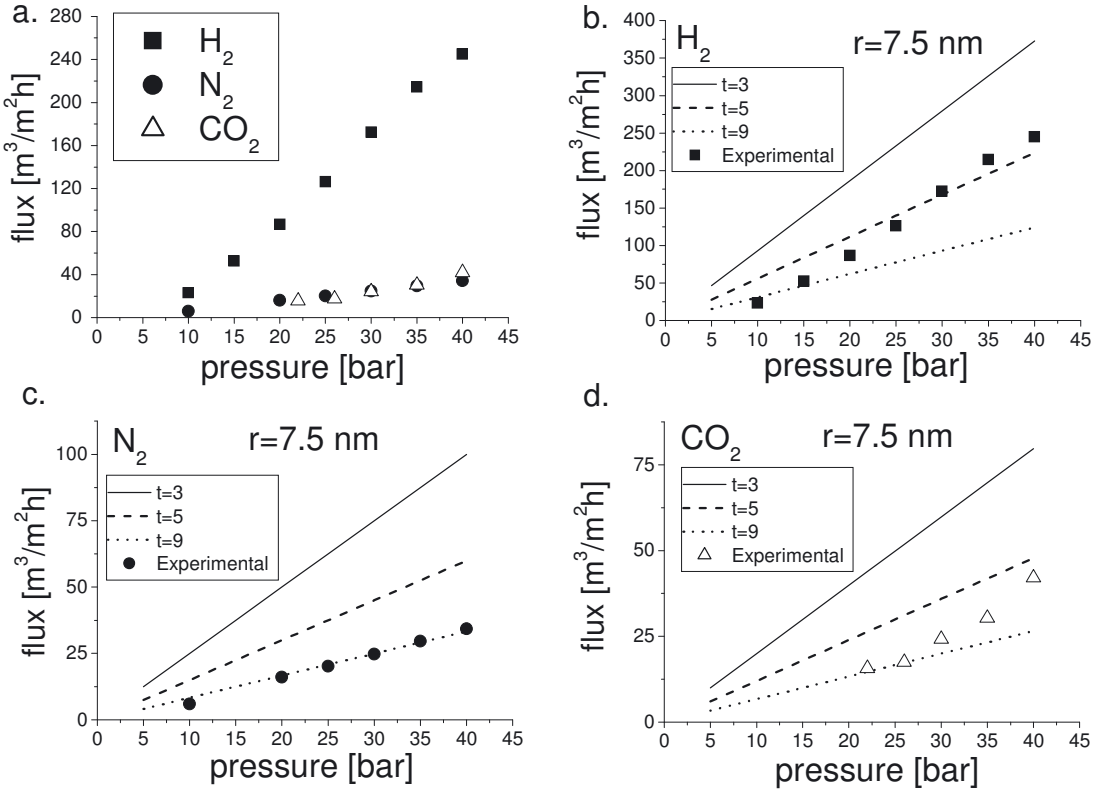

Figure 3 a: Experimental fluxes of H_2 (squares), N_2 (circles) and CO_2 (triangles); b, c and d: experimental (symbols) and theoretical values of flow according to Knudsen equation for pore diameter: 7.5 nm and at four different tortuosity factors: t=3 (solid line); t=5 (dash line); and t=9 (dot line).

The mean free path of Hydrogen gas is higher (98.7 nm) compared to the mean free path of nitrogen (62.0 nm) and carbon dioxide (51.3 nm) at standard conditions whereas the mean free paths of the last two gases are similar. Since the pore diameter of the

nanoporous material is in average 15 nm, that is smaller or similar to the mean free path in all the pressure range tested, the Knudsen diffusion is expected to be the principal regime of gas diffusion in the present experiments [20]:

$$J = \frac{\varepsilon \cdot D_k \cdot \Delta P}{R \cdot T \cdot \tau \cdot l} \qquad \textbf{Equation 1}$$

where J is a volume flux, ε is surface porosity, D_k is Knudsen diffusion coefficient, τ is pore tortuosity and ΔP, R, T and l stand for pressure difference, gas constant, temperature and membrane thickness respectively.

In the case of perpendicularly aligned HEX morphology the porosity ε is equal to the volume fraction f_{vol} of the pores. For the isotropic gyroid morphology the porosity is assumed to scale with the power of dimensionality, therefore the surface porosity ε is related to the volume porosity f_{vol} by: $\varepsilon = \left(f_{vol}\right)^{2/3}$. With $f_{vol} = 0.40$, $\varepsilon = 0.54$.

The tortuosity factor for the gyroid morphology could not be found and is taken as a fitting parameter. The Knudsen diffusion coefficient through a cylindrical channel is proportional to the pore radius *r*:

$$D_k = 0.66 \cdot r \sqrt{\frac{8RT}{\pi M_w}} \qquad \textbf{Equation 2}$$

The pore radius was taken 7.5 nm and the experimental data for all the three gases fall between the tortuosity τ values 5 and 9 (Figure 3). Linear extrapolations of the data trends in figs. 3 b, c to zero flux yield 'residual' pressure values between 3 and 7 bars. This deviation from the prediction of eq. 1, is probably related to the presence of a skin layer on at least one side of the disk. The presence of such a skin layer is plausible due to contribution of interfacial energy in the free energy balance at the sample boundaries. For

example, given the low surface tension of the PDMS block in the precursor polymer it will be energetically favorable for the polymer interface to air to be enriched with PDMS. Therefore it is qualitatively expected that the lamella morphology, thermodynamically stable up to 100°C in the bulk, be stable even at higher temperature at the polymer-air interface [21]. If this phase transition 'retardation' is more than 10°C, then the probability that a thin (few tens of nanometer) layer at the interface gets crosslinked at a less opened morphology than the gyroid bulk is increased. A quantitative calculation of the effect is still missing. The case of CO_2 in fig. 3 d is more uncertain due to difficulties in measuring the flux of this gas with the bubble meter. The possible reason for such difficulties is related to the instability of bubbles in the presence of CO_2. Reliable data on the flux of CO_2 for pressures below 22 bars could not be obtained as shown in fig. 3 d.

Pure solvents fluxes

The flux of MeOH/water (80/20) was 1.1 $l\ m^{-2}\ h^{-1}$ at 38 bar, which is almost identical to the flux of the PEG solution in the same solvent.

Since the mean free path of molecules in the liquid state is much shorter than the pore size the Hagen-Poiseuille equation valid for viscous flow in cylindrical cavities was tested as a possible descriptor of the flux data:

$$J = \frac{\varepsilon \cdot r^2 \cdot \Delta P}{8 \cdot \eta \cdot \tau \cdot l} \qquad \textbf{Equation 3}$$

where η is the liquid viscosity and the other quantities have the same meaning as in eq. 1.

According to this equation the flux through the membrane is calculated between 48 l m^{-2} h^{-1} and 16 l m^{-2} h^{-1}] for $3 < \tau < 9$ at 38 bar for pore diameter 7.5 nm, which are much higher than the experimental value. We speculate that the most important reason for such a failure of eq. 3 to describe the liquid flux data is related to the presence of the skin layer already mentioned in relation to the discussion of gas permeability. The highly networked gyroid porous morphology could disturb the laminar flow and increase the resistance to flow, constituting a second possible reason at the basis of the huge discrepancy.

The flux of MeOH/water (20/80) at 5, 20 and 40 bar on the same nanoporous disc after preconditioning in a methanol rich solvent was 0.22; 0.73 and 2.12 l m^{-2} h^{-1}, respectively. The experimental results were compared to calculated values from the Hagen-Poiseuille equation for three values of the tortuosity factor τ=3; 5 and 9 . The results are presented in Figure 4 which shows a large difference between the experimental and theoretical values.

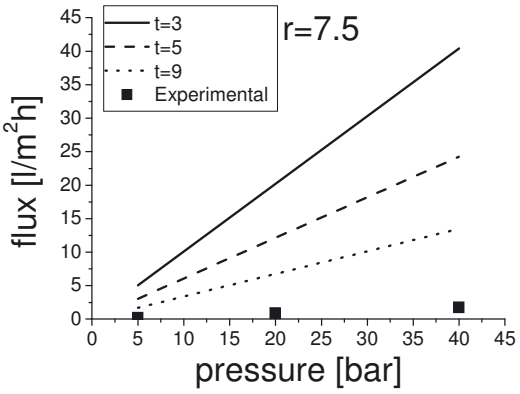

Figure 4 Experimental (symbol) and theoretical values of MeOH/water 20:80 flow according to Hagen-Poiseuille equation at pore radius 7.5 nm and different values of the tortuosity factor τ=3 (solid line); τ=5 (dash line) and τ=9 (dot line).

Size separation of polymers in solution

Results of polymer characterisation

Results of dynamic light scattering obtained with 400 μm pinhole are presented in Table 2. The selection of the pinhole opening in front of the detector was a balance between acceptable photon count rate and quality of correlation function.

Experimental			Literature			Theoretical		
PEG [kg/mol]:	Average $R_h \times 2$ [nm]:	Conc. [mg/ml]:	PEG [kg/mol]:	Average $R_h \times 2$ [nm]:	Conc. [mg/ml]:	PEG [kg/mol]:	$R_g \times 2$ [nm]	$R_h \times 2$ [nm]
1	1.55	20	1.45	2.26	30.98	1	2.94	1.99
3	3.74	20	3.35	3.58	18.23	3	5.81	3.94
8	5.23	10	8.5	5.84	6.50	8	10.47	7.09
10	7.72	10				10	11.97	8.11
12	11.33	10	11.84	6.98	6.00	12	13.36	9.04
35	16.43	5	35	13.18	3.80	35	25.39	17.19
55.6	21.08	3				55.6	33.52	22.69
97.35	36.21	2				97.35	46.91	31.76
230	46.83	2	100	23.9	1.82	230	78.57	52.38

Table 2 Hydrodynamic diameter average value from dynamic light scattering. Literature experimental data and calculated values (see the discussion related to fig. 5 in the main text) are presented for comparison.

The experimental results for the hydrodynamic diameters of the PEG samples were compared to theoretical values calculated in the following way**.** First the radius of gyration R_g for PEG molecules was calculated as:

$$R_g = \frac{1}{6} \cdot R_o^2 \qquad \textbf{Equation 4}$$

where:

R_o^2 - mean square end-to-end distance

R_o^2 in a good solvent, as is the case of PEG in the (methanol : water) mixed solvent, is expressed as:

$$\overline{R}_o^2 = C_n \cdot n^{1.2} \cdot b^2 \qquad \textbf{Equation 5}$$

where:

C_n - the characteristic ratio calculated as a function of chain length [22]

n - number of covalent chain bonds

b - average bond length

The calculated values for the diameter of gyration ($2R_g$)as a function of molecular weight are presented by the solid line in the double logarithmic plot of Figure 5:

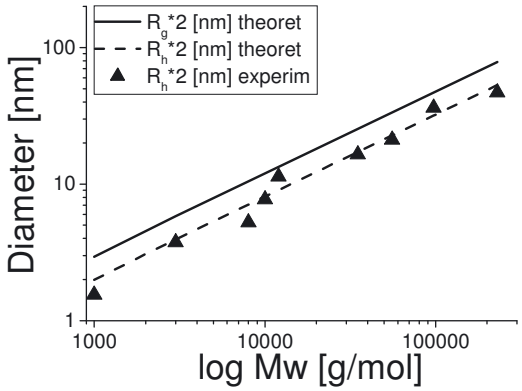

Figure 5 Diameter of gyration (solid line) $2R_g\,[nm]$ calculated from Equation 4; hydrodynamic diameter (dash line) $2R_h\,[nm]$ calculated from the theoretical $R_g\,[nm]$ as described in the main text; experimental data of hydrodynamic diameter $2R_h\,[nm]$ obtained from dynamic light scattering results (triangles).

The R_g values are collected in the eighth column of Table 2. In order to compare the calculated results with the experimental values a proportionality factor between R_g and R_h was needed; such a factor was found in the literature [23]: $R_h \approx \frac{2}{3} R_g$. Based on this ratio values of the theoretical hydrodynamic diameter, $2R_h\left[nm\right]$ were calculated and presented by the segmented line in Figure 5. Values of hydrodynamic diameter are collected in the last column of Table 2. Experimental results of $2R_h\left[nm\right]$ from dynamic light scattering are shown by triangles in Figure 5.

Experimental results from dynamic light scattering are also compared with experimental literature data [24] from quasi-elastic light scattering for polyoxyethylene (POE) prepared in phosphate-buffered saline at 25^{o}C. These data are listed in the middle section of table 2. The overall comparison of our experimental data with the combined literature experimental data and the calculated values is considered satisfactory.

Size separation (ultrafiltration) through the gyroid membranes

10 ml of Feed A, which is a solution of PEG 1+10+100 kg/mol in methanol/water 80/20, and Sample 1(nanoporous disc) were placed in the filtration device. Permeates were analysed by SEC. The '1st Permeate' stands for the first 0.8 ml of permeate collected in the 1ml glass and analysed by SEC. 2nd Permeate and 3rd Permeate were the following 0.8 ml and 0.6 ml of collected volume respectively. Results are presented in Figure 6a, as the detector response in milivolts vs. retention time in minutes. The fluxes of all the PEG solutions through the nanoporous discs were similar to the fluxes of the pure solvents.

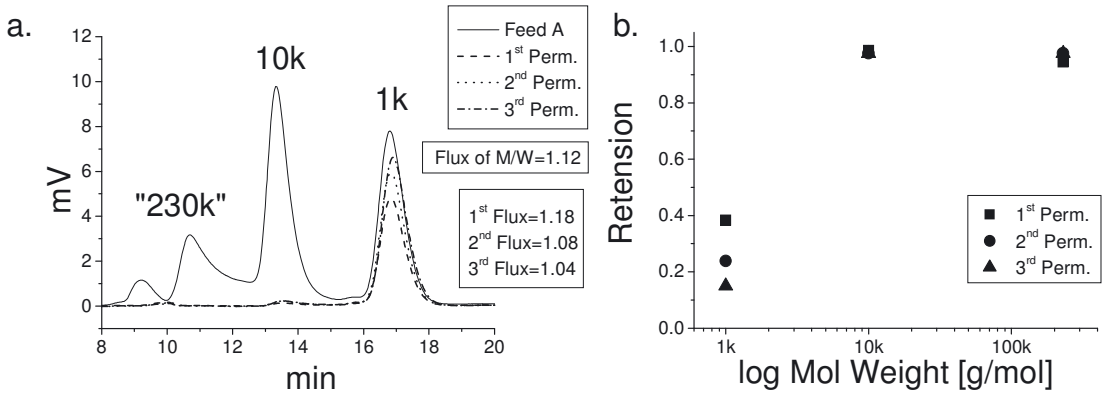

Figure 6 a) Size exclusion chromatography results of filtration Feed A (PEG 1+10+100 kg/mol in methanol/water 80/20) on Sample 1 (nanoporous disc). b) Retention curve based on the analysis of feed and permeates' peaks height

The "PEG 100 000 [g/mol]" showed a bimodal distribution in SEC with MW values of each peak of 230 kg/mol and 60 kg/mol, respectively.

The retention (R) value (Figure 6b) is calculated as: $R = 1 - \frac{C_P}{C_F}$, where C_p and C_F are the concentration of the permeate and the feed, respectively. Knowing the concentration of each of PEG in the Feed A (0.5 mg/ml) we find the permeate concentration from the ratio of permeate and feed peak height.

From Figure 6 it is seen that the membrane is permeable for PEG 1 kg/mol and the retention for this polymer decreases in the successive collected permeates. The peak for PEG 230 kg/mol in all permeates is virtually gone and the retention for these molecules is close to 1.

The same disc was used to filter Feed B, which is a solution of PEG 1+3+8+12+35 kg/mol in methanol/water 80/20. Permeates were analysed by SEC. The1st, 2nd and 3rd Permeate mean the first, second and third 0.8ml of permeate collected. Results are presented in Figure 7.

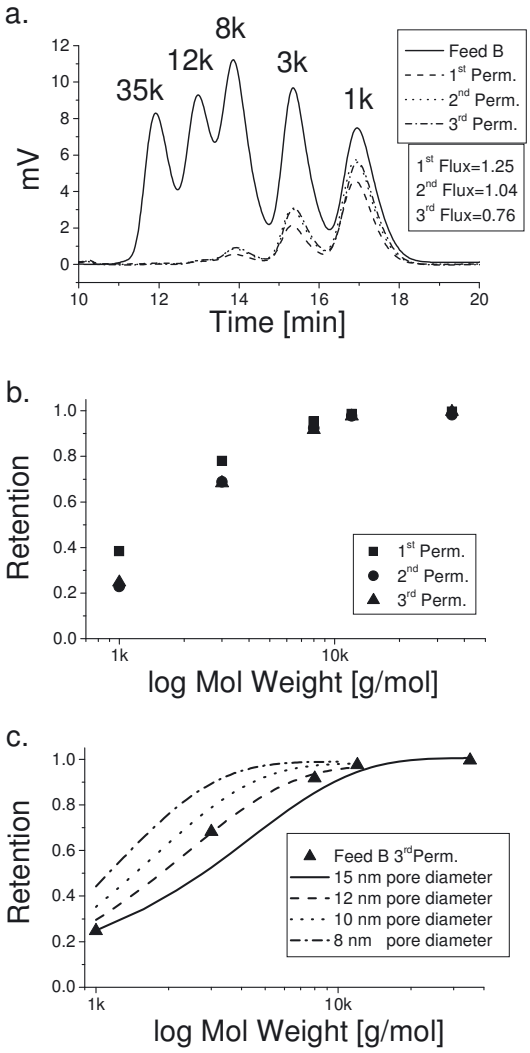

Figure 7 a) Size exclusion chromatography results of filtration Feed B (PEG 1+3+8+12+35 kg/mol in methanol/water 80/20). b) Retention curve based on the analysis

of feed and permeates peaks height. c) Comparison between the retention curve for 3rd Perm from experimental data and calculated maximum retentions for four different pore sizes.

The retention values of the 2nd and 3rd permeates were almost identical as shown in fig. 7 b. The retention profile is also consistent with the profile of fig. 6 b.

Experimental results were compared with a model from literature [25]. In this model the maximum retention of each PEG was calculated for the following values of nanopore diameter: 8 nm, 10 nm, 12 nm and 15 nm. The results are presented in Figure 7 c. The experimental results follow the prediction for a pore diameter of 12 nm, which is within the measured by nitrogen adsorption: 15± 4 nm.

Sample 1 was stored in methanol for 99 days. After a preconditioning in methanol/water 20/80 the disc was used to filtrate Feed C (solution of PEG 1+3+8+12+35 kg/mol in methanol/water 20/80). Four successive permeates (three times 0.8ml and last one 0.6ml) were collected and analysed by SEC. The results are presented in **Figure 8**. Again a good reproducibility of retention profile was observed after the first permeate, as shown in **Figure 8** b. The large difference between 1st and following permeates can come from the fact, that sample was soaked in methanol before PEG filtration. 1st permeate is diluted by solvent left in the sample. 3rd and 4th permeate show that steady state is reached. Same tendency is observed for Feed A (Figure 6) and Feed B (Figure 7).

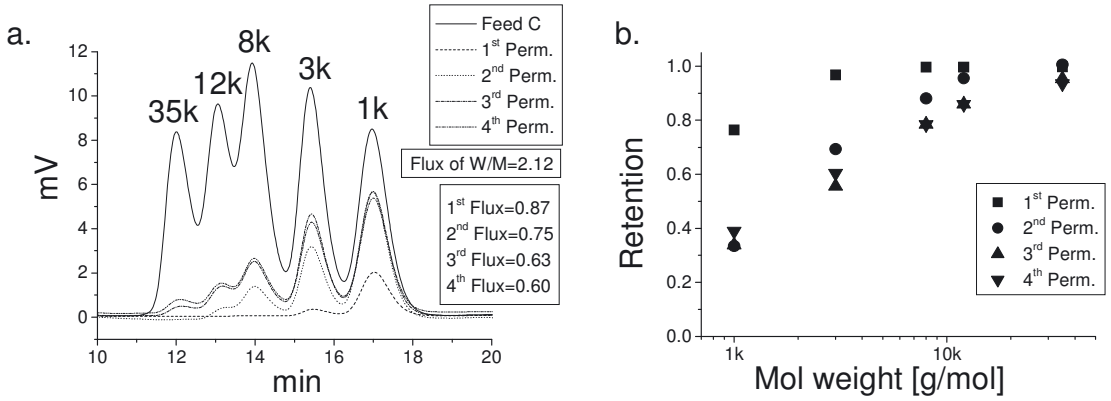

Figure 8 a) SEC results after filtration of Feed C (PEGs in water/MeOH (80/20)) by using Sample 1 at 40 bar. b) retention profiles of four permeates.

The separation properties of a commercial polysulphone membrane, GR61PP by Alfa Laval were investigated and compared to the properties of the nanoporous sample. The results of Feed D (solution of PEG 1+3+8+12+35 kg/mol in 80/20 methanol/water) filtration after overnight membrane conditioning in methanol/water 80/20 are presented in Figure 9. The first permeate at 1 bar shows a low retention value and it further decreases at higher pressures. The results of subsequent Feed E (20/80 methanol/water) filtration are shown in Figure 10. Here the retention values are higher than for Feed D.

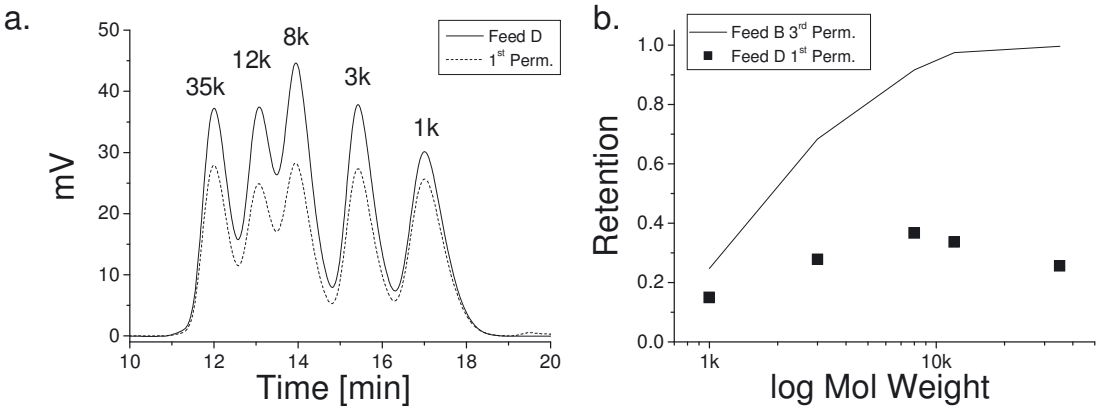

Figure 9 Separation curves for GR61PP. Figure 9a shows curves for Feed D and the following permeates. Figure 9b compares the retention curves for Feed B through the nanoporous disc (see Figure 7), and the filtration of Feed D through the commercial membrane.

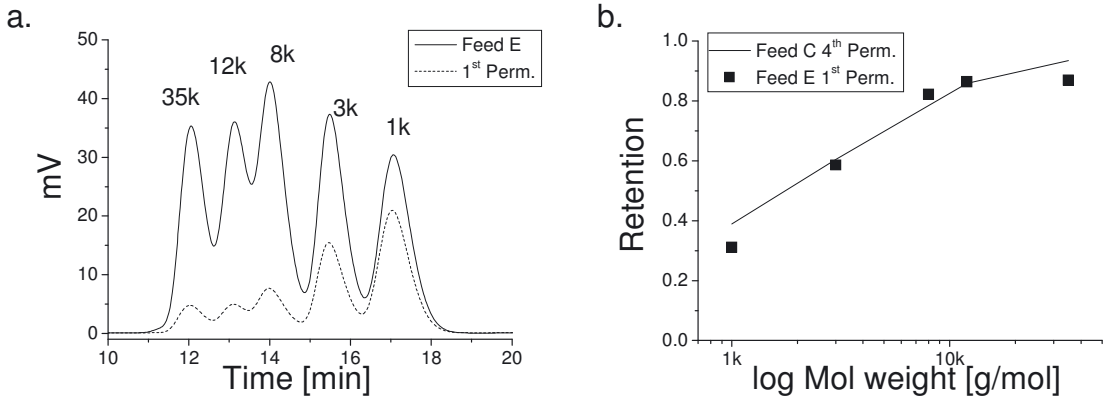

Figure 10 Separation curves for GR61PP. Figure 10a shows curves for Feed E and the following permeates. The retention curves for the commercial membrane and the nanoporous disc (see **Figure 8**) are compared in Figure 10b.

The separation performance of the nanoporous disc was little sensitive to the change of solvent tested in this work, while the sulphone membrane did not show satisfactory separation in the methanol-rich solvent (see fig. 9). The performance of the commercial membrane was also very sensitive to pressure variations. The retention profiles of the nanoporous disc in the two kinds of solvents are superposed as lines in Fig.9 and 10 b and they show at least as good selectivity as the polysulphone membrane when this last performs best.

Before the conclusions an observation about solvent fluxes through the nanoporous disk is in its place. The measured fluxes, of the order of 1 $l\ m^{-2}\ h^{-1}$ at 40 bars, are extremely low. The huge disk thickness in the ultrafiltration membrane context and the presence of the skin layer are the two main reasons responsible for the low flux. The flux at thickness 1 μm and 1 bar can be extrapolated to 13 $l\ m^{-2}\ h^{-1}$ assuming inverse and direct proportionality of flux on thickness and pressure, respectively. For comparison, the flux through the well-performing polysulphone membrane at 1 bar was 26 $l\ m^{-2}\ h^{-1}$. The effect of the skin layer is at the moment more difficult to predict and work for its understanding is in progress and so is the design of supported micrometer thin membranes based on our nanoporous polymers.

Conclusions

Cross-linked 1,2-polybutadiene nanoporous films of gyroid (GYR) morphology, having 40% porosity and pore cross-sectional diameter of 15 $\pm$ 4 nm were tested as ultrafiltration membranes. The fluxes of different fluids (nitrogen, carbon dioxide, hydrogen and mixtures of methanol and water) through 0.5 mm thick nanoporous films were first measured. The molecular size cut-off of the same films was afterwards determined by the filtration of polyethylene glycol (PEG) molecules of different molecular weight dissolved in methanol/water 80/20 or 20/80 mixtures. Permeates and feeds were analyzed by size exclusion chromatography (SEC). A cut-off value in the range between 8000 and 12000 [g/mol] was found, corresponding to molecular hydrodynamic diameters of 7-9 nm, as determined by Dynamic Light Scattering. The membrane characteristics of the GYR nanoporous polymer were compared with one commercial polysulphone ultrafiltration membrane. The GYR membranes were robust to changes in the methanol/water mixtures, while the commercial membrane lost its ultrafiltration characteristics at high methanol content. Work is in progress aiming at the preparation of realistic ultrafiltration systems based on supported nanoporous polymer membranes with thickness in the few micrometer range.

Acknowledgments

This work was financially supported by a grant from the Technical University of Denmark and the Danish Technical Research Foundation (grant no. 26-06-0271). The authors would like to thank Flemming Grumsen from the Technical University of

Denmark for help with TEM and Pia Wahlberg at Danish Technological Institute for help with SEM.

References

[1] G. Liu, J. Ding, A. Guo, M. Herfort and D. Bazett-Jones, Potential Skin Layers for Membranes with Tunable Nanochannels, Macromolecules, 30 (1997)1851-1853

[2] G. Liu, J. Ding and S. Stewart, Preparation and Properties of Nanoporous Triblock Copolymer Membranes, Angew. Chem. Int. Ed., 38 (1999) 835-838

[3] G. Jonsson, Molecular Weight Cut-Off Curves for Ultrafiltration Membranes of Varying Pore Sizes, Desalination, 53 (1985) 3-10

[4] C. Park, J. Yoon and E.L. Thomas, Enabling Nanotechnology With Self Assembled Block Copolymer Patterns, Polymer, 44 (2003) 6725-6760

[5] K.A. Cavicchi, A.S. Zalusky, M.A. Hillmyer and T.P. Lodge, An Ordered Nanoporous Monolith from an Elastomeric Crosslinked Block Copolymer Precursor, Macromol. Rapid Commun., 25 (2004) 704-709

[6] S. Ndoni, M.E. Vigild and R.H. Berg, Nanoporous Materials with Spherical and Gyroid Cavities by Quatitative Etching of Polydimethylsiloxane in Polystyrene-Polydimethylsiloxane Block Copolymers, J. Am. Chem. Soc., 125 (2003) 13366-13367

[7] S.H. Kim, M.J. Misner, T. Xu, M. Kimura and T.P. Russell, Highly Oriented and Ordered Arrays from Block Copolymers via Solvent Evaporation, Advanced Materials, 16 (2004) 226-231

[8] S.Y. Yang, I. Ryu, H.Y. Kim, J.K. Kim, J.K., S.K. Jang and T.P. Russell, Nanoporous Membranes with Ultrahigh Selectivity and Flux for the Filtration of Viruses, Advanced Materials, 18 (2006) 709-712

[9] A. K. Khandpur, S. Förster, F.S. Bates, I.W. Hamley, A.J. Ryan, W. Bras, K. Almdal, and K. Mortensen, Polyisoprene-polystyrene Diblock Copolymer Phase Diagram near the Order-Disorder Transition, Macromolecules, 28 (1995) 8796-8806

[10] S. Ndoni, C.M. Papadakis, F.S. Bates and K. Almdal, Laboratory-Scale Setup for Anionic Polymerization Under Inert Atmosphere, *Rev. Sci. Instrum.*, 66 (1995) 1090-1095

[11] F. Guo, K. Jankova, L. Schulte, M.E. Vigild and S. Ndoni, One-Step Routes from Di- and Triblock Copolymer Precursors to Hydrophilic Nanoporous Poly(acrylic acid)-*b*-polystyrene, *Macromolecules*, 41 (2008) 1486-1493

[12] V. Muralidhalan and C.Y. Hui, Stability of Nanoporous Materials, Macromol. Rapid Commun., 25 (2004) 1487-1490

[13] M.E. Vigild, K. Almdal, K. Mortensen, I.W. Hamley, J.P.A. Fairclough and A.J. Ryan, Transformations To and From the Gyroid Phase in a Diblock Copolymer, Macromolecules, 31 (1998) 5702-5716

[14] F. Guo, J.W. Andreasen, M.E. Vigild and S. Ndoni, Influence of 1,2-PB Matrix Cross-Linking on Structure and Properties of Selectively Etched 1,2-PB-*b*-PDMS Block Copolymers, *Macromolecules*, 40 (2007) 3669-3675

[15] M. R. Jakobsen and A. Grydgaard, Bechelor 'Nano Cavities in Polymeric Materials', B. Sc. Thesis, Technical University of Denmark, 2006

[16] D.A. Hajduk, P.E. Harper, S.M. Gruner, C.C. Honeker, G. Kim, E.L. Thomas and L.J. Fetters, The Gyroid: A New Equilibrium Morphology in Weakly Segregated Diblock Copolymers, Macromolecules, 27 (1994) 4063-4075

[17] T. Hashimoto, K. Tsutsumi and Y. Funaki, Nanoprocessing Based on Bicontinuous Microdomains of Block Copolymers: Nanochannels Coated with Metals, Langmuir, 13 (1997) 6869-6872

[18] T. Hashimoto, Y. Nishikawa and K. Tsutsumi, Identification of the "Voided Double-Gyroid-Channels": A New Morphology in Block Copolymers, Macromolecules, 40 (2007) 1066-1072

[19] G.E. Knözinger and J. Weitkamp editors, Handbook of Heterogeneus Catalysis Vol.2, Wiley-VCH, Weinheim, 1997

[20] M. Mulder, Basic principles of membrane technology, Kluver, Dordrecht, 2003

[21] N. Wu, A. Zheng, Y. Huang and H. Liu, Morphology of Poly(styrene-*block*-dimethylsiloxane) Copolymer Films, Journal of Applied Polymer Science, 104 (2007) 1010-1018

[22] P.J. Flory, Statistical mechanics of chain molecules, Interscience publishers, New York, 1969

[23] G.R. Strobl, The Physics of Polymers, Springer, Berlin, 1996

[24] J.K. Armstrong, R.B. Wenby, H.J. Meiselman and T.C. Fisher, The Hydrodynamic Radii of Macromolecules and Their Effect on Red Blood Cell Aggregation, Biophysical Journal, 87 (2004) 4259-4270

[25] G. Jonsson, C.E. Boesen, Water and Solute Transport Through Cellulose Acetate Reverse Osmosis Membranes, Desalination, 17 (1975) 146-165

E

Journal of Polymer Science Part A: Polymer Chemistry

Nanoporous Materials from Stable and Metastable Structures of 1,2-Polybutadiene-Polydimethylsiloxane Block Copolymers

Journal:	*J. Polym Sci. Part A: Polym. Chem.*
Manuscript ID:	draft
Wiley - Manuscript type:	Original Article
Keywords:	block copolymers < B, crosslinking < C, nanoheterogeneity < N, polysiloxanes < P, phase diagrams < P, polybutadiene < P

Nanoporous Materials from Stable and Metastable Structures of 1,2-Polybutadiene-Polydimethylsiloxane Block Copolymers

Lars Schulte [1], Piotr P. Szewczykowski [1,2], Fengxiao Guo [1,2], Anne Grydgaard [2], Mathilde R. Jakobsen [2], Mads M. Nielsen [1], Martin E. Vigild [2], Rolf H. Berg [1], Sokol Ndoni [1]*

[1]Department of Micro and Nanotechnology, Technical University of Denmark, DK-4000 Roskilde, Denmark

[2]Danish Polymer Centre, Department of Chemical and Biochemical Engineering, Technical University of Denmark, DK-2800 Kgs. Lyngby, Denmark

E-mail: sokol.ndoni@nanotech.dtu.dk

ABSTRACT: Experimental procedures used at the preparation and characterization stages of nanoporous materials (NPM) from 1,2-polybutadiene-polydimethylsiloxane (1,2-PB-PDMS) are presented. The NPM were obtained from self-assembled block copolymers after firstly cross-linking 1,2-PB (the matrix component) and secondly degrading PDMS (the sacrificial component). A number of block copolymers with varying composition and chain length were prepared by 'living' anionic polymerization. The diblock copolymers were characterized by spectroscopy, chromatography, rheology and x-ray scattering. The obtained information enabled to construct part of the micro-phase diagram for 1,2-PB-PDMS. A preliminary step anticipating the production of NPM is free radical cross-linking of 1,2-PB, which provides mechanical stability to the matrix component before the formation of nanocavities. Depending on the temperature of the cross-linking reaction different morphologies can be 'frozen' from the same block copolymer. Starting with a block copolymer precursor of lamellar morphology at room temperature, the gyroid structure or a structure showing hexagonal packing of cylinders (probably related to the metastable hexagonally perforated lamellae morphology) were permanently captured by cross-linking the precursor at 140°C or at 80°C, respectively. PDMS was degraded by reaction with tetrabutylamonium fluoride;

considerations on the mechanism of cleaving reaction are presented. Nanoporous polymers of different morphologies and with an exceptionally high degree of uniformity and order were obtained. The characterization of the obtained NPM includes gravimetry, infrared spectroscopy, small angle x-ray scattering, electron microscopy, isothermal nitrogen adsorption and solvent diffusion experiments.

Keywords: Nanoporous, 1,2-Polybutadiene, Block copolymer, Poly(dimethylsiloxane), Gyroid, HPL, BET.

INTRODUCTION

A diblock copolymer macromolecule consists of two chemically distinct parts (blocks) linked by a covalent bond. Depending on the relative block composition, the total degree of polymerization, temperature and pressure, the interplay between block immiscibility and connectivity can generate a variety of morphologies in the mesoscopic range of scale-lengths. [1] This self-organization in block copolymers is relevant in relation to bottom-up active material nanostructuring.[2,3] The targeted removal of part of the block copolymer molecule in the self-assembled state is an appealing strategy for the preparation of nanoporous polymers and a number of cleaving schemes have been reported[2-8]. Among the possible applications of nanoporous materials (NPM) are templates for electronics, special dielectric materials, substrates for catalysis, design of nano-reactors, micro-filtration membranes and use in medical diagnostics.

A necessary condition for the stability of NPM is mechanical stability of the matrix after the removal of the sacrificial part. Polymers that are glassy at room temperature, like polystyrene (PS), are expected to be stable as matrix component in the dry state or in the presence of non-solvents. However, contact with solvents or heating close to or above the glass transition temperature (T_g) can irreversibly erase polymer's nanoporosity. The introduction of covalent cross-links in the matrix[7-10] can warrant 'memory' of the nanoporous morphology even at such conditions.

We reported about five years ago[8] the preparation of nanoporous polystyrene from block copolymers with polydimethylsiloxane (PS-*b*-PDMS) after the targeted degradation of the PDMS block. Two groups reported shortly afterwards the preparation of nanoporous cross-linked polyisoprene (PI) from PI-*b*-PDMS precursors.[9,10] See reference 10 for a review of the subject. Highly uniform PS-PDMS and polydiene-PDMS block copolymers are readily synthesized by living anionic polymerization;[12] the block copolymer precursors can be aligned in a shear field[11, 13] or an electrical field.[14] Most polydienes show T_g below 0 °C and therefore are unstable as NPM at room temperature. Cross-linking of the polydiene before the removal of PDMS is necessary and feasible[9, 10, 13] in a controlled way.

This contribution presents the procedures for the preparation and characterization of 1,2-Polybutadiene-PDMS (1,2-PB-PDMS) diblock copolymer precursors and of the resulting nanoporous cross-linked 1,2-PB. Compared to the nanoporous polyisoprenes [9], the amount of cross-linker needed to prepare nanoporous 1,2-PB samples with similar mechanical properties is reduced by factors in the range 30-100. This difference is related to the different cross-linking reaction mechanism in the two cases, as shown in the following. A discussion of the PDMS etching reaction mechanism by tetrabutylamonium fluoride is presented. Thermal cross-linking performed at a certain temperature 'freezes' the sample morphology stable at that temperature and therefore is an additional control parameter of nanoporous polymers' morphology. Even thermodynamically metastable block copolymer micro-phases can be stabilized by this strategy. The thorough characterization of the obtained nanoporous materials by a variety of techniques constitutes the central part of the present report.

EXPERIMENTAL

Materials

Block Copolymer Synthesis

The 1,2-PB-PDMS block-copolymers were prepared by sequential 'living' anionic polymerization under Argon.[12] Sec-butyllithium was used as initiator for all the polymerizations. 1,2-PB-PDMS was polymerized in tetrahydrofurane (THF). The temperature of polymerization was either –40 ± 5 ºC or –20 ± 3 ºC, with polymerization times of 13 h and 3 h, respectively. The building unit of PDMS, hexamethyl-cyclotrisiloxane (D_3), was added as a THF solution into the reactor containing the living polybutadienyl Lithium (pale green-yellow) at the respective temperature mentioned above. The temperature then was gradually increased to 0 ºC and D_3 was left to polymerize for up to 3 days at 0 ± 1 ºC. The complete crossover from the hydrocarbon to the siloxy Lithium was associated with colour disappearance within few minutes from the addition of D_3. At that stage of synthesis 3-5 ml samples were taken out of the polymerization reactor. These samples were used for the characterization of the molar mass and molar mass distribution of the hydrocarbon blocks in the block copolymers. After the formation of the PDMS block, all the samples were terminated with a three times molar excess of trimethylchlorosilane. The finished polymers were isolated from the polymerization solutions by first precipitating and washing in excess methanol and then by drying under vacuum over night.

Cross-linking

Dicumyl peroxide (bis(α,α-dimethylbenzyl) peroxide) (DCP) and dilauryl peroxide (DLP) (both from Merck) were used as received for the cross-linking of 1,2-PB. A controlled quantity of 1 % mole cross-linker per mole double bonds were co-dissolved with the polymer prior to solution casting into flat bottom Petri dishes; the solvent was then left overnight to evaporate under a gentle flow of Ar. Smooth films of polymer and cross-linker were thus obtained. The Petri dish with the film was enclosed into a homemade steel cylinder and the air inside the cylinder quantitatively replaced with Argon. The gas tight closed cylinder was placed into a preheated thermostated oven for the cross-linking reaction to happen. DCP alone was used as cross-linking agent for all but one sample and in these cases the reaction temperature was 140°C and the reaction time 2 hours. For

one single sample an equimolar mixture of DLP and DCP was used to carry the cross-linking reaction in two steps: the sample was first kept at 80°C for 8 hours then at 140°C for 2 hours.

Structurally aligned samples of a 1,2-PB-PDMS block copolymer showing hexagonal morphology were prepared by first solvent casting a co-solution of polymer and 1 % DCP (see above). Portions of the dry polymer-DCP mixture were then squeezed between two microscope glasses with 0. 5 mm Teflon spacers in between and shear-aligned by hand: the glasses were moved back and forth relative to each other realizing a shear amplitude of between 400 and 500%. The shear-aligned samples were cross-linked for 2 h at 140°C.

Etching of PDMS

Tetrabutylamonium fluoride (TBAF) (Aldrich) was used as cleaving reactant for PDMS. Cross-linked samples were reacted for 36 h with 1M TBAF in THF at 5-10 times molar excess relative to the concentration of PDMS' repeating unit. After etching each sample was taken out of the solution and rinsed in fresh THF followed by a 24 h methanol bath before gradual solvent evaporation under a stream of Argon.

Characterization Techniques

Chromatography

The molar mass and molar mass distribution of the hydrocarbon blocks in the block copolymer samples were characterized by Size Exclusion Chromatography (SEC) in stabilized THF. Two mixed-D columns (Polymer Laboratories) and a triple detector setup (Viscotek) (right angle light scattering, viscometer and differential refractometer) were used.

Spectroscopy

The average composition of the di-block copolymers was determined by proton magnetic resonance spectroscopy, ^{1}H-NMR in a 250 MHz Avance DPX 250 Bruker instrument. The number of double bonds surviving cross-linking and etching of the 1,2-PB-PDMS samples was monitored by Raman

(Renishaw system 3000) and Fourier transform infrared FT-IR (PerkinElmer Spectrum) spectroscopies.

Rheology

The viscoelastic properties which reflect the diblock copolymer morphology were investigated by isothermal and temperature-gradient dynamic mechanical measurements on a Rheometrics RS 800 using parallel plate geometry. The data included in this paper refer to temperature gradients of 2.5 °C/min.

Small Angle X-ray Scattering

Small angle x-ray scattering (SAXS) was measured using a rotating anode lab-source at Risø, with x-rays of wavelength λ = 1.54 Å. The scattered radiation was collected with a 2-D position-sensitive wire detector at a distance of 1435 mm or 4656 mm from the sample. The data in this paper are raw data, shown as obtained from the detector after sensitivity and distortion corrections.

Electron Microscopy

A typical sample for *Scanning Electron Microscopy (SEM)* was prepared by first freeze fracturing a piece of nanoporous polymer film in liquid nitrogen; the pieces were then mounted onto an aluminum specimen mount using Ted Pella double coated carbon conductive tabs and CCC Carbon Adhesive (Electron Microscopy Science). Each sample was sputter-coated with 2-3 nm gold layer in a Polaron SC7640 and kept under vacuum in the microscopy chamber for 14-16 hours before scanning. A 2 kV electron beam accelerating voltage was chosen in a FIB-SEM Zeiss 1540 EsB Gemini instrument.

Transmission electron microscopy (TEM) was performed in a Jeol 2000F operated at 200 kV or in a Jeol 3000F operated at 300 kV, both at Risø-DTU. Samples for TEM were prepared by pulverizing 50 mg portions of NPM under liquid nitrogen in an agate mortar. The produced powder was suspended in 2 ml toluene (Fluka 99.8% grade) in a glass beaker. The suspension was

ultrasonicated in a Branson 1510 bath for 40 – 60 min and few drops of it were applied onto a copper / carbon grid (Agar Scientific, 04-holey) before toluene evaporation. The dry grids were kept in a grid holder in order to avoid contamination.

Nitrogen adsorption

No particular sample preparation is needed for the nitrogen adsorption experiments. The amount of sample used for the measurements was in the range 100 – 200 mg. The measurements were performed on a Micromerities ASAP 2020 Surface Area and Porosity Analyzer. The isothermal physisorption (adsorbed mass against pressure) was analyzed by the method of Langmuir and Brunauer-Emmett-Teller (BET), while the calculation of the pore size and distribution followed the scheme of Barrett-Joyner-Halenda (BJH).

Pore Accessibility

The kinetics and equilibrium uptake of methanol were measured for all nanoporous 1,2-PB. Pre-weighed dry samples were placed in excess of methanol under gentle stirring. Samples were taken out of the liquid and quickly dried with a tissue on the outer surfaces before weighing. The sample mass was measured as a function of time. The presentation of the subject of solvent uptake by nanoporous 1,2-PB is in focus of a separate publication[13] and only a brief discussion is given here on the uptake of methanol.

RESULTS AND DISCUSSION

Nomenclature

To make nanoporous material the mother polymer was taken via several intermediate steps. In order to keep track of this process the following nomenclature was used for the samples.

Block copolymer precursors' names reflect the monomer composition of the block copolymers: *D* stands for D_3 (the cyclic trimer of dimethylsiloxane) and *B* for butadiene. A sample number is added after the two letters, which uniquely identifies the synthesis batch, e.g., *BD-4*, *BD-14*. Please see Table 1 below for a full listing of the samples.

Cross-linked block copolymers are named by adding an '*x*' to the block copolymer name; Results on one cross-linked sample of *BD-4* and two cross-linked samples of *BD-14* will be presented here: *BD-4-x*., *BD-14-x(80ºC) and BD-14-x(140ºC)* , respectively. The temperature values in brackets refer to the cross-linking start temperature as explained in the Experimental/Cross-linking section.

Etched samples are named by adding a suffix *E* to the name of the cross-linked sample, e.g., *BD-4-x-E*. All the NPM samples presented in this work were prepared by degrading the PDMS block with tetrabutylamonium fluoride (TBAF).

Characterization of the Block Copolymer Precursors

Table 1 summarizes properties of 12 block copolymer precursor samples prepared by sequential anionic polymerization. The molar masses of the hydrocarbon blocks shown in the second column of Table 1 were determined by size exclusion chromatography (SEC). The SEC results combined with the compositional information from ^{1}H-NMR of the finished block copolymer allowed to calculate the total average mass values listed in the third column. The polydispersity index of the block copolymer samples (fourth column in table 1) was determined by SEC. In addition to composition (fifth column) ^{1}H-NMR analyses provided information on the microstructure of the polybutadiene block: 89.5 ± 1.5% of the repeating units were 1,2-units and the rest were *trans*-1,4-units. The morphology at room temperature was determined by small angle x-ray scattering (SAXS) measurements. Some samples showed multiphase behaviour and the transition temperatures were determined by rheology, which also gave indications to the morphology, as the different diblock copolymer structures exhibit distinctive viscoelastic properties.[15] Five equilibrium morphologies were observed, lamellar (*LAM*), gyroid or $Ia\bar{3}d$ (*GYR*), hexagonally packed cylinders (*HEX*), body centred cubic (*BCC*) and disordered morphology. An additional structure between the *LAM* and *GYR* was observed both by rheology and by SAXS. It will be shown further on in this paper that the nanoporous samples prepared from samples cross-linked within the stability temperature region of this morphology show cylindrical pore structure with some skewed hexagonal packing, therefore we call it phase *'H'*. The relation of this phase to previously reported hexagonally perforated

lamellae (*HPL*)[16] metastable phase will be shortly discussed. The fact that cross-linking takes place at 140°C (and in one case at 80°C) and effectively freezes the morphology at that temperature, introduces the possibility to gain evidence for the morphology at elevated temperatures by performing room temperature SAXS measurements on samples cross-linked at the respective elevated temperature.

Partial Phase Diagram for 1,2-PB-PDMS Block Copolymers

The data on the series of samples in Table 1 created the basis for constructing a region of the micro-phase diagram for the 1,2-PB-PDMS diblock copolymer. Following the scheme of Flory and Huggins, as customary in this context, the change in the free energy for mixing at the monomer unit scale is determined by an empirical dimensionless interaction parameter χ_{12} (shortly χ).[17] The main part χ_H of the Flory-Huggins interaction parameter χ is of enthalpic nature; an estimation of χ_H and its temperature dependence were made on the basis of the blocks' solubility parameters:

$$\chi_H = \frac{V_r(\delta_1 - \delta_2)^2}{RT}$$

where δ_1, δ_2 are the solubility parameters of the blocks. V_r is a reference volume calculated here as a molar average of the monomer volumes for 1,2-PB and PDMS:

$$V_r = x_1 V_{r1} + x_2 V_{r2}$$

where x_1 and x_2 are the monomer molar fractions for the 1,2-PB and the PDMS blocks, respectively ($x_1 + x_2 = 1$). The monomer reference volumes were calculated from density data for 1,2-PB and PDMS[18, 19]: V_{r1} = 100 Å^3 and V_{r2} = 128 Å^3.[18] δ_1 = 17.4 MPa$^{1/2}$ and δ_2 = 15.1 MPa$^{1/2}$ are the chosen values of solubility parameters for 1,2-PB and PDMS, respectively.[18, 19] The uncertainty in the values of the solubility parameters is larger for 1,2-PB; the literature data for this polymer are quite scarce. In the case of the more studied 1,4-PB polymers the reported solubility parameters vary in the range 14.6-17.6 MPa$^{1/2}$.[18, 19] It was not possible to estimate the temperature dependence of the

solubility parameters. On the basis of these data the enthalpic part of the interaction parameter was estimated to:

$$\chi_H = \frac{48.9 - 10.7 x_1}{T}$$

The introduction of a composition dependent reference volume does not follow the 'usual' literature trend, where a fixed, composition-independent reference volume is used. The reason for this choice is related to the following. The important parameter in considering the micro-phase behaviour is the product of the Flory-Huggins interaction parameter with the total degree of polymerization: χN. The (number average) degree of polymerisation $\overline{N}_n \equiv N$ for each of the 1,2-PB-PDMS samples was calculated from the respective number average molar masses and compositions: $N = \overline{M}_n / \overline{m}$ with $\overline{m}$ the average monomer mass: $\overline{m} = x_1 m_1 + x_2 m_2$. The overall expression proposed here is therefore:

$$\chi_H N = \frac{V_r (\delta_1 - \delta_2)^2}{RT} N = \frac{(\delta_1 - \delta_2)^2}{RT} \overline{M}_n \frac{x_1 V_{r1} + x_2 V_{r2}}{x_1 m_1 + x_2 m_2} \equiv \frac{(\delta_1 - \delta_2)^2}{RT} \frac{\overline{M}_n}{\overline{\rho}} \equiv \frac{(\delta_1 - \delta_2)^2}{RT} \overline{V}_n$$

which is formally identical to the expression for χ_H in which the monomer reference volume V_r is substituted by the number average molar volume of the block copolymer, $\overline{V}_n$ (= N V_r). This average volume is temperature, composition and molecular weight dependent. Neglecting the temperature dependence of $\overline{V}_n$ and of the solubility parameters (literature data missing), and substituting the respective values for the monomer molar masses (m_1 = 54.1 g/mol and m_2 = 74.2 g/mol) the relation in the case of 1,2-PB-PDMS diblock copolymer reads:

$$\chi_H N = \frac{48.9 - 10.7 x_1}{74.2 - 20.1 x_1} \frac{\overline{M}_n}{T} = (0.532 + \frac{1}{7.88 - 2.14 x_1}) \frac{\overline{M}_n}{T}$$

This is the expression used to calculate the y-axes values of the micro-phase diagram in Figure 1; for each block copolymer sample composition, mass and transition temperature data are listed in Table 1.

Fluctuations [20] are expected to be important in the range of chain lengths considered here; an estimation of this effect in the symmetrical case f_{PB} = 0.5 for 1,2-PB-PDMS samples of total polymerization degree in the range 100-300 yields order-to-disorder (ODT) values 7-5 χN units above the mean field spinodal [21] (thin continues line in figure 1). It was not possible to estimate a similar contribution for the asymmetric di-blocks.[20] It's also uncertain how the fluctuations effect the order-to-order transition temperatures (OOT) between the micro-phases shown in figure 1. The actual data in figure 1 around the symmetrical composition are 3-4 χN units above the mean field spinodal. On the one side the fluctuation contribution to ODT seems to be quite significant, and on the other side it was not possible to estimate such effects for all the compositions and transitions in the microphase diagram. Given the mentioned uncertainties no tentative was made to further calculate the residual (entropic) contribution χ_S to the Flory-Huggins interaction parameter χ (= χ_H − χ_S). We adopted instead the pragmatic choice of presenting an operationally well-defined microphase diagram.

The circles in figure 1 show the OOT or ODT as determined by rheology. The crosses indicate morphology data obtained by SAXS measurements. The two arrows at f_{PB} equal to 0.61 and 0.71 point to the two samples *BD-14* and *BD-4*, respectively. These are the precursor polymers for all the nanoporous samples presented in this contribution. For a given composition the SAXS data with the highest $\chi_H N$ value represent block copolymer melts measured at 20 ºC. In the case of sample *BD-14* with f_{PB} = 0.61, shown by one of the arrows in figure 1, two additional morphologies, '*H*' stable (at the time-scale of few hours) at 80 ºC and *GYR* stable at 140 ºC were characterized by SAXS as well. The respective data are shown by the crosses at ordinates 21 and 18, respectively. As already mentioned these data refer to measurements made at 20 ºC on samples cross-linked at the respective higher temperatures. Figure 2 shows the azimuthally averaged SAXS profiles of (a) *BD-14* melt, (b) *BD-14* cross-linked at 140ºC (*BD-14-x(140ºC)*), (c) same sample after PDMS cleavage (*BD-14-x(140ºC)-E*), and (d) *BD-14* cross-linked at 80 ºC and etched (*BD-14-x(80ºC)-E*). Profile (a) shows at least three equidistant peaks as is typical for lamella structure with periodicity 22 nm. Profiles (b)

and (c) are both characteristic for the gyroid (GYR) cubic structure, while profile (d) shows some similarities with both GYR and the hexagonal structures. The structure revealed by profile (d) is labelled 'H' in the present paper. It is probably related to the metastable hexagonally perforated lamella (HPL) structure, as will be discussed below in the paragraph 'Nanoporosity'. The samples showing SAXS profiles (c) and (d) are both nanoporous; direct-space scanning electron microscopy images of these fascinating structures are shown in Figures 6, 7 below.

Cross-linking of 1,2-Polybutadiene

The cross-linking reaction of 1,2-PB by peroxides is quite different from the cross-linking of polyisoprene (PI).[9, 22, 23] At the same cross-linking conditions as for PI, just one single addition of 1 molar % of DCP relative to the double bonds was sufficient to generate a wide range of cross-linking degrees simply by changing the reaction time. E.g., at 140 ºC, 1 molar % DCP suffices to generate networks which range from rubbery to glassy matrices, simply by changing the reaction time in the interval 0.5 h to 4 h. This is a clear indication that the cross-linking reaction in this case is a chain reaction, where one peroxide molecule can generate more than one cross-link, in neat contrast to the 1:1 proportion in the case of PI. This can only happen by direct involvement of double bonds as shown in Scheme 1.

The alcoxy radical produced from the thermal scission of the peroxide (Scheme 1(a)) initiates the reaction by generating a free radical onto the polymer either by subtraction of allylic Hydrogen or by direct attack on the double bond (Scheme 1(b)). Both the tertiary and the secondary Carbon free radicals thus produced can start a chain of reaction on other double bonds of PB (propagation), as shown in Scheme 1 (c), (d) and (e). In each propagation step of the reaction chain either an intramolecular cyclization (as in (d)) or an intermolecular cross-link (as in (e)) and a new free radical on the polymer chain are formed. The secondary free radicals in (b-d) may also rearrange into more stable tertiary free radicals by displacement of the neighbour allylic Hydrogen (not shown). A cross-linking cluster thus forming is ended either by transfer of free radical to other molecules (e.g., by subtraction of an allylic H) or by recombination of two free radicals (not shown).

This last is a true termination reaction of the kinetic chain and may produce merger of two cross-linking clusters. The intramolecular cyclization between double bonds of two adjacent 1,2-units shown in (d) results into substituted cyclohexane units along the main chain with possibility for fused rings. There are different factors affecting these intra-molecular reactions, such as tacticity, conformation statistics of adjacent 1,2-units and the presence of 1,4-units. Increased reaction time augments the fraction of peroxide transformed into free radicals and therefore the number of kinetic chains. The half-life of DCP at 140ºC (from measurements in dodecane solution) is estimated to 1.5 h;[23] therefore 85 % of DCP is expected to be decomposed after 4 h at 140 ºC. As shown in a recent publication[13] FT-IR and Raman spectroscopy measurements can be used to monitor the disappearance of double bonds as a function of cross-linking reaction time/temperature. This information can be used to calculate the kinetic chain length of the cross-linking reaction: 39 - 69 double bonds disappear during cross-linking per free radical equivalent of DCP.[13]

The cross-linking conditions for *BD-4-x* and *BD-14-x* are summarized in Table 2. The second to fourth columns in Table 2 include data on cross-linker amount and cross-linking time. These data confer in a nutshell the significant difference between the mechanisms of cross-linking reactions of 1,2-PB contra PI - as described in the previous paragraph. As an illustration, in order to obtain *BD-4-x-E* with similar mechanical properties as a corresponding nanoporous PI, 35 times less DCP was used in just 1/7-th of cross-linking time. The fifth column contains data on the fraction of double bonds surviving cross-linking relative to the double bonds in the diblock copolymer precursor, as measured by FT-IR. The dependence of consumed double bonds on the cross-linking degree and on the degree of collapse of the resulting materials after the removal of PDMS are discussed in a separate publication.[13]

Etching of PDMS

The reaction of TBAF with PDMS in THF (containing approx. 5% w/w H_2O) is much gentler than the reaction with anhydrous HF.[7, 24] While anhydrous HF is a strong protonating acid with acidity function (H_0) of about –11,[25] TBAF is perhaps a base in polar aprotic solvents such as THF. It's

reasonable to expect that cleavage with HF operate by an S_N1-type process, via silicon-oxygen cleavage to give water and silico-cations, which react with fluoride anions. In contrast, cleavage with TBAF probably proceeds via the so-called S_N2-Si pathway (Scheme 2) known from the rapid cleavage of silyl ethers to alcohols by treatment with 2-3 eq. TBAF in THF at 25°C.[26 a, b]

Data on the fabrication of three1,2-PB-PDMS samples (*BD-4-x-E*, *BD-14-x(80°C)-E* and *BD-14-x(140°C)-E*) are summarized in the last two columns of Table 2. *BD-4-x-E* exhibited hexagonally packed cylinder cavities while *BD-14-x(80°C)-E* and *BD-14-x(140°C)-E* exhibited 'H' and gyroid morphology, respectively, as will be demonstrated in the next section. The data in the sixth and seventh columns of the table reflect the quantitative removal of PDMS after the reaction with TBAF.

Nanoporosity

The nanoporosity of the samples fabricated from the several block copolymer precursors was analyzed by combining data obtained by SAXS, electron microscopy and isothermal Nitrogen adsorption measurements.

Figure 3 shows SAXS profiles of 2-D raw data in the direction of shear (right panel) and 1-D reduced data (left panel) for the nanoporous sample *BD-4-x-E*. This sample was subjected to reciprocal shearing before cross-linking and etching. The SAXS instrument measures the scattering from a sample volume of approximately one cubic millimeter. The extraordinarily well-resolved 2-D scattering indicates that the sample is aligned to such a degree that the order can be compared to a single crystal-like hexagonal arrangement of the cylindrical cavities. The shear planes were parallel to the (10) crystallographic plane of the morphology. Figure 4 shows SEM and TEM micrographs of the same sample (*BD-4-x-E*). The single crystal-like order of the cavities is clearly evident in the two pictures. The SEM micrograph shows the area around the diagonally running edge of two (fracture) surfaces that are tilted with respect to one another. The upper right-hand part of the picture displays an "end view" of the cavities, which gives a perfectly uniform hexagonal pattern. The lower left-hand part of the picture displays a "side view" of the structure, where the cylindrical

cavities are exposed along their length, which clearly exceeds the frame of the SEM picture. Both micrographs yield information on the characteristic length scales of the NPM.

Table 3 summarizes the characteristic geometrical scales obtained by different techniques for precursors and NPM samples of the present study. Both the diblock copolymer precursor BD-4 and the derived samples cross-linked at 140 °C show hexagonally packed cylindrical structure as the only observed ordered phase in the microphase diagram (see the arrow at f_{PB} = 0.71 in Fig. 1). The etched sample (BD-4-x-E) shows a 9% smaller characteristic distance between primary Bragg planes compared to the diblock copolymer precursor (19.3 nm against 21.1 nm) as can be seen in Tab. 3. This shrinkage is mainly due to increased density of the 1,2-PB phase in the process of cross-linking. The characteristic length-scales estimated from the SEM pictures were in good agreement with those calculated by SAXS. The pore radius of the *BD-4-x-E* sample shown in Figure 4 was 6.0 ± 0.9 nm. The calculated average pore radius for the sample *BD-4-x-E* from the SAXS profile was 6.64 nm.

Figure 5 shows the 1-D and 2-D SAXS profiles of the nanoporous sample *BD-14-x-E*. The 1-D scattering curve is indexed to match the reflections of the gyroid morphology. We have previously demonstrated a gyroid NPM in a PS matrix;[8] to the best of our knowledge *BD-14-x-E* is the first realization of nanoporous gyroid morphology from cross-linked polydiene. The lattice constant of the cubic lattice calculated from the position of the first allowed SAXS diffraction peak was 47.5 nm. Scanning and transmission electron microscopy pictures of *BD-14-x-E* are shown in Figure 6. The SEM micrograph shows the (211) projection known also as ‚knitting pattern', while the (111) or the ‚wagon wheel' projection is visible in the TEM micrograph. 1-D SAXS profiles from the block copolymer precursor, the cross-linked and the etched samples *BD-14*, *BD-14-x*, *BD-14-x-E*, respectively, were already shown in Fig. 2 above. The crystallographic cell size estimated from the TEM micrograph was 47 ± 6 nm, in good agreement with the one calculated from SAXS. A pore radius of 6 nm was roughly estimated from the SEM image and listed in tab. 3. A strut length of 18 nm was estimated from TEM.

Figure 7 is the SEM image of the nanoporous polymer with structure labelled 'H' in the micro-phase diagram of figure 1; this is the structure captured by cross-linking sample BD-14 at 80°C. The image shows clearly a pattern of channels packed in some 'disturbed' hexagonal symmetry. It does not show clear evidence of some hexagonally perforated lamella structure (*HPL*).[16] This could hint that what is known as the metastable *HPL* micro-phase is actually a more or less continuous set of different morphologies in the transition between the thermodynamically stable *LAM* and *GYR* micro-phases. The pore radius was estimated to 10 nm from fig. 7. It's quite interesting that a structure of (skewed) hexagonally packed cylindrical channels of 40 % porosity can be realized from a thermodynamically metastable morphology. It's also interesting that the pore radius is quite large, for example much larger than the radii of the nanoporous samples with gyroid and hexagonal structures (figs. 4 and 6, respectively). To the best of our knowledge stabilization of such a micro-phase by cross-linking and the production of the corresponding nanoporous polymer has not been previously reported.

Finally Figure 8 shows the results from isothermal adsorption of Nitrogen into the nanoporous sample *BD-14-x(140ºC)-E* and the resulting pore size and pore size distribution as calculated from the Barrett-Joyner-Halenda (BJH) scheme.[27] The plot of pore radius as calculated from the desorption branch (4.8 ± 0.5 nm) is shown by the red line in fig. 8. The corresponding radius calculated from the adsorption branch peaks at 7.1 nm. This last is the value conventionally reported in the literature from BJH analysis of gas sorption data. The pore sizes calculated for both the hexagonal and the gyroid nanoporous samples are shown in the sixth column of tab. 3. The pore sizes listed in tab. 3 as measured/calculated by different methods are reasonably consistent. The specific surface area of the HEX and the GYR samples shown in the last column of tab. 3 were derived from Nitrogen sorption measurements analyzed by the BET scheme. The calculation of surface area for the NPM *BD-4-x-E* was straightforward; it's shown in the next to last column of tab. 3 (139 m^2/g). It is significantly higher than A_{BET} (75 ± 20 m^2/g), hinting to the possibility that part of the cylindrical pores were not accessible to Nitrogen, probably due to hindered percolation from

the outer surface. The A_{BET} for the sample *BD-14-x-E* with gyroid structure was 260 ± 30 m^2/g. The specific surface area for the same sample was also estimated from a mathematical model of the 'double gyroid'.[28] The model represents gyroid surfaces (or interfaces) by surfaces of constant mean curvature (cmc) and the surfaces are measured by triangulation. The surface area of a cmc enclosing same volume fraction and scaled to same crystallographic cell size as our gyroid sample was calculated to 151 m^2/g. This value is significantly smaller than A_{BHT} (260 ± 30 m^2/g); at the moment we have no clue on the reason of this discrepancy.

Methanol Uptake

In a series of experiments it was possible to demonstrate that despite the non-solvent character of methanol (MeOH) relative to both PS and polydienes, it fills the nanocavities. This subject is in focus of a separate publication.[13] Suffice it to say here that the key parameter for the filling capillary effect is the contact angle θ between the polymer and the solvent. In the case of MeOH it was measured to be less than $90°$ for all the three polymers PS, PI and 1,2-PB; therefore a filling capillary effect is expected and observed in all the three cases. Young's equation[29] relates the interfacial tension between pairs of phases:

$$\gamma_{ls} = \gamma_{sv} - \gamma_{lv} \cos\theta < \gamma_{sv} \qquad \text{for} \qquad 0° < \theta < 90°$$

where *lv*, *ls* and *sv* are the liquid-vapor, liquid-solid and solid-vapor interfaces, respectively. The driving force for the cavity filling is of course the reduction of the total interface energy. This finding provides an easy way to measure porosity. It also opens up for the possibility to specifically address the cavities by a reactive solution in case that a physico-chemical modification of the pore walls is wished without affecting the 'bulk' of the matrix polymer. Depending on the quality of the solvent relative to the nanoporous matrix, a whole range of behaviors is expected to be observed as for the cavity size and the matrix degree of swelling.

CONCLUSIONS

The preparation procedure of nanoporous materials from diblock copolymers of PDMS with 1,2-polybutadiene was presented. The 1,2-PB matrix was stabilized by cross-linking before the production of nanoporosity. Free radical cross-linking of the polydiene block was initiated by a thermally scissioned peroxide, DCP. A possible reaction scheme for the cross-linking of 1,2-PB was presented. TBAF in THF was used to quantitatively degrade PDMS from the cross-linked samples. A short discussion of the possible degradation reaction mechanism was presented. The morphology of the remaining polymer matrix was largely conserved after PDMS cleaving as ascertained by SAXS. Images in direct space realised by scanning and transmission electron microscopy were shown as a direct proof of the morphology and alignment and were in quantitative agreement with the SAXS data. An important 'bonus' of the present work was the first publication of part of the micro-phase diagram of the 1,2-PB-PDMS diblock constructed on the basis of data on composition, molar mass and morphology. Controlling the temperature of cross-linking reaction of same block copolymer precursor allowed capturing different accessible morphologies from the phase diagram. Pore size, size distribution and specific surface area were measured by isothermal Nitrogen adsorption. Finally, a short discussion on pore accessibility by methanol was presented. This is the first report describing the preparation of nanoporous cross-linked polydienes with gyroid and 'H' morphologies. This last is a stabilized structure derived from a probably metastable structure of the precursor block copolymer.

ACKNOWLEDGMENTS

We thank the Danish Agency for Research, Technology and Innovation (FTP) for supporting the project. We acknowledge Jens W. Andreasen (Risø/POL, Denmark) for his help with the SAXS measurements. We thank Pia Wahlberg from The Danish Technological Institute for helping with scanning electron microscopy (SEM) imaging, Jørgen Bilde-Sørensen (Risø National Laboratory DTU) and Flemming Grumsen (Dept. Manufacturing Engineering and Management DTU). Marina

Kustova and Søren K. Klitgaard (Centre of Sustainable and Green Chemistry, DTU) supported with the nitrogen adsorption characterization.

REFERENCES AND NOTES

1. For an early summary of the subject, see e.g., Aggarwal, S. L., Ed., Block copolymers, Plenum Press, New York, 1970

2. See, e.g., Lee, J.-S.; Hirao, A. Nakahama, S. Macromolecules 1988, 21, 274-276.

3. Hashimoto, T.; Tsutsumi, K.; Funaki, Y. Langmuir 1997, 13, 6869-6872.

4. Park, M.; Harrison, C.; Chaikin, P. M.; Register, R. A.; Adamson, D. H. Science 1997, 276, 1401-1404.

5. Thurn-Albrecht, T.; Schotter, J.; Kastle, G. A.; Emley, N.; Shibauchi, T.; Krusin-Elbaum, L.; Guarini, K.; Black, C. T.; Tuominen, M. T.; Russell, T. P. Science 2000, 290, 2126-2129.

6. Zalusky, A. S.; Olayo-Valles, R.; Wolf, J. H.; Hillmyer, M. A. J Am Chem Soc 2002, 124, 12761-12773.

7. Liu, G.; Ding, J.; Guo, A.; Herfort, M.; Bazzett-Jones, D. Macromolecules 1997, 30, 1851-1853.

8. Ndoni, S.; Vigild, M. E.; Berg, R. H. J Am Chem Soc 2003, 125, 13366-13367.

9. Hansen, M. S.; Vigild, M. E.; Berg, R. H.; Ndoni, S. Polymer Bulletin 2004, 51, 403-409; Hansen, M. S. "Polyisoprene Glass with Nanopores" Jan 2003, Diplom K Thesis, Technical University of Denmark, Dept of Chemical Engineering, Lyngby, Denmark.

10. Cavicchi, K. A.; Zalusky, A. S.; Hillmyer, M. A.; Lodge, T. P. Macromol Rapid Commun 2004, 25, 704-709.

11. Hillmyer, M. A. Adv Polym Sci 2005, 190, 137-181.

12. Ndoni, S.; Papadakis, C. M.; Almdal, K.; Bates, F. S. Rev Sci Instrum 1995, 66, 1090-1095.

13. Guo, F; Andreasen, J. W.; Vigild, M. E.; Ndoni, S. Macromolecules 2007, 40, 3669-3675.

14. A manuscript is in preparation based on the project work of Hentschel, T. "Electrical field alignmed nanoporous polymers obtained by a 1,2-PB-PDMS block copolymer" 2006, Polymer Dept., Risø National Laboratory and Danish Polymer Centre, Institute of Chemical Engineering, Technical University of Denmark.

15. Frederickson, G. H.; Bates, F. S, Dynamics of block copolymers: theory and experiment, Annu. Rev. Mater. Sci. 26, 501-50 (1996)

16. Förster, S.; Khandpur, A. K.; Zhao, J.; Bates, F. S.; Hamley, I. W.; Ryan, A. J.; Bras, W. Macromolecules 1994, 27, 6922

17. See e.g., Strobl, G. R. The Physics of Polymers, Springer-Verlag: Berlin, Heidelberg, New York, 1996.

18. Mark, J. E. editor, Polymer Data Handbook, Oxford University Press, 1999.

19. Brandrup, J.; Immergut, E. H. Polymer Handbook, 3rd ed., John Wiley & Sons: New York, 1989.

20. Frederikson, G. H.; Helfand, E. J Chem Phys 1987, 87, 697-705.

21. Matsen, M. W.; Bates, F. S. Macromolecules 1996, 29, 1091-1098.

22. Van Krevelen, D. W. editor, Properties of Polymers, Elsevier: Amsterdam, Oxford, New York, Tokyo, 1990.

23. See, e.g., Encyclopedia of Polymer Science and Engineering, 2nd ed., John Wiley & Sons: New York, 1985-1989; Vol. 14.

24. Booth, H. S.; Freedman, M. L. J Am Chem Soc 1950, 72, 2847-2850.

25. Hyman, H. H.; Garber, R. A. J Am Chem Soc 1959, 81, 1847-1849.

26. (a) Corey, E. J.; Venkateswarlu, A. J Am Chem Soc 1972, 94, 6190-6191; (b) Corey, E. J.; Snider, B. B. J Am Chem Soc 1972, 94, 2549-2550.

27. Barrett, E. P.; Joyner, L. G.; Halenda, P. P. J Am Chem Soc 1951, 73, 373-380

28. Grosse-Brauckmann, K. J Coll Interface Sci 1997, 187, 418-428

29. See, e.g., Atkins, P. W. Physical Chemistry, 4th ed., Oxford University Press: Oxford, 1990; p 150.

FIGURE LEGENDS

Figure 1. Part of the micro-phase diagram for 1,2-PB-PDMS diblock copolymers from data of Table 1. Thick solid line connects experimentally determined points of order to disorder transition. 'H' stands for the phase detected between the lamella and the gyroid micro-phases (possibly related to the metastable hexagonally perforated lamellae, HPL phase). All ordered phases were characterized by SAXS of the 1,2-PB-PDMS melts or the cross-linked BD samples. The thinner solid lines connect points of order-to-order transition. Segmented lines are used as guide for the eyes showing 'guessed' extrapolations in regions of the micro-phase diagram where data is missing. The thinnest solid line depicts the mean field order-to-disorder transition line.[21] The more accurately determined zone of the phase diagram is shown in the inset. Two arrows point to the block copolymer precursors of the nanoporous samples presented in this work.

Figure 2. Azimuthally integrated SAXS profiles for samples derived from the same block copolymer precursor: *BD-14* (see tab. 1 and fig. 1). (a) SAXS profile of the precursor *BD-14*, consistent with a lamella morphology of 21.6 nm spacing; (b) sample cross-linked at 140 ºC of gyroid morphology with first allowed Bragg peak corresponding to 19.8 nm and a (cubic) crystallographic cell of 48.5 nm; (c) nanoporous gyroid sample obtained from previous sample after etching of PDMS, with first allowed Bragg peak corresponding to 19.4 nm and crystallographic cell size of 47.5 nm; (d) nanoporous sample of 'H' morphology obtained from *BD-14* cross-linked at 80 ºC; the first allowed Bragg peak corresponds to 19.5 nm in direct space. The q-values

corresponding to the four peaks visible in (d) show relative ratios 1 : $(8.3/6)^{½}$: $3^{½}$: $4^{½}$: $7^{½}$. With the exception of the second peak the above ratios are characteristic for the hexagonal symmetry (see Fig. 3 below). The second peak is reminiscent, but not at exactly the same position as the second allowed peak of the gyroid symmetry (see Fig. 5 below).

Figure 3. 2-D and 1-D SAXS profiles for shear-oriented *BD-4-x-E* in the direction parallel to the shear direction. The scattering profiles show characteristic peaks for hexagonally packed cylinder morphology; the profiles are consistent with a high degree of shear-alignment.

Figure 4. SEM and TEM micrographs of *BD-4-x-E*. Characteristic length-scales of the structure were calculated from the picture (see Table 3).

Figure 5. 1-D and 2-D SAXS profiles of a nanoporous sample *BD-14-x(140ºC)-E*. The [211], [220] and other characteristic peaks for the gyroid morphology are marked in the 1-D profile (the marked positions, expected for scattering from gyroid have the following q ratios: $6^{1/2}$, $8^{1/2}$, $14^{1/2}$, $16^{1/2}$, $20^{1/2}$, $22^{1/2}$, $24^{1/2}$, $26^{1/2}$, $30^{1/2}$, $32^{1/2}$, $38^{1/2}$, $40^{1/2}$, $42^{1/2}$, $50^{1/2}$). The lattice constant is 47.5 nm.

Figure 6. SEM and TEM images of *BD-14-x(140°C)-E* clearly showing gyroid morphology. Projection (1,1,1) known also as knitting pattern is clearly visible in the SEM micrograph; (2,1,1) or wagon wheel pattern is clearly visible in the TEM micrograph.[3]

Figure 7. SEM image of *BD-14-x(80°C)-E* with 'H' morphology, showing cylindrical channels with some kind of 'deformed' hexagonal packing. The SAXS profile of the same sample is shown in Figure 2.

Figure 8. BET nitrogen adsorption data. Cumulative (black) and differential (red) distribution of adsorbed Nitrogen per unit mass of nanoporous polymer as a function of pore size as calculated

from the BJH scheme.[28] The profiles are typical for mesoporous materials with well-defined pore size. Both the adsorption and desorption branches are shown for the cumulative distribution, together with the differential distribution relative to the desorption branch. The average value of the radius was 48 Å. The average pore radius from the adsorption branch was 71 Å (not shown). The reason for showing the radius calculated from the desorption branch is that the region of condensation (i.e. the region showing steepest increase) is more accurately determined on this branch, while the data points for the adsorption branch at the same region are more sparse.

Scheme 1. Suggested cross-linking scheme of 1,2-PB by heating in inert atmosphere in the presence of a peroxide. The wavy lines stand for the polymer chain.

Scheme 2. Proposed PDMS cleaving reaction mechanism by TBAF through the S_N2-Si pathway, which involves a pentacoordinate silicon intermediate anion. The wavy lines depict the polymer chain.

GRAPHICAL ABSTRACT

Lars Schulte, Piotr P. Szewczykowski, Fengxiao Guo, Anne Grydgaard, Mathilde R. Jakobsen, Mads. M. Nielsen, Martin E. Vigild, Rolf H. Berg and Sokol Ndoni *

Nanoporous Materials from Stable and Metastable Structures of 1,2-Polybutadiene-Polydimethylsiloxane Block Copolymers

Selective degradation of silicone in silicone containing block copolymers permits to prepare macroscopoic, well-controlled, nanoporous samples of cross-linked polydienes. Our favourite is 1,2-polybutadiene; scanning electron microscopy images of nanoporous samples with three different morphologies are shown: Gyroid, ‘H’ (related to the metastable HPL?) and Hexagonal.

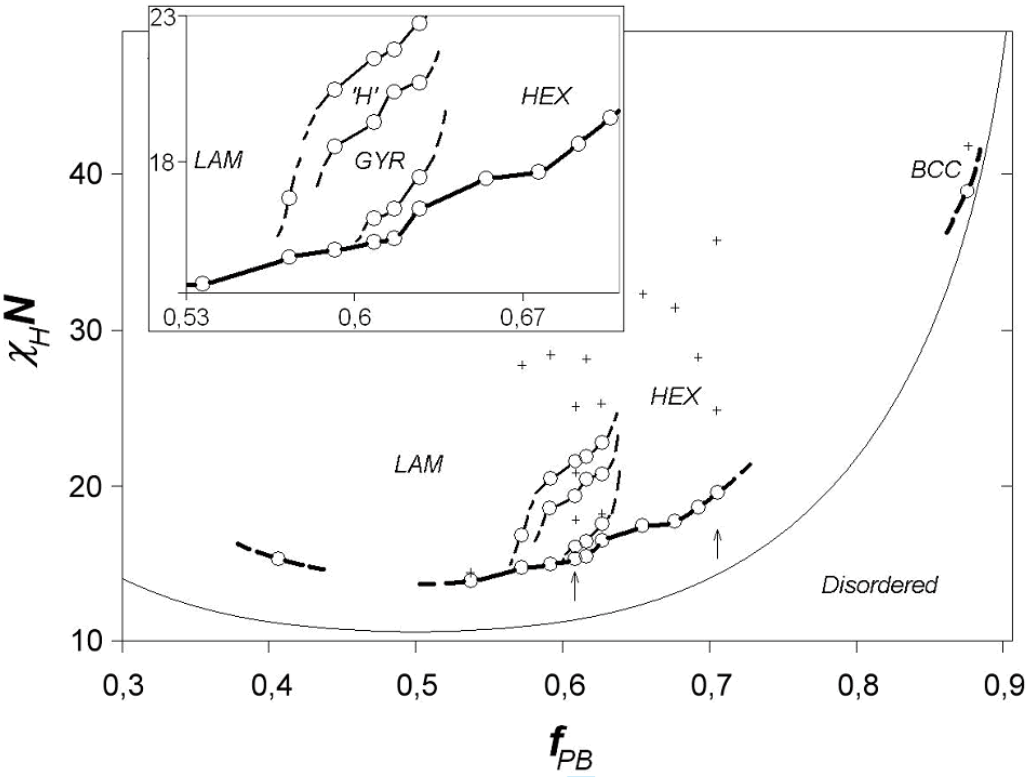

Figure 1

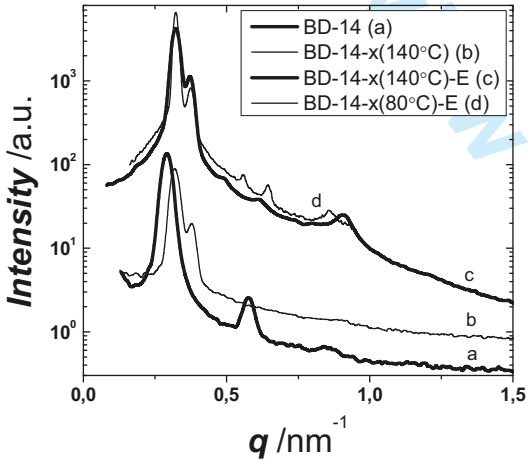

Figure 2

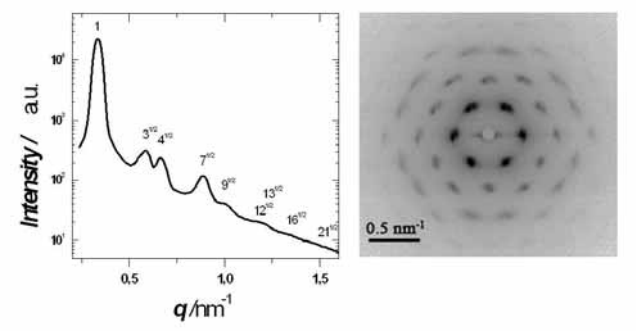

Figure 3

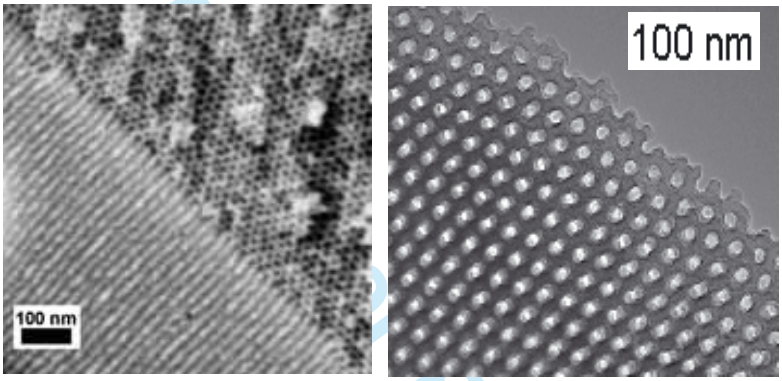

Figure 4

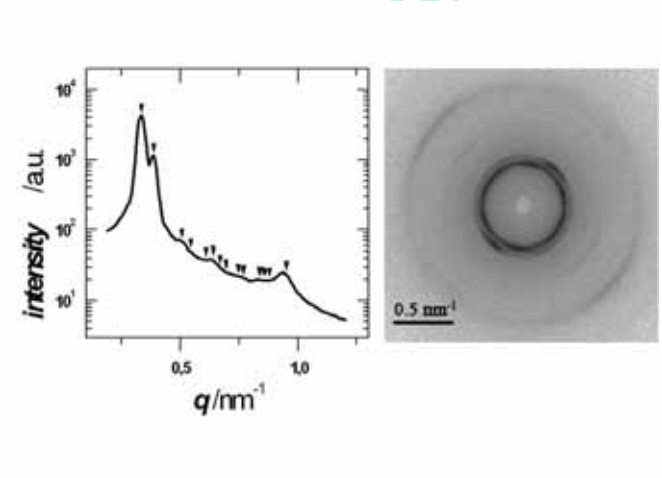

Figure 5

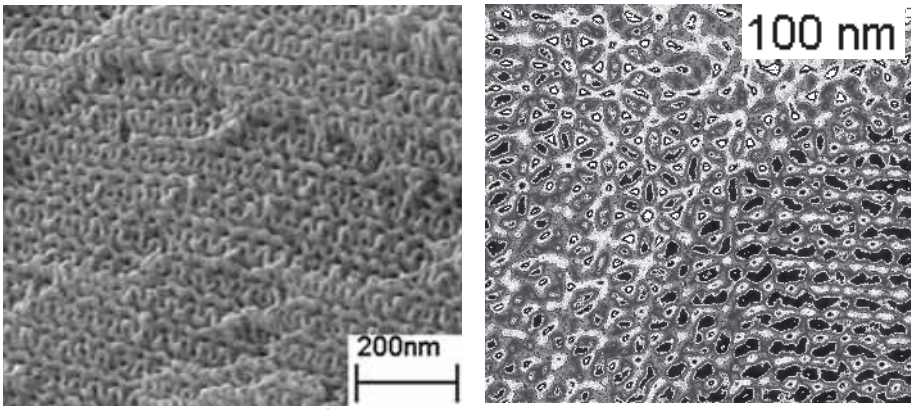

Figure 6

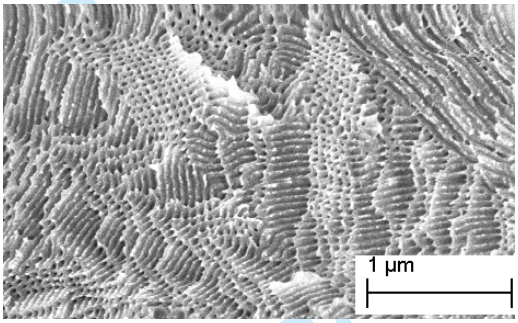

Figure 7.

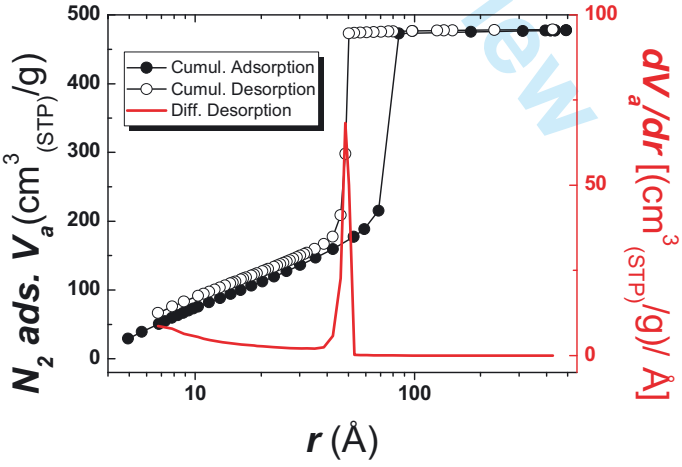

Figure 8.

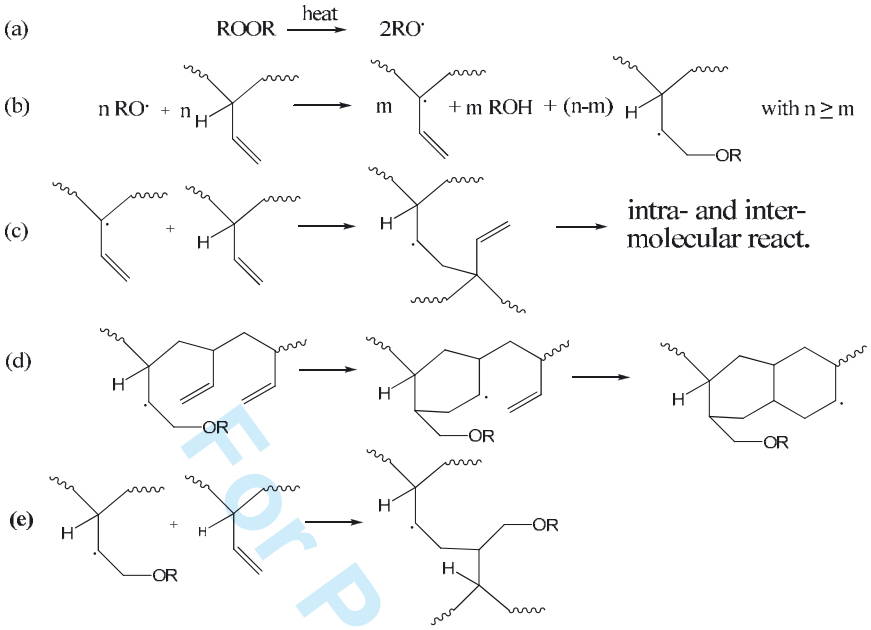

Scheme 1

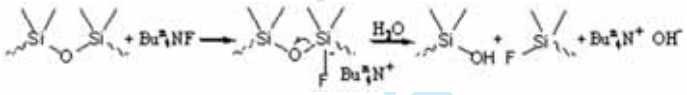

Scheme 2

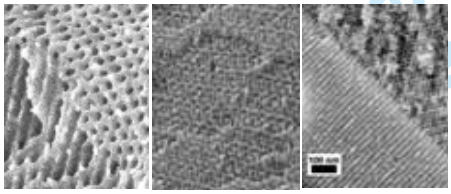

'H' 'GYR' 'HEX'

Graphic abstract

Table 1. Summary of molecular mass (MW) and composition data on 12 block copolymers. The transition order-to-order and order-to-disorder temperatures, T_{OOT} and T_{ODT}, respectively were determined by rheology.

Sample	$\langle M_n \rangle_1$ (g mol^{-1})[a]	$\langle M_n \rangle_{total}$ (g mol^{-1})[b]	PDI_{total}[c]	w_{PDMS}[d]	f_{PDMS}[e]	Morphology	T_{OOT} and T_{ODT} (ºC)
BD-1	2400	6200	1.25	0.610	0.594	LAM	0 (ODT)
BD-2	3200	6100	1.09	0.480	0.463	LAM	30 (ODT)
BD-4	10400	15000	1.22	0.308	0.294	HEX	260 (ODT)
BD-7	15200	17500	1.05	0.132	0.124	BCC	42 (ODT)
BD-8	7000	12100	1.13	0.425	0.408	LAM HPL GYR	133 (OOT) 175 (OOT) 281 (ODT)
BD-10	8100	11900	1.07	0.322	0.307	HEX	170 (ODT)
BD-11	8700	13700	1.06	0.361	0.345	HEX	267 (ODT)
BD-12	8800	13300	1.13	0.339	0.324	HEX	245 (ODT)
BD-14	6300	10700	1.04	0.408	0.392	LAM HPL GYR HEX	68 (OOT) 106 (OOT) 183 (OOT) 207 (ODT)
BD-15	7200	12000	1.06	0.400	0.384	LAM HPL GYR HEX	103 (OOT) 130 (OOT) 226 (OOT) 261 (ODT)

BD-16	6600	10700	1.09	0.389	0.373	LAM HPL GYR HEX	52 (OOT) 84 (OOT) 150 (OOT) 177 (ODT)
BD-18	6600	11800	1.18	0.444	0.427	LAM HPL	210 (OOT) 276 (ODT)

[a] Number average MW of the 1,2-PB block as obtained by SEC.

[b] Number average MW obtained by SEC and ^{1}H-NMR.

[c] Polydispersity index PDI = $<M_w>/<M_n>$ ($<M_w>$ is the weight average MW) obtained by SEC.

[d] mass fraction of PDMS determined by ^{1}H-NMR.

[e] volume fraction of PDMS at 20°C; density values: $\rho_{1,2\text{-PB}} = 0.902$ g/cm^3 and $\rho_{PDMS} = 0.966$ g/cm^3.[18, 19]

Table 2. Data on cross-linking and etching of three 1,2-PB-PDMS samples. The temperature of cross-linking reaction was 140 ºC for the first two samples. The last sample was first cross-linked at 80 ºC for 8 h and then at 140 ºC for 2 h.

Sample	$n_{DLP}/n_{=,0}$ [a]	$n_{DCP}/n_{=,0}$ [a]	t / h [b]	$n_{=,x}/n_{=,0}$ [c]	$\Delta m_E/\Delta m_0$ [d]	$\Delta m_E/\Delta m_{E,max}$ [e]
BD-4-x-E	0	0.01	2	0.36	0.30	0.97
BD-14-x(140ºC)-E	0	0.01	2	0.34	0.40	0.99
BD-14-x(80ºC) -E	0.01	0.01	8 (*80ºC*) 2 (*140ºC*)	0.30	0.39	0.98

[a] Molar ratio between cross-linker (DCP or DLP) and polydiene double bonds in the block copolymer precursor.

[b] Cross-linking reaction time in hours.

[c] Fraction of double bonds measured by FT-IR in the cross-linked sample relative to the double bonds in the block copolymer precursor (uncertainty ± 5%).

[d] Fractional mass loss due to etching of PDMS.

[e] Fractional mass loss relative to maximal expectation.

Table 3. Geometric characteristics of nanoporous materials obtained from SAXS, electron microscopy and Nitrogen adsorption data. Uncertainties were estimated from at least three measurements.

Sample	d^*_{SAXS} /nm [a]	d^*_{EM} / nm [b]	r_{calc} / nm [c]	r_{EM} / nm [d]	r_{BJH} / nm [e]	A_{calc} [f]	A_{BET} [g]
BD-4-x-E	19.3	18.3 ± 3.4	6.64	6.0 ± 0.9	6.1 ± 1.5	139	75 ± 20
BD-14-x (140°C)-E	19.4 (GYR)	19.3 ± 2.5	n.m/c [h]	6 ± 1	7.1 ± 0.5	151	260 ± 30
BD-14-x (80°C)-E	19.5 ('H')	n.m/c	n.m/c	10 ± 2	n.m/c	n.m/c	n.m/c

[a] Characteristic length-scales corresponding to the first structural peak from SAXS; [b] Distance between principal Bragg planes from SEM/TEM; [c] Cylinder/Pore radius calculated from SAXS, composition and density data; [d] Pore radius from SEM/TEM; [e] Pore radius from N_2 isothermal adsorption; [f] Specific surface area calculated from SAXS data; [g] Specific surface area from N_2 isothermal adsorption; [h] Not measured / calculated.

F

Macromolecules
COMMUNICATION TO THE EDITOR

Macromolecules **2009**, *42*, 3877–3880 **3877**
DOI: 10.1021/ma900485q

Controlled Photooxidation of Nanoporous Polymers

Sokol Ndoni,*,† Li Li,†,‡ Lars Schulte,†,‡ Piotr P. Szewczykowski,†,‡ Thomas W. Hansen,§ Fengxiao Guo,†,‡ Rolf H. Berg,† and Martin E. Vigild*,‡

†*Department of Micro- and Nanotechnology, Technical University of Denmark, DK-4000 Roskilde, Denmark,* ‡*Department of Chemical and Biochemical Engineering Technical University of Denmark, DK-2800 Kgs. Lyngby, Denmark, and* §*Center for Electron Nanoscopy, Technical University of Denmark, DK-2800 Kgs. Lyngby, Denmark*

Received March 5, 2009
Revised Manuscript Received May 3, 2009

The general phenomenon of photooxidation[1−5] involves oxygen gas permeation[6,7] into the material under photochemical reaction, typically mediated by UV radiation. It has been extensively studied mainly driven by material degradation concerns.[1−5] The effects of photooxidation to the emerging class of nanoporous polymers[8−14] (NP) are unexplored and hold great potential for both the fundamental understanding of polymer photooxidation in general and for nanotechnological applications. Uses of NP as ultrafiltration membranes[10] or as cladding for liquid core wave guides[12] are worth mentioning in the context of the present work. Nanoporous polymers derived from self-organized block copolymers[15] show crystalline-like order with typical structural length scales in the range 10−100 nm; they have vast internal surfaces (50−500 $m^2\ g^{-1}$), which in the presence of pore percolation are readily accessible to gases. For structural length scales much smaller than the wavelength of UV-A, B radiation ($\lambda > 280$ nm), radiation penetration depth is not seriously limited by scattering.[16] No experimental or modeling report was found on the photooxidative stability of nanoporous polymers. One report describes treatment of a nonpolymeric matrix[17] with UV-254 nm and ozone; the survival of nanoporosity was uncertain.

We demonstrate that the polymer−air interface of nanoporous polymers can be altered by controlled photooxidation in air, without compromising nanostructure. Patterned hydrophilicity can be generated, spawning interesting applications. We also illustrate, by the straightforward calculation of the oxygen fixation quantum yield,[1,2] that NP open new possibilities for fundamental surface studies of polymers. The effect of photooxidation is described here for the case of nanoporous cross-linked 1,2-polybutadiene[18] of gyroid morphology[19] derived from a self-assembled 1,2-polybutadiene-*b*-polydimethylsiloxane (PB−PDMS) diblock copolymer. The conceptual scheme of the present contribution is shown in Figure 1. Figure S1 of the Supporting Information demonstrates the nanoporosity-enhanced photooxidation of another polymer, polystyrene.

PB−PDMS was prepared by "living" anionic polymerization.[20] The number-average molecular mass of the 1,2-PB block was 6300 g mol^{-1} and its mass fraction 0.59. The 1,2-PB microphase was first cross-linked at 140 °C for 2 h under argon, and then PDMS was specifically and quantitatively removed by tetrabutylammonium fluoride, following our recently reported procedure.[18] Either aromatic dicumyl peroxide or aliphatic diamyl peroxide was used as free radical generators at 1% molar concentration relative to the PB repeating units. 0.50 mm NP films were photooxidized in air at either 32 ± 2 or 42 ± 2 °C, for times of up to 50 h by UV generated from Philips Cleo 25W RS UV lamps. Lithographic masks were used for micropatterning, while the coarser masks were machined on aluminum sheets. The radiation wavelength range chosen for the modification of *x*-PB was 310−420 nm, peaking at 350 nm; the radiant flux at the samples' position was measured to 31 ± 2 mW cm^{-2}. Finally, copper electrotemplating was realized at 40 V at an electrode separation of 20 mm from 1 M copper(II) chloride solution (see Figure 4c).

Figure 2a−d shows transmission electron microscopy (TEM) images of the NP after 0, 10, 30, and 40 h of UV treatment. The morphology is conserved in the time window as confirmed by small-angle X-ray scattering (SAXS) (Figure 2e). The equality of length scales shown by SAXS indicates that oxygen photofixation for irradiation times of up to 40 h mainly happens at the polymer−air interface.[21−23]

The sample dry mass increases with irradiation time due to oxygen fixation as plotted in Figure 3a. After 50 h of irradiation the mass increases by 21% relative to the nanoporous native sample. Figure 3b shows the equilibrium value for water uptake of samples submerged in water after increasing UV-irradiation times. The sigmoid trend shows that there is a lower limit of roughly 6−8 h in irradiation time before spontaneous wetting can start. This can be interpreted as the time needed to reach a critical value for the surface density of the generated hydrophilic groups. At 30 h the water uptake is 0.63 ± 0.03, which together with the dry oxidation mass adds up to a total volume fraction of 0.44 ± 0.02 (1 g cm^{-3} overall density assumed). The pore volume fraction of the original NP as measured by methanol uptake is 0.43 ± 0.01, nicely matching the above value and reconfirming structure stability. For the samples irradiated at 40 and 50 h the total volume fraction of absorbed water and fixed oxygen exceeds by up to 7% the pore volume fraction of the original NP, probably due to slight sample swelling in water. Detailed analyses of the results are complicated by the depth gradient of sample photooxidation degree.

The effects of temperature and cross-linking agent on the photooxidation reaction were tested by operating at two temperatures (32 and 42 °C) and with two cross-linkers (one aromatic and one aliphatic peroxide).[24] Within experimental uncertainty samples irradiated at 32 and 42 °C cannot be discriminated by the data in Figure 3a. However, Figure 3b hints to a sharper "hydrophilic transition" taking place at the lower temperature. The effect of temperature on the sharpness of the transition is more evident in Figure S3, where the *x*-axis is the absorbance at 350 nm. The lower temperature therefore favors the formation of hydrophilic groups at the polymer−air interface throughout the sample thickness. A more systematic study of the effect of temperature in the range 0−50 °C is in progress.

The distinctive possibilities the present materials open for fundamental studies of photooxidation of polymers in general is illustrated below by the calculation of the initial oxygen fixation quantum yield,[1,2] $\overline{Q^0_{O_2}}$, which is the wavelength averaged probability for an absorbed photon to create a covalent bond between polymer and oxygen:

$$\overline{Q^0_{O_2}} = \left(\frac{dN_{O_2,\,fix}}{dN_{h\nu,\,abs}}\right)_{time=0} = \left(\frac{dN_{O_2,\,fix}/dt}{dN_{h\nu,\,abs}/dt}\right)_{t=0}; \quad 310\ nm < \lambda < 400\ nm$$

*Corresponding authors. E-mail: sokol.ndoni@nanotech.dtu.dk (S.N.); mev@kt.dtu.dk (M.E.V.).

Published on Web 05/19/2009

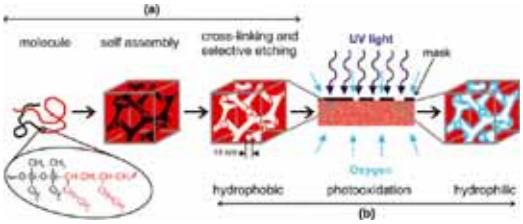

Figure 1. Conceptual scheme showing (a) preparation of a cross-linked nanoporous polymer of gyroid morphology from a self-assembled diblock copolymer and (b) controlled photofixation of oxygen onto the pore walls. Hydrophilic patterns can be created by application of UV masks. The polymer matrix (red zone) constitutes the pore walls (0.57 volume fraction, 20−30 nm thick). The wall volume separated ~1 nm from the air−polymer interface is referred to as "polymer bulk" in the text.

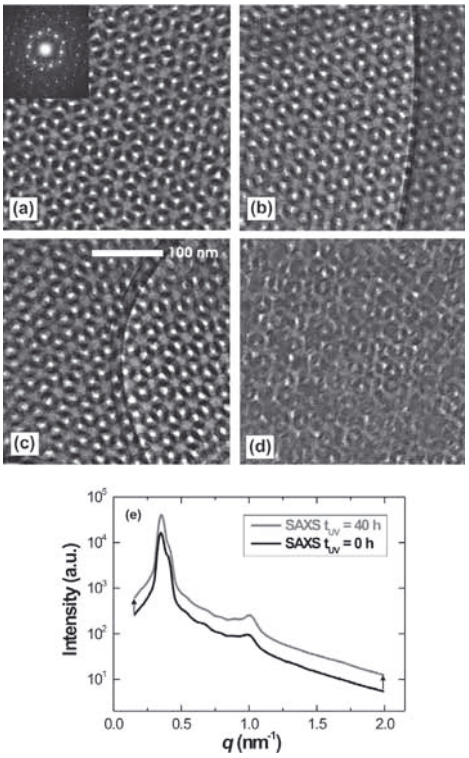

Figure 2. Structural characterization by TEM and SAXS of nanoporous *x*-PB after (a) 0, (b) 10, (c) 30, and (d) 40 h of UV treatment. The "wagon wheel" (111) projection of the gyroid structure is neatly visible in all the TEM micrographs. The light regions correspond to the interconnected porous structure of tripod struts with the white spots marking the struts with highest projected porosity. The inset in (a) is a fast Fourier transform of the image illustrating the high degree of order. The micrograph (d) shows less regularity than the other three; we argue that this is not due to loss of nanoporous morphology but probably to sample brittleness caused by inhomogeneous oxidation at different depths. TEM specimen preparation becomes difficult for such samples, resulting in fractured microtomed surface at the scale of the micrographs. The preservation of morphology is directly supported by the similarity of the SAXS profiles after 0 and 40 h of UV irradiation shown in (e). For most applications modification depths 10−100 times smaller than the present sample thickness will be of interest; in such cases irradiation times of 8−15 h will be sufficient at equal UV intensity.

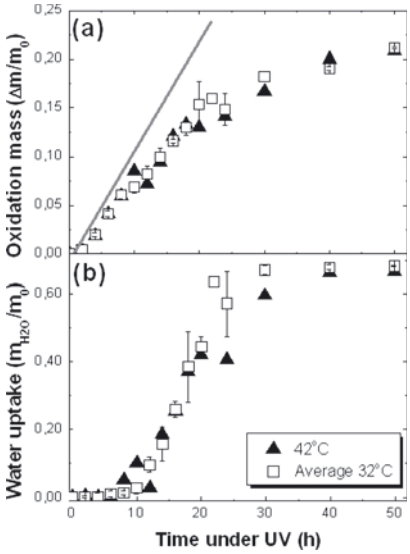

Figure 3. Mass change due to oxygen photofixation and equilibrium of water uptake as a function of UV irradiation time and temperature. (a) Degree of oxygen fixation expressed as dry mass increase relative to the unmodified samples for three sets of samples irradiated at 32 °C and one set at 42 °C. The straight line marks the initial slope of the mass growth used to calculate the O_2-fixation quantum yield. (b) Equilibrium water uptake of samples treated at different times by UV-350 nm. The increase of water uptake after 8 h of UV treatment is due to an increased volume of the NP sample being rendered hydrophilic starting from the side directly exposed to UV. After 22−30 h the whole sample of thickness 0.50 mm is rendered hydrophilic.

$N_{O_2,fix}$ and $N_{h\nu,abs}$ are the number of O_2 molecules covalently bond to the polymer and the number of photons absorbed by the NP, respectively. The numerator in the last expression can be readily evaluated from the initial slope in Figure 3a; the denominator is calculated from the polymer transmission UV spectrum at time $t = 0$ and the lamp emission profile, as illustrated in Figure S2 of the Supporting Information. The possibility to calculate $Q^0_{O_2}$ (0.24 ± 0.03, no literature value could be found for comparison) by using an analytical balance is directly related to the concentrated interface area and the high oxygen permeability in the nanoporous samples. Accurate mapping of the $Q^0_{O_2}$ dependence on λ is possible by using monochromatic radiation of known wavelength. Other important parameters, difficult to obtain in other ways, such as the kinetics of photooxidation and the type and distribution of the generated chemical groups can be gained by the present procedure.

The ability of the UV-modified samples to take up water remained unchanged for at least 6 months, during which dry samples stored under argon for the period behaved in the same way as freshly UV-irradiated ones.[25] This is an attractive feature since many hydrophilically modified polymers show irreversible hydrophobic recovery[26] after few days of storage in the dry state.

Figure 4 illustrates the UV patterning of the hydrophobic matrix and two derived applications on wave guiding and metal nanotemplating. Patterning of hydrophilic regions into hydrophobic surrounding is straightforward by utilizing appropriate masks. Fine patterns in the micrometer scale were fabricated, as shown in Figure 4a (see also Figure S4). The spatial decorations realized here are fascinating as they are a convolution of nanoporosity into micropatterns. When submerged into water such samples wet exclusively in the irradiated zones. The added water increases the refractive index in the hydrophilic regions,

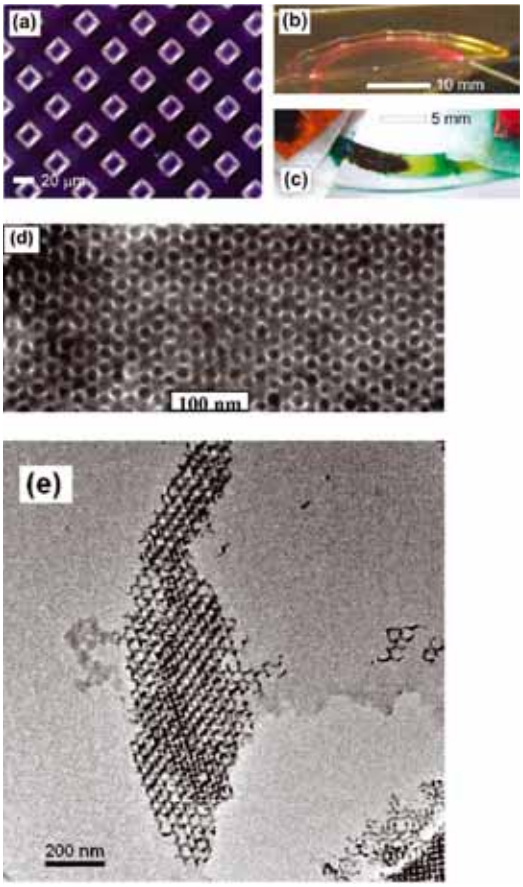

Figure 4. Examples of NP with added functionality by photooxidative decoration. (a) Grid of hydrophilic squares of size 20 μm in a 2-D square lattice of 40 μm principal distance (for a 5 μm feature pattern see Figure S4). The wet patterned NP was placed between two microscope glasses in order to prevent water evaporation. The presence of water exclusively in the hydrophilic regions gives rise to an increased contrast of refractive indices between the two zones. (b) Demonstration of principle of 630 nm laser light guiding along a wet nanoporous zone formed as a 140° arch of 1 mm width and 0.3 mm depth. The light source (laser light passing through a syringe needle of 0.8 mm opening) is visible at the right bottom corner. (c) Copper electrodeposition along a 2.0 mm wide hydrophilic zone surrounded by hydrophobic nanoporous polymer. (d) TEM image from the metal filled zone (Figures S6 and S7 show a high-resolution TEM of the template). (e) TEM of template "finger" with visible gyroid copper scaffold.

providing picture contrast under the optical microscope. Again, the refractive index contrast allows light guiding at total internal reflection, as demonstrated in Figure 4b.[27]

Figure 4c shows directed electrodeposition of copper through a 2 mm wide and 0.5 mm thick hydrophilic strip (cathode on the left; both electrodes embrace the NP sample through copper sheets and filter paper helping to keep the sample extremities wet). The growing finger pattern of the nanotemplated (black) copper on the cathode (left) is evident. Nanotemplating was confirmed by SAXS (not shown), by TEM shown in Figure 4d,e, and by high-resolution TEM shown in Figures S5 and S6. The conservation of the gyroid morphology after electrotemplating is evident from Figure 4d,e. The hydrophilic nanopores are filled with copper which is the reason for the inversed contrast in Figure 4d relative to the TEM images of Figure 2. The length scale is unchanged in the two cases. Figure 4e shows a TEM image from sample's margin where the copper gyroid scaffold is very clear. Now, the TEM imaging was made several weeks after the electrodeposition experiment. The sample was kept in air in the mean time, in which case copper is expected to oxidize.[28] The crystalline patterns in the high-resolution TEM images of Figures S5 and S6 show periodicity of 2.54 ± 0.06 Å, consistent with the d_{111} crystal spacing observed in nanoparticles of cuprite, Cu_2O, from in-air-oxidized copper nanoparticles.[28]

In conclusion, we have presented a simple method for generating hydrophilic nanoporous materials of conserved nanostructure by photooxidation in air of hydrophobic nanoporous polymers. The vast knowledge on photooxidation of polymers accumulated in the field of polymer degradation is expected to play a constructive role within the method presented. The typical chemical groups responsible for the hydrophilicity are carboxyl and hydroxyl groups. Hydrophilic patterns of few micrometer length scale were easily produced. Conversely, it was argued that nanoporous polymers constitute unique model materials for the study of the general phenomenon of polymer photooxidation.

The overall method presented combines molecular self-organization as a bottom-up procedure for the production of nanoporous polymers with UV patterning as a top-down procedure for changing the chemical composition of the concentrated polymer−air interface. A number of added and structure-related physicochemical properties such as water self-confinement and flow, refractive index contrast, large surface area, accessible chemically reactive functional groups, and nanoporosity can be combined to generate a multitude of new application possibilities.

Acknowledgment. We thank Mogens H. Jakobsen and Gabriella Blagoi (DTU Nanotech) for permission to use their UV reactor, Jens W. Andreasen (Risø-DTU) for assistance with SAXS, Niels B. Larsen (DTU Nanotech) for providing the lithographic UV masks, and Kell Mortensen (KU-Life, University of Copenhagen) for useful discussions. We acknowledge the financial support from the Danish Research Agency for Technology and Production.

Supporting Information Available: Figures S1−S6. This material is available free of charge via the Internet at http://pubs.acs.org.

References and Notes

(1) Rabek, J. F. *Polymer Photodegradation*; Chapman & Hall: London, 1995; Chapters 1−3.
(2) Rabek, J. F. *Photodegradation of Polymers*; Springer: Berlin, 1996.
(3) Adam, C.; Lacoste, J.; Lemaire, J. *Polym. Degrad. Stab.* **1990**, *29*, 305.
(4) Piton, M.; Rivaton, A. *Polym. Degrad. Stab.* **1996**, *53*, 343.
(5) Lucki, J.; Ranby, B.; Rabek, J. F. *Eur. Polym. J.* **1979**, *15*, 1101.
(6) Vieth, W. R.; Howell, J. M.; Hsieh, J. H. *J. Membr. Sci.* **1976**, *1*, 177.
(7) Paul, D. R. *Phys. Chem. Chem. Phys.* **1979**, *83*, 294.
(8) Lee, J.-S.; Hirao, A.; Nakahama, S. *Macromolecules* **1988**, *21*, 274.
(9) Thurn-Albrecht, T.; Schotter, J.; Kastle, G. A.; Emley, N.; Shibauchi, T.; Krusin-Elbaum, L.; Guarini, K.; Black, C. T.; Tuominen, M. T.; Russell, T. P. *Science* **2000**, *290*, 2126.
(10) Yang, S. Y.; Ryu, I.; Kim, H. Y.; Kim, J. K.; Jang, S. K.; Russell, T. P. *Adv. Mater.* **2006**, *18*, 709.
(11) Urbas, A. M.; Maldovan, M.; DeRege, P.; Thomas, E. L. *Adv. Mater.* **2002**, *14*, 1850.
(12) Risk, W. P.; Kim, H. C.; Miller, R. D.; Temkin, H.; Gangopadhyay, S. *Opt. Express* **2004**, *12*, 6446.
(13) Hillmyer, M. A. *Adv. Polym. Sci.* **2005**, *190*, 137.
(14) Ndoni, S.; Vigild, M. E.; Berg, R. H. *J. Am. Chem. Soc.* **2003**, *125*, 13366.
(15) Bates, F. S.; Frederickson, G. H. *Annu. Rev. Phys. Chem.* **1990**, *41*, 525.

(16) We visually observe that 0.5 mm thick NP films of hexagonally packed cylindrical pores are opaque or translucent, despite structural length scales of ~20 nm. This might be due to birefringent light scattering from a multidomain material, with cylinder orientational domain size in the micrometer range. Shear aligned samples are more transparent.
(17) Guo, F.; Andreasen, J. W.; Vigild, M. E.; Ndoni, S. *Macromolecules* **2007**, *40*, 3669.
(18) Hajduk, D. A.; Harper, P. E.; Gruner, S. M.; Honeker, C. C.; Kim, G.; Thomas, E. L.; Fetters, L. J. *Macromolecules* **1994**, *27*, 4063.
(19) Kim, H.-C.; Kreller, C. R.; Tran, K. A.; Sisodiya, V.; Angelos, S.; Wallraff, G.; Swanson, S.; Miller, R. D. *Chem. Mater.* **2004**, *16*, 4267.
(20) Ndoni, S.; Papadakis, C. M.; Almdal, K.; Bates, F. S. *Rev. Sci. Instrum.* **1995**, *66*, 1090.
(21) Oxygen fixation on these highly cross-linked matrices should mainly happen at the interface; otherwise, a change in the length scale should be observed by SAXS. The free radicals formed in the process of photooxidation fix oxygen mostly at the air interface due to higher oxygen concentration in the pore volume than in the polymer bulk. At increasing irradiation times the oxidized layer expands into the matrix bulk.
(22) Ito, M.; Matsumoto, M.; Doi, M. *Fluid Phase Equilib.* **1998**, *144*, 395. A molecular dynamic simulation of O_2 permeation into a polyethylene film showing polymer−air interface enriched with O_2 and a sharp fall (within 1−2 nm) in O_2 concentration in the bulk; this can be relevant for the present situation.
(23) There are three relevant time scales in the process of NP photooxidation related to O_2 diffusion into the nanopores (τ_K), O_2 diffusion into the bulk polymer (τ_B), and O_2 consumption by photoreaction (τ_R). O_2 transport through the nanopores occurs by Knudsen diffusion. In the present case Knudsen diffusion coefficient is $\sim 10^6$ larger than bulk diffusion coefficient. For a given NP the mentioned characteristic times are sample thickness dependent, and they are expected to change in the course of photofixation due to material's chemical and optical property changes. In the present case the initial absorbance of UV is low so that photooxidation in the majority of the sample is expected initially to happen at conditions of quasi-equilibrium in oxygen concentration in the pores and in the bulk, $\tau_K \leq \tau_B \ll \tau_R$. The bulk concentration can be taken equal to O_2 solubility in the polymer matrix, which in the present case is expected to be 10−20 times lower than O_2 concentration in air.
(24) The possibility of a special role in oxygen photofixation of in situ generated photoinitiator (benzophenone, one of the scission products of dicumyl peroxide during the oxygen-free cross-linking reaction) was excluded by the observation that the sample series cross-linked by the aliphatic diamyl peroxide showed the same behaviour under UV treatment as the DCP series.
(25) Li, L. Surface Modification of Nanoporous 1,2-Polybutadiene Matrices by Near UV-Induced Photooxidation, M.Sc. Thesis, Technical University of Denmark, **2007**.
(26) Larsson, A.; Dérand, H. *J. Colloid Interface Sci.* **2002**, *246*, 214.
(27) The estimated refractive index at 633 nm is 1.30 for the dry NP and 1.43 for the water-filled NP. The edges of the hydrophilic pattern visibly scatter light due to roughness of length scale ~1−10 μm, conveyed from the "coarse" aluminum UV mask during the patterning process.
(28) Urban, J.; Sack-Kongehl, H.; Hweiss, K. *Z. Phys. D* **1995**, *36*, 73.

Department of Chemical
and Biochemical Engineering

DTU Building 229
Søltofts Plads
DK-2800 Kgs. Lyngby
www.kt.dtu.dk